NASA TECHNICAL NOTE

NASA TN D-5945

NASA TN D-5945

C. 1

WIND-TUNNEL INVESTIGATION OF VARIOUS SMALL-SCALE ROTOR/WING CONFIGURATIONS FOR VTOL COMPOSITE AIRCRAFT IN THE CRUISE MODE

by James P. Shivers

Langley Research Center
Hampton, Va. 23365

NATIONAL AERONAUTICS AND SPACE ADMINISTRATION • WASHINGTON, D. C. • OCTOBER 1970

1. Report No.	2. Government Accession No.	3. Recipient's Catalog No.
NASA TN D-5945		

4. Title and Subtitle
WIND-TUNNEL INVESTIGATION OF VARIOUS SMALL-SCALE ROTOR/WING CONFIGURATIONS FOR VTOL COMPOSITE AIRCRAFT IN THE CRUISE MODE

5. Report Date
October 1970

6. Performing Organization Code

7. Author(s)
James P. Shivers

8. Performing Organization Report No.
L-7133

10. Work Unit No.
721-01-10-01

9. Performing Organization Name and Address
NASA Langley Research Center
Hampton, Va. 23365

11. Contract or Grant No.

13. Type of Report and Period Covered
Technical Note

12. Sponsoring Agency Name and Address
National Aeronautics and Space Administration
Washington, D.C. 20546

14. Sponsoring Agency Code

15. Supplementary Notes

16. Abstract

A subsonic wind-tunnel investigation of a small-scale rotor/wing VTOL airplane has been conducted in a low-speed tunnel with a 12-foot (3.66 meter) octagonal test section at the Langley Research Center to determine the aerodynamic characteristics of the model in the cruise mode. Five three-blade and three four-blade rotor/wing planforms were tested on a model with a conventional fuselage and tails. The investigation consisted of tests in the cruise configuration to determine lift, drag, static stability and control characteristics, and the dynamic rolling-stability derivatives. Studies with the rotor/wing fixed at various azimuth angles were made to determine the rolling and pitching moments due to variation of the azimuth angle and the effectiveness of the controls for countering these moments.

17. Key Words (Suggested by Author(s))
Aerodynamics
Configurations
Stability and control

18. Distribution Statement
Unclassified – Unlimited

19. Security Classif. (of this report)	20. Security Classif. (of this page)	21. No. of Pages	22. Price*
Unclassified	Unclassified	225	$3.00

*For sale by the Clearinghouse for Federal Scientific and Technical Information
Springfield, Virginia 22151

WIND-TUNNEL INVESTIGATION OF VARIOUS SMALL-SCALE ROTOR/WING CONFIGURATIONS FOR VTOL COMPOSITE AIRCRAFT IN THE CRUISE MODE

By James P. Shivers
Langley Research Center

SUMMARY

A subsonic wind-tunnel investigation of a small-scale rotor/wing VTOL airplane model has been conducted in a low-speed tunnel with a 12-foot (3.66 meter) octagonal test section at the Langley Research Center to determine the cruise-mode aerodynamic characteristics for eight planforms using the same fuselage. The rotor/wing VTOL aircraft concept is one in which a rotor is used for hovering and low-speed flight, whereas for high-speed flight the rotor is stopped and serves as a fixed wing. Five three-blade and three four-blade rotor/wing planforms were tested on a model with a conventional fuselage and tails. The investigation consisted of tests in the cruise configuration to determine lift, drag, static stability and control characteristics, and the dynamic rolling-stability derivatives. Studies with the rotor/wing fixed at various azimuth angles were made to determine the rolling and pitching moments due to variation of the azimuth angle and the effectiveness of the controls for countering these moments.

The results of the investigation showed that the longitudinal stability and control characteristics for most of the wings were generally satisfactory and the lateral stability and control characteristics were generally satisfactory when twin vertical tails were mounted at the tips of the horizontal tail. The three-blade rotor/wings experienced large pitching and rolling moments due to center-of-pressure shift as the blades were rotated through the azimuth range. The use of cyclic pitch control was found to be effective in reducing or eliminating these moments. The four-blade rotor/wing did not experience appreciable moment changes with azimuth angle.

INTRODUCTION

A wind-tunnel investigation of a small-scale rotor/wing VTOL aircraft model has been conducted in a low-speed tunnel with a 12-foot (3.66 meter) octagonal test section at the Langley Research Center to determine the aerodynamic and stability and control characteristics for eight planforms in the cruise mode. The rotor/wing VTOL aircraft concept is one in which a rotor is used for hovering and low-speed flight, whereas for

high-speed flight the rotor is stopped and serves as a fixed wing. This concept is intended to combine the low downwash effects and high hovering efficiency of the helicopter rotor system with the high cruise-speed efficiency of the conventional fixed-wing airplane. In the present investigation five three-blade and three four-blade rotor/wing configurations were tested on the same fuselage. Tests were made for a range of horizontal-tail heights with a single vertical tail and also with a twin-vertical-tail configuration on the center fuselage.

The investigation consisted of tests to determine: (1) the lift, drag, and static longitudinal stability and control characteristics; (2) the static lateral stability and control characteristics; (3) the dynamic rolling-stability derivatives (for the five three-blade rotors only); (4) the rolling- and pitching-moment characteristics as a function of rotor azimuth position; and (5) the effect of cyclic pitch inputs to control the rolling and pitching moments associated with azimuth changes in starting and stopping the rotor system.

SYMBOLS

Longitudinal forces and moments are referred to the stability system of axes. Lateral forces and moments are referred to the body system of axes. Both axes systems are shown in figure 1. The moments are referred to the center-of-gravity position shown in figure 2. Dimensional quantities are given in both U.S. Customary Units and the International System of Units (SI). Conversion factors relating the two systems are given in reference 1.

A_o constant term in expression for θ; hence, mean-blade-pitch angle, deg

A_1 coefficient of $-\cos\psi$ in expression for θ, deg or rad

B_1 coefficient of $-\sin\psi$ in expression for θ, deg or rad

b wing span, ft (m)

c chord, ft (m)

c_{av} average wing chord, S/b, ft (m)

C_L lift coefficient, F_L/qS

$C_{L,t}$ lift coefficient of horizontal tail based on its area

C_D	drag coefficient, F_D/qS
$C_{D,t}$	drag coefficient of horizontal tail based on its area
C_m	pitching-moment coefficient, M_Y/qSc_{av}
$C_{m,t}$	tail pitching-moment coefficient
C_Y	lateral-force coefficient, F_Y/qS
C_l	rolling-moment coefficient, M_X/qSb
$C_{l,t}$	tail rolling-moment coefficient
C_n	yawing-moment coefficient, M_Z/qSb
$C_{n,t}$	tail yawing-moment coefficient
F_D	drag, lb (N)
F_L	lift, lb (N)
F_Y	lateral force, lb (N)
i_t	horizontal-tail incidence (positive for leading-edge-upward deflection), deg
$i_{t,mean}$	mean horizontal-tail incidence when right- and left-tail planes are deflected differentially for roll control, deg
$i_{t,R}$	incidence of right-horizontal-tail plane, deg
$i_{t,L}$	incidence of left-horizontal-tail plane, deg
k	reduced-frequency parameter, $\omega b/2V$
M_X	rolling moment, ft-lb (m-N)
M_Y	pitching moment, ft-lb (m-N)

M_Z	yawing moment, ft-lb (m-N)
p	rolling velocity, rad/sec
$\dot{p}$	aircraft rolling acceleration, rad/sec^2
q	free-stream dynamic pressure, lb/ft^2 (N/m^2)
S	wing area, ft^2 (m^2)
S_t	tail area, ft^2 (m^2)
V	free-stream velocity, ft/sec (m/sec)
X,Y,Z	body reference axes
x,y	ordinates for horizontal tail, ft (m)
α	angle of attack of wing, deg
β	angle of sideslip, deg
$\dot{\beta}$	aircraft yawing acceleration, rad/sec^2
ϵ	average downwash angle, deg
θ	feathering motion of blades with respect to plane of tip for rotating-rotor condition, $A_0 - A_1 \cos \psi - B_1 \sin \psi \ldots$, deg or rad
Θ	incidence of rotor blades relative to rotor hub measured perpendicular to rotor radius, deg; positive incidence indicates that leading edges of right and left blades (in stopped rotor condition) are deflected upward
Θ_{mean}	mean incidence of right and left rotor blades when deflected differentially for roll control in stopped-rotor condition, deg
Θ_R	incidence of right rotor blade, deg
Θ_L	incidence of left rotor blade, deg

ψ blade azimuth angle measured from downwind position in direction of rotation, deg or rad

Λ rotor-blade-sweep angle, deg

ω angular velocity, rad/sec

Δ increment between coefficient for mean-control-surface angle setting and coefficient for differentially deflected control surfaces

$$C_{l_\beta} = \frac{\partial C_l}{\partial \beta} \qquad C_{n_\beta} = \frac{\partial C_n}{\partial \beta} \qquad C_{Y_\beta} = \frac{\partial C_Y}{\partial \beta}$$

$$C_{l_p} = \frac{\partial C_l}{\partial \frac{pb}{2V}} \qquad C_{n_{\beta,t}} = \frac{\partial C_{n,t}}{\partial \beta}$$

$$C_{l_{\dot\beta}} = \frac{\partial C_l}{\partial \frac{\dot\beta b}{2V}} \qquad C_{n_p} = \frac{\partial C_n}{\partial \frac{pb}{2V}}$$

$$C_{l_{\dot p}} = \frac{\partial C_l}{\partial \frac{\dot p b^2}{4V^2}} \qquad C_{n_{\dot\beta}} = \frac{\partial C_n}{\partial \frac{\dot\beta b}{2V}}$$

$$C_{n_{\dot p}} = \frac{\partial C_n}{\partial \frac{\dot p b^2}{4V^2}}$$

A dot over a symbol represents a derivative with respect to time.

MODEL

A drawing of the model with rotor/wing 2 installed is shown in figure 2. Figure 3 shows the model with rotor/wing 8 installed. Figure 4 shows the planforms of all eight rotor/wings that were investigated.

The rotor/wing was oriented as shown in figure 2 for the three-blade rotors and as shown in figure 3 for the four-blade rotors. The incidence of all rotor blades was adjustable about the 50-percent chord line. The airfoil section of the wing was a flat plate with rounded leading and trailing edges and tips.

The horizontal tail, which is shown in figure 2, had an NACA 0012 airfoil section and could be mounted in any of the three vertical positions (high, mid, and low) as shown

in figure 2. The incidence of the horizontal tail was adjustable for pitch control, and the incidence of the right and left tail planes could be adjusted differentially for roll control.

The model had a center vertical tail which had an NACA 0012 airfoil section and was constructed to be detachable from the fuselage for vertical-tail-off tests. The lower, or ventral, part of the center vertical tail was used only when the horizontal tail was in the low position. Twin vertical flat-plate surfaces were added to the tips of the horizontal tails (for mid-height position, only) to provide additional tail area for some of the initial lateral-stability investigations. When it was found that the lateral stability was improved, new vertical twin tails and a new horizontal tail were constructed and installed on the fuselage as shown in figure 3. These vertical tails had NACA 0012 airfoil sections and the horizontal tail had a cambered airfoil section instead of the symmetrical section originally used. The ordinates for the cambered tail are listed in the table in figure 3.

TESTS

Static-stability wind-tunnel tests were made in a 12-foot (3.66 meter), low-speed, atmospheric tunnel with an octagonal cross section. The model was sting mounted on an internal strain-gage balance to measure the forces and moments on the model. The tests were made over an angle-of-attack range from 0° to 36°. The schedule of tests for all eight rotor/wings followed the same general pattern, although the tests were more detailed or more extensive for some rotor/wings than for others. Initially, rotor/wing 2 was tested extensively and analysis of the results permitted reduction in the test matrix for the other configurations.

Tests were made on the five three-blade rotor/wings to determine the lift, drag, and longitudinal stability and control characteristics of the model for three horizontal-tail height positions and for the tails-off condition. Similar parameters were measured with the cambered horizontal tail mounted on the fuselage. These configurations were similar to a three-blade configuration tested on a powered model in the Langley full-scale tunnel and reported in reference 2.

Lateral tests were made at angles of sideslip of 5° and -5° to determine the static lateral-stability derivatives over the test angle-of-attack range. A few lateral tests were also made for each rotor configuration over a range of sideslip angles of 20° to -20°, to determine whether the lateral characteristics were linear functions of sideslip angles. Lateral-control tests were made to determine the effectiveness of the rotor blades and of the horizontal tails as roll-control devices.

In addition to the investigation with the rotor/wing stopped for the airplane mode, tests were also made to determine the rolling and pitching moments generated with the rotor/wing stopped at several different azimuth angles to obtain aerodynamic data for use in analysis of the transition phase of flight.

Forced-oscillation tests were made to determine the dynamic rolling-stability derivatives of the model with the five three-blade rotors. These tests were made in the Langley full-scale tunnel by using the apparatus and technique described in reference 3. The oscillation tests were made at a frequency of 1 cycle per second (1 Hz) which gave a value of the reduced frequency parameter k of about 0.20. The tests were generally made at a dynamic pressure of about 4.0 psf (191.5 N/m^2), which corresponds to a value of Reynolds number of 400 000 based on the average wing chord of rotor/wing 2.

As a supplement to the force tests, tuft studies were made early in the program with rotor/wing 2 to determine the stall pattern of the wing, with particular emphasis placed on determining the effect of blade incidence in relieving blade stall. These studies were used as a guide in choosing the range of test variables. During all tests, several tufts were used on the horizontal tail as a visual means of detecting tail stall. No tunnel wall corrections were applied to the data since the model was small relative to the size of either of the tunnels.

RESULTS AND DISCUSSION

An index to the test data figures is presented in table I. Each of the eight parts of the table pertains to one of the eight rotor/wings sketched in figure 4. For convenience in data comparison for the various wings, summary plots have been made from the basic data figures to show the relative aerodynamic characteristics of the rotor/wings. The basic data are presented in figures 5 to 31 and figures 34 to 145. The summary plots are presented in figures 146 to 153. Most of the discussion will be relative to these summary data.

Wing-Flow Characteristics

Photographs of tufts showing the flow over rotor/wing 2 are presented as figures 32 and 33. Figure 32 shows the flow pattern on the model in the airplane cruise condition and indicates an increase in spanwise flow of the boundary layer with increasing angle of attack that is typical of swept and delta wings. Figure 32 also shows that stalling on the blades starts at a lower angle of attack than on the triangular hub part of the wing. The development of the pronounced spanwise flow and the stalling on the blades were delayed to higher angles of attack by the use of negative blade incidence. It appears from the tuft studies that it is desirable to use a blade incidence of 0° for angles of attack near 0°, and to use a blade incidence of at least -20° for angles of attack near that for wing stall. Consequently, values of blade incidence of 0°, -10°, and -20° were included in most of the series of force tests.

The next series of photographs, figure 33, shows the flow behavior on the rotor/wing when it is oriented to different azimuth positions. At azimuth angles of 30° and 90° the

photographs show that the spanwise flow is asymmetrical. At those two azimuth angles the out-of-trim rolling moments are at a maximum. The positions shown in the photographs are representative of those for the rotor as it starts and stops when in the transition mode. The rotor blades, for the case shown, are set at zero angle relative to the rotor hub.

Lift and Drag

A comparison of the lift and drag characteristics of the eight rotor/wing configurations tested is presented in figures 146 and 147 for the horizontal tail off and the horizontal tail on, respectively. The nondimensional aerodynamic coefficients are based on the actual areas of each wing as listed in figure 4. The lift-curve slopes of the three-blade configurations are generally linear up to the stall except that rotor/wing 4 has a reduction in slope beginning at an angle of attack of about 12°. This reduction in slope is probably a result of tip stall on the swept rotor blades. The data of figure 146 for the four-blade configurations show that rotor/wing 8 experienced an abrupt stall and change in lift-curve slope near an angle of attack of about 8°, whereas the other four-blade configurations show a much higher stall angle of attack. This higher stall angle of attack of rotor/wings 6 and 7 is believed to result, mainly, from a favorable interference effect between the fuselage and wing, since it is much too large to be attributed to differences in aspect ratio of the four-blade configurations. To determine the effect of blade sweep for rotor/wing 6 the blades were swept 30° and 45°. There was a small increase in maximum lift coefficient for these sweep angles. (See fig. 113.)

Longitudinal Stability and Control

From tests made with the horizontal tail at different vertical positions, it was found that best stability characteristics were obtained, generally, with the horizontal tail located in the mid-tail position for the single vertical tail or center-fuselage position for the twin vertical tails. (See figs. 2 and 3.) The summary data of figure 147 are presented for the model with the horizontal tail in center-fuselage position. (See fig. 3.)

The pitching-moment data of figure 146 show that, as expected, all the configurations were statically unstable with tail off except for rotor/wings 3 and 4 at low angles of attack. Planforms 3 and 4, which have practically all their exposed area behind the center of gravity, were statically stable until an increase in angle of attack caused the tips to stall. This tip stall, in turn, caused a forward shift in the aerodynamic center and thereby induced static instability for these rotor/wings.

The data presented in figure 147 show that stability was achieved by the addition of the tail for all the rotor/wing configurations with the exception of the delta wing (rotor/wing 5). Since the tail size remained constant for these tests, those rotor/wings

with smaller areas generally have proportionally greater amounts of stability because of the large values of S_t/S. In figure 148 where $\partial C_m/\partial C_L$ is plotted as a function of S_t/S, it is seen that for reasonable static stability the tail areas for most of the configurations could be reduced considerably. The major exception to this condition, however, is the case of the delta wing (rotor/wing 5). Past experience with delta wings has shown that a horizontal tail is generally ineffective behind such a planform because of the adverse variation in downwash characteristics. The downwash factor $\left(1 - \frac{\partial \epsilon}{\partial \alpha}\right)$, determined from the basic data (in the low angle-of-attack range) and presented in figure 149, shows that for rotor/wing 5 the value of $\left(1 - \frac{\partial \epsilon}{\partial \alpha}\right)$ is only about 0.26, whereas for the other rotor/wings the values range between 0.36 to 0.58.

Static Lateral Stability

Effect of rotor/wing planform.- The data presented in figure 150 show the static lateral-stability characteristics for the configurations with vertical tail off. These data show, as expected, that all the configurations were directionally unstable with vertical tail off and that the instability generally increased at the higher angles of attack. The dihedral effect was positive $\left(-C_{l_\beta}\right)$ at low angles of attack for most of the rotor/wings and was negative $\left(C_{l_\beta}\right)$ at the higher angles of attack. Rotor/wings 3 and 4 had negative dihedral effect at much lower angles of attacks than did the other rotor/wings, apparently because of the very early tip stall which occurred with these configurations.

Effect of vertical-tail arrangement.- From the basic data plots it was found that the model with the center vertical tail was directionally unstable except at low angles of attack. (For example, see figs. 68 and 69.) For this reason, vertical flat plate surfaces were installed on the tips of the horizontal tail as a means of improving the directional stability with angle of attack. Since this tail configuration was found to be more satisfactory than the center tail for directional stability, newly designed twin vertical tails were used for the remainder of the investigation. All the comparison plots showing the effects of rotor/wing configuration on the lateral-stability characteristics, presented in figure 151, are made for the twin-tail configuration.

The data of figure 151 indicate that all the configurations had directional stability over the test angle-of-attack range with the exception of the delta-wing planform (rotor/wing 5) at high angles of attack. Rotor/wings 3 and 4 show the largest values of directional stability of the rotor/wings tested. It should be pointed out that the relative values of C_{n_β} are compared for a tail of constant area. Thus, wings having the smallest areas, such as rotor/wings 3 and 4, would be expected to have the highest values of directional stability because of the higher ratios of tail area to wing area. The dihedral effects of the rotor/wings with vertical tails on and off were generally similar.

Lateral Control

The lateral control that can be provided by differential incidence of the right and left rotor blades is shown in figure 152. The data show that the rolling moment due to control deflections diminishes about 50 percent as the angle of attack is increased from 0° to angles near the stall. The yawing moments due to control deflections are generally adverse, particularly for the higher angles of attack. It should be pointed out that the summary plots of figure 152 were made for the configurations having constant blade-pitch settings. The basic data plots (fig. 53 being typical) for the respective rotor/wings indicate that it is possible to achieve increased rolling moments and reduced adverse yawing moments through the use of increasingly negative mean settings of the blade incidence (avoiding blade stall) as angle of attack is increased.

In addition to the roll control provided by differential incidence of the right and left rotor blades, the basic data plots (fig. 54 being typical) for the respective rotor/wings also show that appreciable roll control can be achieved by differential deflection of the right and left horizontal-tail planes. This control remains essentially constant with angle of attack when the tail surfaces are deflected differentially from increasingly negative mean-incidence settings. The rolling moment produced by differential horizontal-tail deflection is more or less independent of wing planform and is not presented in the summary figures.

Dynamic Rolling-Stability Derivatives

Rolling-oscillation tests were made only for the five three-blade rotor/wings. The results of these tests, as summarized in figure 153, indicate that the model maintains damping in roll $\left(\text{negative values of } C_{l_p} + C_{l_{\dot{\beta}}}\right)$ throughout the angle-of-attack range for rotor/wings 1, 2, and 5 and that rotor/wings 3 and 4 maintain damping in roll up to angles of attack of 26° and 28°, respectively. Subsequent loss of damping in roll for rotor/wings 3 and 4 is associated with the early tip stall that occurred for these configurations.

A comparison of the data of figure 153 with some of the basic data for tail-off conditions indicates that the contribution of the tails to the damping in roll was insignificant for rotor/wings 1, 2, and 5. (See figs. 29, 56, and 109.) For rotor/wings 3 and 4, however, the contributions of the tails to damping in roll became appreciable over some portions of the angle-of-attack range. (See figs. 79 and 94.)

Effect of Rotor Azimuth Angle

In order to determine the effect of moment changes in roll and pitch with a change in rotor azimuth angle, a series of angle-of-attack tests at different azimuth angles were run. The number of azimuth angles was determined by the number needed to produce a smooth rolling- or pitching-moment curve. The rotor was first tested through an

azimuth-angle range with zero cyclic pitch to determine the magnitude of the rolling and pitching moments. Secondly, a first harmonic sine function of 15^{o} was programed into the cyclic controls and then later a sine function of 30^{o} was used to check moment variation for varying degrees of cyclic pitch. Most of the cyclic control variations were made with rotor/wing 2, since data from this rotor/wing were needed to compare with a powered rotor/wing model with a similar wing planform that had been tested in the Langley full-scale tunnel (ref. 4). Enough data were taken with the other rotor/wing models at different azimuth angles and cyclic pitch angles to determine the reaction of each rotor/wing to the various controls.

The pitching- and rolling-moment coefficients (see fig. 58(b)) resulting from center-of-pressure shift on the three-blade rotor/wing as the blades were rotated through an azimuth angle could be reduced (see fig. 58(c)) or eliminated (see fig. 58(d)) by the use of cyclic pitch. It was found that the four-blade rotor/wings did not experience appreciable changes in rolling and pitching moments with changes in azimuth angle (see figs. 123 and 133) since there was no significant center-of-pressure shift as the blades were rotated.

CONCLUSIONS

A subsonic wind-tunnel investigation of a small-scale rotor/wing VTOL airplane has been conducted in a low-speed tunnel with a 12-foot (3.66 meter) octagonal test section at the Langley Research Center to determine the aerodynamic characteristics of the model in the cruise mode. Five three-blade and three four-blade rotor/wing planforms were tested on a model with a conventional fuselage and tails. The results of the investigation may be summarized as follows:

1. The rotor blades had a tendency to stall at the higher test angles of attack. Stalling could generally be relieved by the use of negative blade incidence (of the order of 10^{o} to 20^{o}) with attendant improvements in longitudinal stability, dihedral effect, and roll-control effectiveness of the blades.

2. The longitudinal stability and control characteristics were generally satisfactory for the rotor/wings, except for the delta planform wing, which produced downwash characteristics that caused the horizontal tail to be relatively ineffective.

3. With vertical tails located on the tips of the horizontal tail, the model had positive directional stability over the angle-of-attack range for most of the rotor/wings. A center vertical tail was less satisfactory.

4. The dihedral effect was generally positive at low angles of attack but became negative at higher angles of attack for most of the rotor/wings. For some of the

rotor/wings, the dihedral effect changed from positive to negative at very low angles of attack because of wing-tip stall.

5. Differential deflection of the right and left rotor blades appeared to be a satisfactory means of obtaining lateral control for the rotor/wing configurations. Differential deflection of the horizontal tail was also effective.

6. The three-blade rotor/wings experienced large pitching and rolling moments due to center-of-pressure shift as the blades were rotated through the azimuth range. The use of cyclic pitch control was found to be capable of reducing or eliminating these moments.

7. The four-blade rotor/wings did not experience significant changes in rolling and pitching moments with changes in azimuth angle since there was no appreciable center-of-pressure shift as the blades were rotated.

Langley Research Center,
National Aeronautics and Space Administration,
Hampton, Va., July 13, 1970.

REFERENCES

1. Mechtly, E. A.: The International System of Units – Physical Constants and Conversion Factors. NASA SP-7012, 1964.

2. Winston, Matthew M.; and Huston, Robert J.: Wind-Tunnel Investigation of Steady-State Aerodynamics of a Composite-Lift VTOL Aircraft Model. NASA TN D-5232, 1969.

3. Chambers, Joseph R.; and Grafton, Sue B.: Investigation of Lateral-Directional Dynamic Stability of a Tilt-Wing V/STOL Transport. NASA TN D-5637, 1970.

4. Huston, Robert J.; and Shivers, James P.: A Wind-Tunnel and Analytical Study of the Conversion From Wing Lift to Rotor Lift on a Composite-Lift VTOL Aircraft. NASA TN D-5256, 1969.

TABLE I.- SCHEDULE OF TESTS AND INDEX OF TEST DATA FIGURES

(a) Rotor/wing 1

Type of test	Vertical tail	Horizontal tail		Blade incidence, Θ, deg	Special characteristics	Figures
		Position	Incidence, i_t, deg			
Static longitudinal stability	Off	Off	----------	0, -10, -20		5
	Center	Low	0, -10, -20	0 -10 -20		6 7 8
	Center	Mid	0, -10, -20	0 -10 -20		9 10 11
	Center	High	0	0		12
	Twin	Center fuselage	0, -10, -20	0 -10 -20		13 14 15
Static lateral stability	Off	Off	----------	-10	β, variable	16
	Twin	Center fuselage	-10	-10	β, variable	17
	Off	Off	----------	0, -10, -20	$\beta = \pm 5^o$	18
	Off	Off	----------	-10	$\beta = \pm 5^o$	19
	Twin	Center fuselage	0, -10	-10	$\beta = \pm 5^o$	19
	Twin	Center fuselage	0	0, -10, -20	$\beta = \pm 5^o$	20
	Twin	Center fuselage	0, -10, -20	0, -10, -20	$\beta = \pm 5^o$	21
Roll control effectiveness (blades)	Off	Off	----------	$\Theta_{mean} = 0$	Differential Θ	22
	Twin	Center fuselage	0	$\Theta_{mean} = 0$	Differential Θ	22
	Twin	Center fuselage	0	$\Theta_{mean} = 0$	Differential Θ	23
	Twin	Center fuselage	-10	$\Theta_{mean} = -10$	Differential Θ	24
	Twin	Center fuselage	-20	$\Theta_{mean} = -20$	Differential Θ	25
Roll control effectiveness (horizontal tail)	Twin	Center fuselage	$i_{t,mean} = 0$	0	Differential i_t	26
	Twin	Center fuselage	$i_{t,mean} = -10$	0	Differential i_t	27
	Twin	Center fuselage	$i_{t,mean} = -20$	0	Differential i_t	28
Roll oscillation	Off	Off	----------	0	Dynamic stability	29
	Center	Mid	-10	0	Dynamic stability	29
	Center	Mid	-10	0, -10, -20	Dynamic stability	30
Cyclic control	Twin	Center fuselage	-5	$\Theta = 0$	ψ, variable	31

TABLE I.- SCHEDULE OF TESTS AND INDEX OF TEST DATA FIGURES – Continued

(b) Rotor/wing 2

Type of test	Vertical tail	Horizontal tail		Blade incidence, Θ, deg	Special characteristics	Figures
		Position	Incidence, i_t, deg			
Tuft	----------	----------	----------	0, -10, -20	α, variable	32
	----------	----------	----------	0	ψ, α, variable	33
Static longitudinal stability	Center	Off	----------	0, -10, -20		34
	Center	Low	0, -5, -10	0		35(a)
				-10		35(b)
				-20		35(c)
	Center	Mid	0, -5, -10, -15	0		36(a)
				-10		36(b)
				-20		36(c)
	Center	High	0, -5, -10	0		37(a)
				-10		37(b)
	Twin	Center fuselage	0, -10, -20, -30	0		38(a)
				-10		38(b)
				-20		38(c)
Horizontal tail characteristics	Center	Mid	Variable	0	Symetrical airfoil section	39
Static lateral stability	Off	Off	----------	-10	β, variable	40
	Center	Mid	-5	-10	β, variable	41
	Center	Mid	-10	-20	β, variable	42
	Twin	Center fuselage	-10	-10	β, variable	43
	Off	Off	----------	0, -10, -20	$\beta = \pm 5^o$	44
	Center	Off	----------	-10	$\beta = \pm 5^o$	45
	Center	Mid	0, -5, -10	-10	$\beta = \pm 5^o$	45
	Twin	Center fuselage	0, -10	-10	$\beta = \pm 5^o$	46
	Center	Mid	0	0, -10, -20	$\beta = \pm 5^o$	47
	Twin	Center fuselage	0	0, -10, -20	$\beta = \pm 5^o$	48
	Center	Mid	0, -5, -10	0, -10, -20	$\beta = \pm 5^o$	49
	Twin	Center fuselage	0, -10, -20	0, -10, -20	$\beta = \pm 5^o$	50
	Center + tip	Mid	-5	-10	$\beta = \pm 5^o$	51(a), 51(b)
	Twin	Center fuselage	-10	-10	$\beta = \pm 5^o$	51(a)
Roll control effectiveness (blades)	Center, off/on	Mid, off/on	----------	$\Theta_{mean} = 0$	Differential Θ	52
	Center	Mid	0	$\Theta_{mean} = 0$	Differential Θ	53(a)
			-5	$\Theta_{mean} = -10$		53(b)
			-10	$\Theta_{mean} = -20$		53(c)
Roll control effectiveness (horizontal tail)	Center	Mid	$i_{t,mean} = 0$	0	Differential i_t	54(a)
			$i_{t,mean} = -5$			54(b)
			$i_{t,mean} = -10$			54(c)
	Twin	Center fuselage	$i_{t,mean} = 0$	0	Differential i_t	55(a)
			$i_{t,mean} = -10$			55(b)
			$i_{t,mean} = -20$			55(c)
Roll oscillation	Center, off/on	Mid, off/on	----------	0	Dynamic stability	56
	Center, off/on	Mid	-10	0, -10, -20	Dynamic stability	57
Cyclic control	Center	Mid	0	Hub alone	ψ, variable	58(a)
	Center	Mid	0	$\Theta = 0$	ψ, variable	58(b)
	Twin	Center fuselage	-10	$\Theta = -15 \sin \psi$	ψ, variable	58(c)
	Center	Mid	0	$\Theta = -30 \sin \psi$	ψ, variable	58(d)

TABLE I.- SCHEDULE OF TESTS AND INDEX OF TEST DATA FIGURES – Continued

(c) Rotor/wing 3

Type of test	Vertical tail	Horizontal tail		Blade incidence, Θ, deg	Special characteristics	Figures
		Position	Incidence, i_t, deg			
Static longitudinal stability	Center	Off	----------	0, -10, -20		59
	Center	Low	0, -10, -15	0 -10 -20		60(a) 60(b) 60(c)
	Center	Mid	0, -10, -20	0 -10 -20		61(a) 61(b) 61(c)
	Center	High	0	0		62
	Twin	Center fuselage	0, -10, -20	0 -10 -20		63(a) 63(b) 63(c)
Static lateral stability	Off	Off	----------	-10	β, variable	64
	Center	Mid	-10	-10	β, variable	65
	Twin	Center fuselage	-10	-10	β, variable	66
	Off	Off	----------	0, -10, -20	$\beta = \pm 5^o$	67
	Center	Off	----------	-10	$\beta = \pm 5^o$	68
	Center	Mid	0, -10	-10	$\beta = \pm 5^o$	68
	Center	Mid	0	0, -10, -20	$\beta = \pm 5^o$	69
	Twin	Center fuselage	0	0, -10, -20	$\beta = \pm 5^o$	70
	Center	Mid	0, -10, -20	0, -10, -20	$\beta = \pm 5^o$	71
	Twin	Center fuselage	0, -10, -20	0, -10, -20	$\beta = \pm 5^o$	72
	Center and twin	Mid and center fuselage	-10	-10	$\beta = \pm 5^o$	73
Roll control effectiveness (blades)	Off	Off	----------	$\Theta_{mean} = 0$	Differential Θ	74
	Center	Mid	0	$\Theta_{mean} = 0$	Differential Θ	74
	Center	Mid	0	$\Theta_{mean} = 0$ $\Theta_{mean} = -10$ $\Theta_{mean} = -20$	Differential Θ	75(a) 75(b) 75(c)
	Twin	Center fuselage	0 -10 -20	$\Theta_{mean} = 0$ $\Theta_{mean} = -10$ $\Theta_{mean} = -20$	Differential Θ	76(a) 76(b) 76(c)
Roll control effectiveness (horizontal tail)	Center	Mid	$i_{t,mean} = 0$ $i_{t,mean} = -10$ $i_{t,mean} = -20$	0	Differential i_t	77(a) 77(b) 77(c)
	Twin	Center fuselage	$i_{t,mean} = 0$ $i_{t,mean} = -10$ $i_{t,mean} = -20$	0	Differential i_t	78(a) 78(b) 78(c)
Roll oscillation	Off	Off	----------	0	Dynamic stability	79
	Center	Mid	-10	0	Dynamic stability	79
	Center	Mid	0	0, -10, -20	Dynamic stability	80
Cyclic control	Center	Mid	0	$\Theta = 0$	ψ, variable	81

TABLE I.- SCHEDULE OF TESTS AND INDEX OF TEST DATA FIGURES – Continued

(d) Rotor/wing 4

Type of test	Vertical tail	Horizontal tail		Blade incidence, Θ, deg	Special characteristics	Figures
		Position	Incidence, i_t, deg			
Static longitudinal stability	Off	Off	----------	0, -10, -20		82
	Center	Low	0, -10, -20	0 -10 -20		83(a) 83(b) 83(c)
	Center	Mid	0, -10, -20	0 -10 -20		84(a) 84(b) 84(c)
	Center	High	0, -10, -20	0 -10 -20		85(a) 85(b) 85(c)
	Twin	Center fuselage	0, -10, -20	0 -10 -20		86(a) 86(b) 86(c)
Static lateral stability	Off	Off	----------	-10	β, variable	87
	Twin	Center fuselage	-10	-10	β, variable	88
	Off	Off	----------	0, -10, -20	$\beta = \pm 5^o$	89
	Twin	Center fuselage	0	0, -10, -20	$\beta = \pm 5^o$	90
	Twin	Center fuselage	0, -10, -20	0, -10, -20	$\beta = \pm 5^o$	91
Roll control effectiveness (blades)	Twin	Center fuselage	0 -10 -20	$\Theta_{mean} = 0$ $\Theta_{mean} = -10$ $\Theta_{mean} = -20$	Differential Θ	92(a) 92(b) 92(c)
Roll control effectiveness (horizontal tail)	Twin	Center fuselage	$i_{t,mean} = 0$ $i_{t,mean} = -10$ $i_{t,mean} = -20$	$\Theta = 0$	Differential i_t	93(a) 93(b) 93(c)
Roll oscillation	Off	Off	----------	0	Dynamic stability	94
	Center	Mid	-10	0	Dynamic stability	94
	Center	Mid	-10	0, -10, -20	Dynamic stability	95
Cyclic control	Center	Mid	0	0	ψ, variable	96

TABLE I.- SCHEDULE OF TESTS AND INDEX OF TEST DATA FIGURES – Continued

(e) Rotor/wing 5

Type of test	Vertical tail	Horizontal tail		Blade incidence, Θ, deg	Special characteristics	Figures
		Position	Incidence, i_t, deg			
Static longitudinal stability	Off	Off	----------	0, -10, -20		97
	Center	Low	0, -10, -20	0 -10 -20		98(a) 98(b) 98(c)
	Center	Mid	0, -10, -20	0 -10 -20		99(a) 99(b) 99(c)
	Center	High	0	0		100
	Twin	Center fuselage	0, -10, -20	0 -10 -20		101(a) 101(b) 101(c)
Static lateral stability	Off	Off	----------	-10	β, variable	102
	Twin	Center fuselage	-10	-10	β, variable	103
	Off	Off	----------	0, -10, -20	$\beta = \pm 5^{o}$	104
	Twin	Center fuselage	0	0, -10, -20	$\beta = \pm 5^{o}$	105
	Twin	Center fuselage	0, -10, -20	0, -10, -20	$\beta = \pm 5^{o}$	106
Roll control effectiveness (blades)	Twin	Center fuselage	0 -10 -20	$\Theta_{mean} = 0$ $\Theta_{mean} = -10$ $\Theta_{mean} = -20$	Differential Θ	107(a) 107(b) 107(c)
Roll control effectiveness (horizontal tail)	Twin	Center fuselage	$i_{t,mean} = 0$ $i_{t,mean} = -10$ $i_{t,mean} = -20$	0	Differential i_t	108(a) 108(b) 108(c)
Roll oscillation	Off	Off	----------	0	Dynamic stability	109
	Center	Mid	-10	0	Dynamic stability	109
Cyclic control	Center	Mid	0	0	ψ, variable	110

TABLE I.- SCHEDULE OF TESTS AND INDEX OF TEST DATA FIGURES – Continued

(f) Rotor/wing 6

Type of test	Vertical tail	Horizontal tail		Blade incidence, Θ, deg	Special characteristics	Figures
		Position	Incidence, i_t, deg			
Static longitudinal stability	Off	Off	----------	0, -5, -10, -15		111
	Twin	Center fuselage	-5, -10, -15	0 -5 -10 -15		112(a) 112(b) 112(c) 112(d)
	Twin	Center fuselage	-5	0	Blade sweep angle 0^o, 30^o, 45^o	113
Horizontal tail characteristics	Twin	Center fuselage	Variable	0	$\alpha = 0^o$	114
Static lateral stability	Off	Off	----------	-10	β, variable	115
	Twin	Center fuselage	-10	-10	β, variable	116
	Off	Off	----------	0, -5, -10, -15	$\beta = \pm 5^o$	117
	Twin	Center fuselage	-5, -10, -15	-5, -10, -15	$\beta = \pm 5^o$	118
	Twin	Center fuselage	Off, -10	-10	$\beta = \pm 5^o$	119
Roll control effectiveness (blades)	Twin	Center fuselage	Off, -5	$\Theta_{mean} = 0$	Differential Θ	120
	Twin	Center fuselage	-5	$\Theta_{mean} = -5$	Differential Θ	121(a)
			-10	$\Theta_{mean} = -10$		121(b)
			-15	$\Theta_{mean} = -15$		121(c)
Roll control effectiveness (horizontal tail)	Twin	Center fuselage	$i_{t,mean} = 0$ $i_{t,mean} = -5$ $i_{t,mean} = -10$ $i_{t,mean} = -15$	0	Differential i_t	122(a) 122(b) 122(c) 122(d)
Cyclic control	Twin	Center fuselage	-10	0	ψ, variable	123

TABLE I.- SCHEDULE OF TESTS AND INDEX OF TEST DATA FIGURES – Continued

(g) Rotor/wing 7

Type of test	Vertical tail	Horizontal tail		Blade incidence, Θ, deg	Special characteristics	Figures
		Position	Incidence, i_t, deg			
Static longitudinal stability	Off	Off	----------	0, -5, -10, -15		124
	Twin	Center fuselage	-5, -10, -15	0		125(a)
				-5		125(b)
				-10		125(c)
				-15		125(d)
Static lateral stability	Off	Off	----------	-10	β, variable	126
	Twin	Center fuselage	-10	-10	β, variable	127
	Off	Off	----------	0, -5, -10, -15	$\beta = \pm 5^o$	128
	Twin	Center fuselage	-5, -10, -15	-5, -10, -15	$\beta = \pm 5^o$	129
Roll control effectiveness (blades)	Twin, off/on	Center fuselage, off/on	Off, -5	$\Theta_{mean} = 0$	Differential Θ	130
	Twin	Center fuselage	-5	$\Theta_{mean} = -5$	Differential Θ	131(a)
			-10	$\Theta_{mean} = -10$		131(b)
			-15	$\Theta_{mean} = -15$		131(c)
Roll control effectiveness (horizontal tail)	Twin	Center fuselage	$i_{t,mean} = 0$	0	Differential i_t	132(a)
			$i_{t,mean} = -5$			132(b)
			$i_{t,mean} = -10$			132(c)
			$i_{t,mean} = -15$			132(d)
Cyclic control	Twin	Center fuselage	-5	$\Theta = 0$	ψ, variable	133

TABLE I.- SCHEDULE OF TESTS AND INDEX OF TEST DATA FIGURES – Concluded

(h) Rotor/wing 8

Type of test	Vertical tail	Horizontal tail		Blade incidence, Θ, deg	Special characteristics	Figures
		Position	Incidence, i_t, deg			
Static longitudinal stability	Off	Off	----------	0, -5, -10, -15, -20		134
	Twin	Center fuselage	0, -5, -10, -15	0 -5 -10 -15		135(a) 135(b) 135(c) 135(d)
Static lateral stability	Off	Off	----------	-10	β, variable	136
	Twin	Center fuselage	-10	-10	β, variable	137
	Off	Off	----------	0, -5, -10, -15	$\beta = \pm 5^o$	138
	Twin	Center fuselage	-5	0, -5, -10, -15	$\beta = \pm 5^o$	139
	Twin	Center fuselage	-5, -10, -15	0, -5, -10, -15	$\beta = \pm 5^o$	140
Roll control effectiveness (blades)	Twin, off/on	Center fuselage, off/on	Off, 0	$\Theta_{mean} = 0$	Differential Θ	141
	Off	Off	----------	$\Theta_{mean} = 0$	Differential Θ	142
	Twin	Center fuselage	0	$\Theta_{mean} = 0$	Differential Θ	143(a)
			-5	$\Theta_{mean} = -5$		143(b)
			-10	$\Theta_{mean} = -10$		143(c)
			-15	$\Theta_{mean} = -15$		143(d)
Roll control effectiveness (horizontal tail)	Twin	Center fuselage	$i_{t,mean} = 0$	0	Differential i_t	144(a)
			$i_{t,mean} = -5$			144(b)
			$i_{t,mean} = -10$			144(c)
			$i_{t,mean} = -15$			144(d)
Cyclic control	Twin	Center fuselage	-5	$\Theta = 0$	ψ, variable	145(a)
	Twin	Center fuselage	-5	$\Theta = -10 \sin 4\psi$	ψ, variable	145(b)

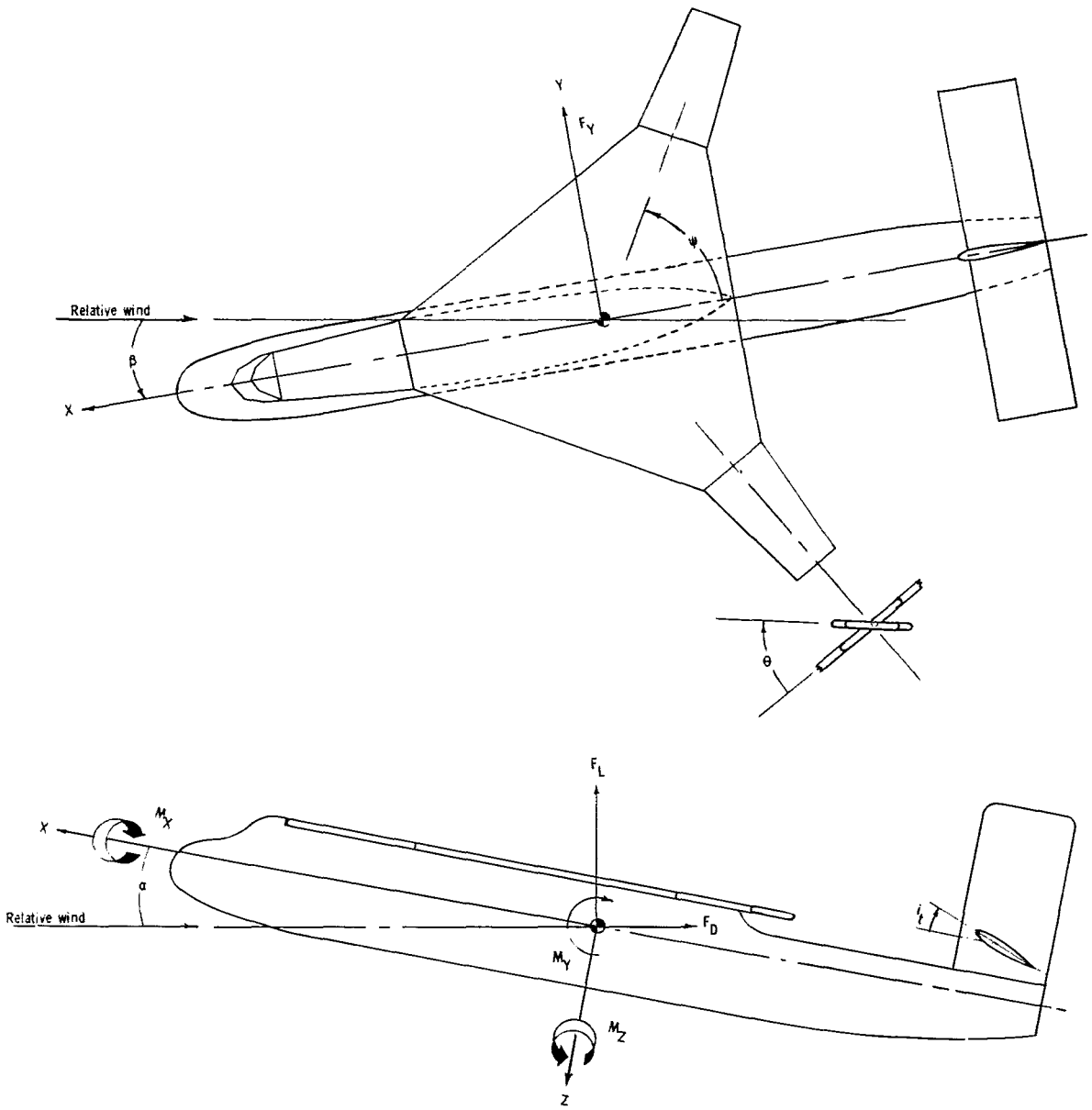

Figure 1.- System of axes used in the investigation. Arrows indicate positive directions of moments, forces, and angles.

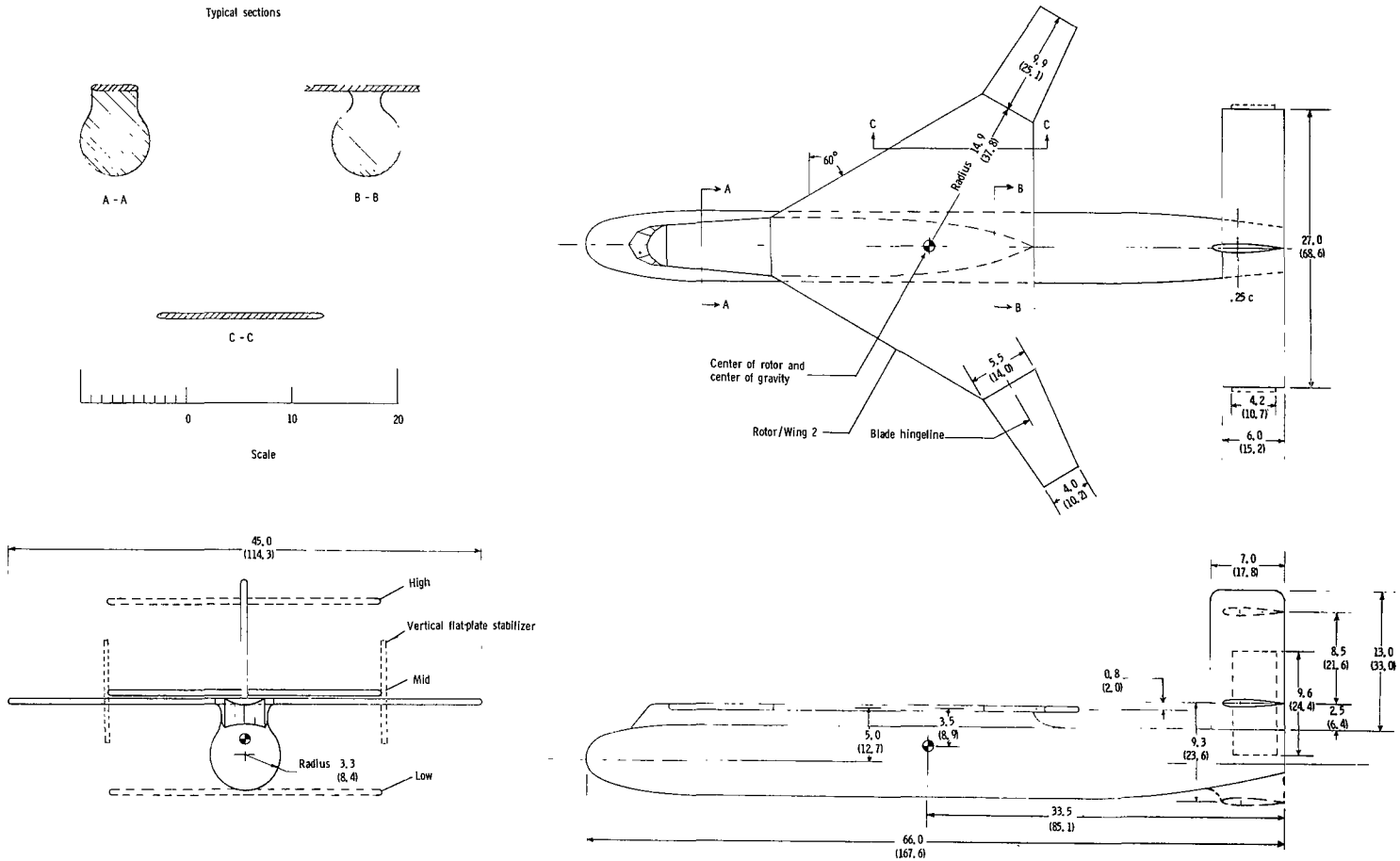

Figure 2.- Drawing of model with rotor/wing 2. Dimensions in inches (cm).

ORDINATES FOR HORIZONTAL TAIL SURFACE			
Station, percent chord	x in. (cm)	y upper in. (cm)	y lower in. (cm)
0	0	0.224 (0.569)	0.224 (0.569)
1.25	0.075 (0.191)	.397 (1.008)	.093 (.236)
2.50	.150 (.381)	.475 (1.207)	.056 (.142)
5.00	.300 (.762)	.580 (1.473)	.027 (.069)
7.50	.450 (1.143)	.672 (1.707)	.0144 (.037)
10.00	.600 (1.524)	.735 (1.867)	0
15.00	.900 (2.286)	.832 (2.113)	0
20.00	1.200 (3.048)	.898 (2.281)	0
30.00	1.800 (4.572)	.910 (2.311)	0
40.00	2.400 (6.096)	.867 (2.202)	0
50.00	3.000 (7.620)	.798 (2.027)	0
60.00	3.600 (9.144)	.688 (1.748)	0
70.00	4.200 (10.668)	.546 (1.387)	0
80.00	4.800 (12.192)	.378 (.960)	0
90.00	5.400 (13.716)	.189 (.480)	0
95.00	5.700 (14.478)	.0976 (.248)	0
100.00	6.000 (15.240)	.012 (.030)	0

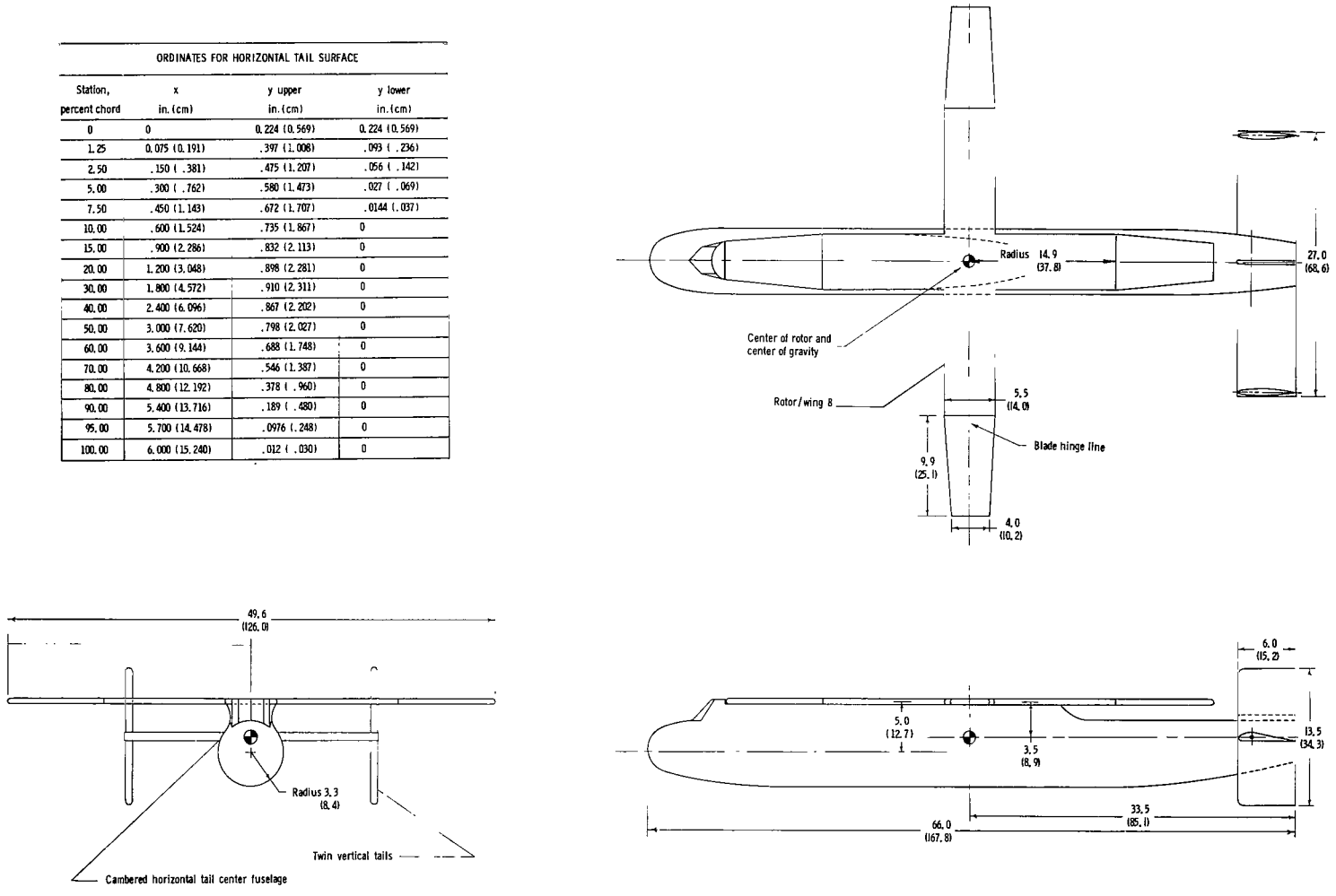

Figure 3.- Drawing of model with rotor/wing 8. Dimensions in inches (cm).

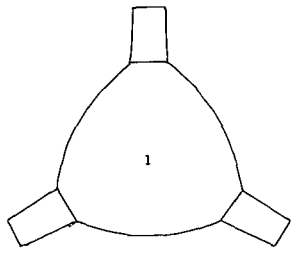

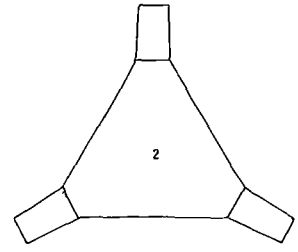

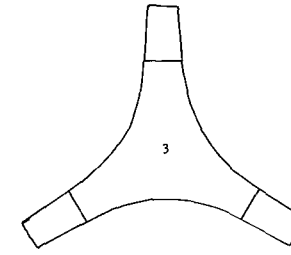

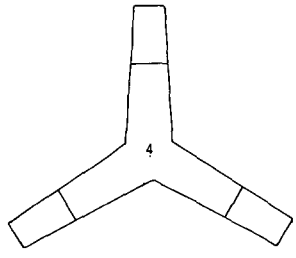

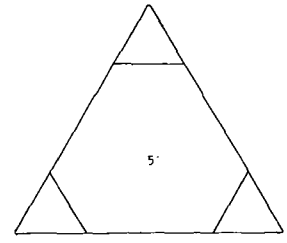

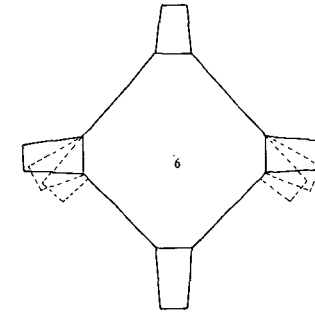

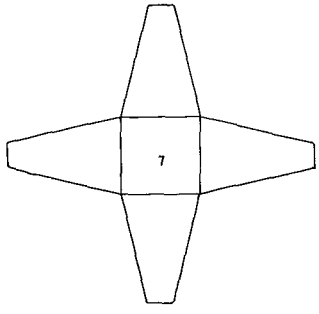

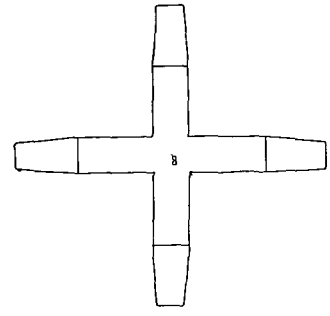

TABLE OF ROTOR/WING PROPERTIES				
Rotor Hub	Area S ft^2 (m^2)	Span b ft (m)	Chord c ft (m)	Aspect Ratio AR
1	5.07 (0.47)	3.75 (1.14)	1.35 (0.41)	2.79
2	4.18 (0.39)	3.75 (1.14)	1.11 (0.34)	3.37
3	3.38 (0.31)	3.75 (1.14)	0.90 (0.27)	4.17
4	2.88 (0.27)	3.75 (1.14)	0.77 (0.23)	4.87
5	5.56 (0.52)	3.58 (1.09)	1.55 (0.47)	2.32
6	5.43 (0.50)	4.133 (1.26)	1.315 (0.401)	3.14
7	5.43 (0.50)	4.133 (1.26)	1.315 (0.401)	3.14
8	3.37 (0.31)	4.133 (1.26)	0.816 (0.249)	5.05

Figure 4.- Sketch of rotor/wing planforms and table of properties.

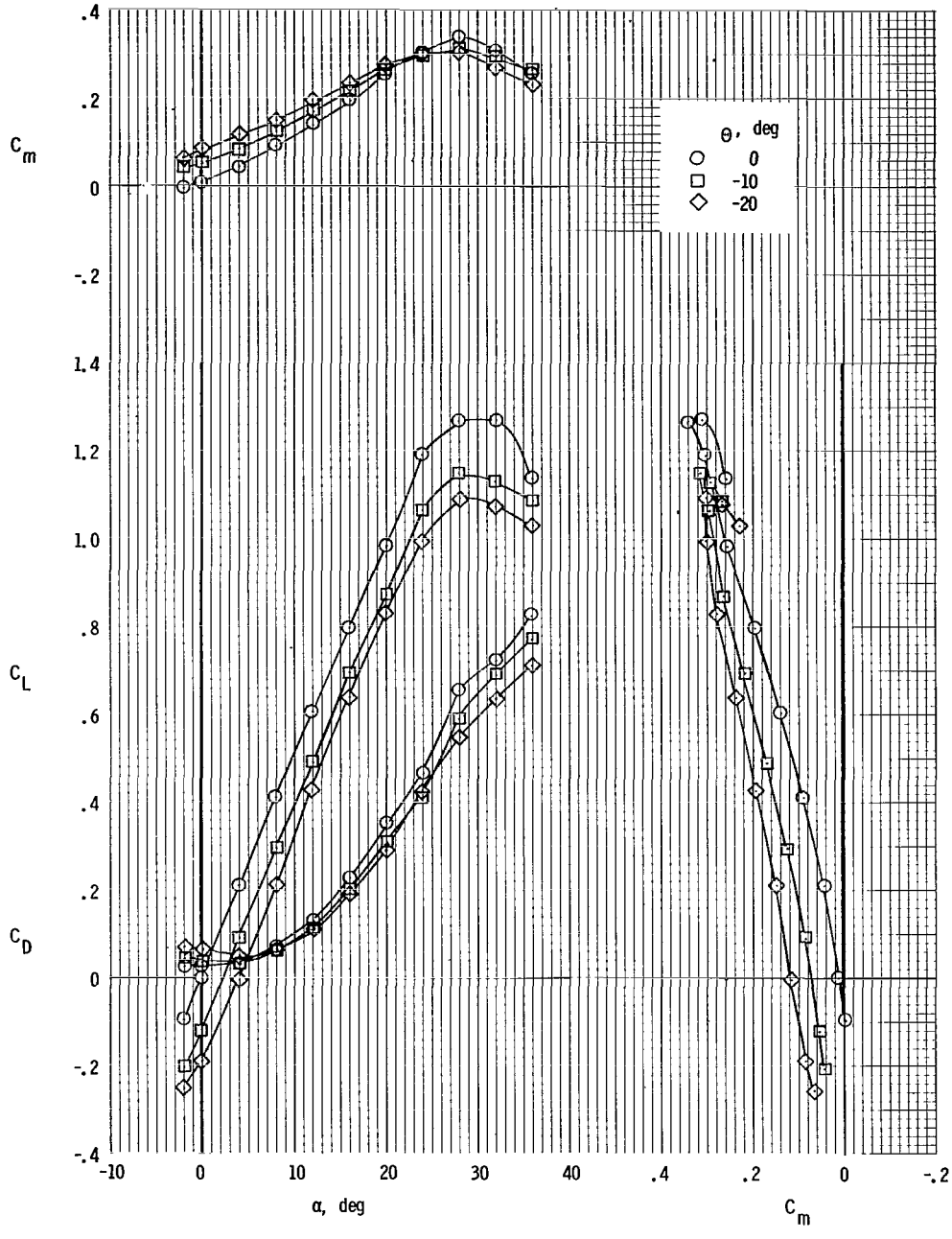

Figure 5.- Longitudinal aerodynamic characteristics. Tails off; rotor/wing 1.

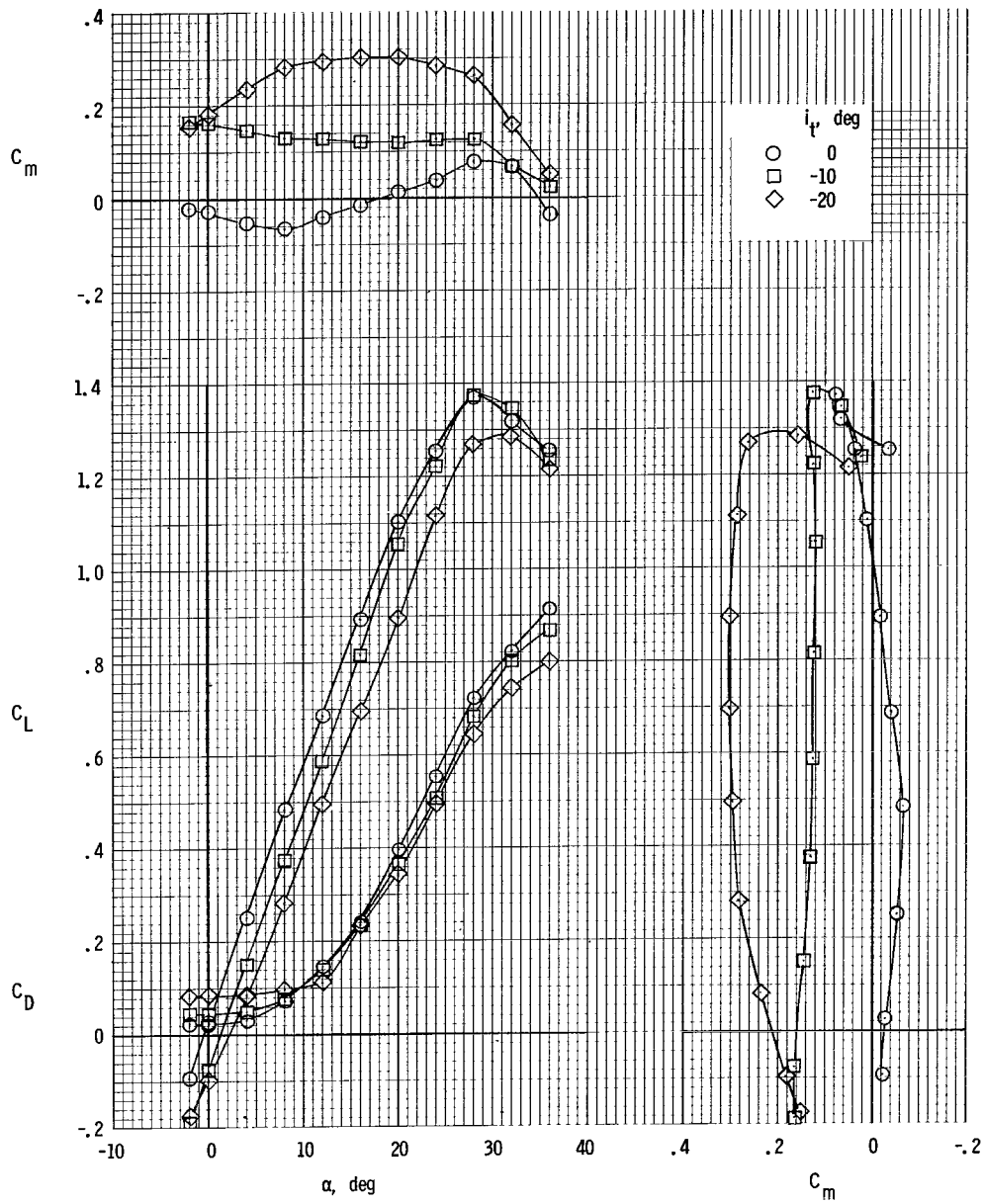

Figure 6.- Longitudinal aerodynamic characteristics. Low horizontal tail; center vertical tail; $\Theta = 0^{\circ}$; rotor/wing 1.

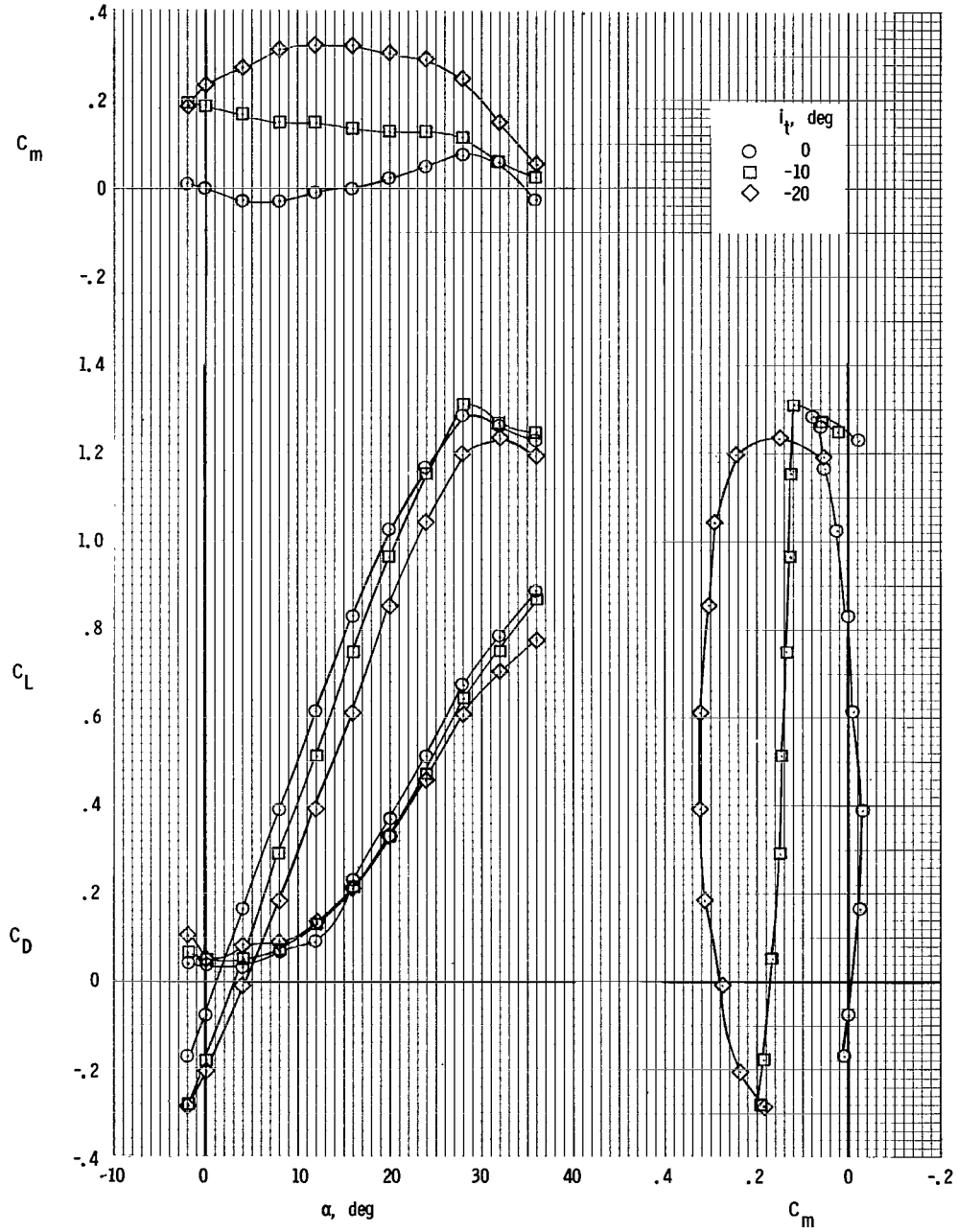

Figure 7.- Longitudinal aerodynamic characteristics. Low horizontal tail; center vertical tail; $\Theta = -10^{\circ}$; rotor/wing 1.

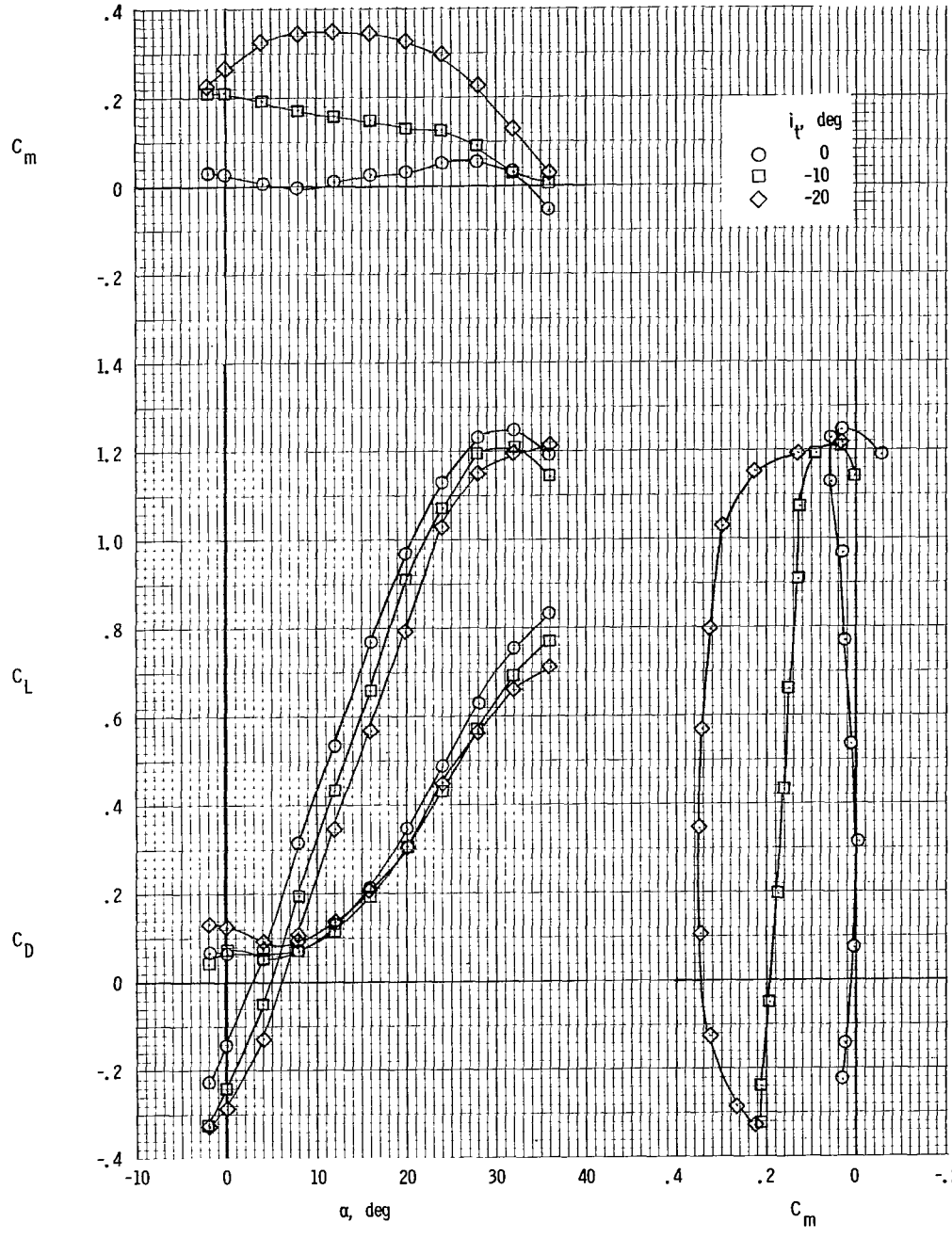

Figure 8.- Longitudinal aerodynamic characteristics. Low horizontal tail; center vertical tail; $\Theta = -20^{\circ}$; rotor/wing 1.

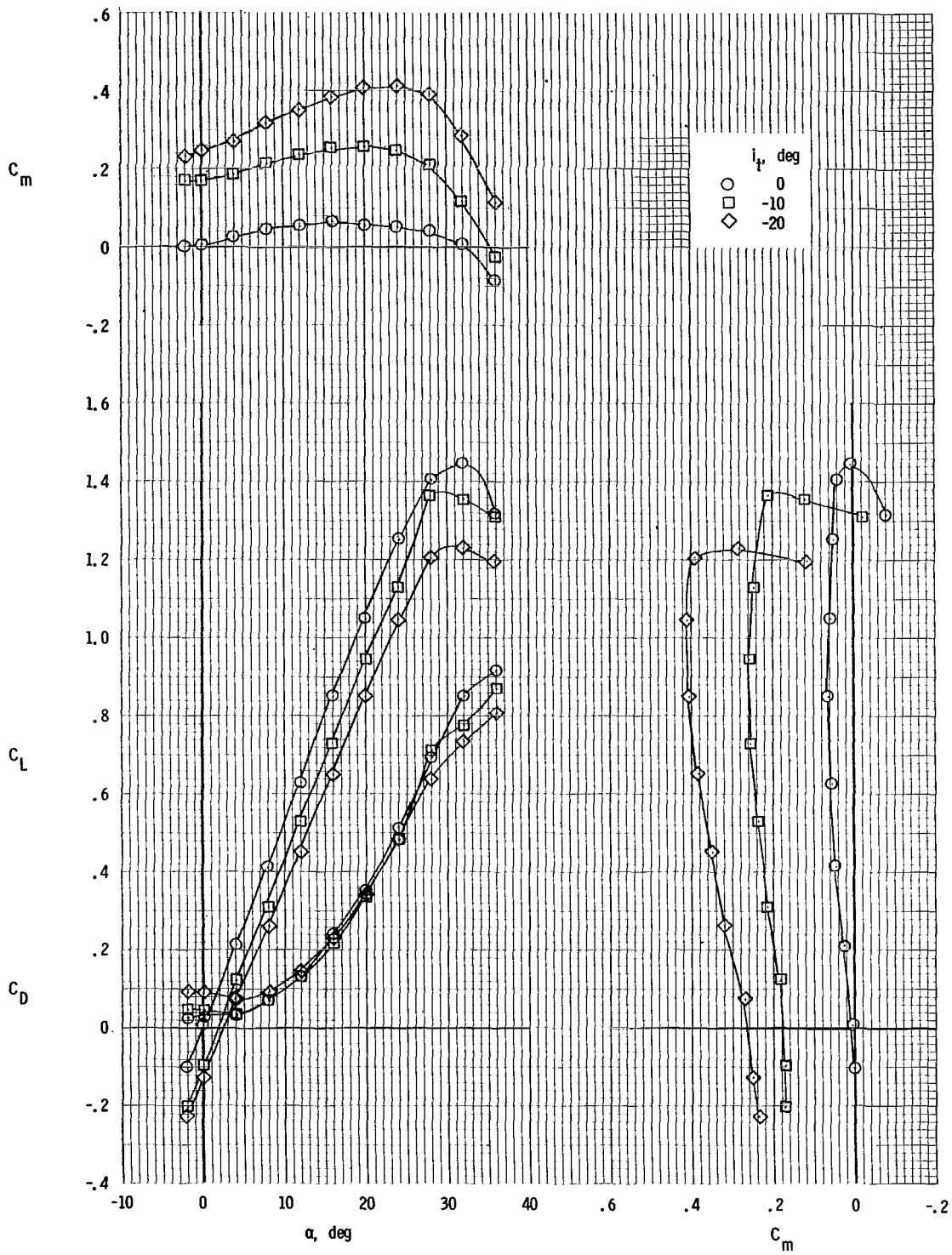

Figure 9.- Longitudinal aerodynamic characteristics. Mid horizontal tail; center vertical tail; $\Theta = 0^{\circ}$; rotor/wing 1.

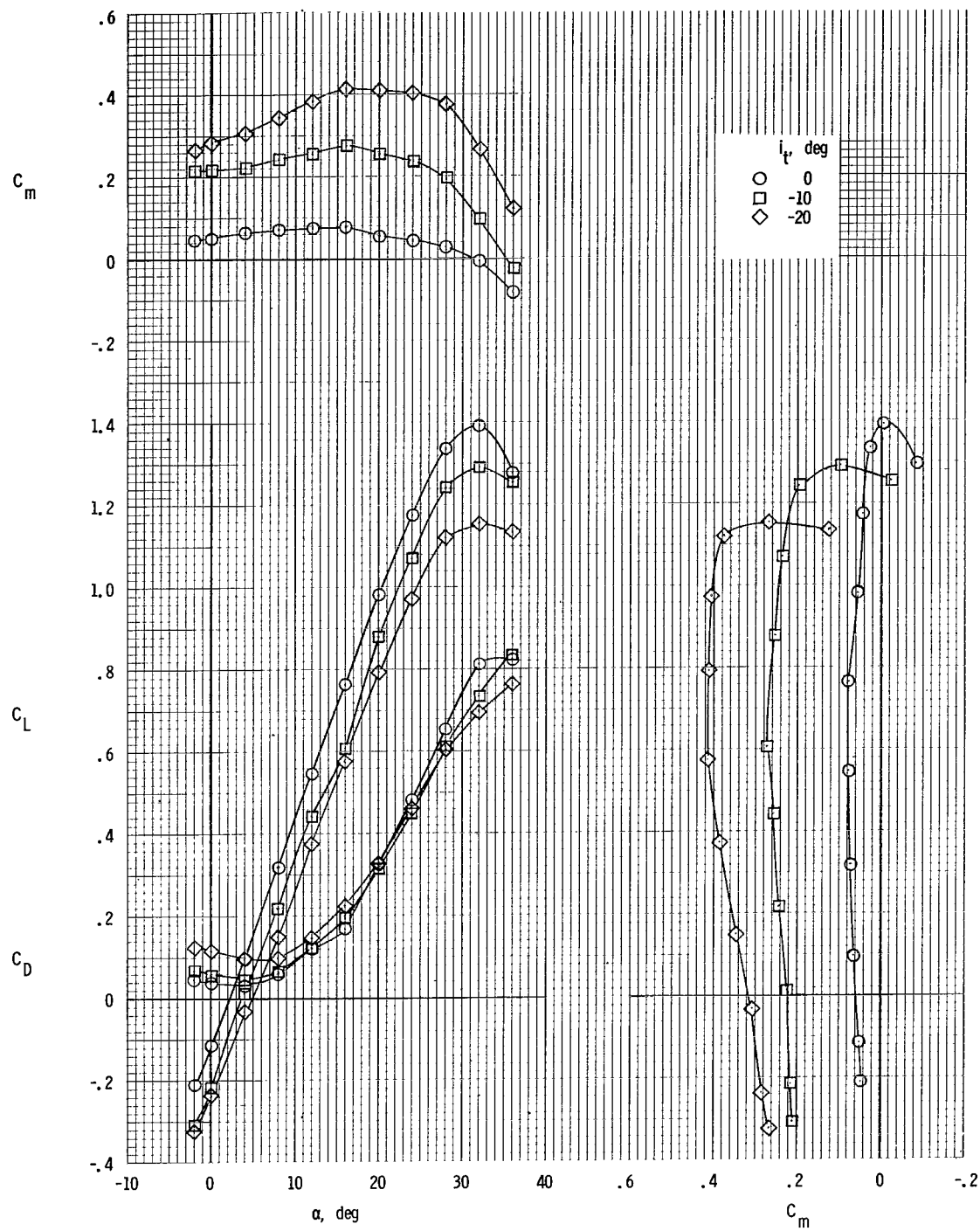

Figure 10.- Longitudinal aerodynamic characteristics. Mid horizontal tail; center vertical tail; $\Theta = -10^{\circ}$; rotor/wing 1.

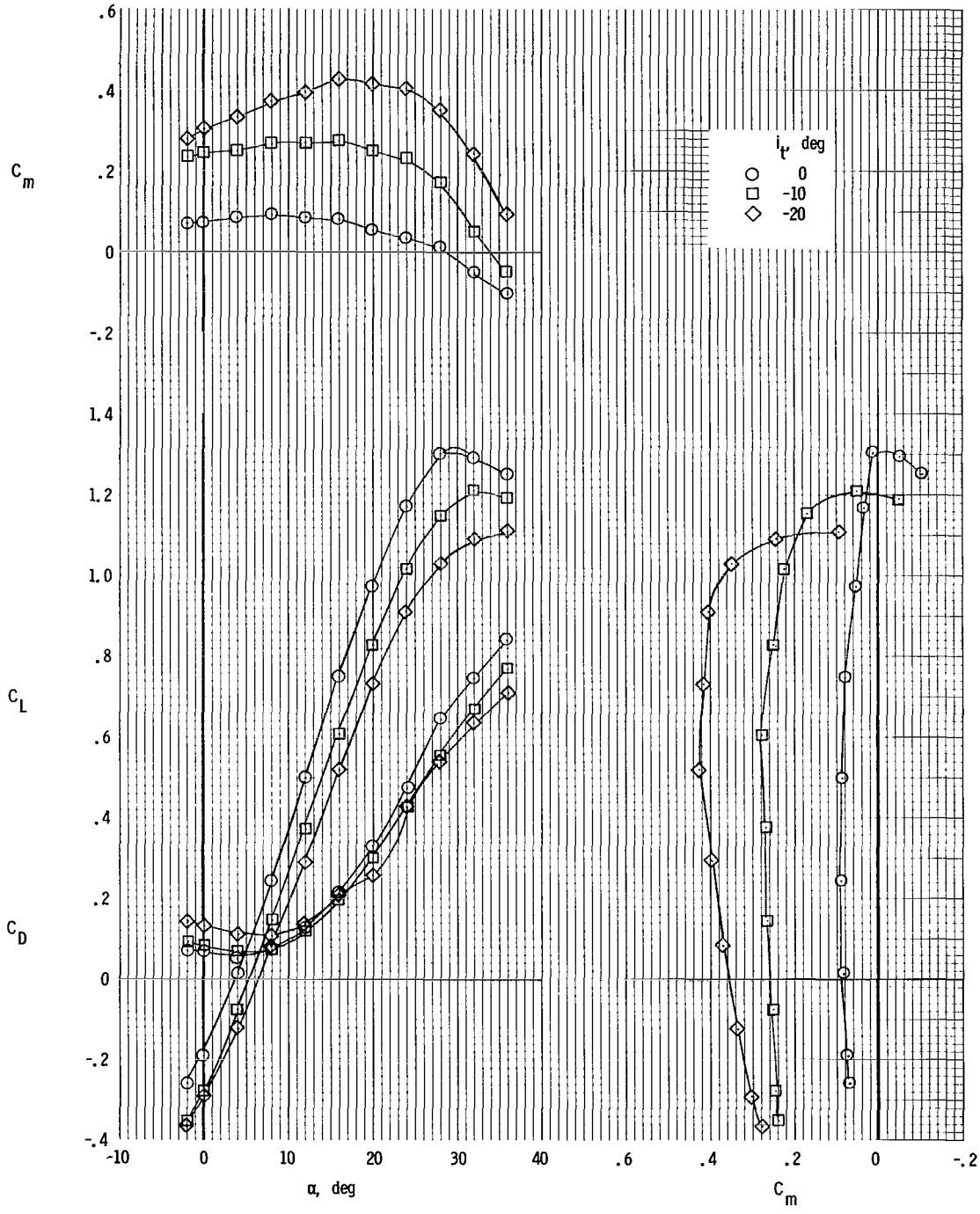

Figure 11.- Longitudinal aerodynamic characteristics. Mid horizontal tail; center vertical tail; $\Theta = -20^{\circ}$; rotor/wing 1.

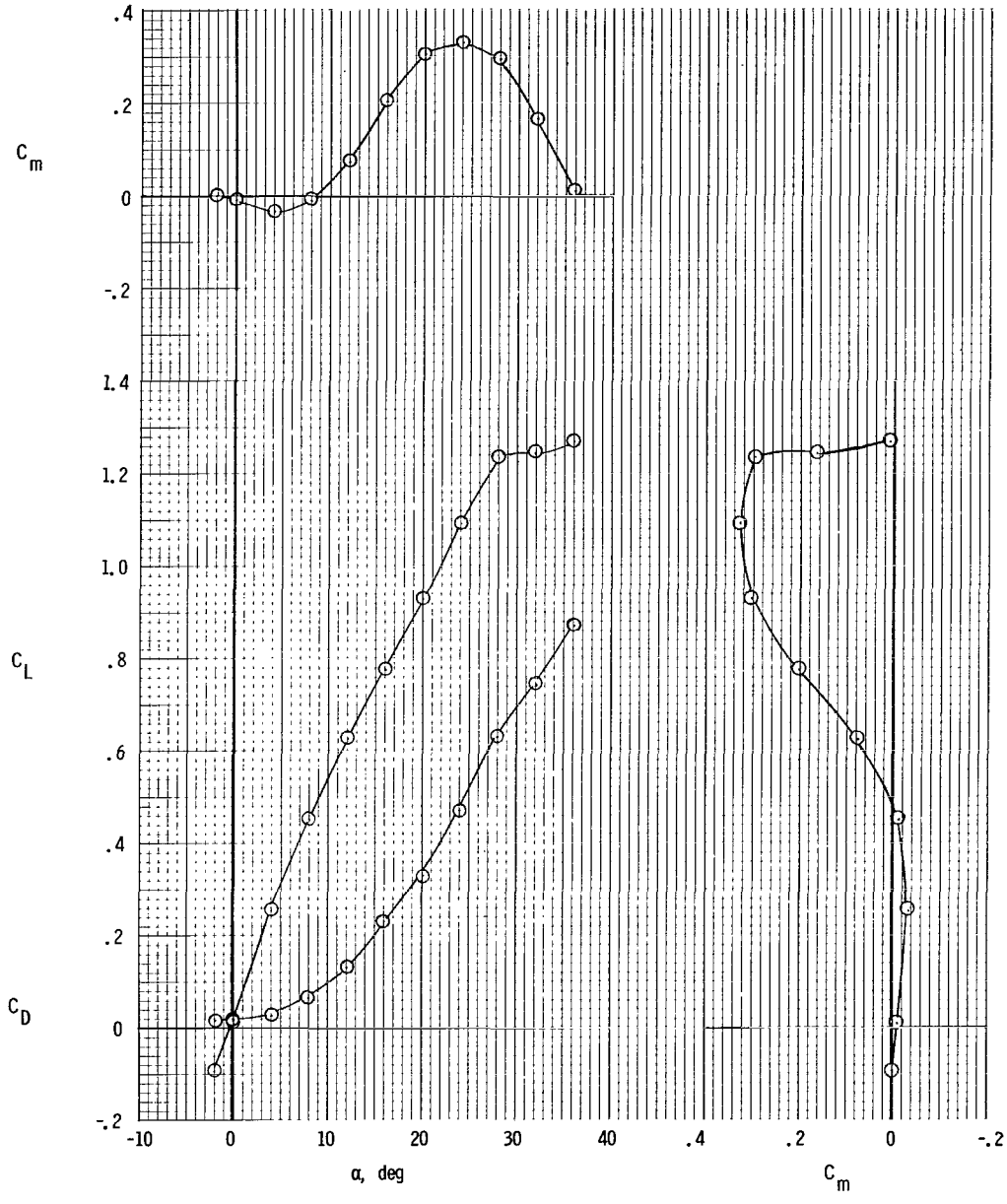

Figure 12.- Longitudinal aerodynamic characteristics. High horizontal tail; center vertical tail; $i_t = 0^o$; $\Theta = 0^o$; rotor/wing 1.

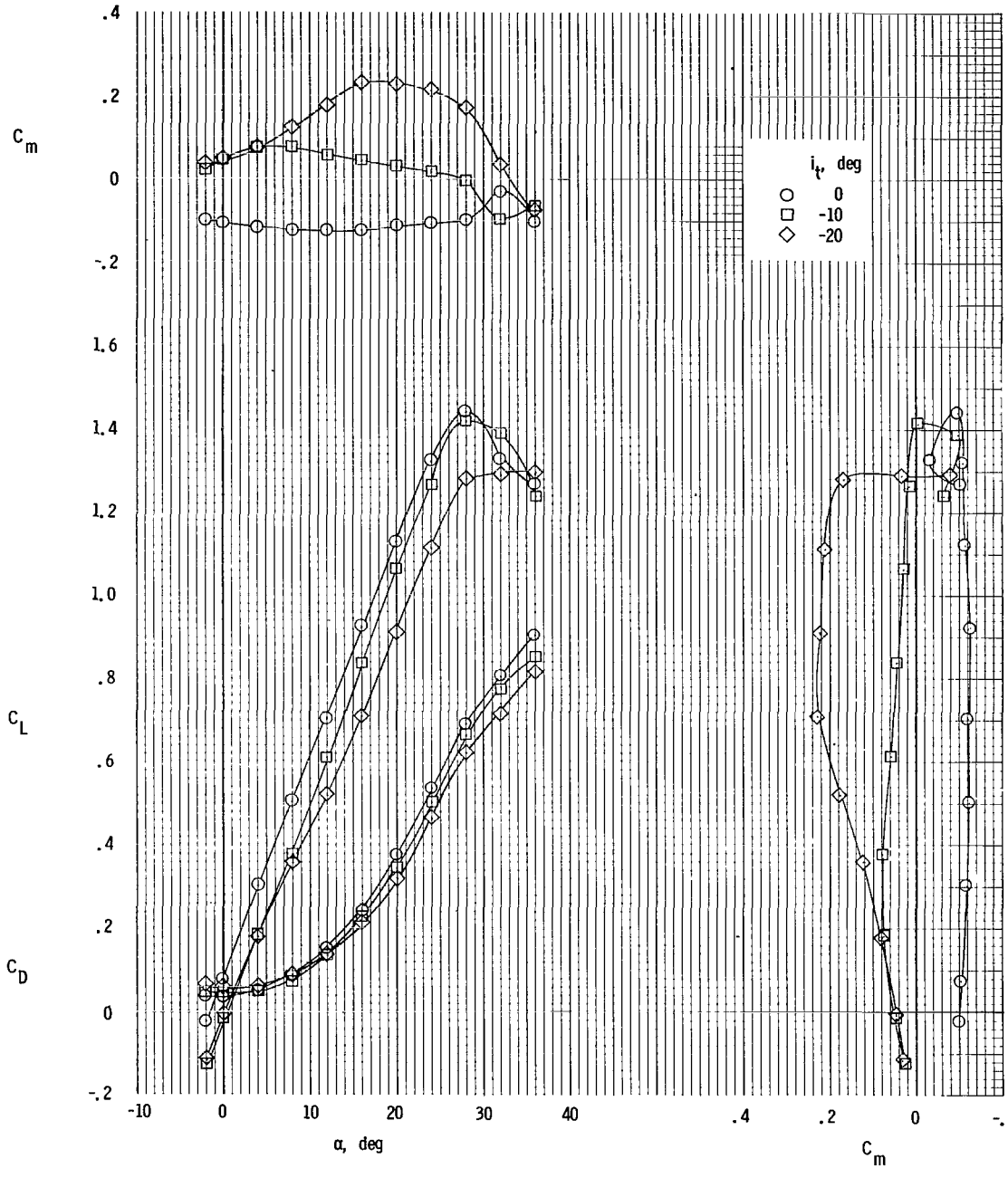

Figure 13.- Longitudinal aerodynamic characteristics. Horizontal tail at center fuselage; twin vertical tails at tip of horizontal tails; $\Theta = 0^{\circ}$; rotor/wing 1.

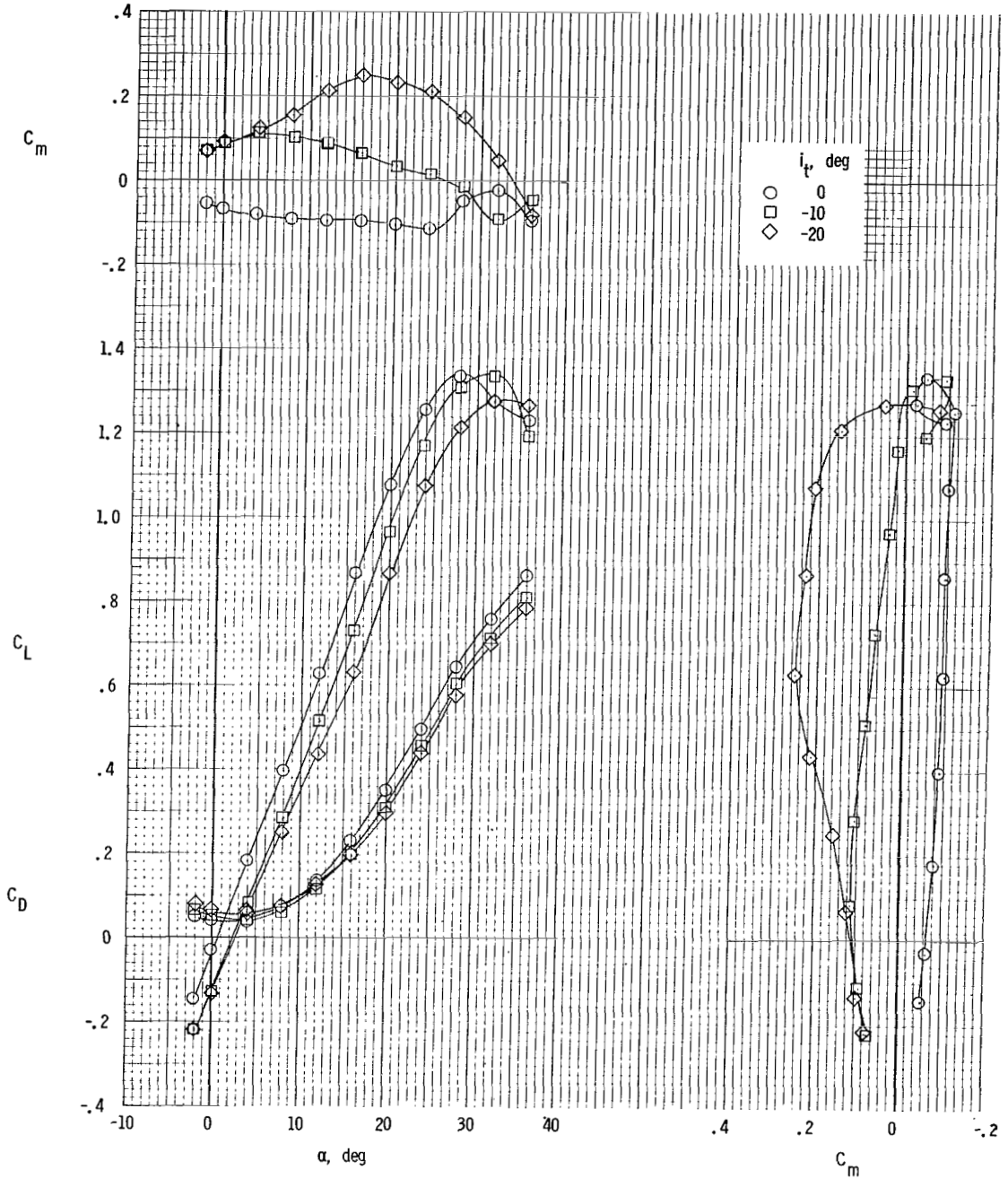

Figure 14.- Longitudinal aerodynamic characteristics. Horizontal tail at center fuselage; twin vertical tails at tip of horizontal tails; $\Theta = -10^{\circ}$; rotor/wing 1.

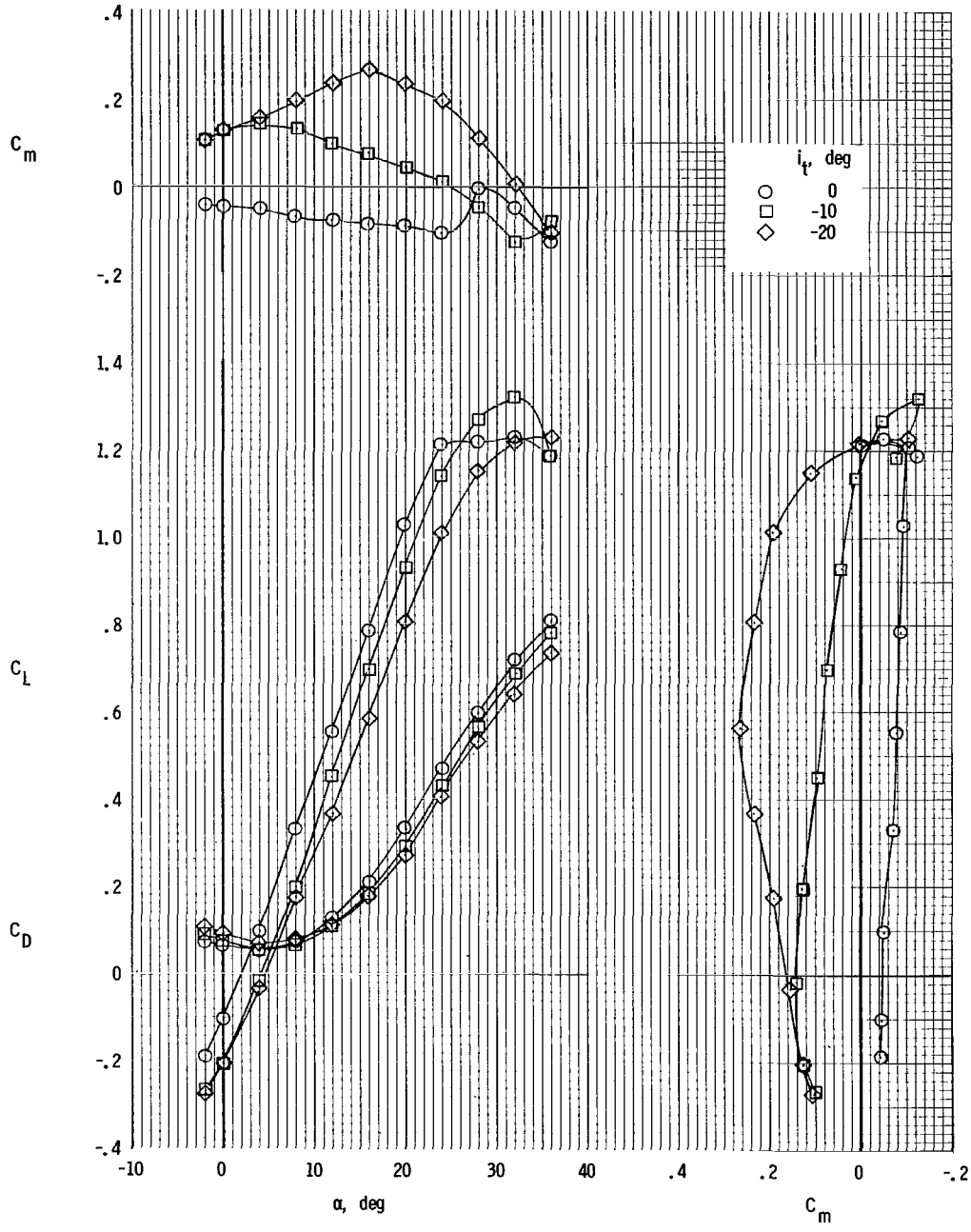

Figure 15.- Longitudinal aerodynamic characteristics. Horizontal tail at center fuselage; twin vertical tails at tip of horizontal tail; $\Theta = -20^{\circ}$; rotor/wing 1.

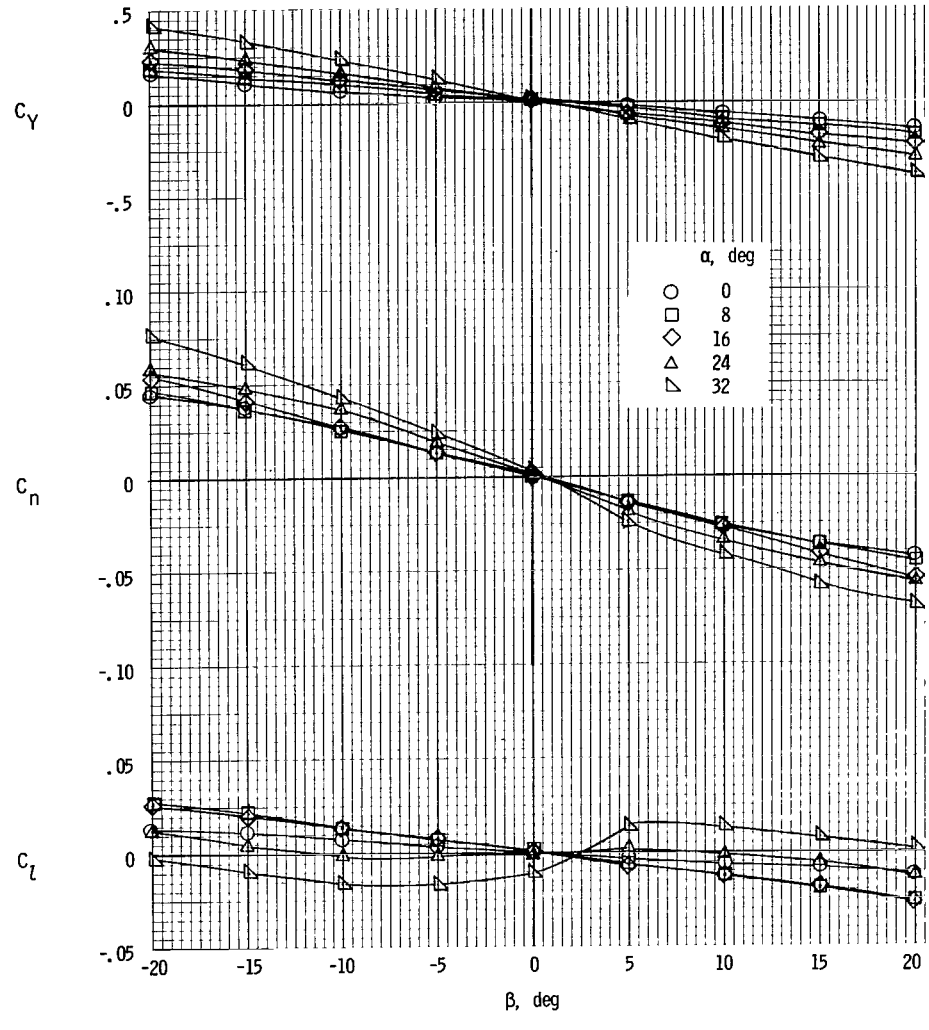

Figure 16.- Sideslip characteristics. Tails off; $\Theta = -10^{\circ}$; rotor/wing 1.

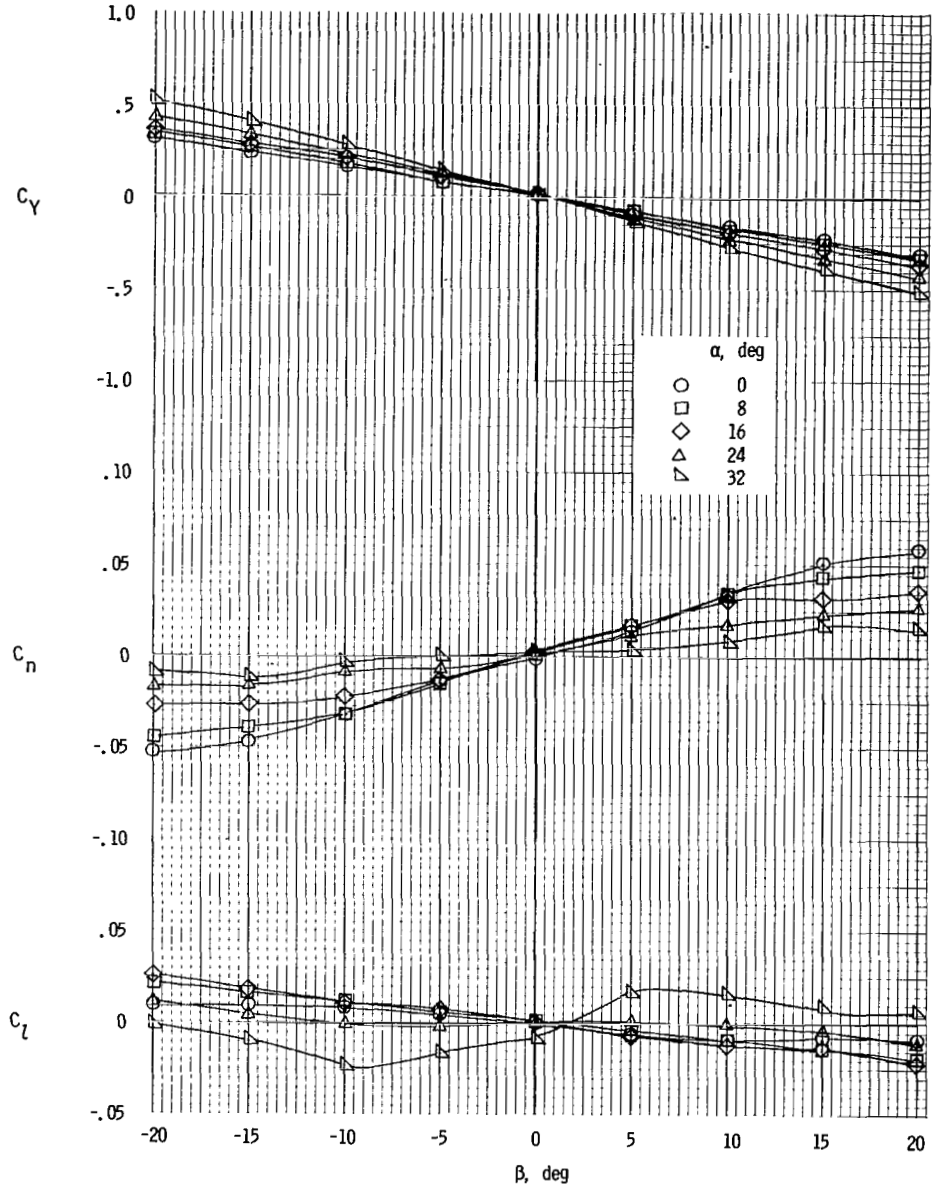

Figure 17.- Sideslip characteristics. Horizontal tail at center fuselage; twin vertical tails at tip of horizontal tail; $i_t = -10^\circ$; $\Theta = -10^\circ$; rotor/wing 1.

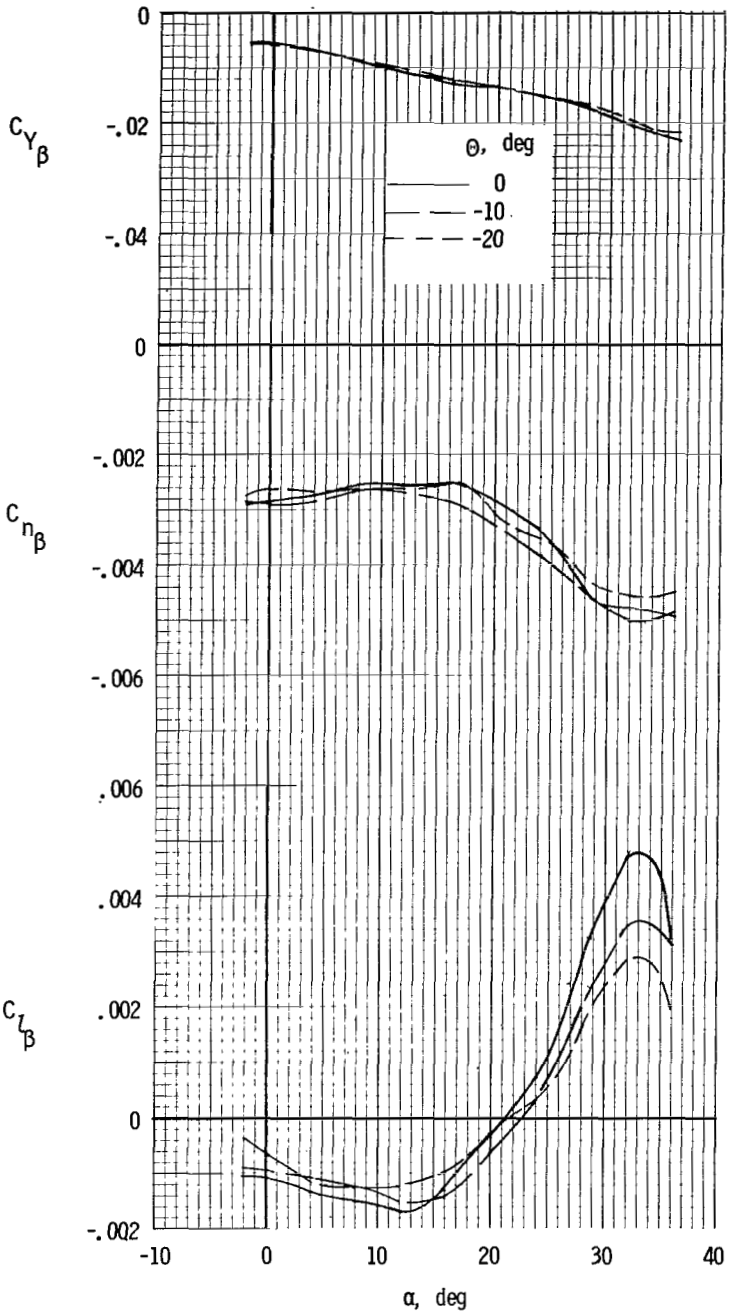

Figure 18.- Static lateral stability derivatives. Tails off; rotor/wing 1.

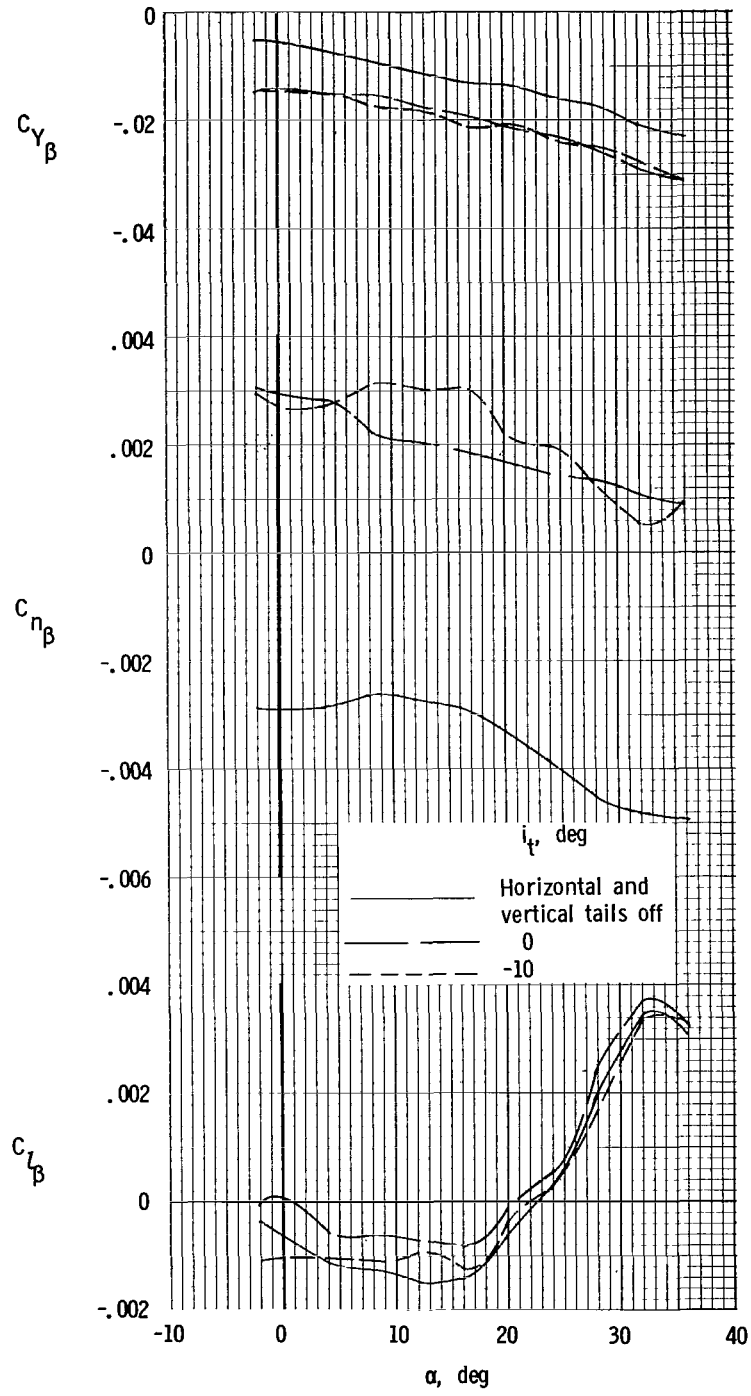

Figure 19.- Effect of vertical and horizontal tail on static lateral-stability derivatives. Twin vertical tails; horizontal tail at center fuselage; $\Theta = -10^{\circ}$; rotor/wing 1.

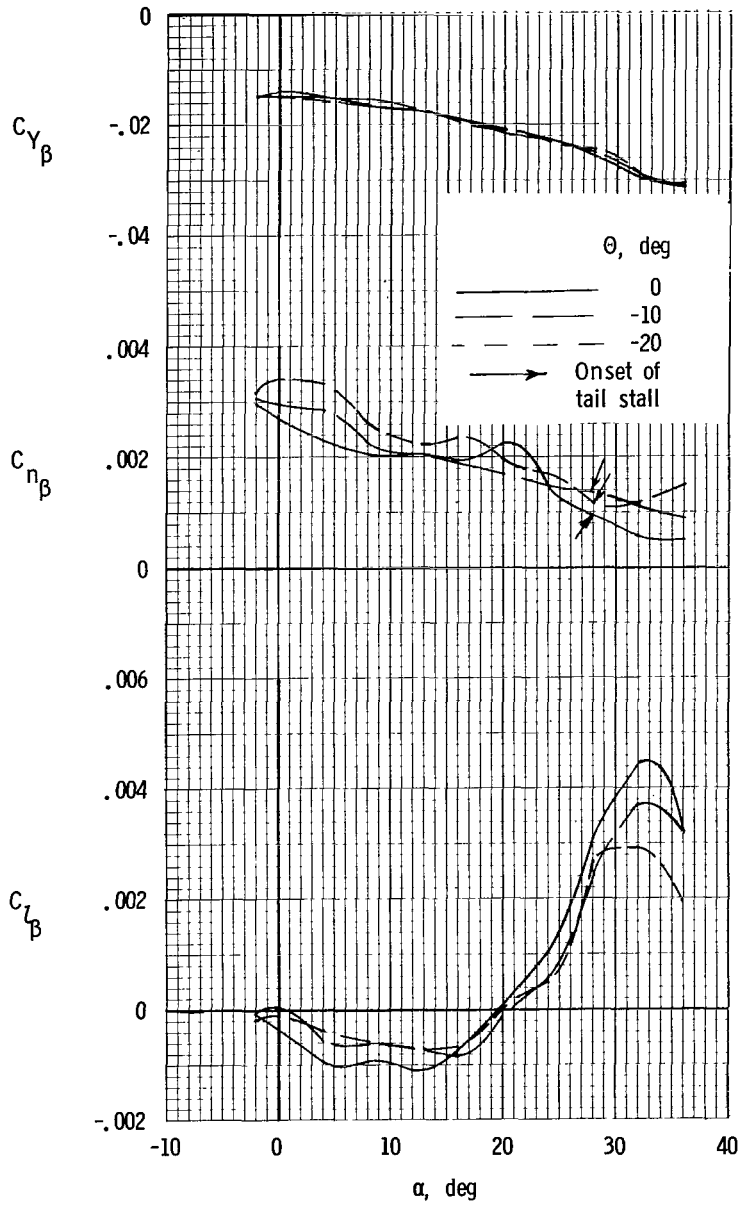

Figure 20.- Static lateral-stability derivatives. Twin vertical tails at tip of horizontal tail; horizontal tail at center fuselage; $i_t = 0^\circ$; rotor/wing 1.

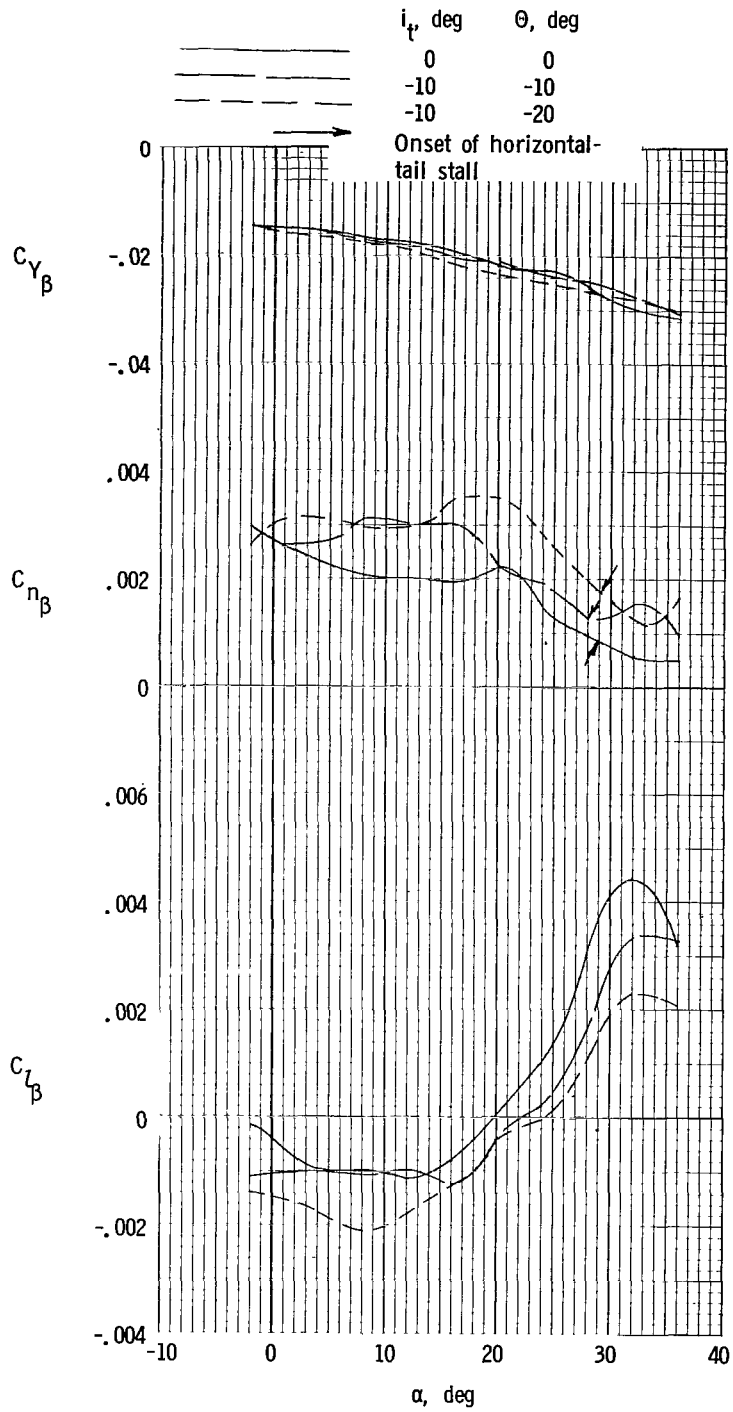

Figure 21.- Static lateral-stability derivatives for combinations of Θ and i_t. Twin vertical tails; horizontal tail at center fuselage; rotor/wing 1.

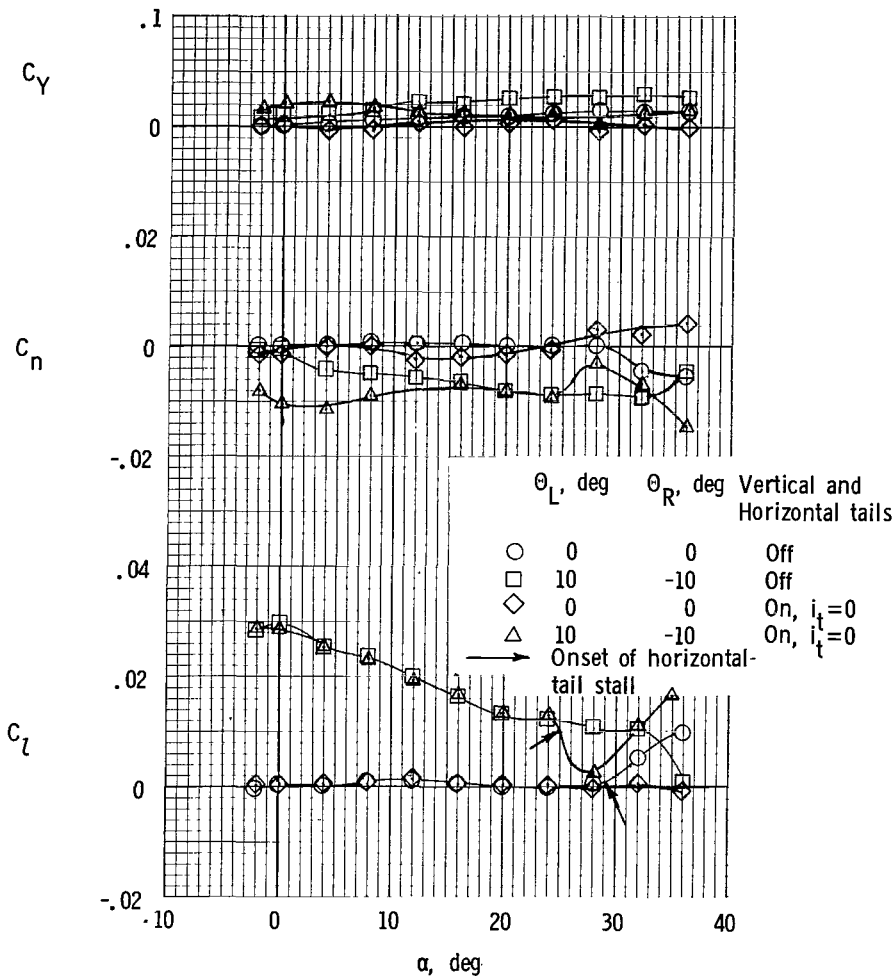

Figure 22.- Effect of tails on lateral-control characteristics with rotor blades used for control. Twin vertical tails; horizontal tail at center fuselage; rotor/wing 1.

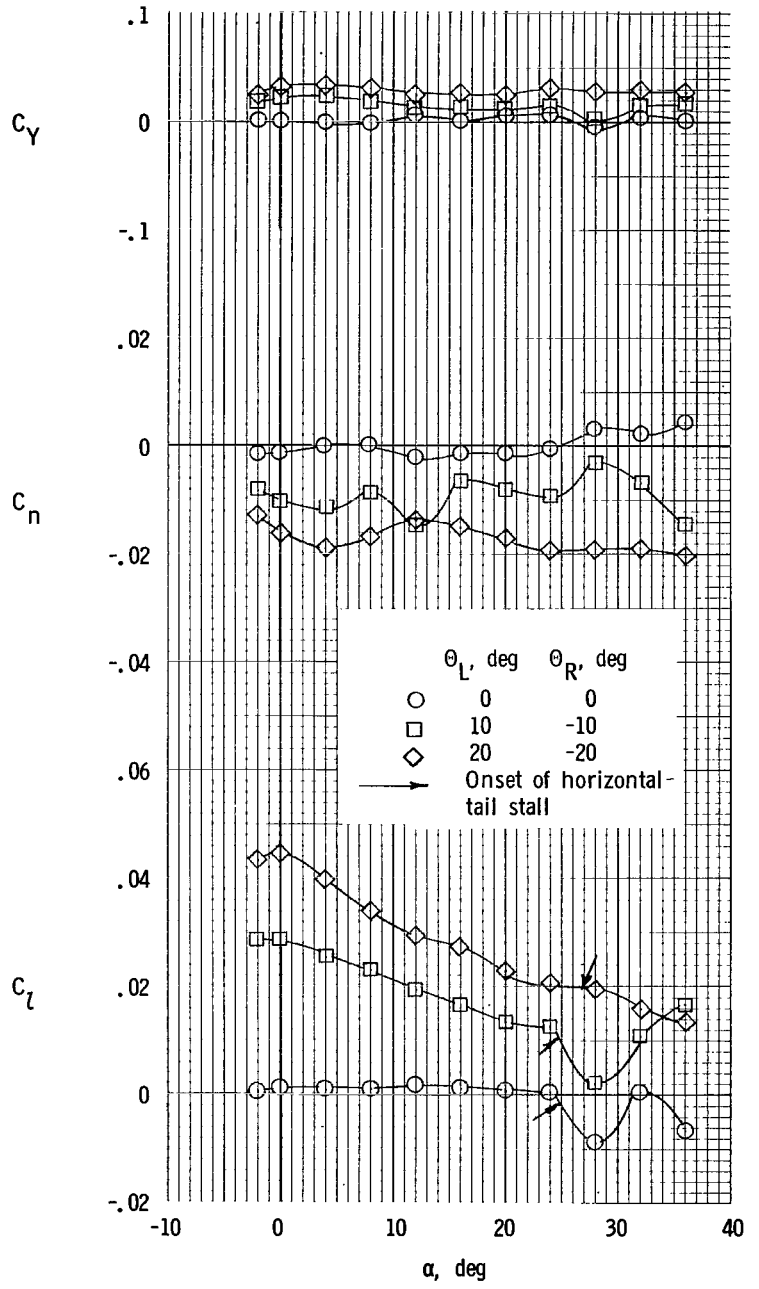

Figure 23.- Lateral-control characteristics with rotor blades used for control. Twin vertical tails; horizontal tail at center fuselage; $i_t = 0^\circ$; $\Theta_{mean} = 0^\circ$; rotor/wing 1.

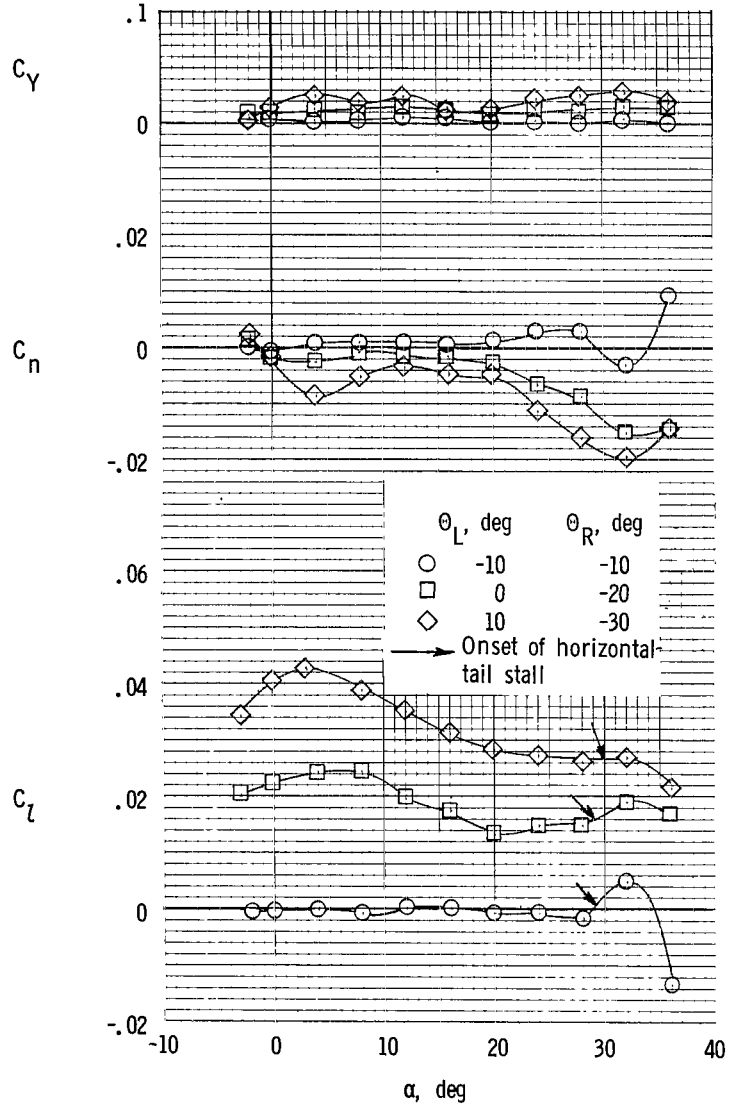

Figure 24.- Lateral-control characteristics with rotor blades used for control. Twin vertical tails; horizontal tail at center fuselage; $i_t = -10^\circ$; $\Theta_{mean} = -10^\circ$; rotor/wing 1.

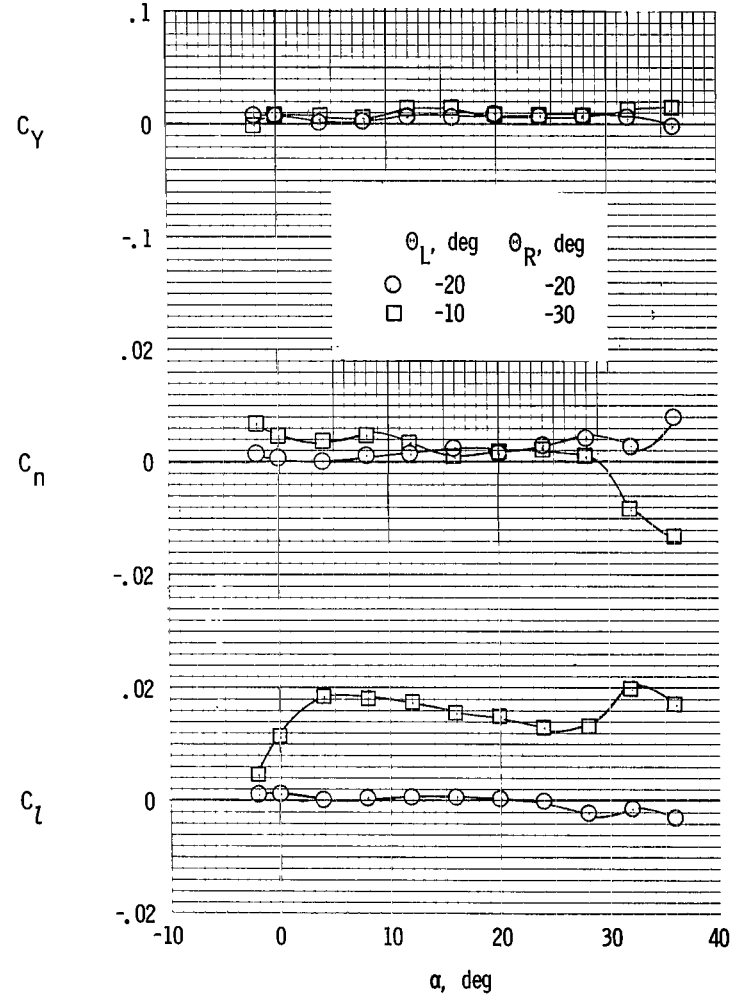

Figure 25.- Lateral-control characteristics with rotor blades used for control. Twin vertical tails; horizontal tail at center fuselage; $i_t = -20^\circ$; $\Theta_{mean} = -20^\circ$; rotor/wing 1.

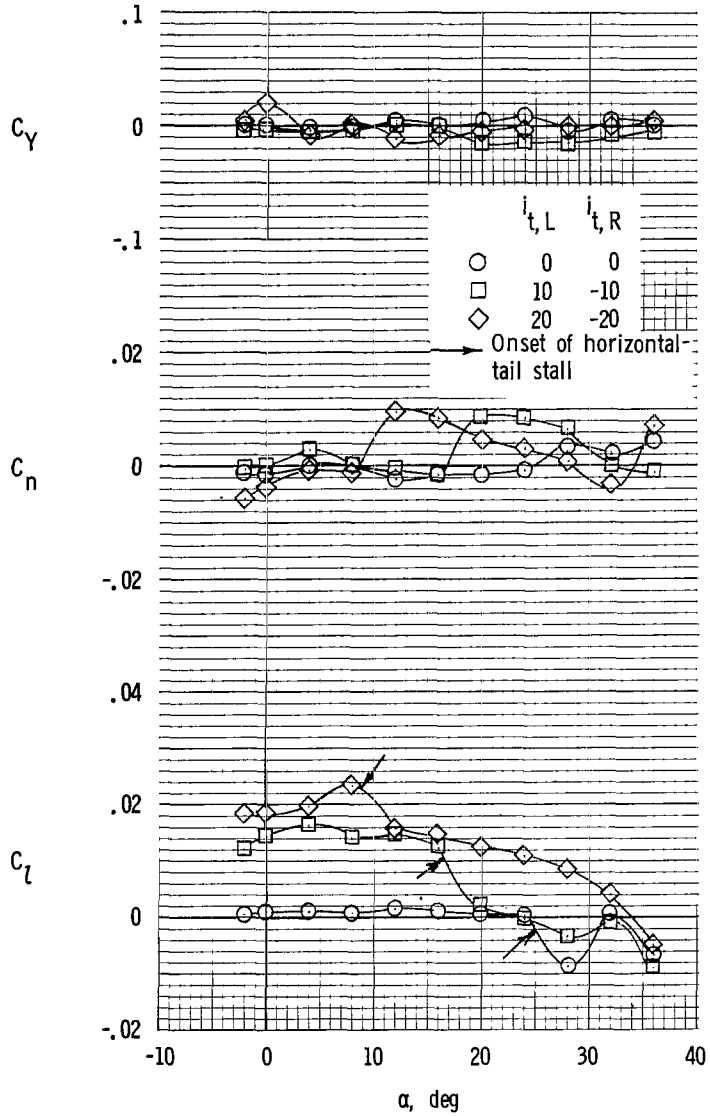

Figure 26.- Lateral-control characteristics with horizontal tail used for control. Twin vertical tails; horizontal tail at center fuselage; $\Theta = 0^\circ$; $i_{t,mean} = 0^\circ$; rotor/wing 1.

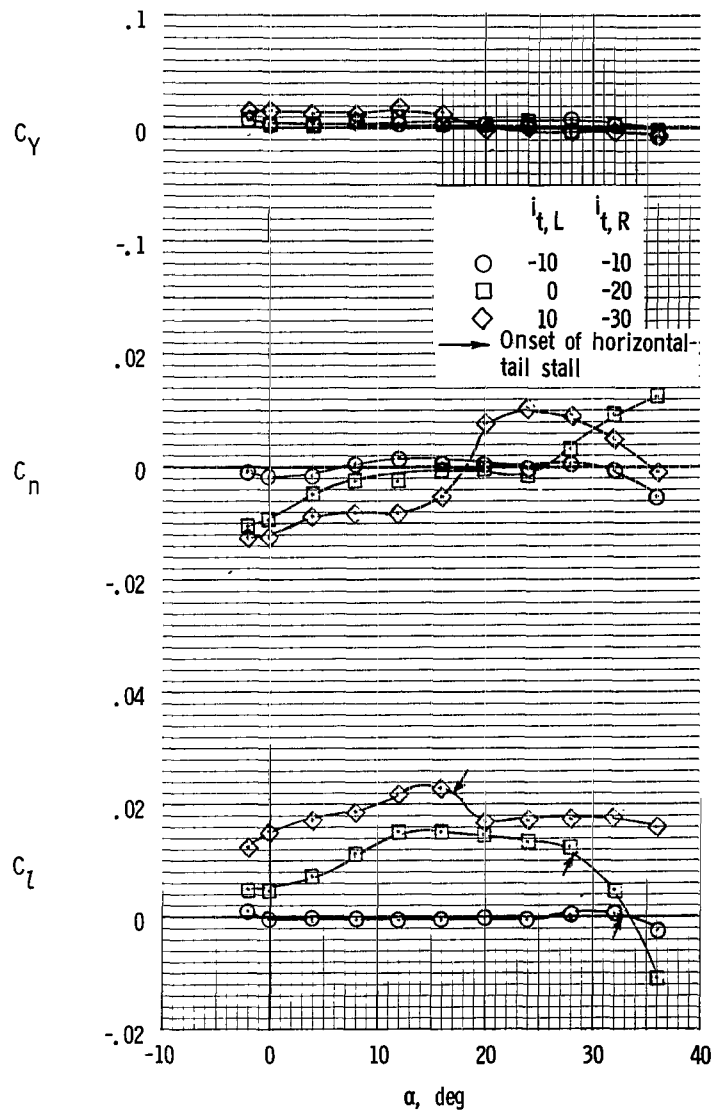

Figure 27.- Lateral-control characteristics with horizontal tail used for control. Twin vertical tails; horizontal tail at center fuselage; $\Theta = 0^\circ$; $i_{t,mean} = -10^\circ$; rotor/wing 1.

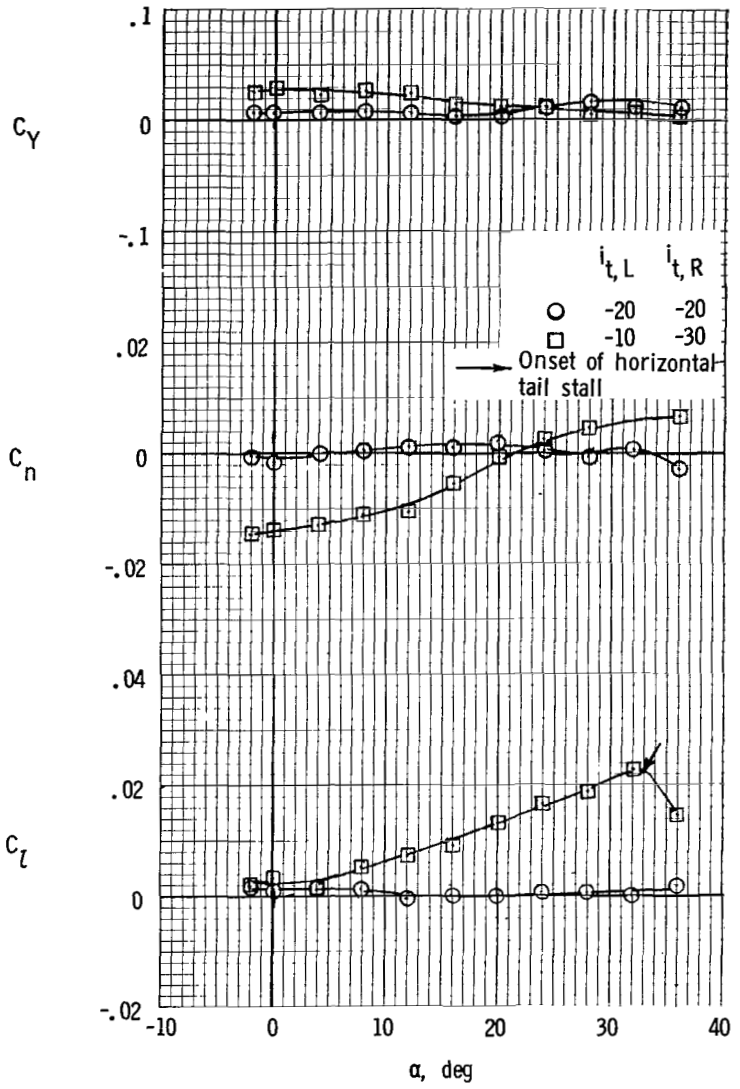

Figure 28.- Lateral-control characteristics with horizontal tail used for control. Twin vertical tails; horizontal tail at center fuselage; $\Theta = 0^\circ$; $i_{t,mean} = -20^\circ$; rotor/wing 1.

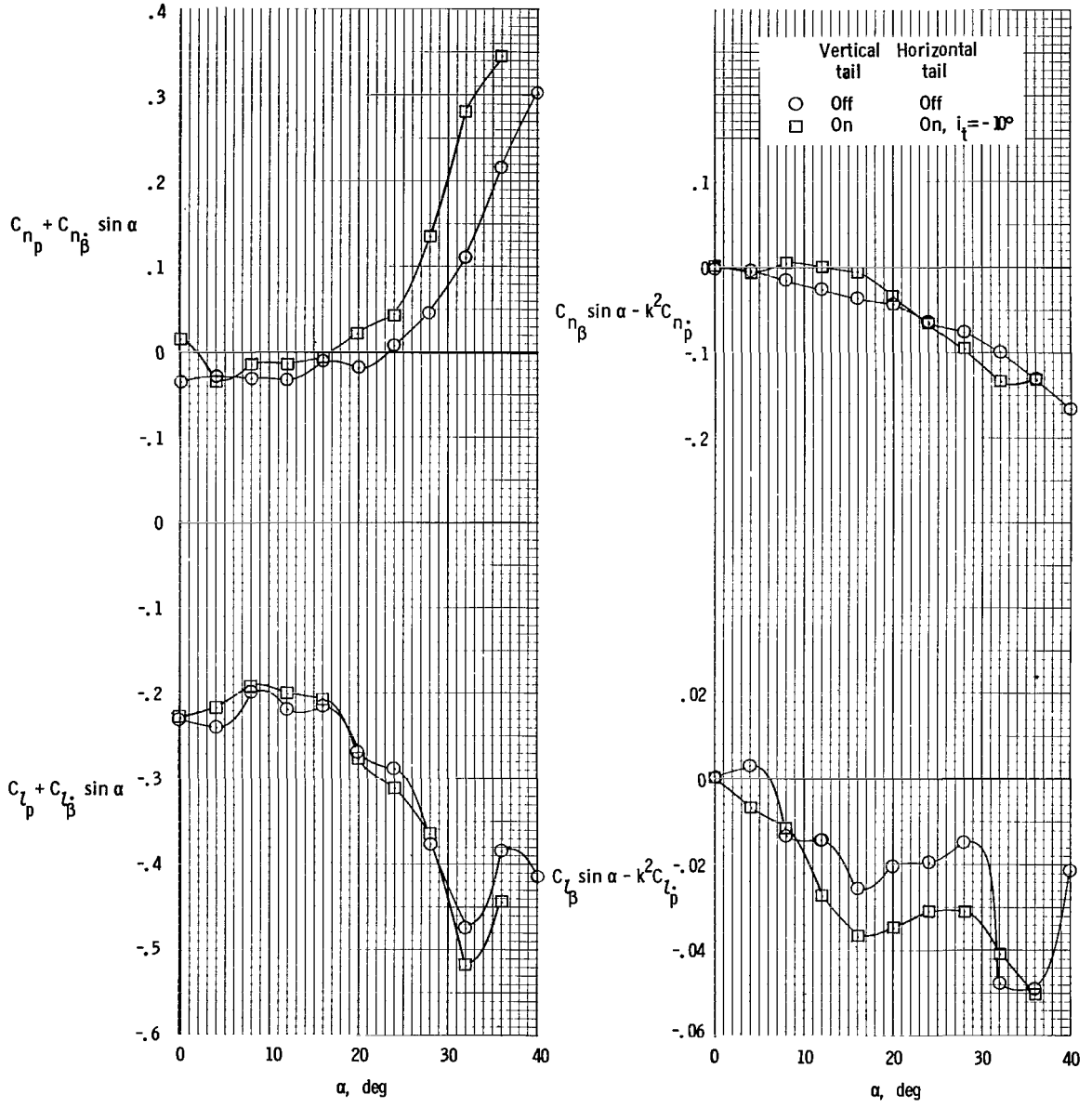

(a) Out-of-phase derivatives.

(b) In-phase derivatives.

Figure 29.- Effect of tails on dynamic-stability derivatives measured in rolling-oscillation tests. Center vertical tail; mid horizontal tail; Θ = 0°; rotor/wing 1.

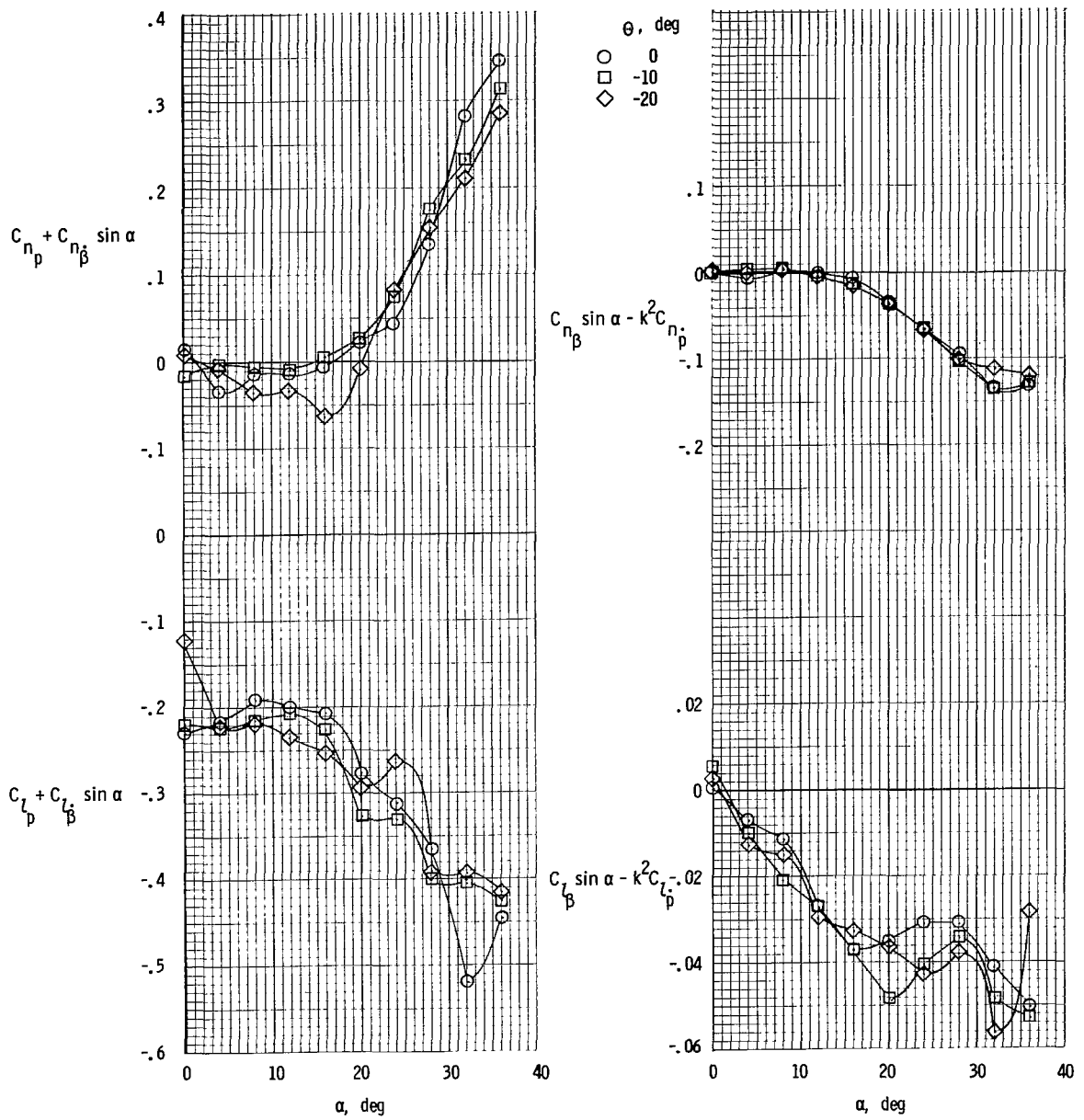

(a) Out-of-phase derivatives.

(b) In-phase derivatives.

Figure 30.- Effect of rotor blade incidence on dynamic-stability derivatives measured in rolling-oscillation tests. Center vertical tail; mid horizontal tail; $i_t = -10^\circ$; rotor/wing 1.

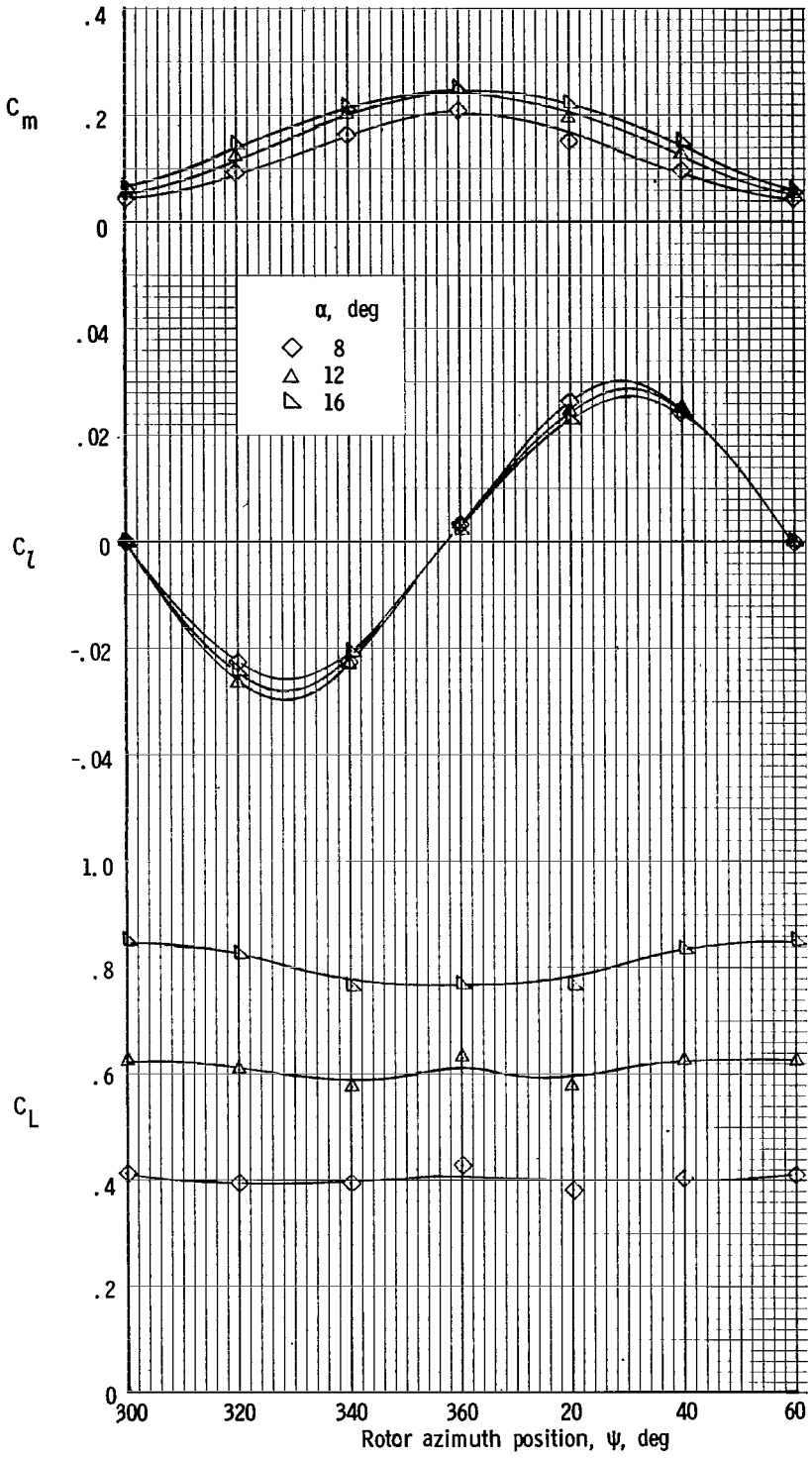

Figure 31.- Effect of azimuth position on lift coefficient and rolling- and pitching-moment coefficient for changes in model angle of attack. $\Theta = 0^\circ$; $i_t = -5^\circ$; horizontal tail at center fuselage; rotor/wing 1.

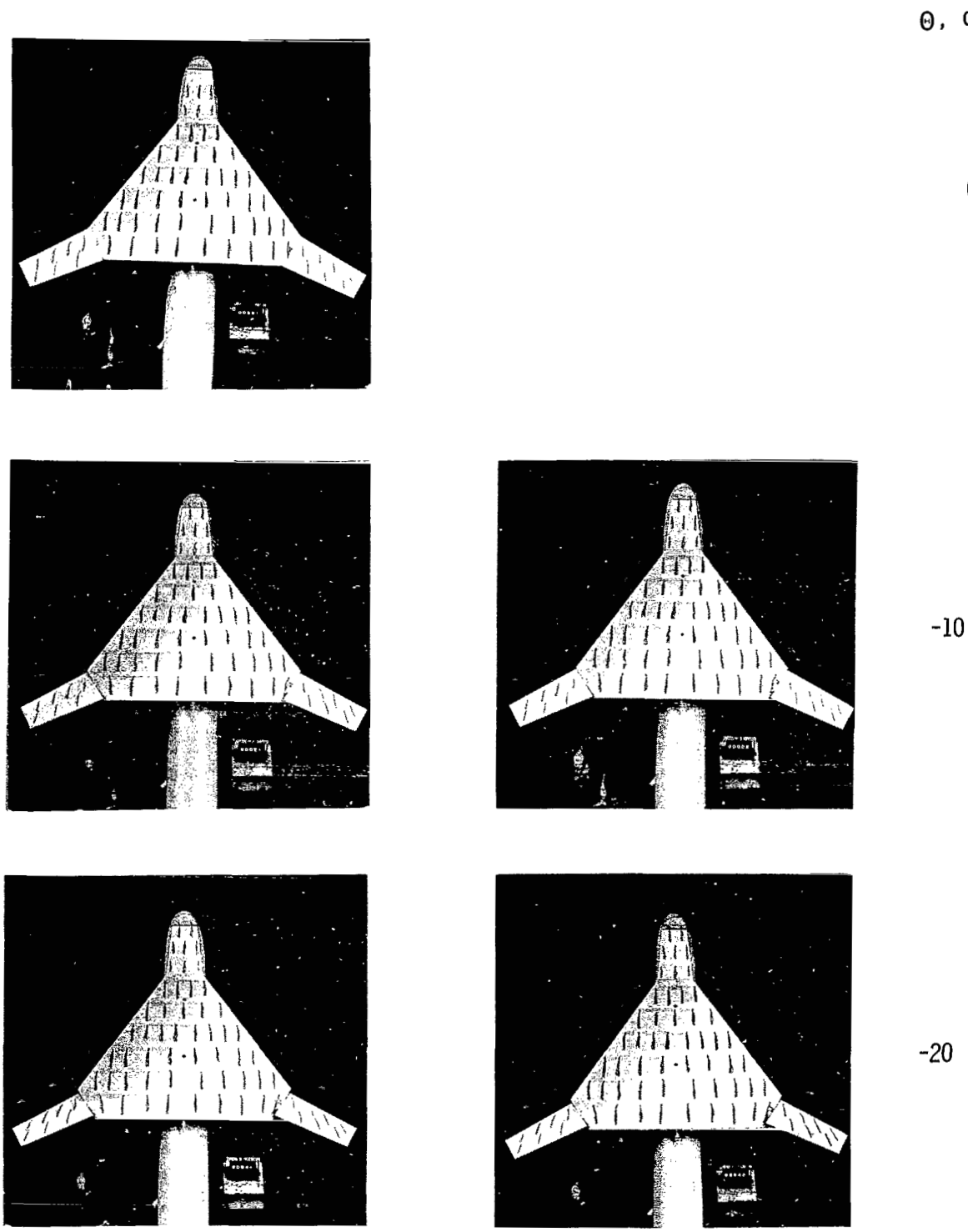

(a) $\alpha = -2^{\circ}$; $\alpha = 0^{\circ}$. L-70-4723

Figure 32.- Tuft-test results for rotor/wing in stopped mode. Rotor/wing 2.

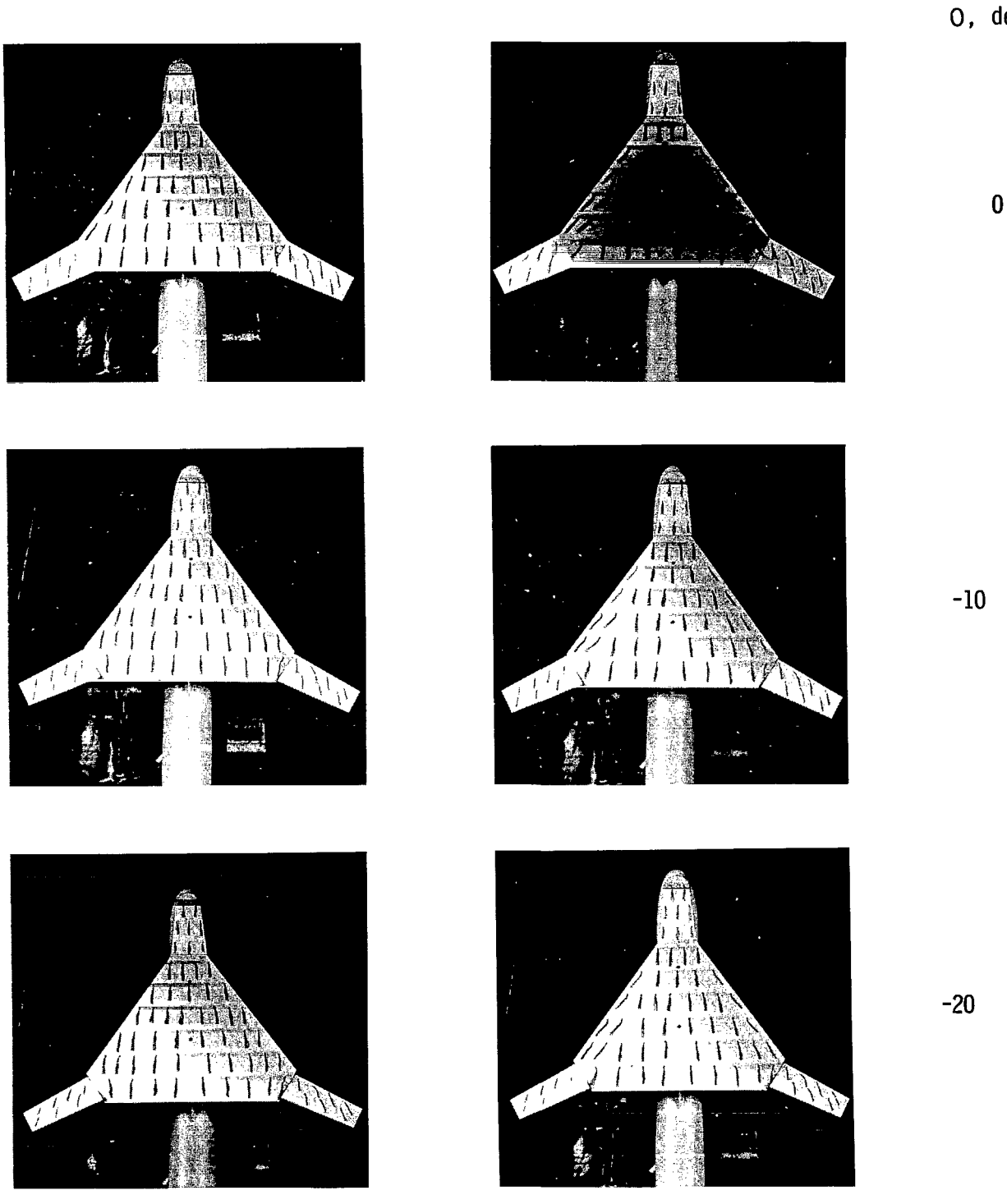

(b) $\alpha = 2^{\circ}$; $\alpha = 4^{\circ}$. L-70-4724

Figure 32.- Continued.

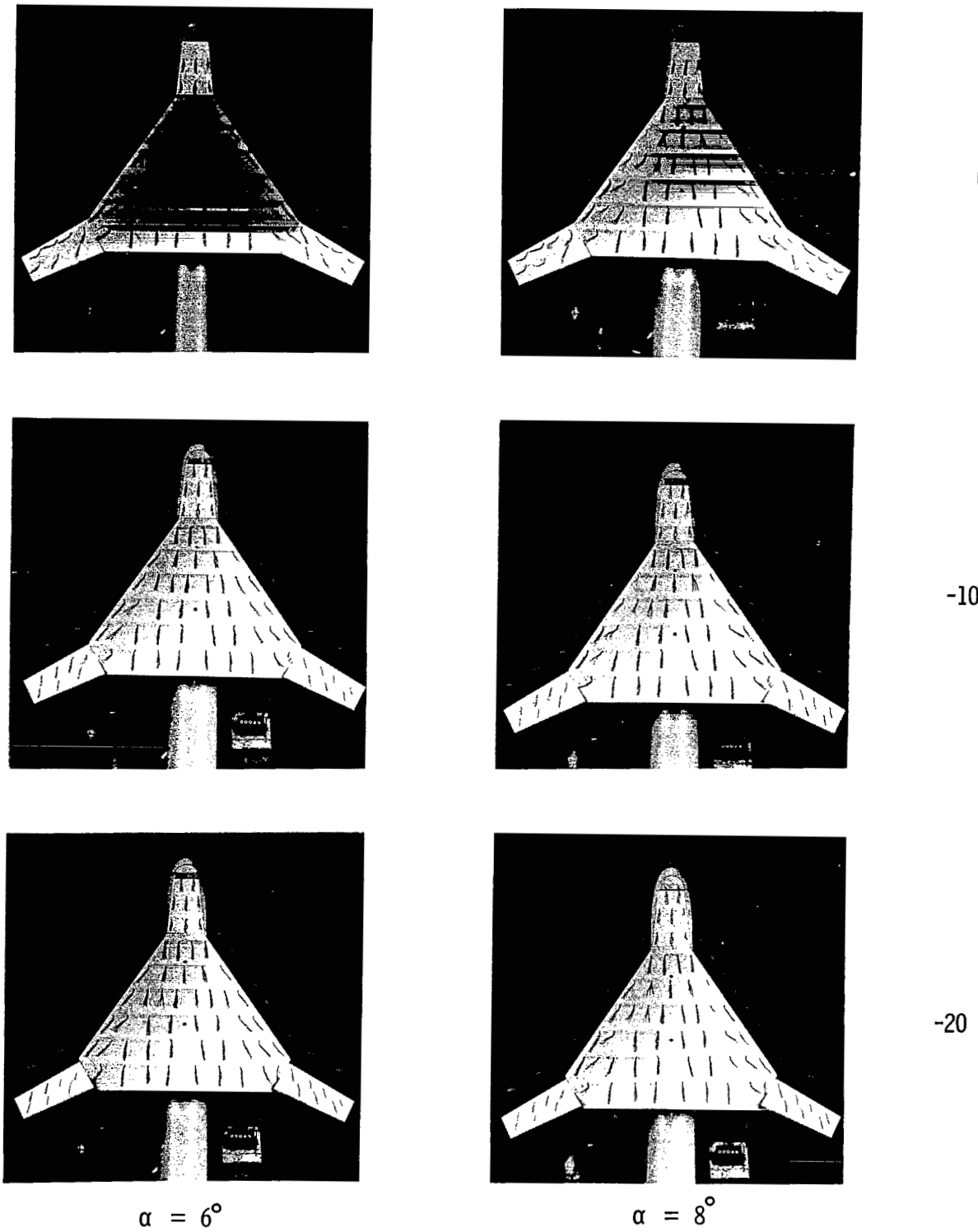

(c) $\alpha = 6^\circ$; $\alpha = 8^\circ$. L-70-4725

Figure 32.- Continued.

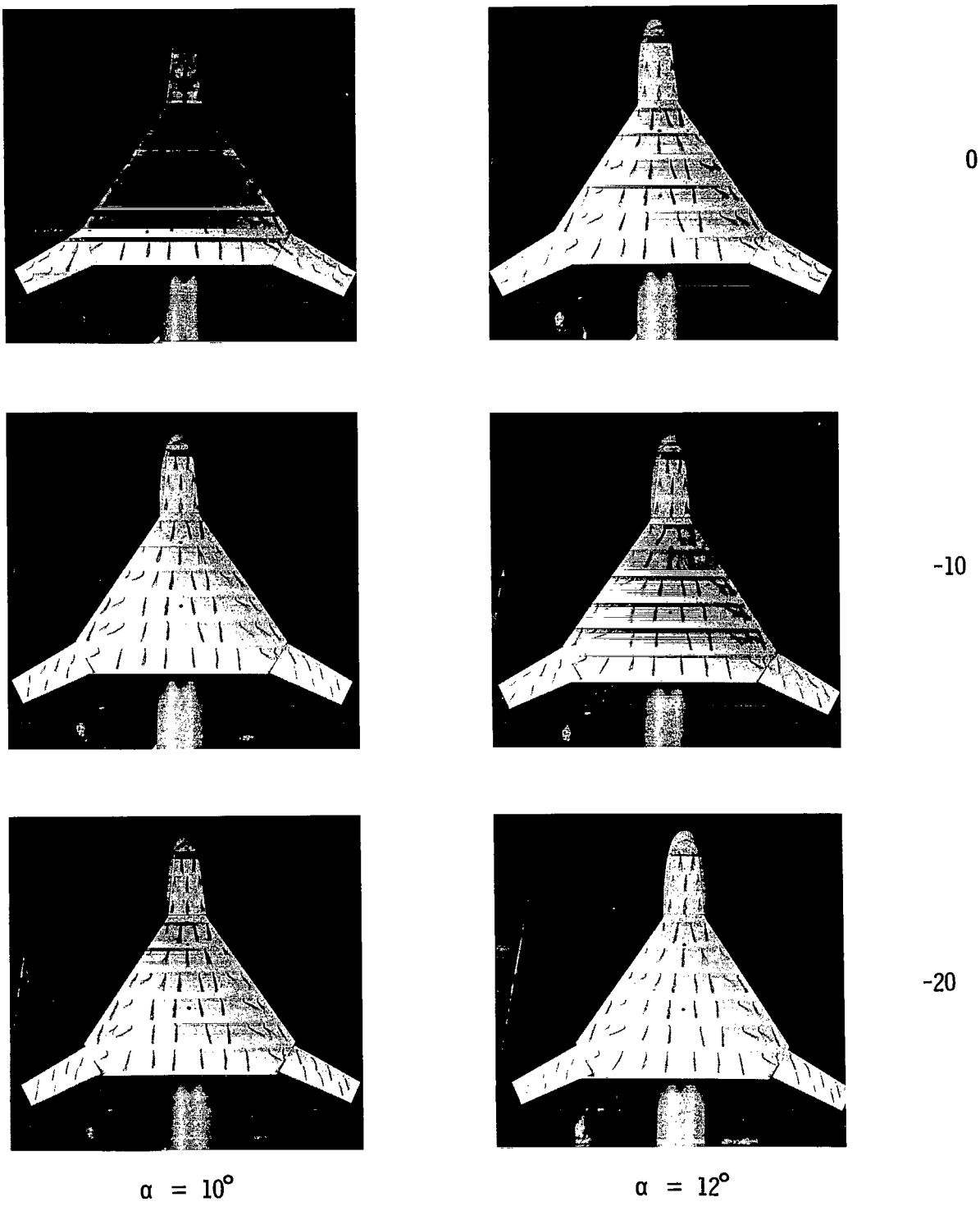

(d) $\alpha = 10^{\circ}$; $\alpha = 12^{\circ}$. L-70-4726

Figure 32.- Continued.

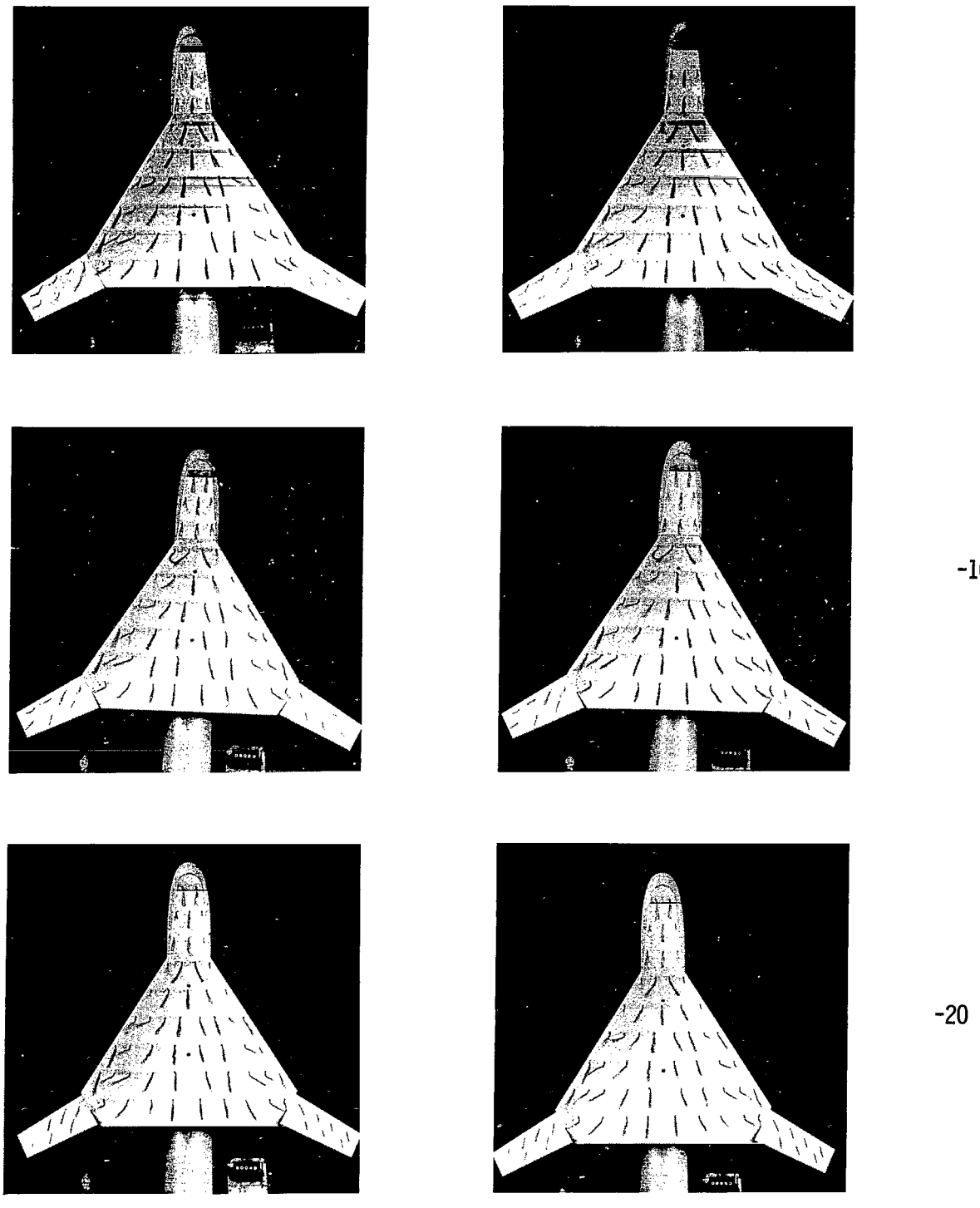

(e) $\alpha = 14^\circ$; $\alpha = 16^\circ$. L-70-4727

Figure 32.- Continued.

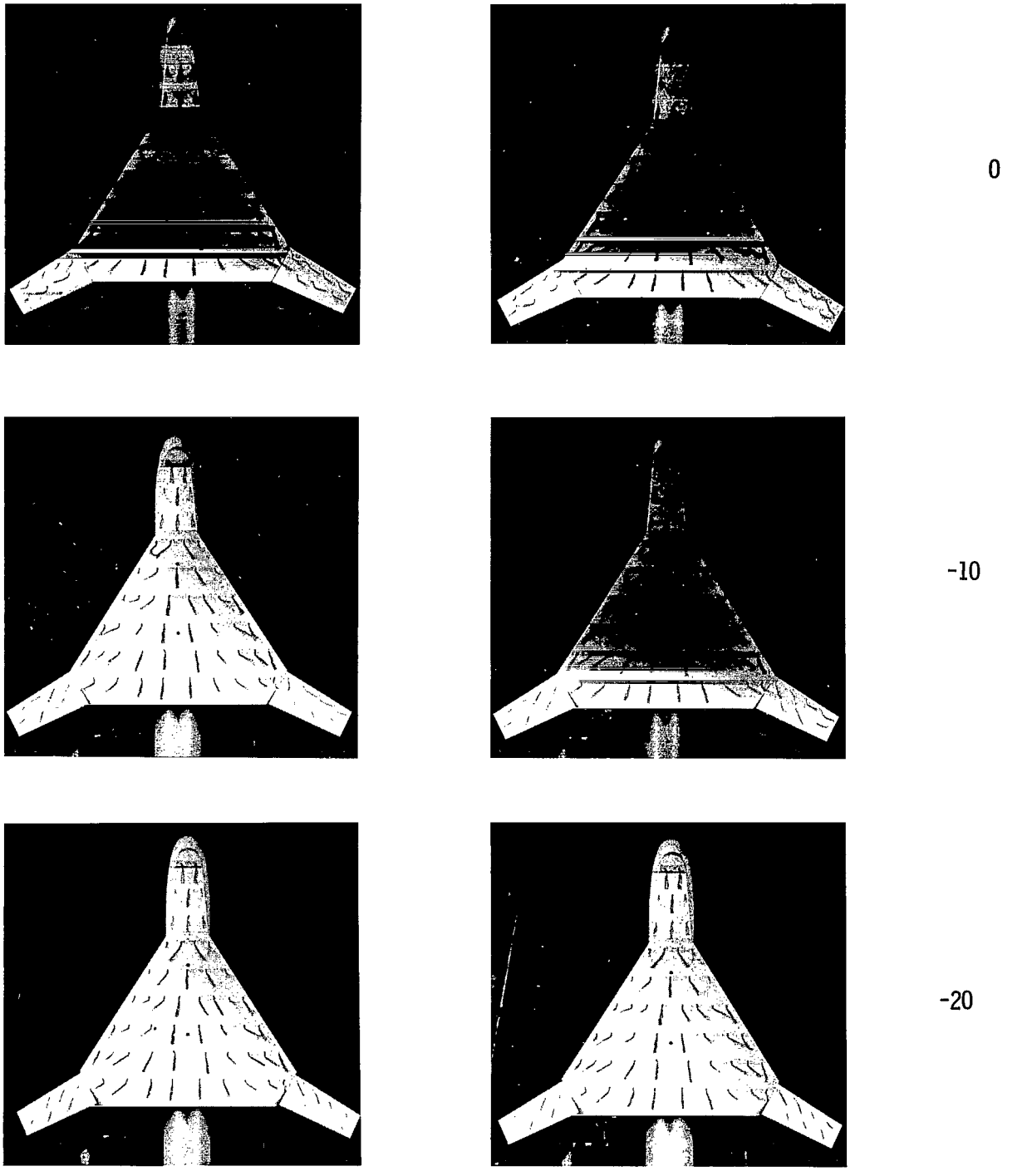

(f) $\alpha = 18°$; $\alpha = 20°$. L-70-4728

Figure 32.- Continued.

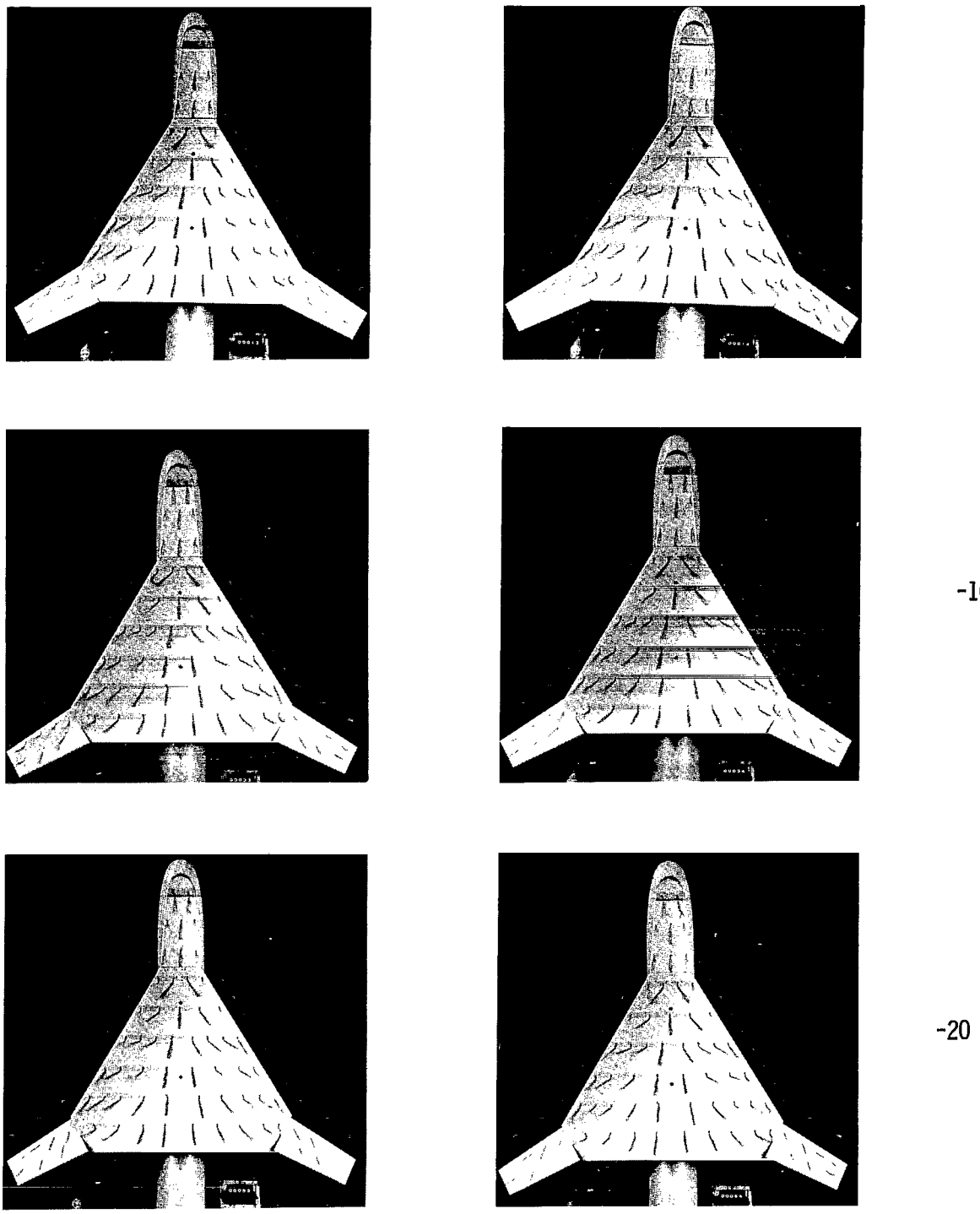

(g) $\alpha = 22^{\circ}$; $\alpha = 24^{\circ}$. L-70-4729

Figure 32.- Continued.

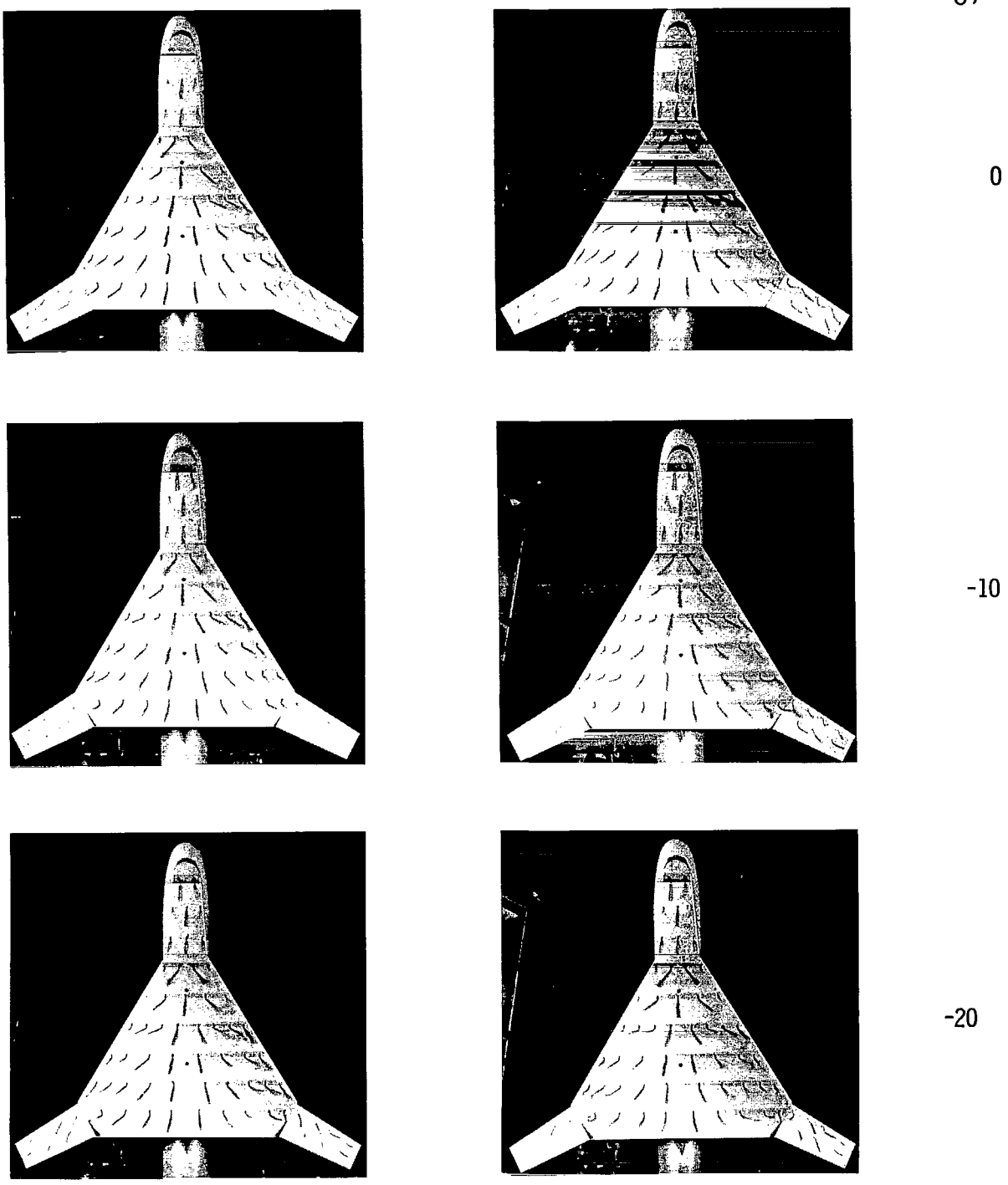

(h) $\alpha = 26°$; $\alpha = 28°$. L-70-4730

Figure 32.- Continued.

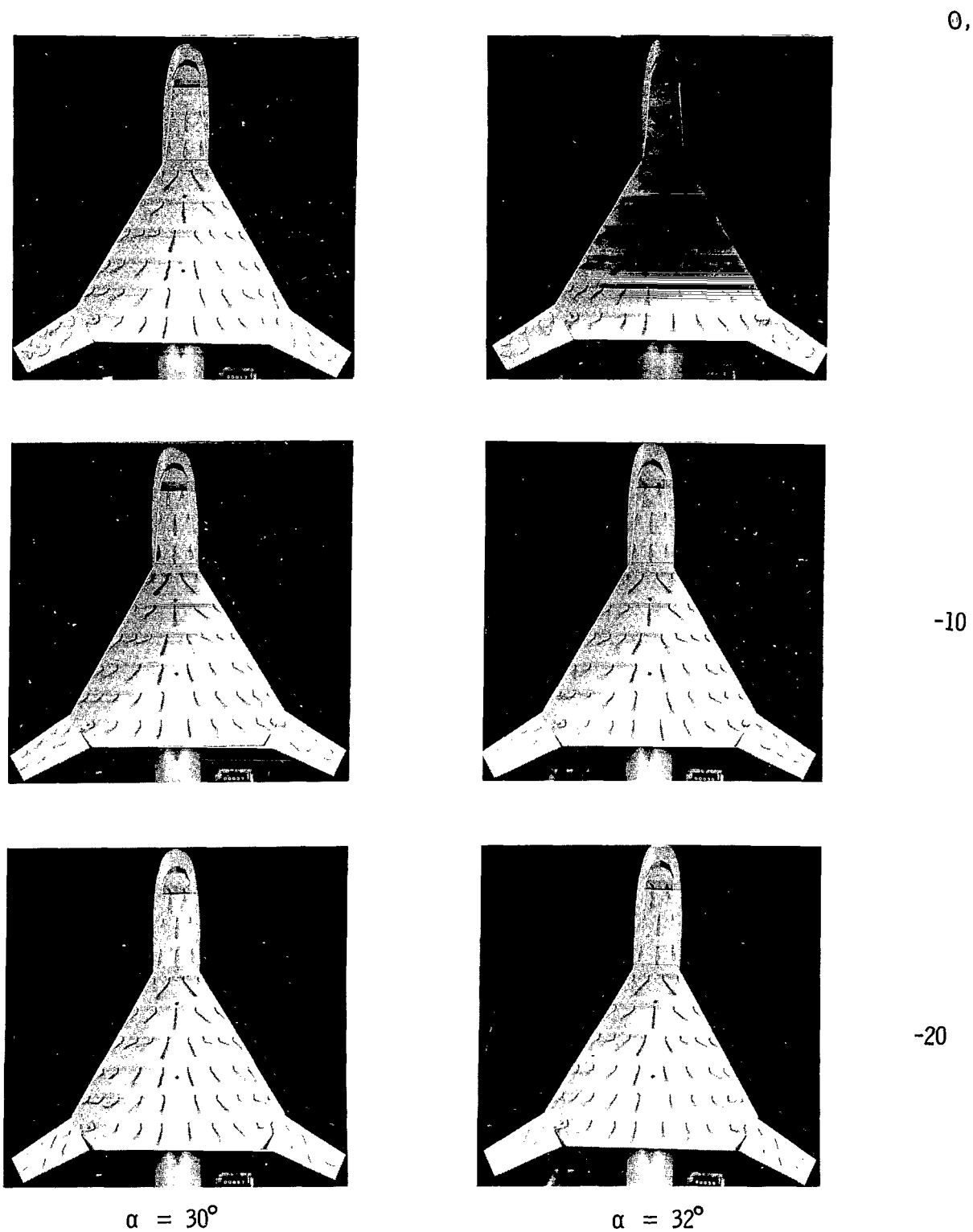

(i) $\alpha = 30^{\circ}$; $\alpha = 32^{\circ}$. L-70-4731

Figure 32.- Continued.

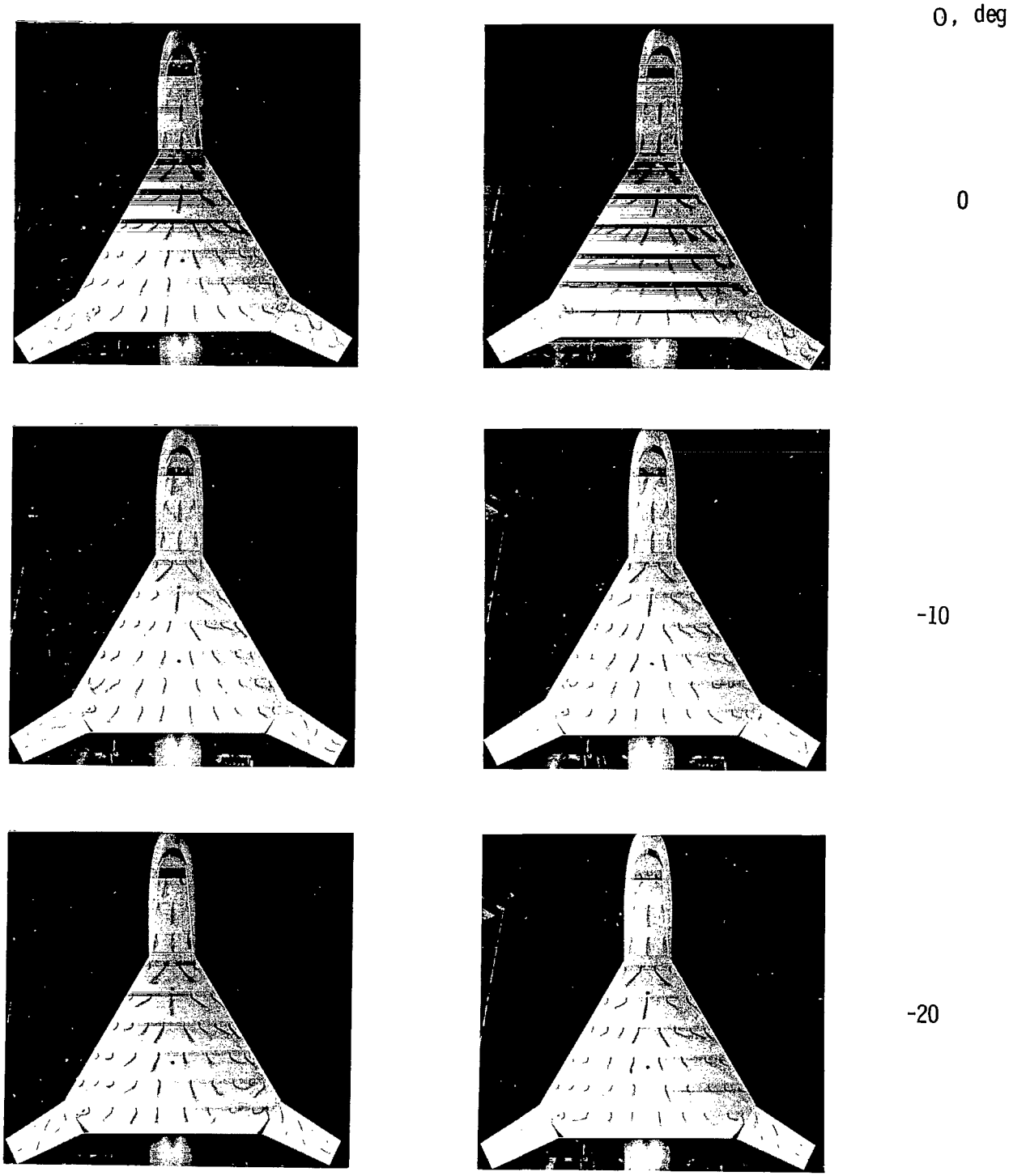

(j) $\alpha = 34^{\circ}$; $\alpha = 36^{\circ}$. L-70-4732

Figure 32.- Concluded.

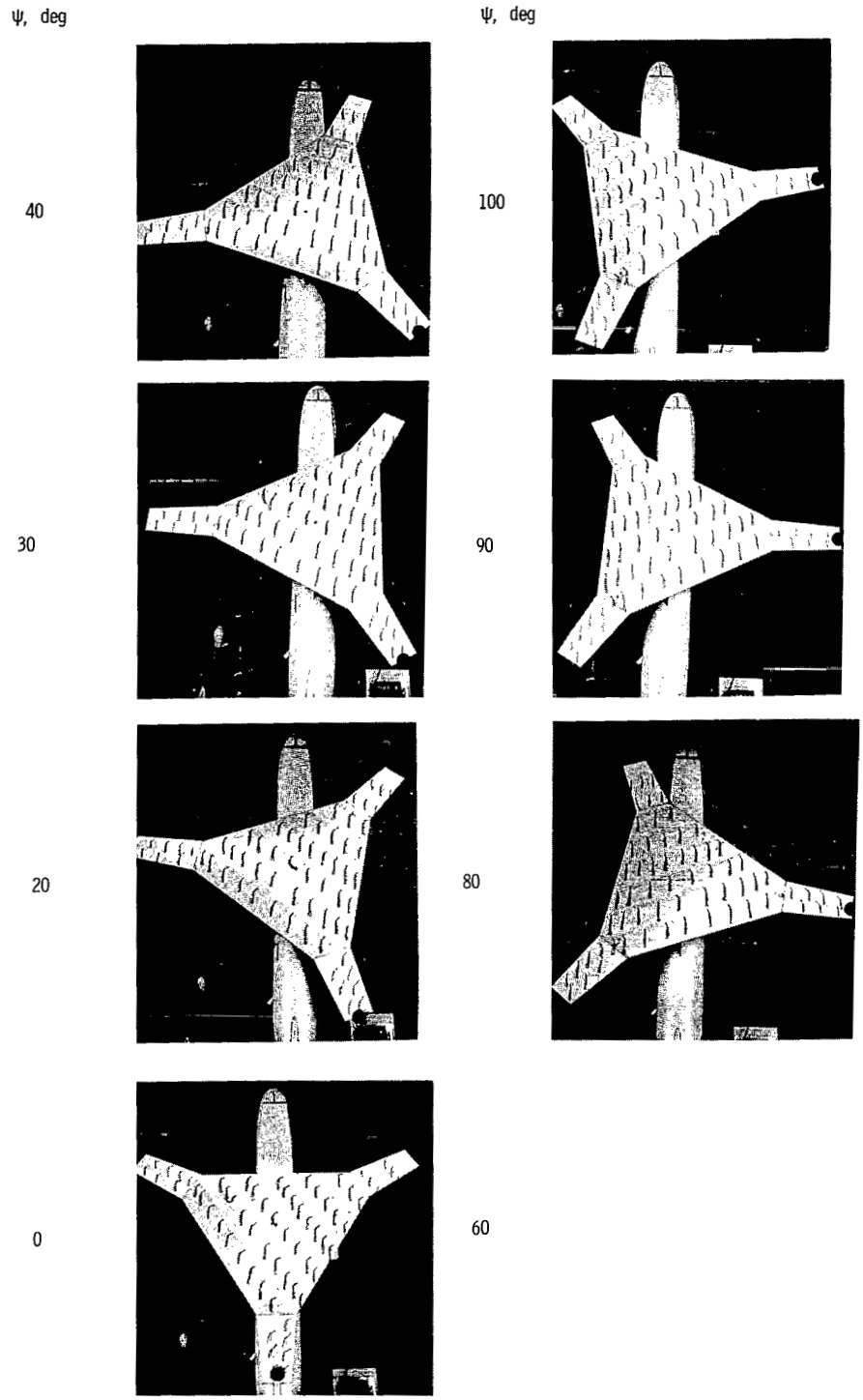

(a) $\alpha = 0^{\circ}$. L-70-4733

Figure 33.- Tuft-test results for rotor/wing at various azimuth angles. $\Theta = 0^{\circ}$; rotor/wing 2.

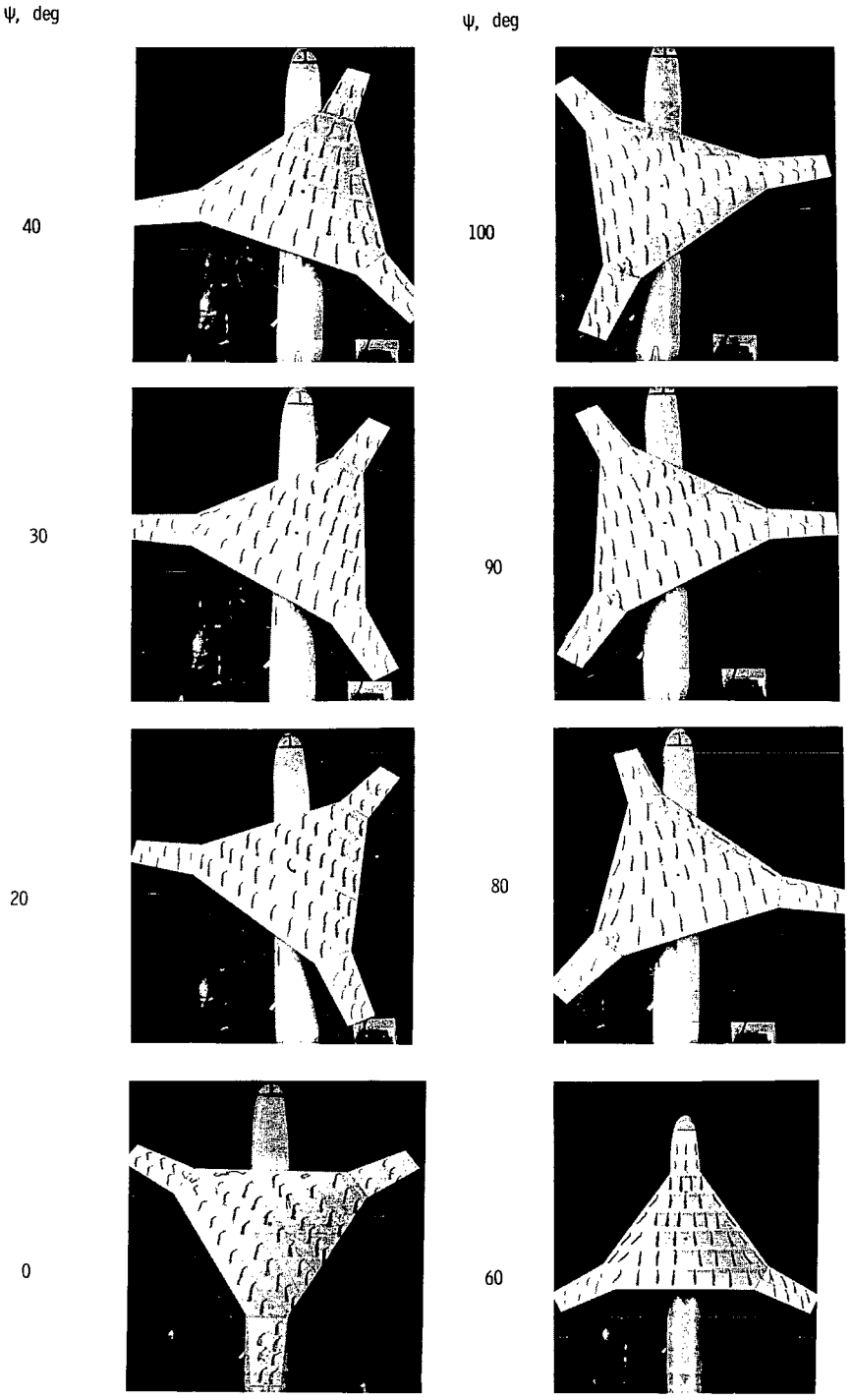

(b) $\alpha = 4^{\circ}$.

L-70-4734

Figure 33.- Continued.

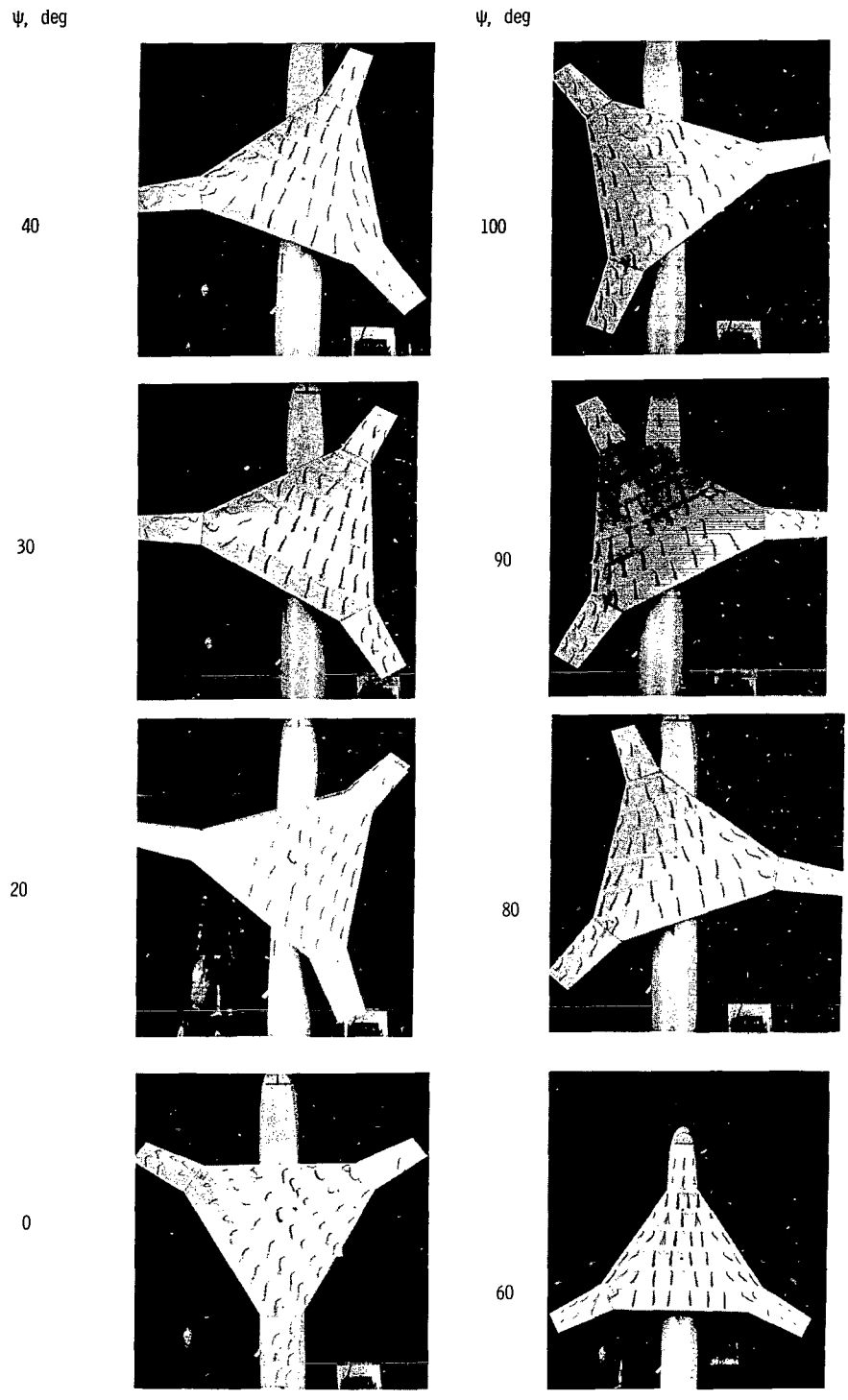

(c) $\alpha = 8^{\circ}$. L-70-4735

Figure 33.- Continued.

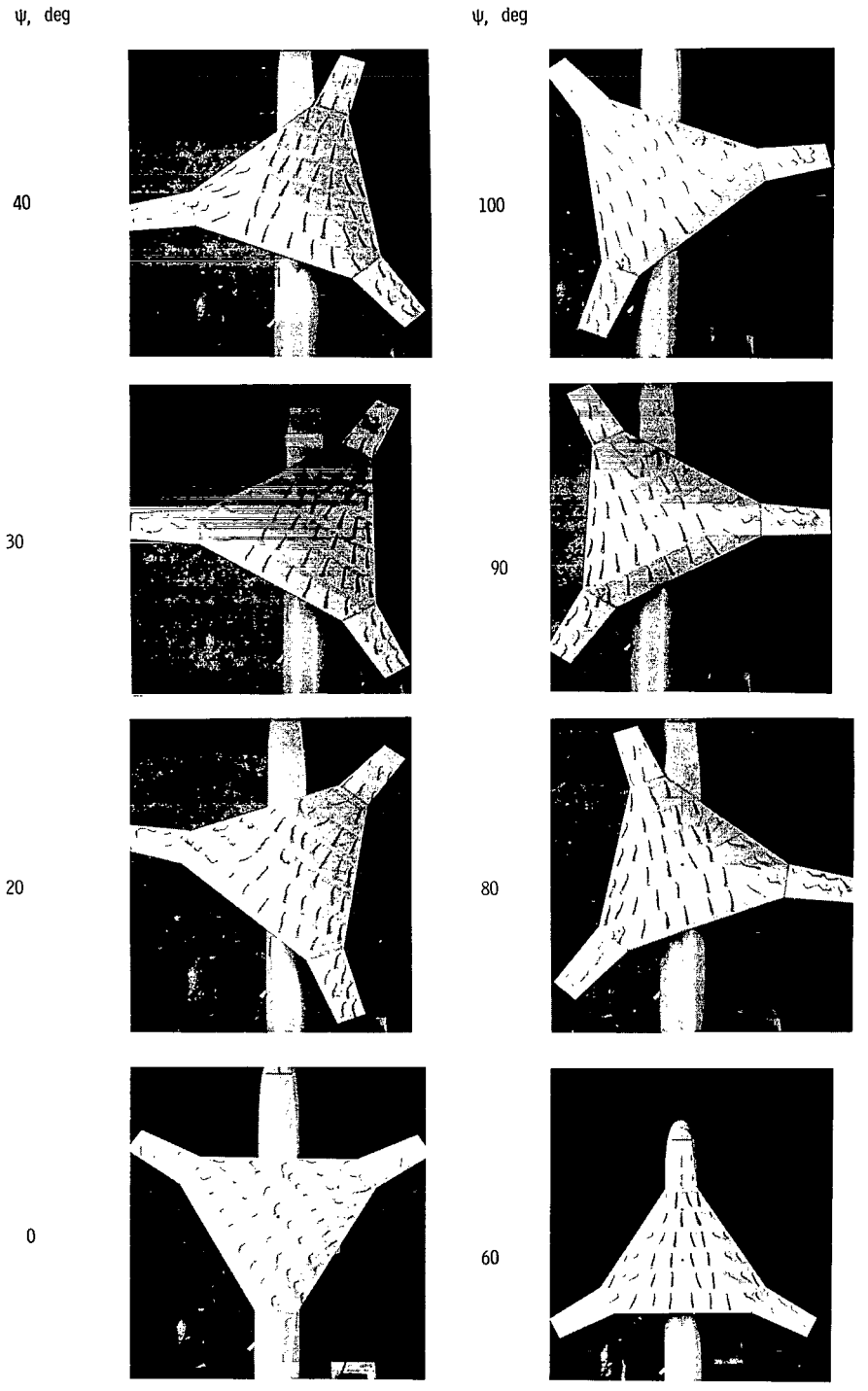

(d) $\alpha = 12^{\circ}$. L-70-4736

Figure 33.- Continued.

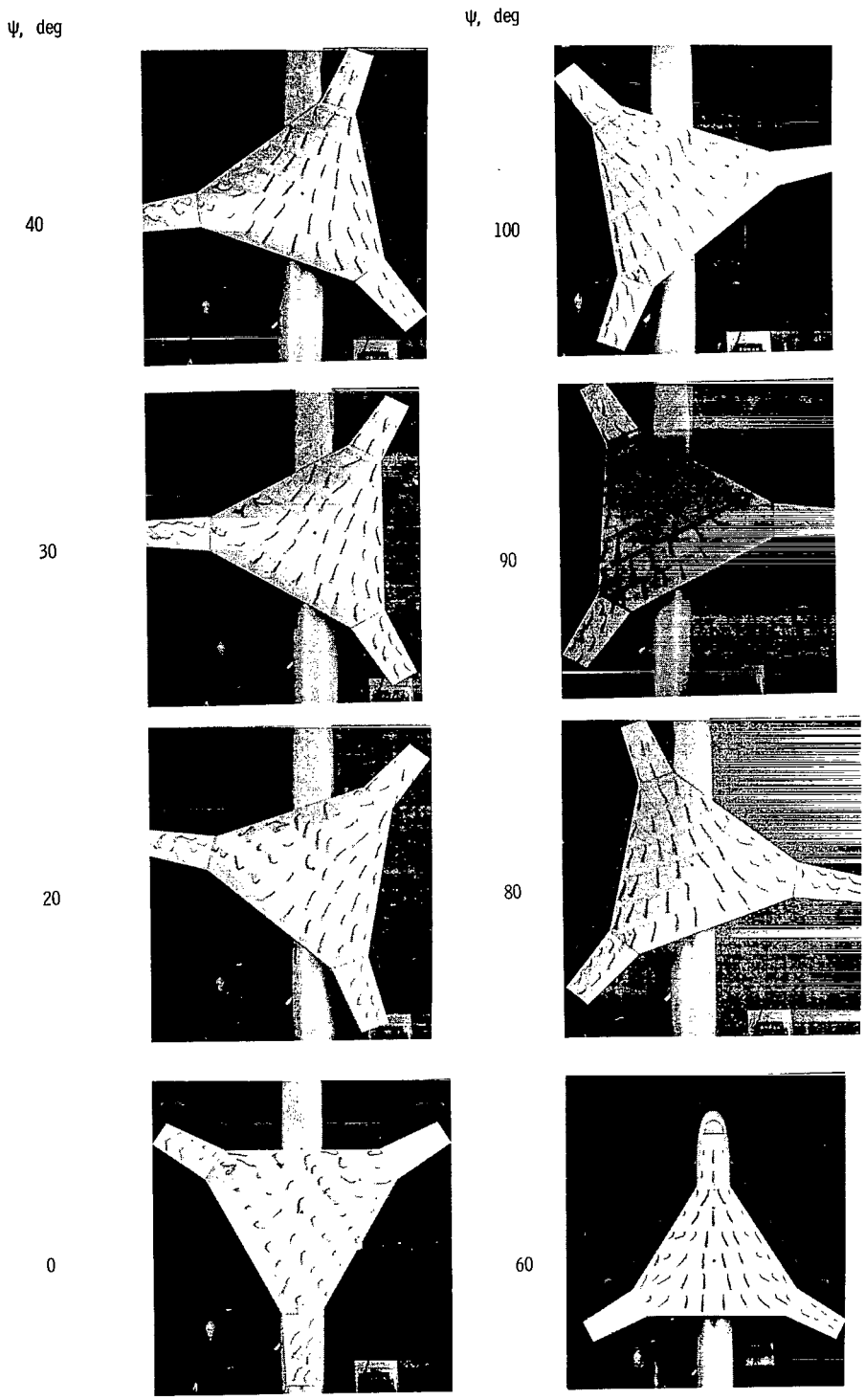

(e) $\alpha = 16^{\circ}$. L-70-4737

Figure 33.- Continued.

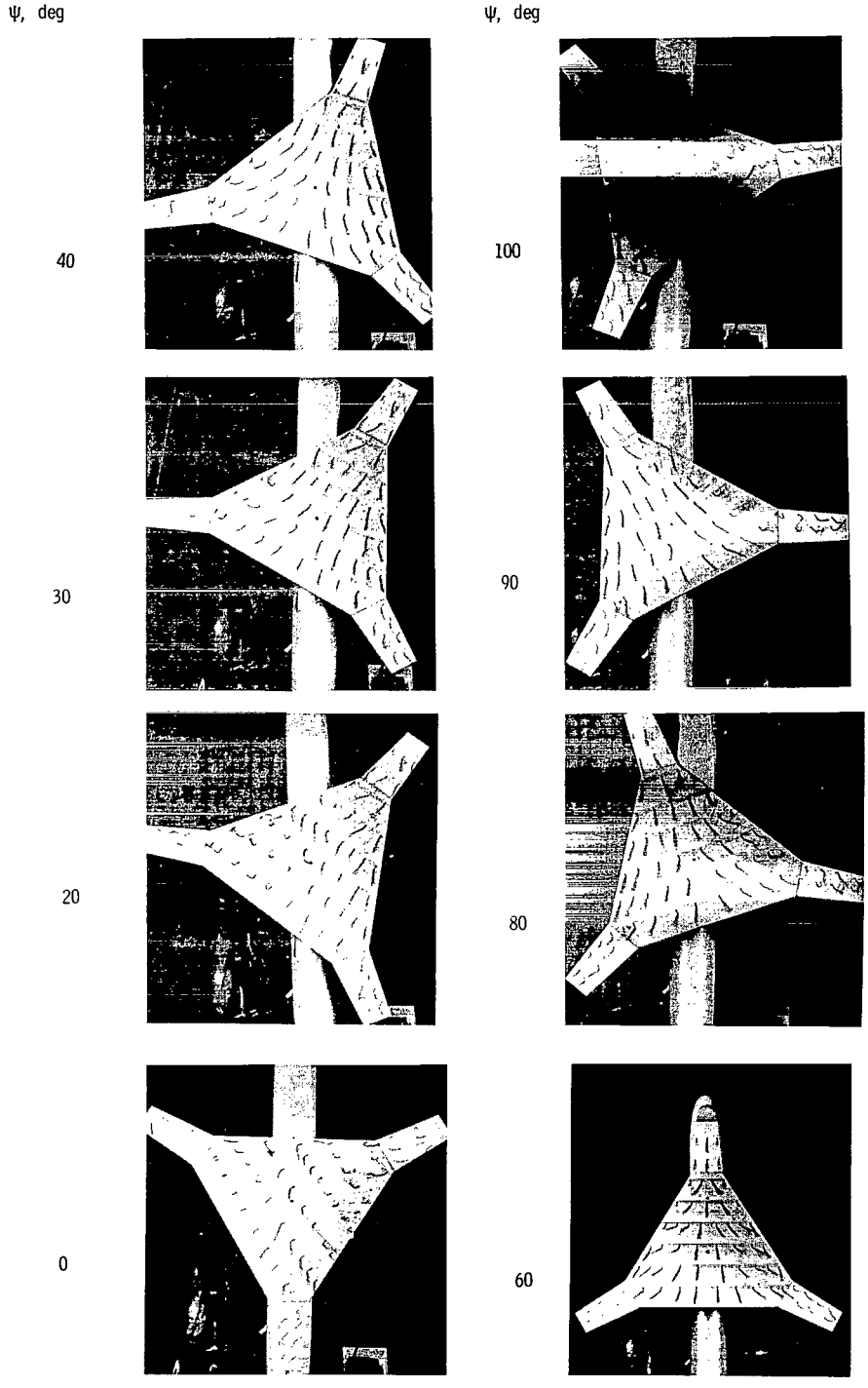

(f) $\alpha = 20^{\circ}$. L-70-4738

Figure 33.- Continued.

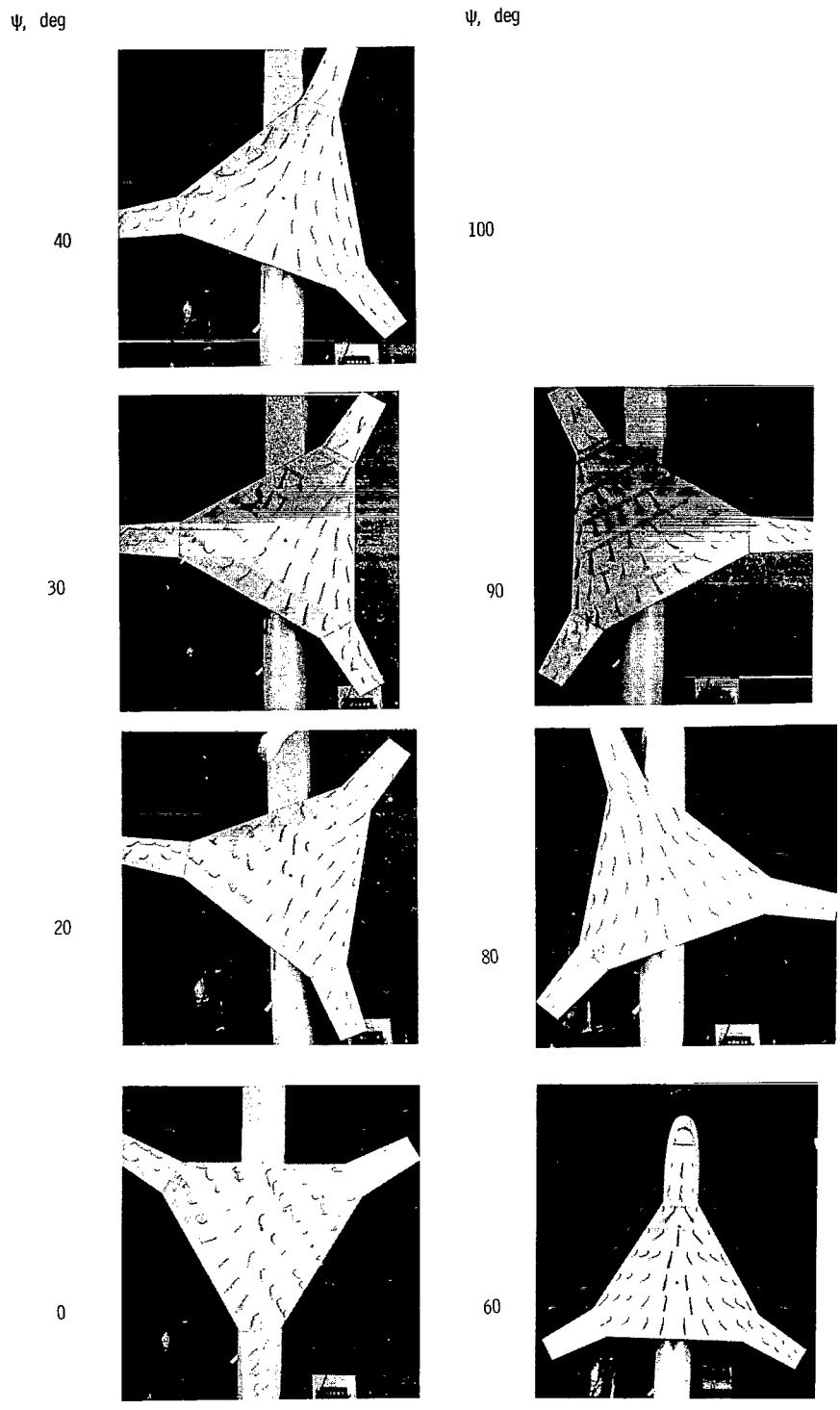

(g) $\alpha = 24^{\circ}$. L-70-4739

Figure 33.- Concluded.

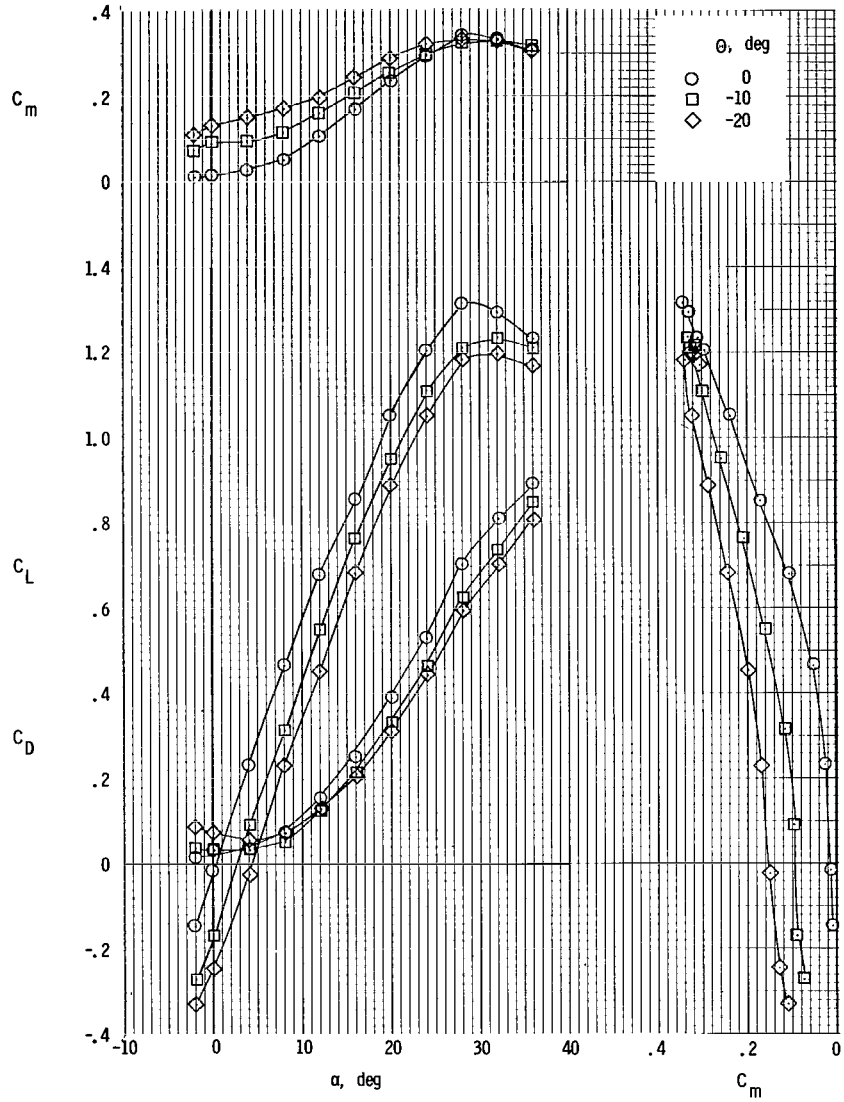

Figure 34.- Longitudinal aerodynamic characteristics. Horizontal tail off; center vertical tail; rotor/wing 2.

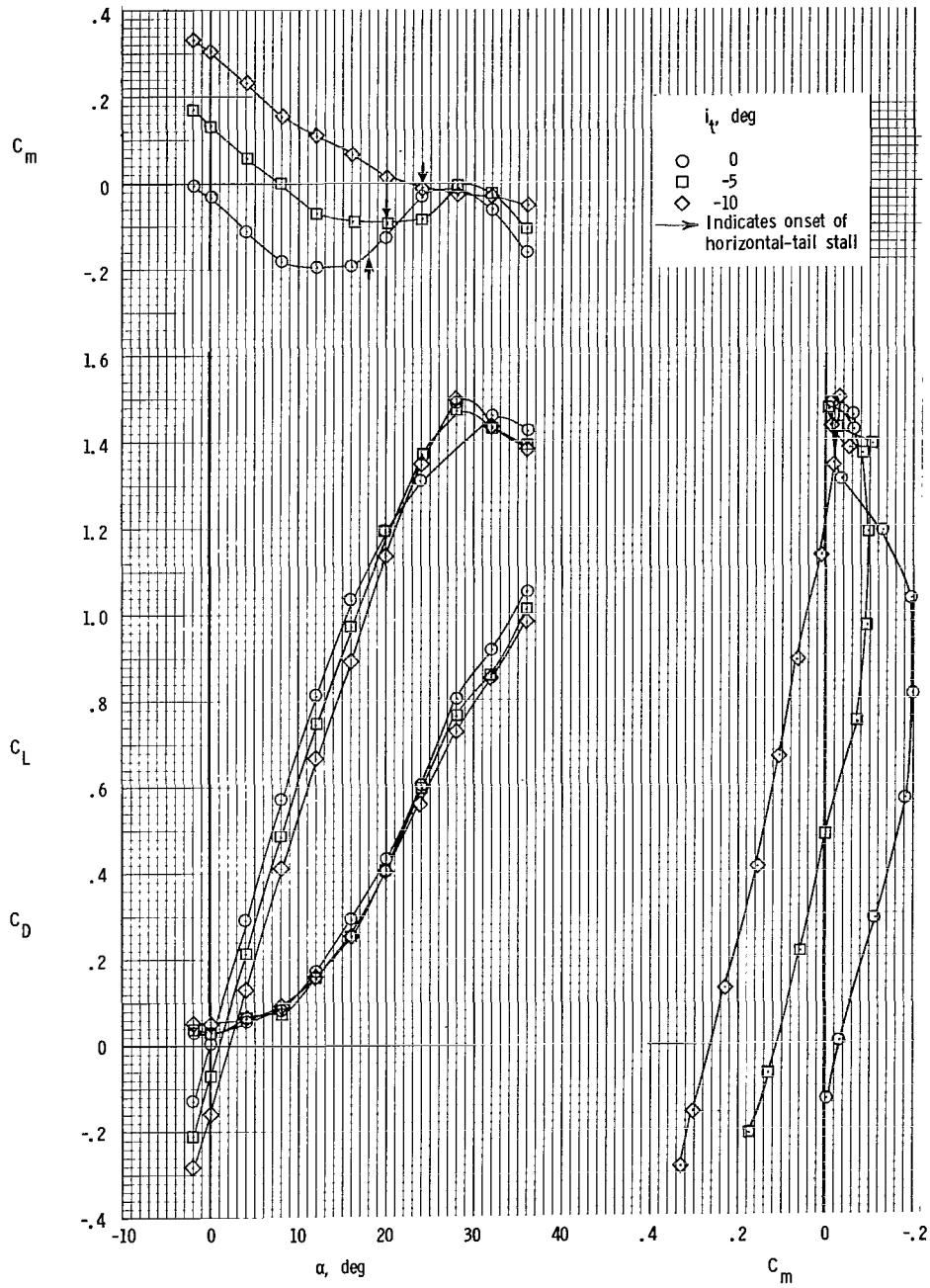

(a) $\Theta = 0^\circ$.

Figure 35.- Longitudinal aerodynamic characteristics. Low horizontal tail; center vertical tail; rotor/wing 2.

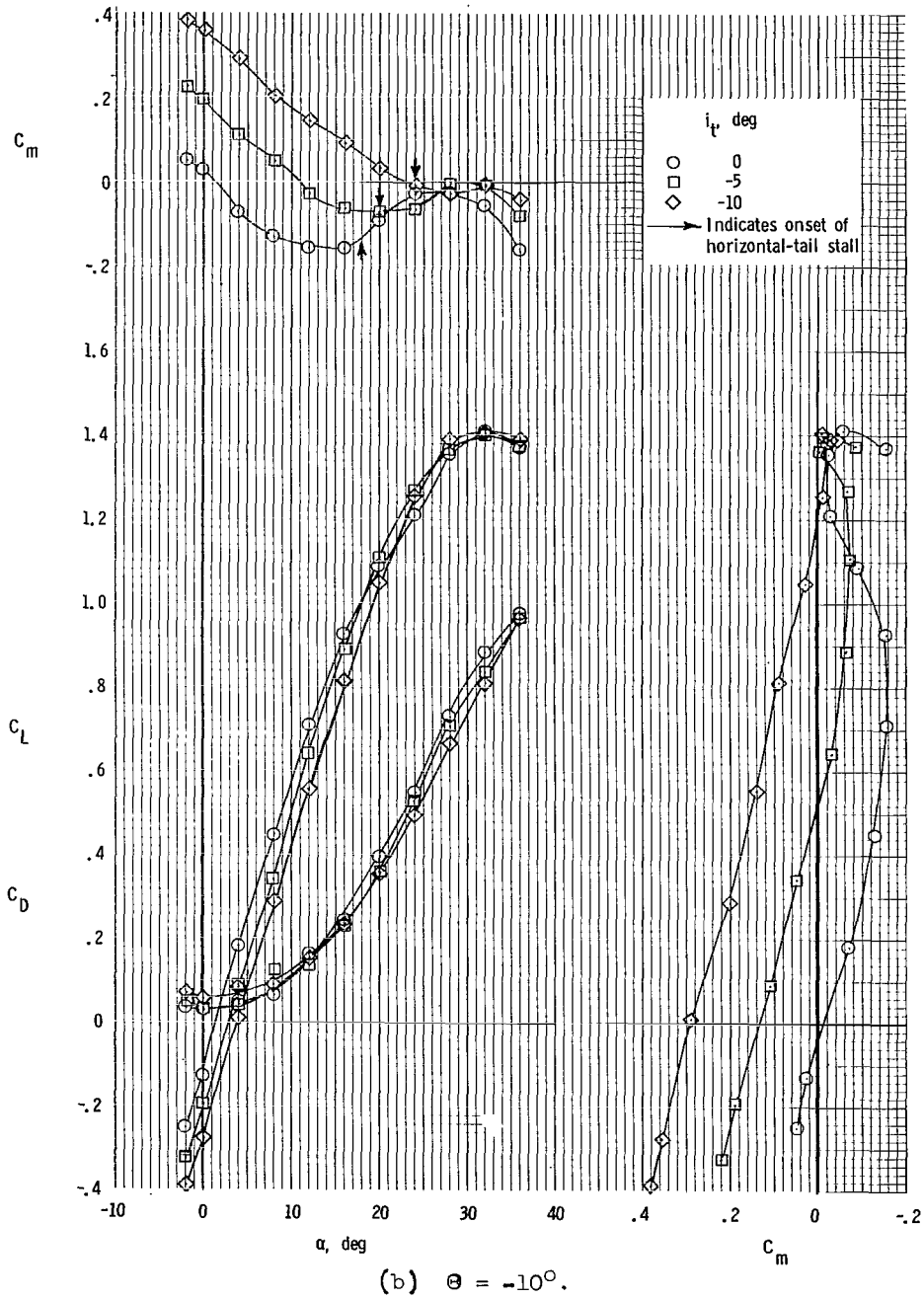

(b) $\Theta = -10^{\circ}$.

Figure 35.- Continued.

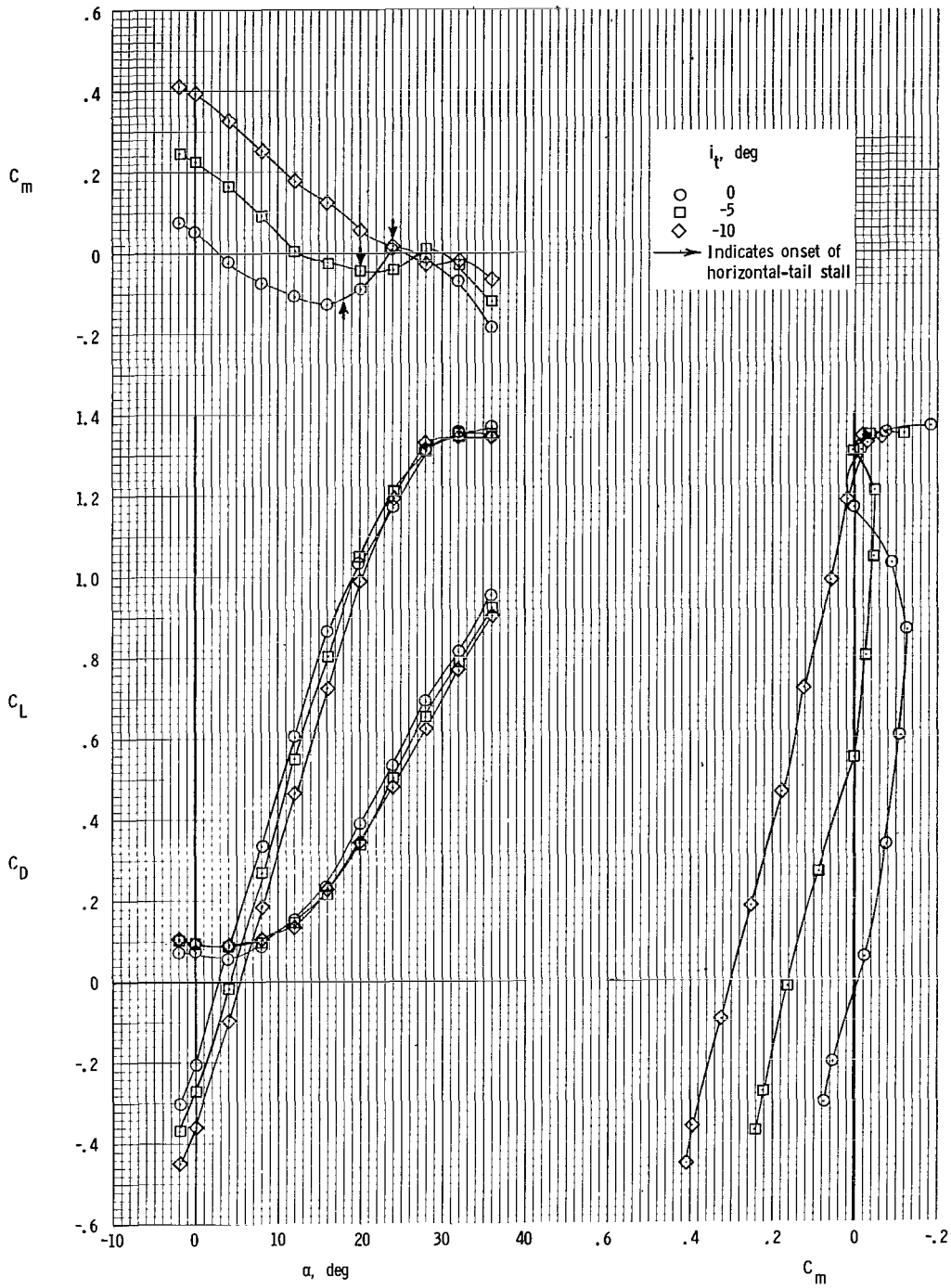

(c) $\Theta = -20^\circ$.

Figure 35.- Concluded.

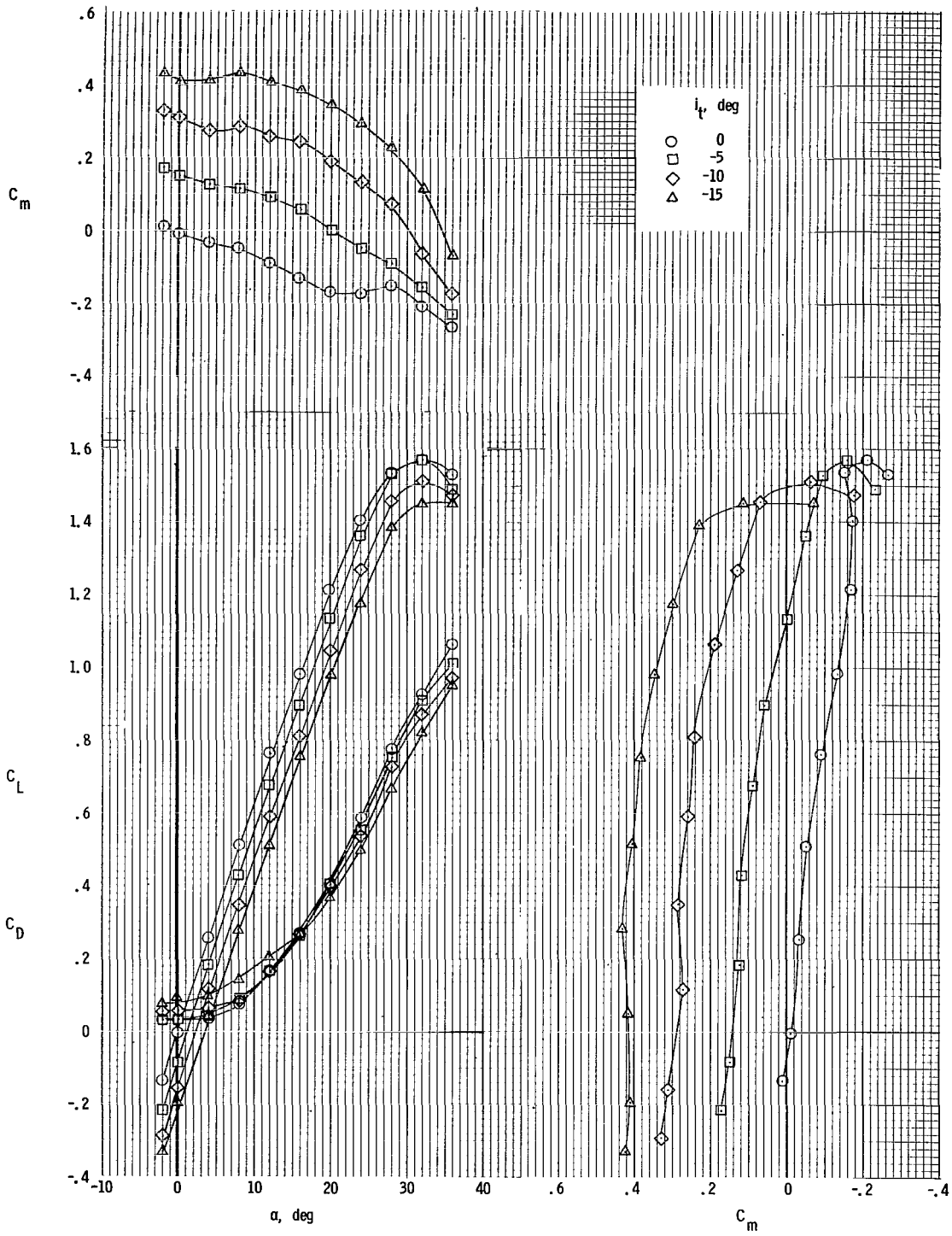

(a) $\Theta = 0^{\circ}$.

Figure 36.- Longitudinal aerodynamic characteristics. Mid horizontal tail; center vertical tail; rotor/wing 2.

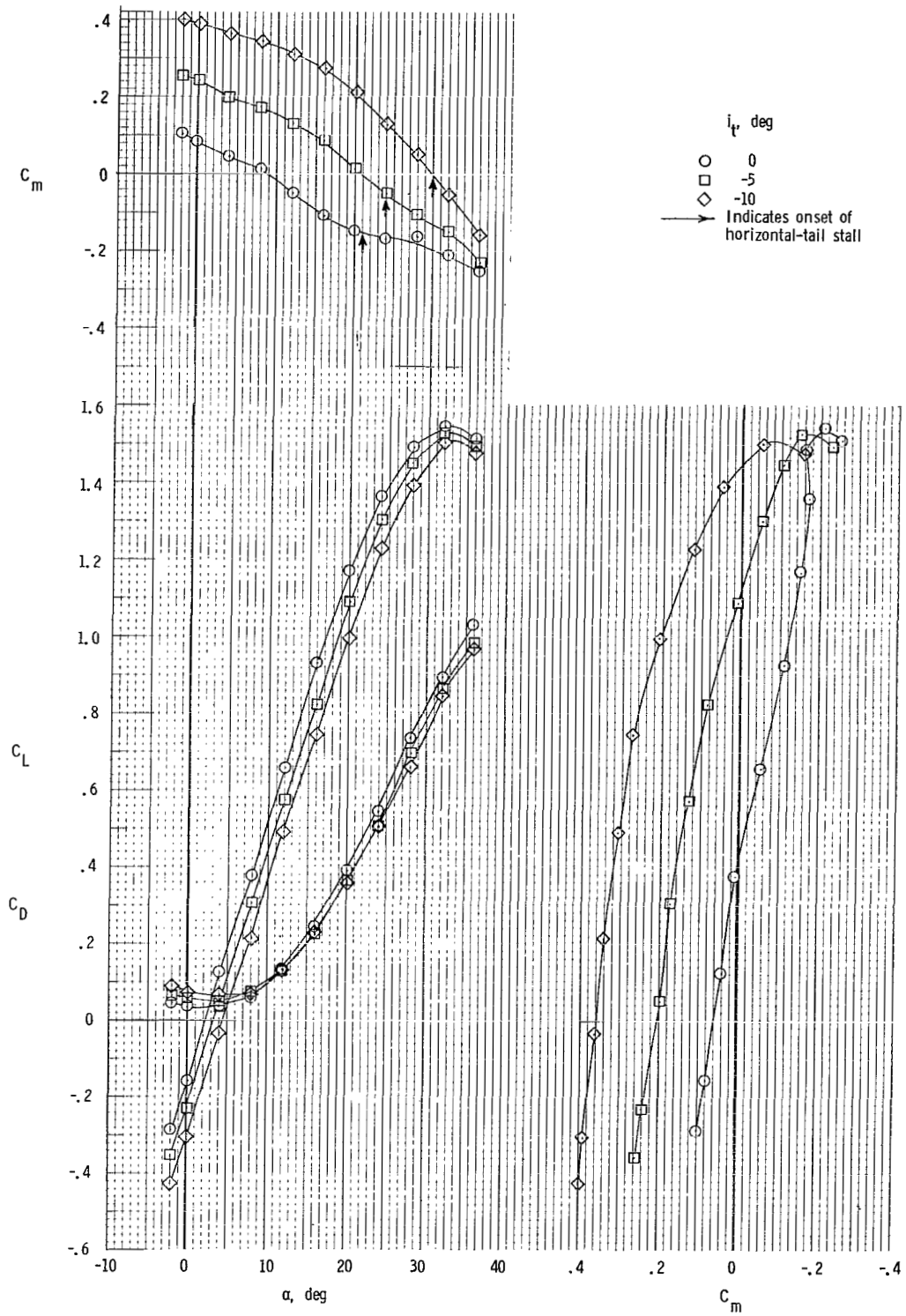

(b) $\Theta = -10^\circ$.

Figure 36.- Continued.

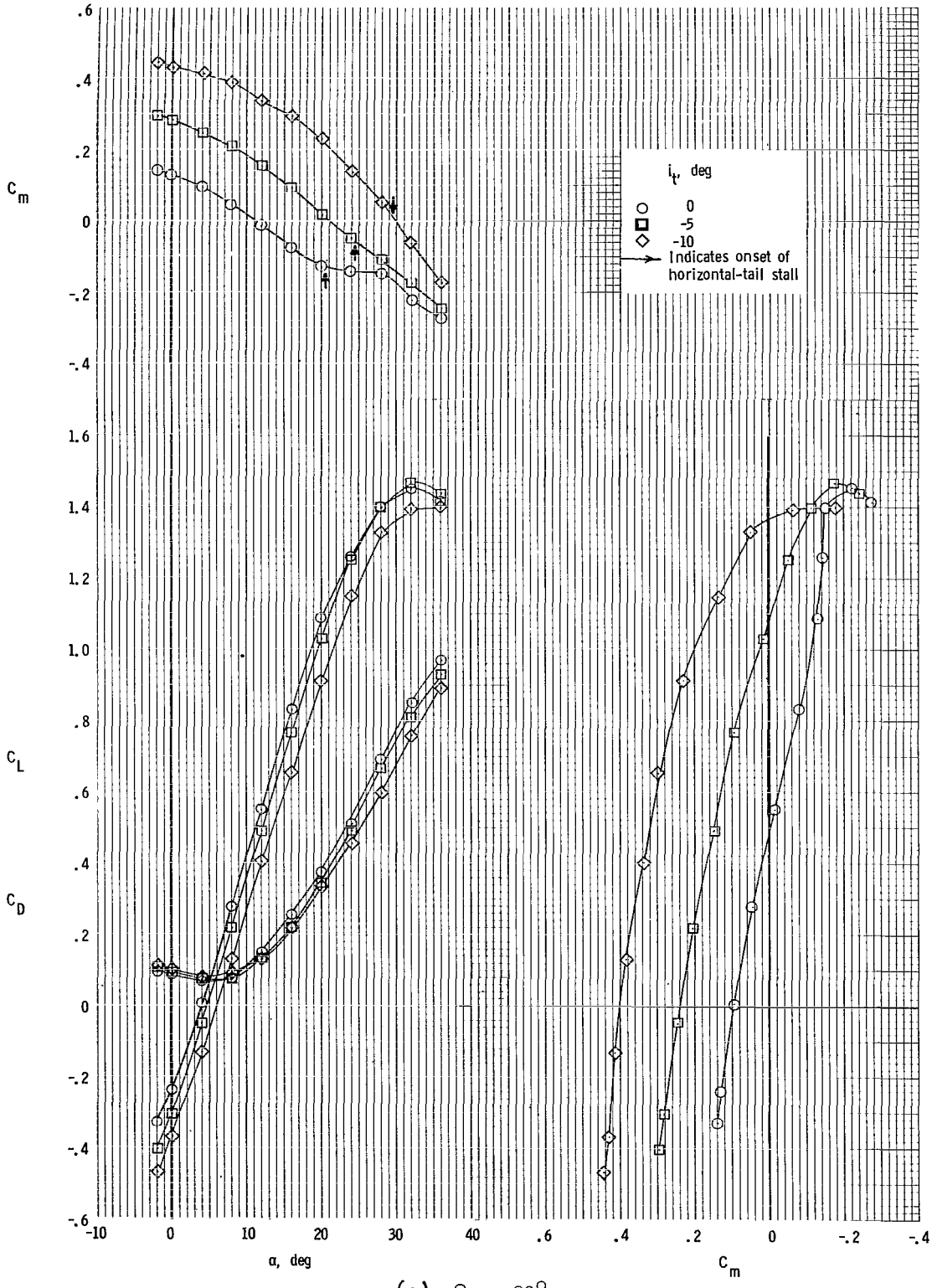

(c) $\Theta = -20^\circ$.

Figure 36.- Concluded.

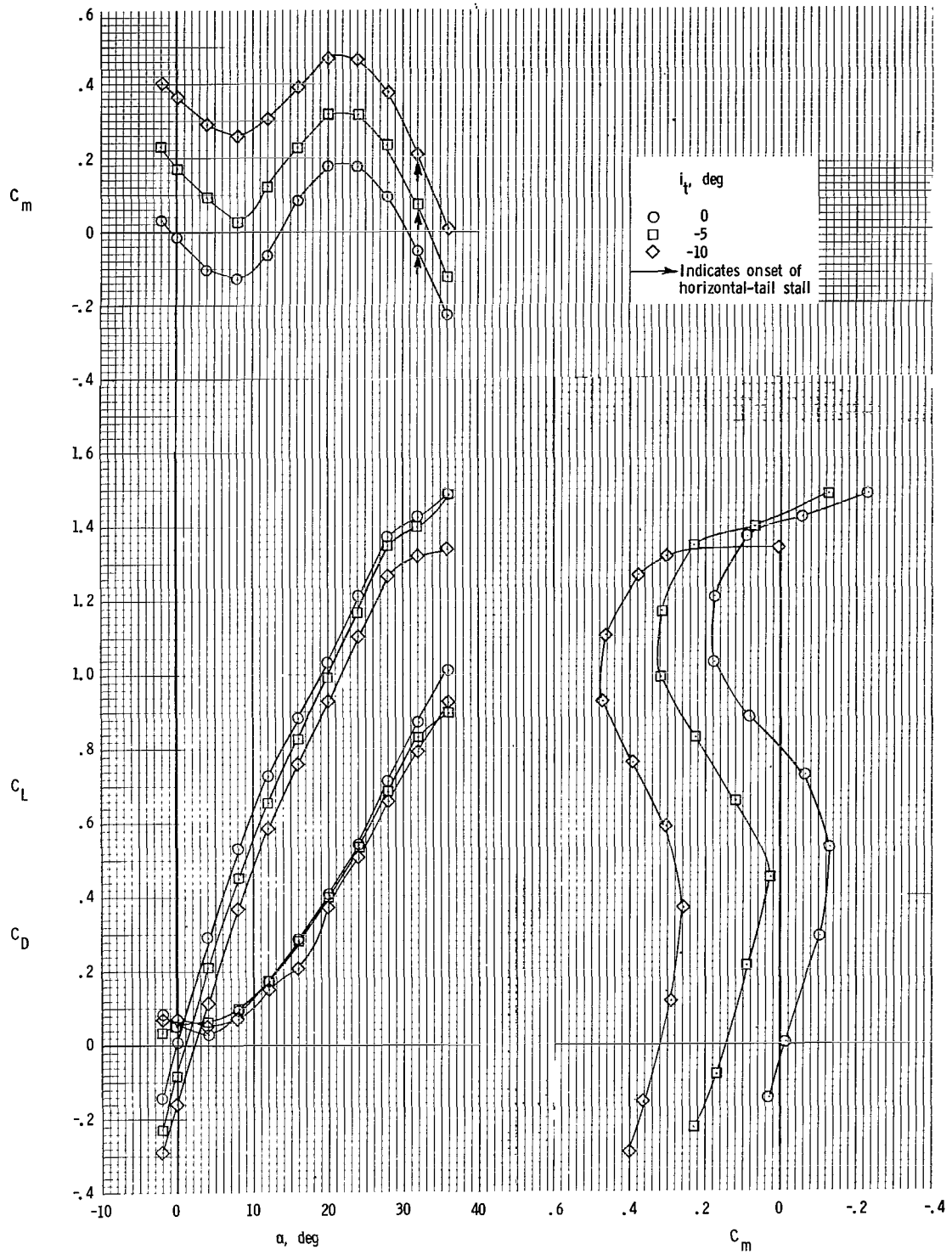

(a) $\Theta = 0^{\circ}$.

Figure 37.- Longitudinal aerodynamic characteristics. High horizontal tail; center vertical tail; rotor/wing 2.

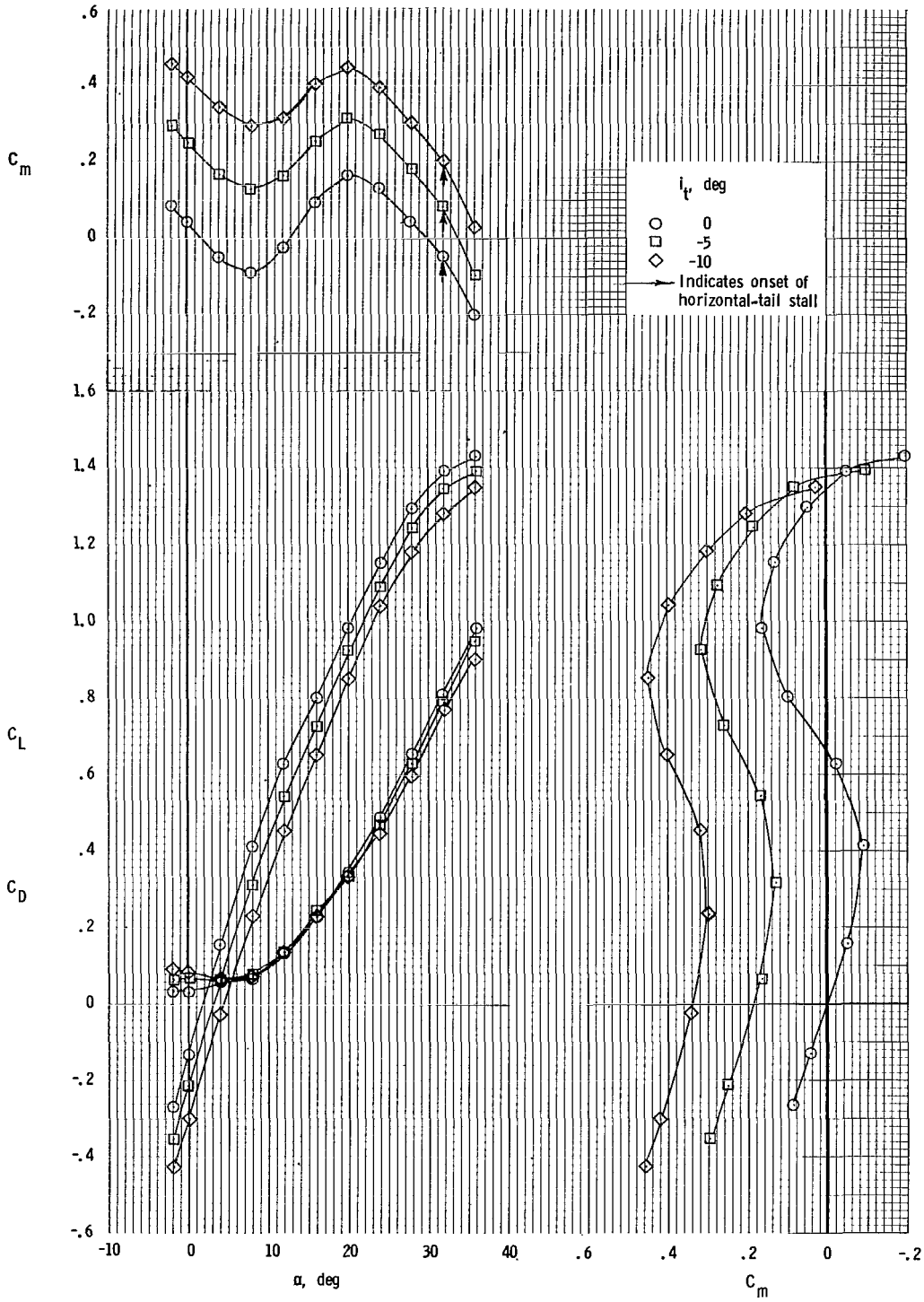

(b) $\Theta = -10^{\circ}$.

Figure 37.- Concluded.

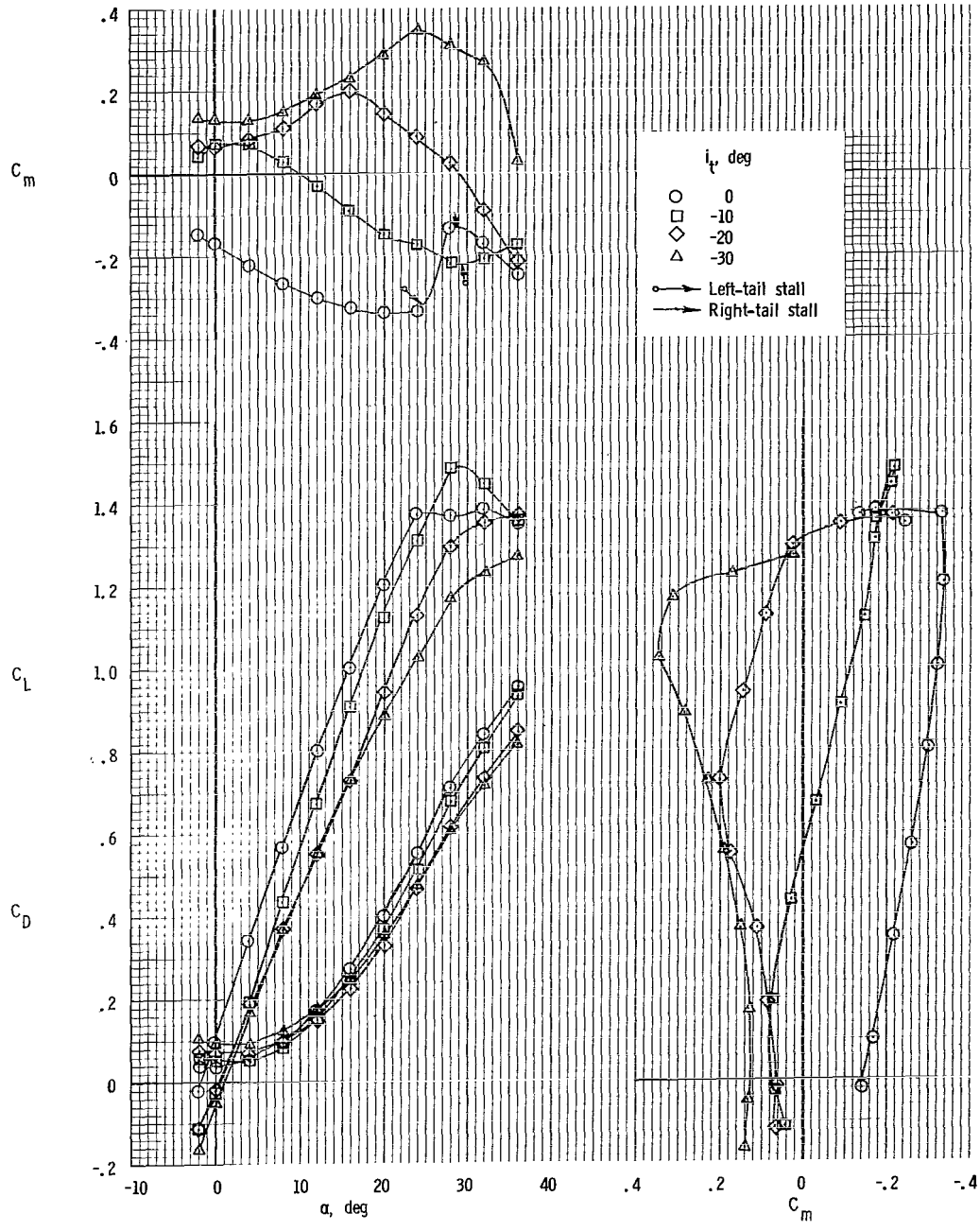

(a) $\Theta = 0^{\circ}$.

Figure 38.- Longitudinal aerodynamic characteristics. Twin vertical tails; horizontal tail at center fuselage; rotor/wing 2.

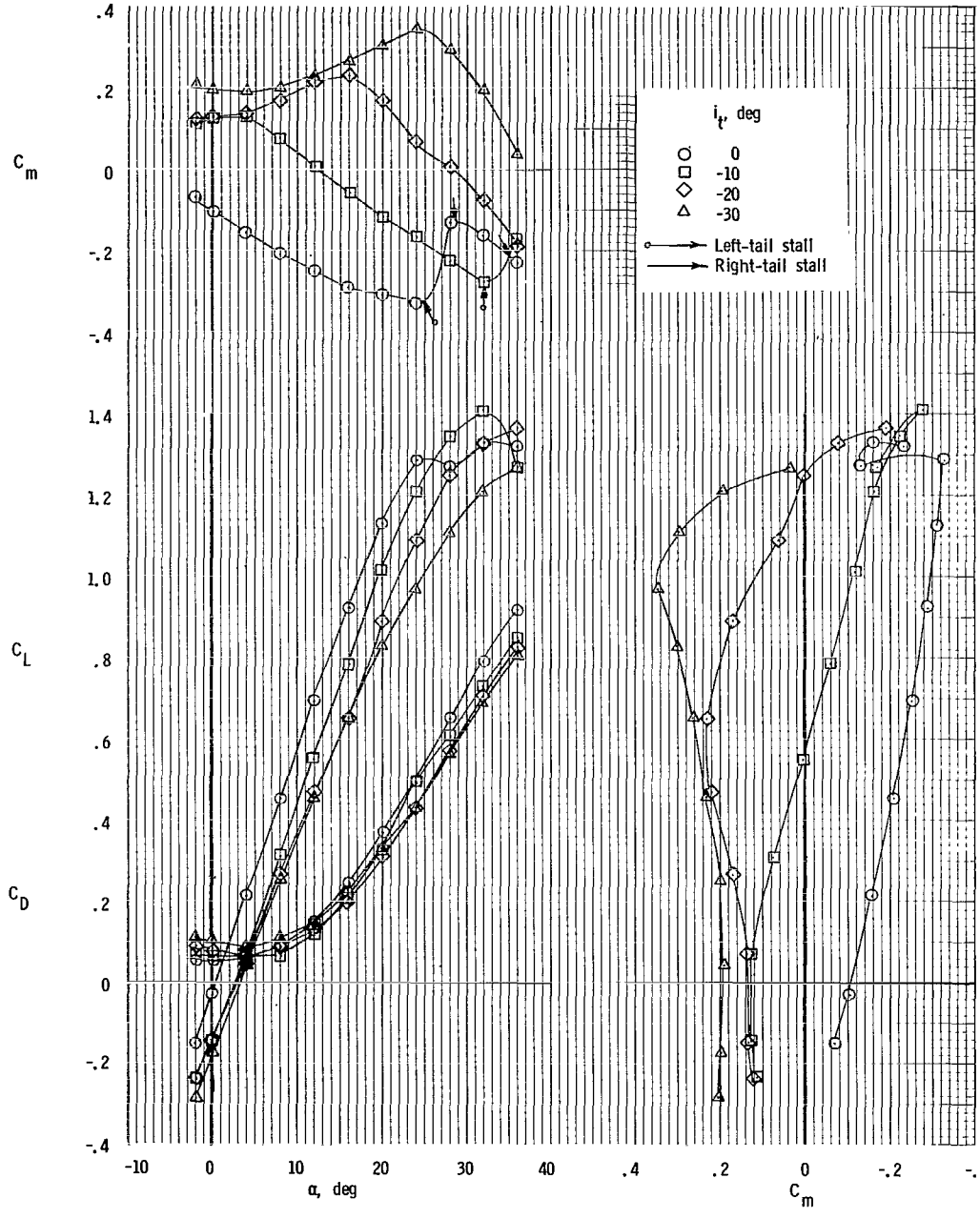

(b) $\Theta = -10^{\circ}$.

Figure 38.- Continued.

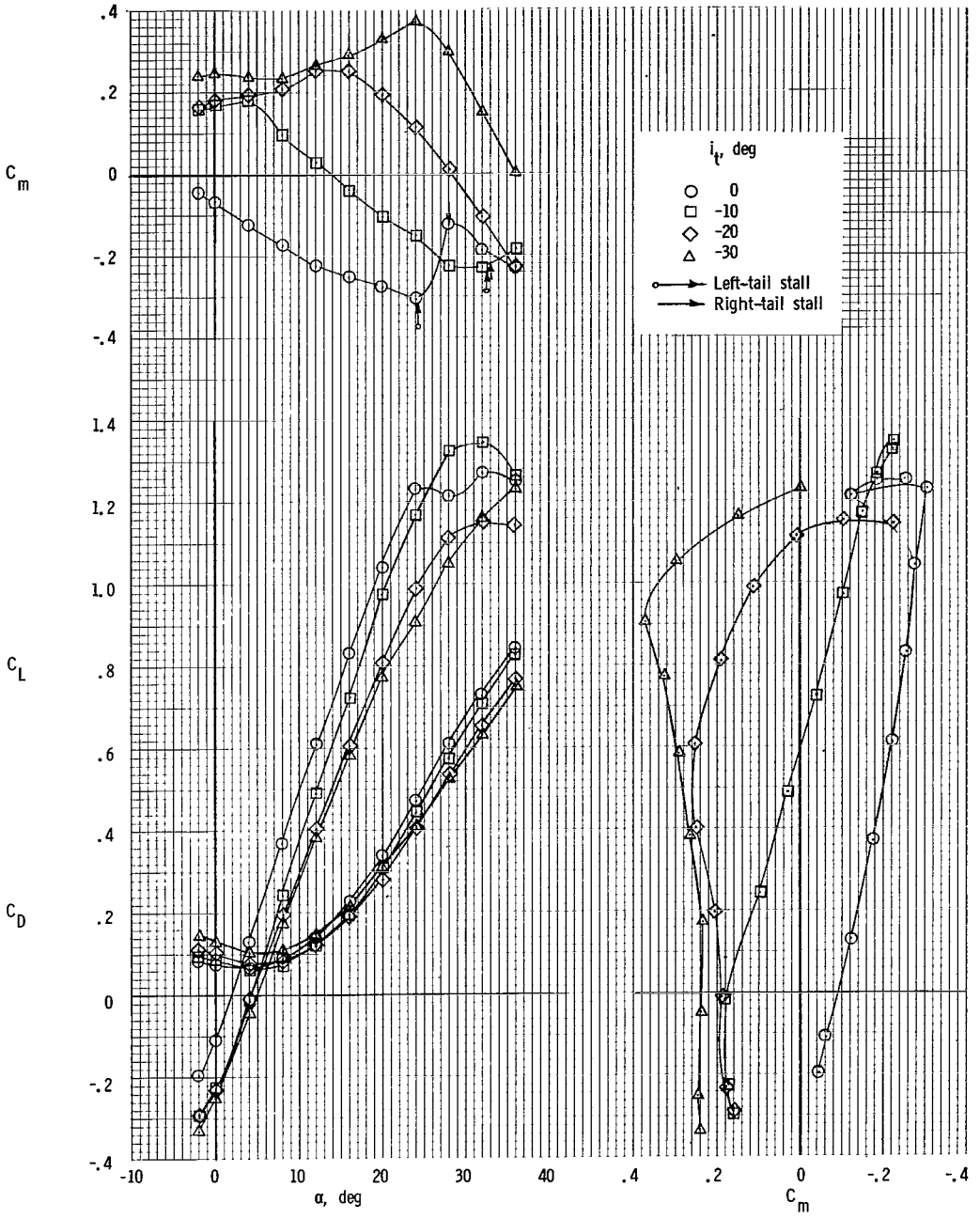

(c) $\Theta = -20^{\circ}$.

Figure 38.- Concluded.

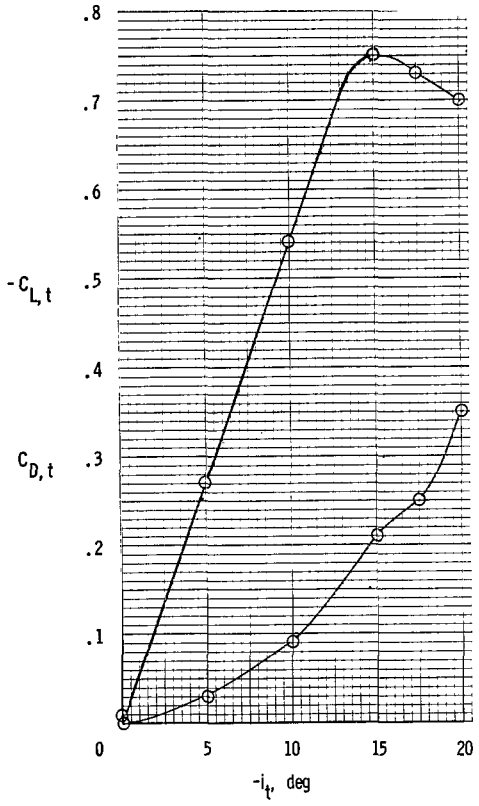

Figure 39.- Lift and drag characteristics of horizontal tail based on tail area. Center vertical tail; mid horizontal tail; $\Theta = 0^{\circ}$; $\alpha = 0^{\circ}$; rotor/wing 2.

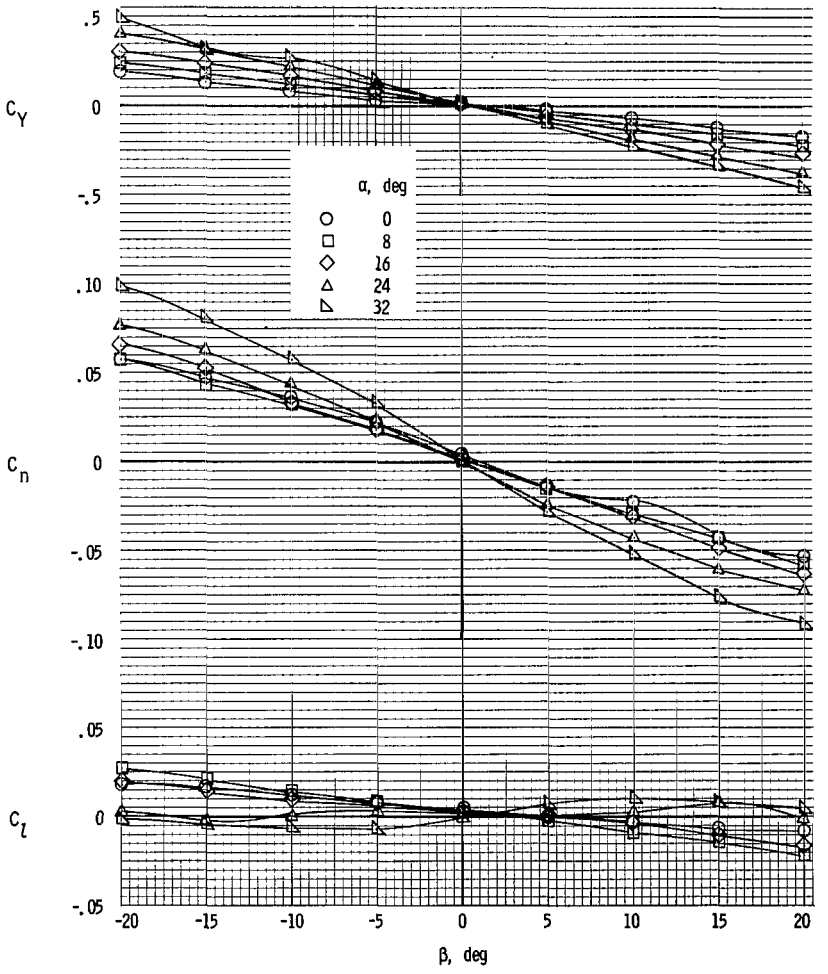

Figure 40.- Sideslip characteristics. Tails off; $\Theta = -10^{\circ}$; rotor/wing 2.

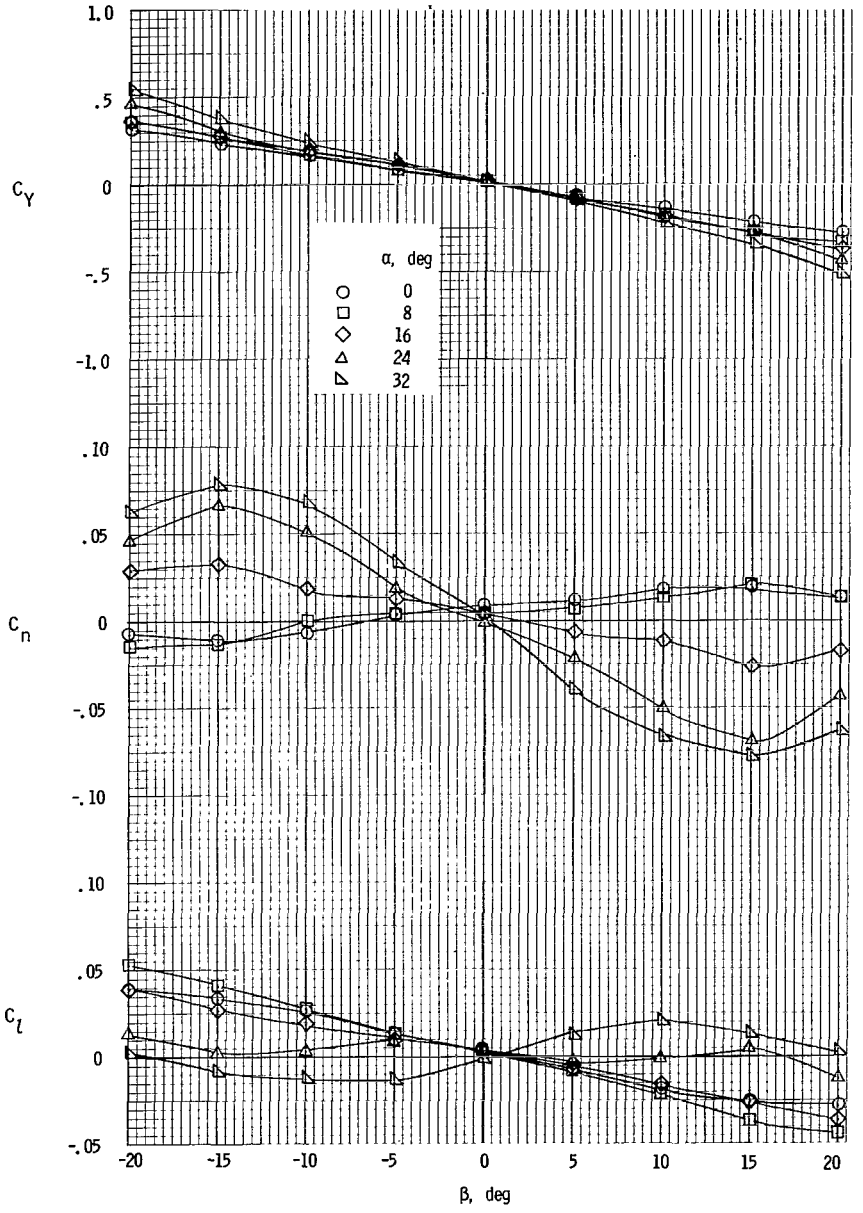

Figure 41.- Sideslip characteristics. Center vertical tail; mid horizontal tail; $i_t = -5^\circ$; $\Theta = -10^\circ$; rotor/wing 2.

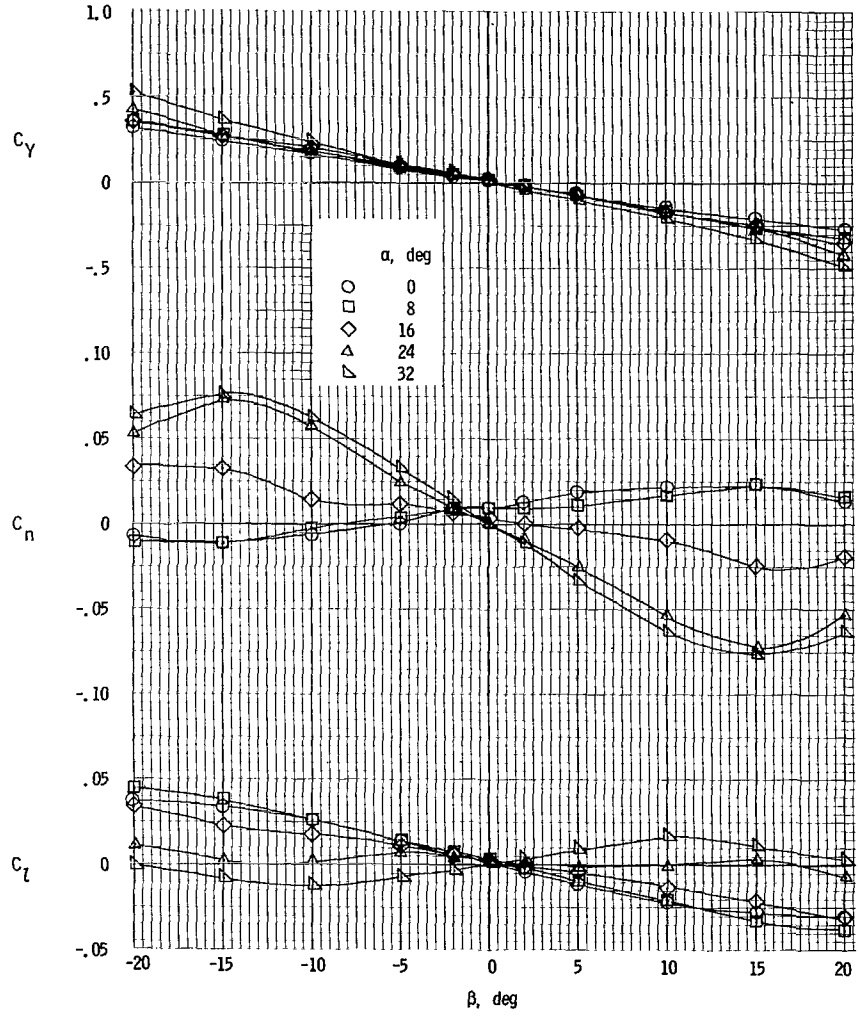

Figure 42.- Sideslip characteristics. Center vertical tail; mid horizontal tail; $i_t = -10^\circ$; $\Theta = -20^\circ$; rotor/wing 2.

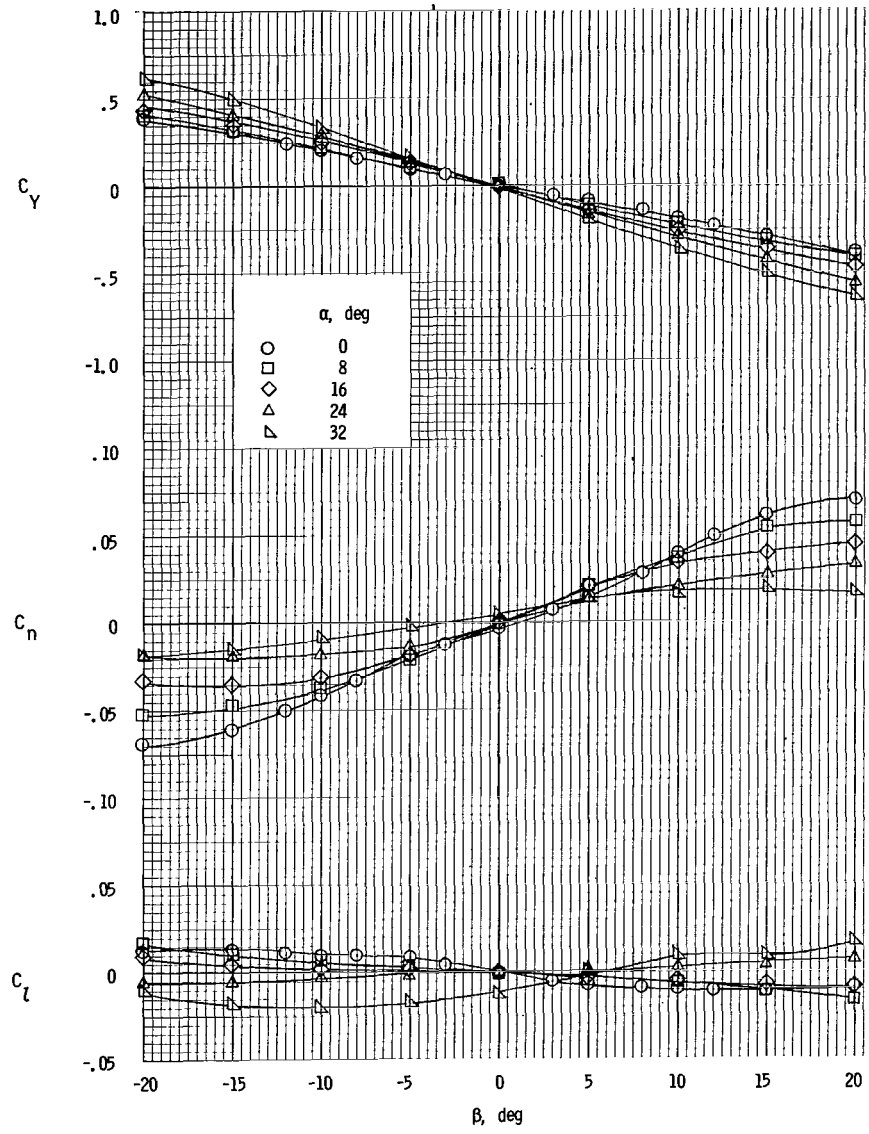

Figure 43.- Sideslip characteristics. Twin vertical tails; horizontal tail at center fuselage; $i_t = -10^\circ$; $\Theta = -10^\circ$; rotor/wing 2.

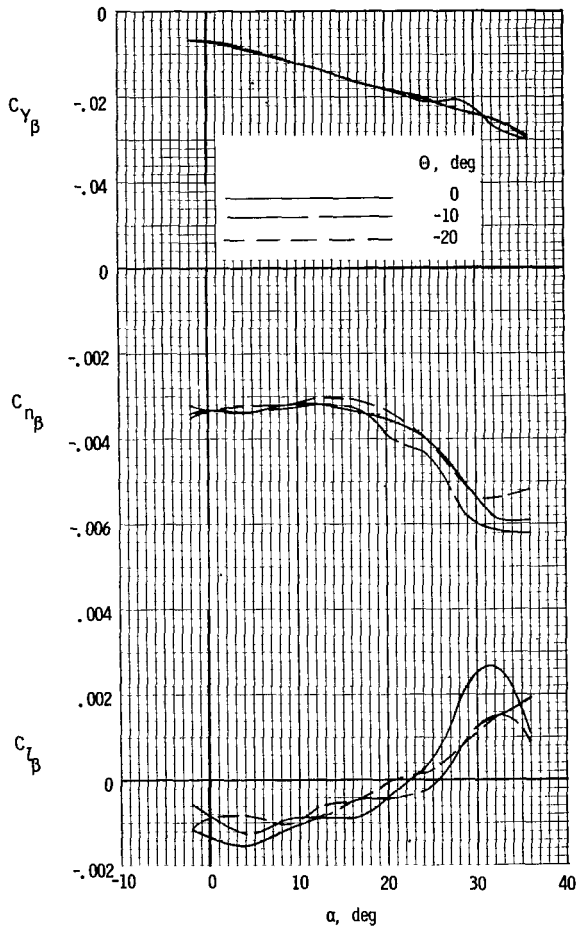

Figure 44.- Static lateral-stability derivatives. Tails off; rotor/wing 2.

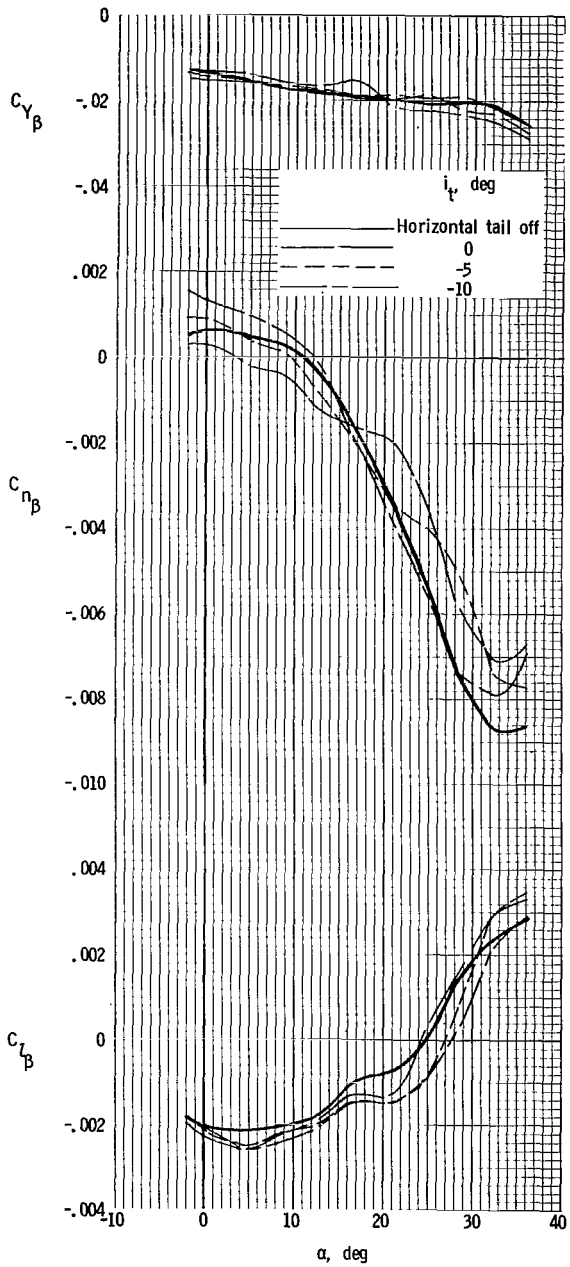

Figure 45.- Effect of horizontal tail on static lateral-stability derivatives. Center vertical tail; mid horizontal tail; $\Theta = -10^\circ$; rotor/wing 2.

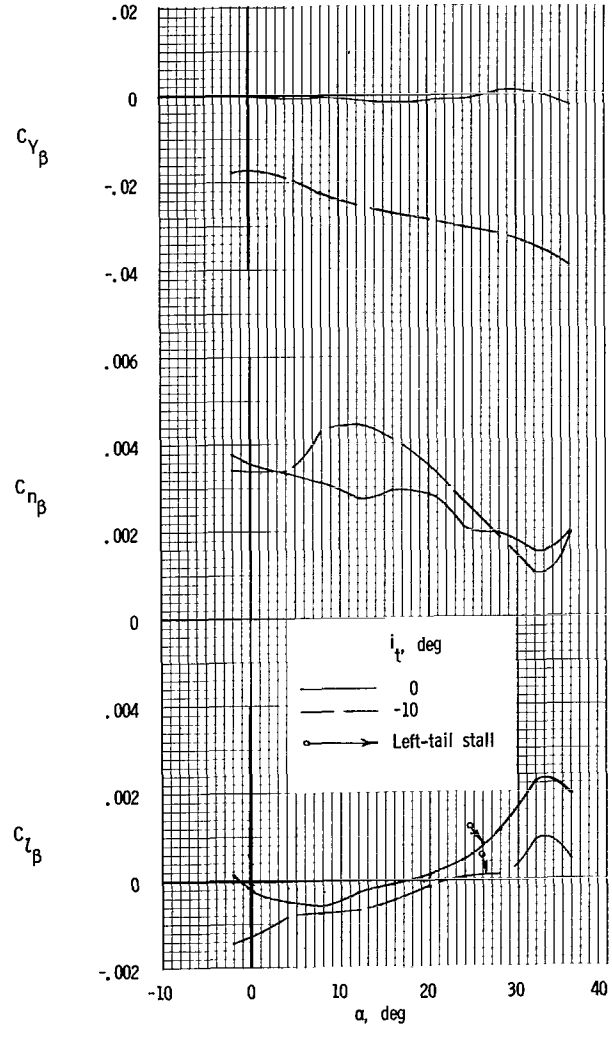

Figure 46.- Effect of horizontal tail on static lateral-stability derivatives. Twin vertical tails; horizontal tail at center fuselage; $\Theta = -10^{\circ}$; rotor/wing 2.

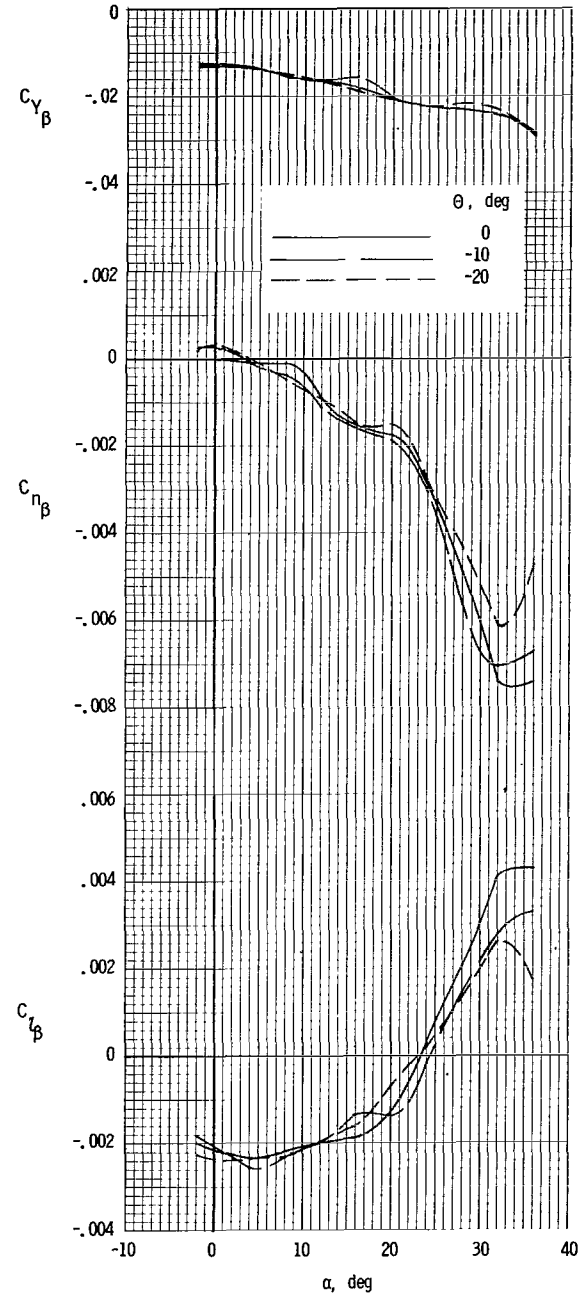

Figure 47.- Static lateral-stability derivatives. Center vertical tail; mid horizontal tail; $i_t = 0^{\circ}$; rotor/wing 2.

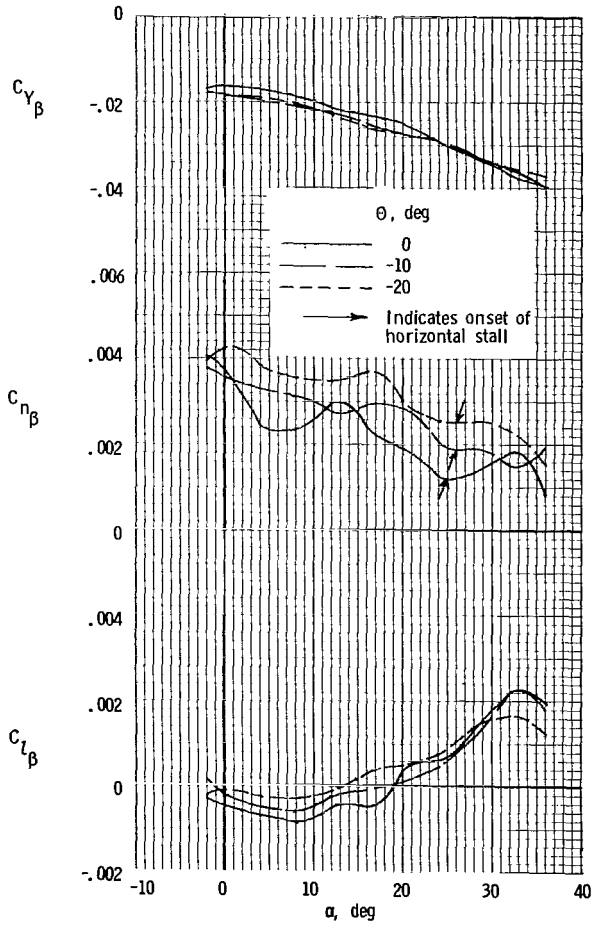

Figure 48.- Static lateral-stability derivatives. Twin vertical tails; horizontal tail at center fuselage; $i_t = 0^o$; rotor/wing 2.

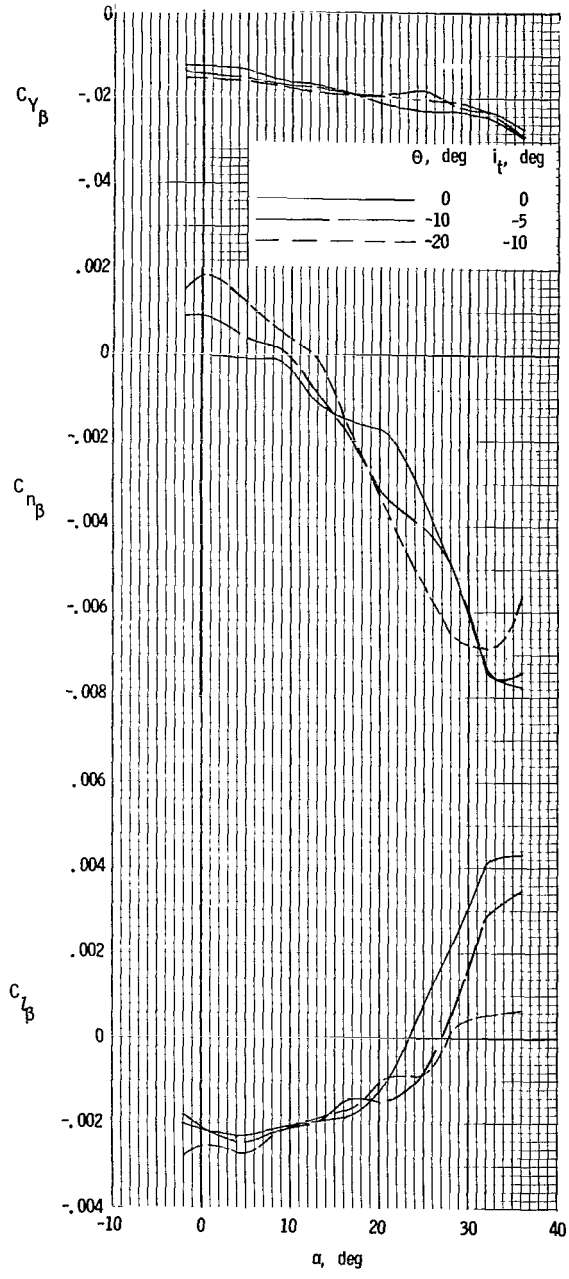

Figure 49.- Static lateral-stability derivatives for combinations of Θ and i_t. Center vertical tail; mid horizontal tail; rotor/wing 2.

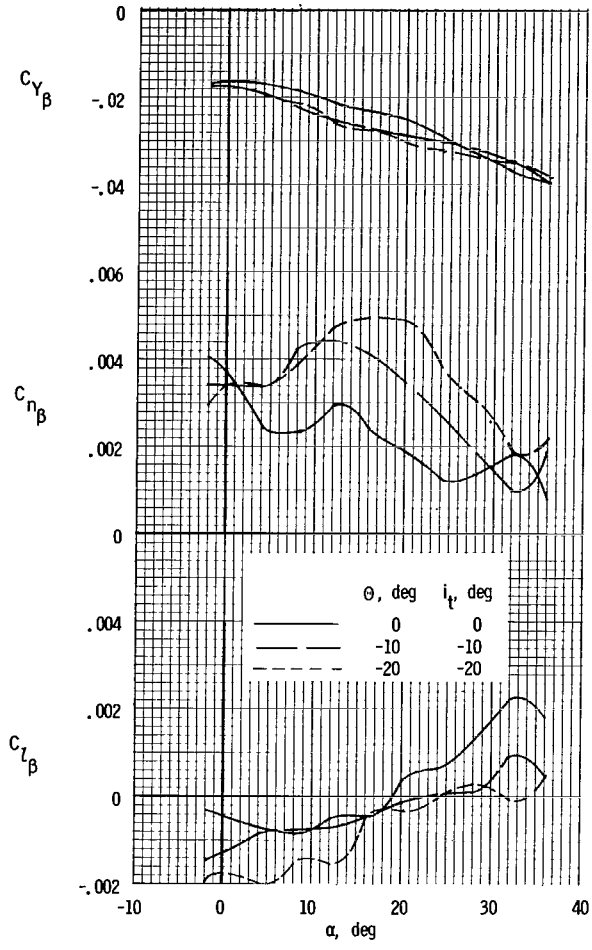

Figure 50.- Static lateral-stability derivatives for combinations of Θ and i_t. Twin vertical tails; horizontal tail at center fuselage; rotor/wing 2.

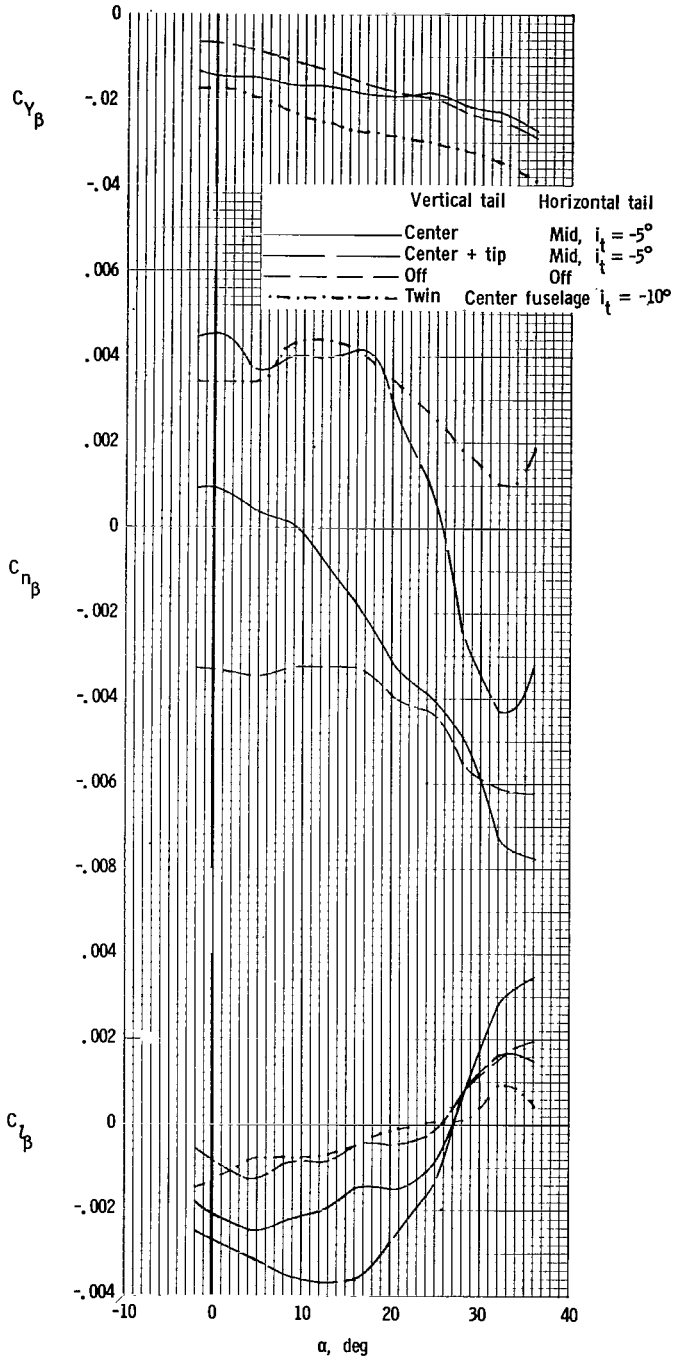

(a) Complete model characteristics.

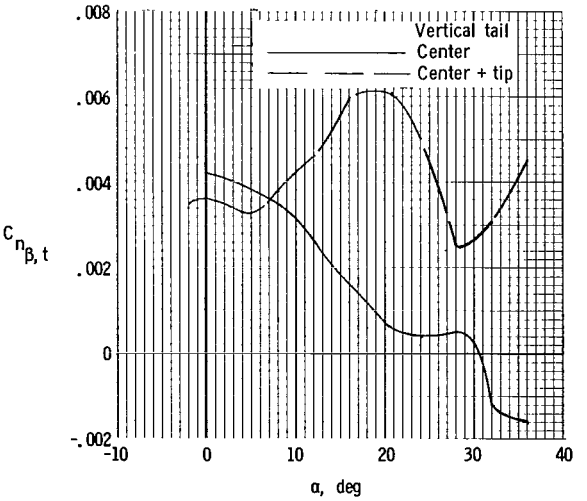

(b) Vertical-tail contribution.

Figure 51.- Effect of vertical-tail configuration on static lateral-stability derivatives. $\Theta = -10^\circ$; rotor/wing 2.

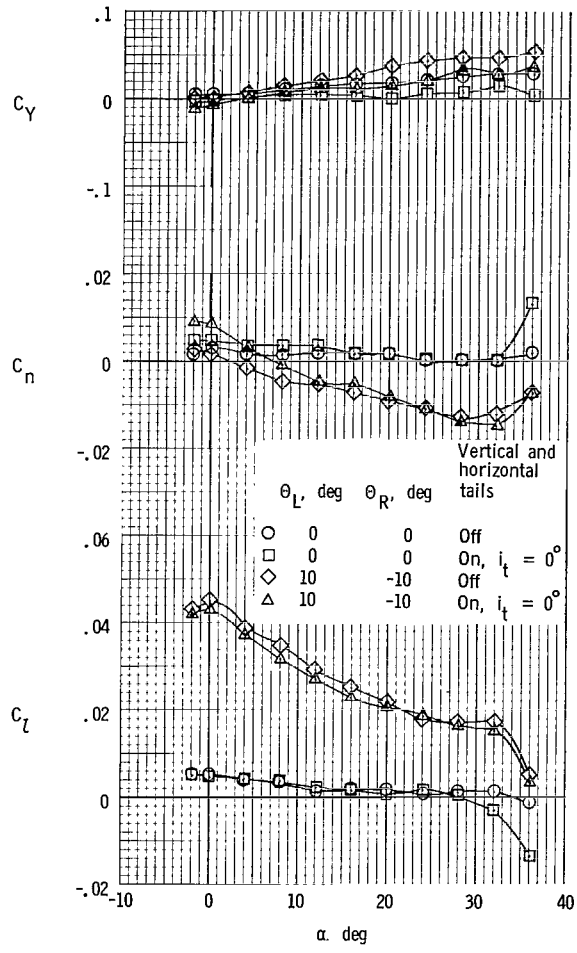

Figure 52.- Effect of tails on lateral-control characteristics with rotor blades used for control. Center vertical tail; mid horizontal tail; Θ_{mean} = 0°; rotor/wing 2.

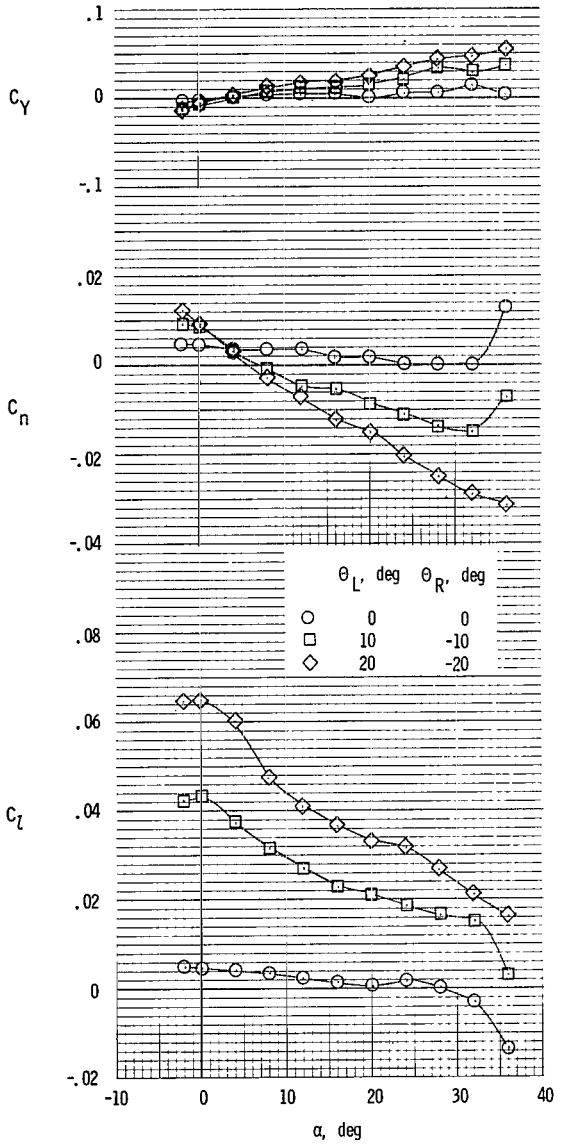

(a) $i_t = 0^\circ$; $\Theta_{mean} = 0^\circ$.

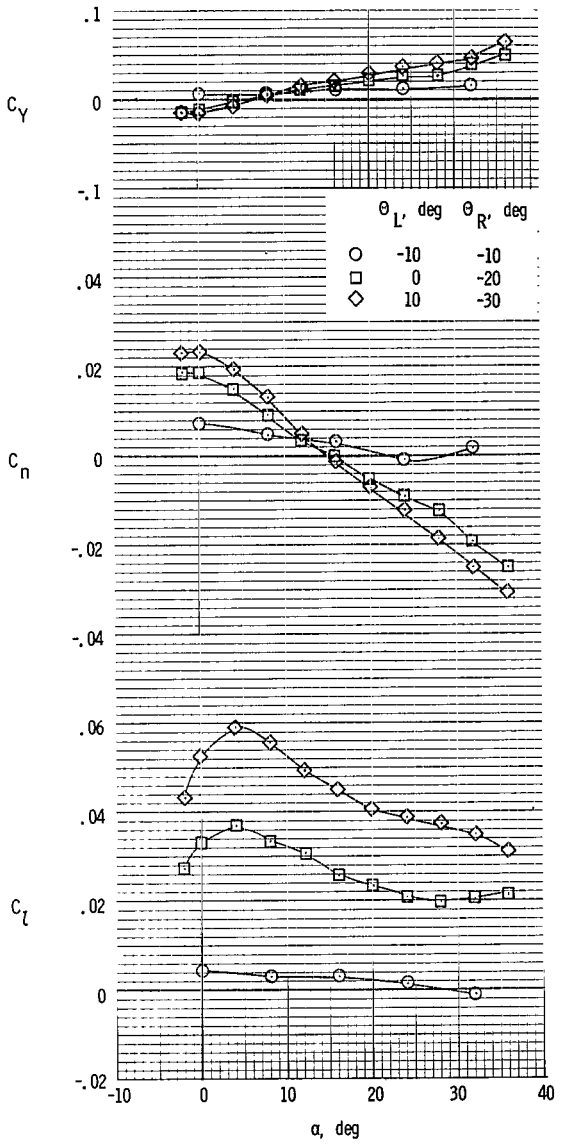

(b) $i_t = -5^\circ$; $\Theta_{mean} = -10^\circ$.

Figure 53.- Lateral-control characteristics with rotor blades used for control. Center vertical tail; mid horizontal tail; rotor/wing 2.

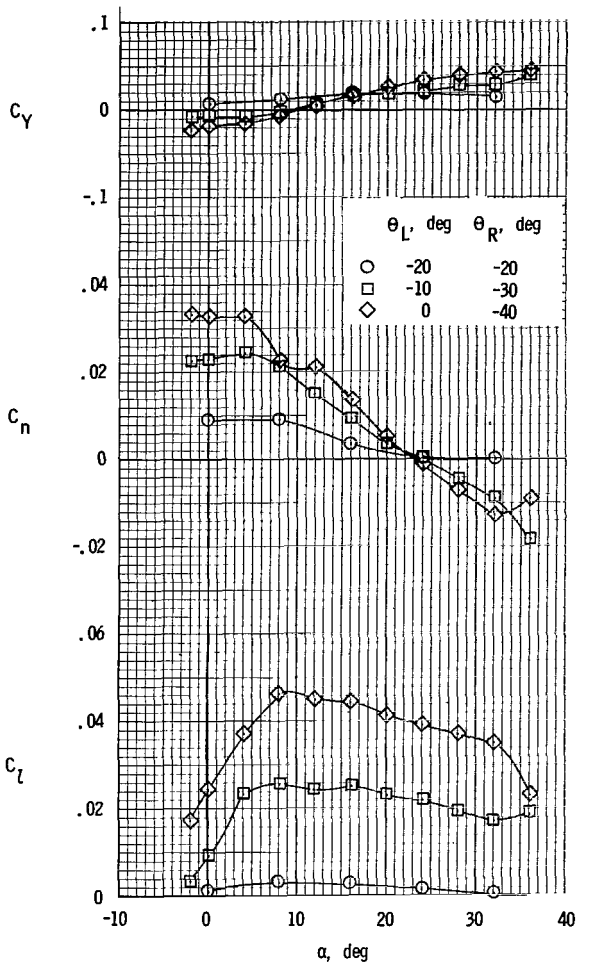

(c) $i_t = -10^\circ$; $\Theta_{mean} = -20^\circ$.

Figure 53.- Concluded.

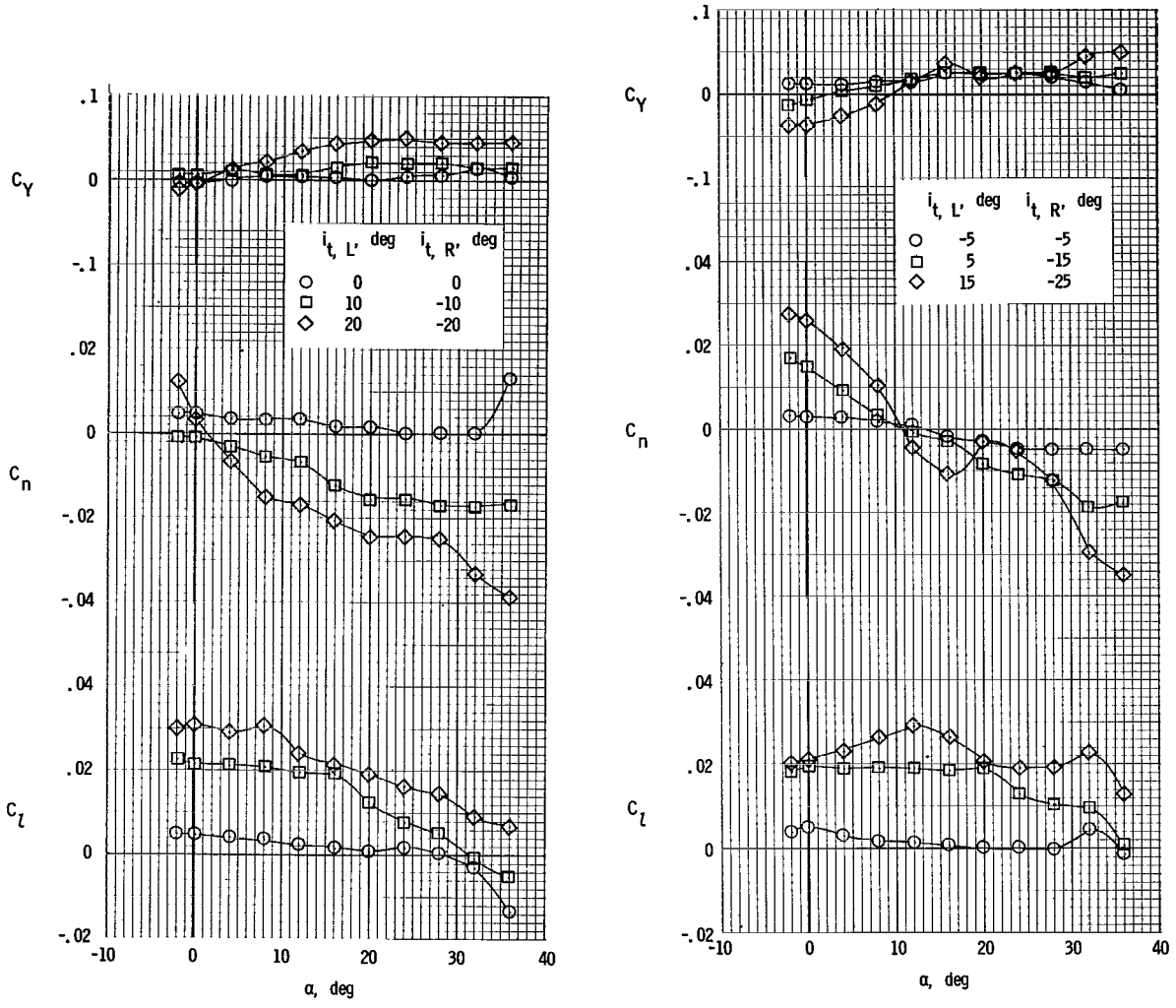

(a) $i_{t,mean} = 0^\circ$.

(b) $i_{t,mean} = -5^\circ$.

Figure 54.- Lateral-control characteristics with horizontal tail used for control. Center vertical tail; mid horizontal tail; $\Theta = 0^\circ$; rotor/wing 2.

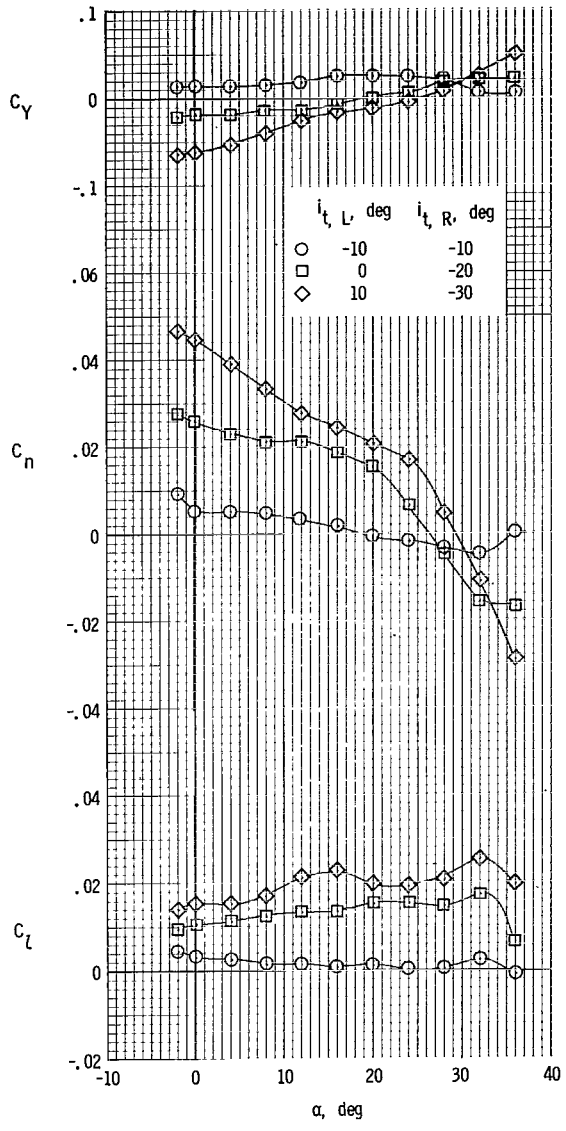

(c) $i_{t,mean} = -10^{\circ}$.

Figure 54.- Concluded.

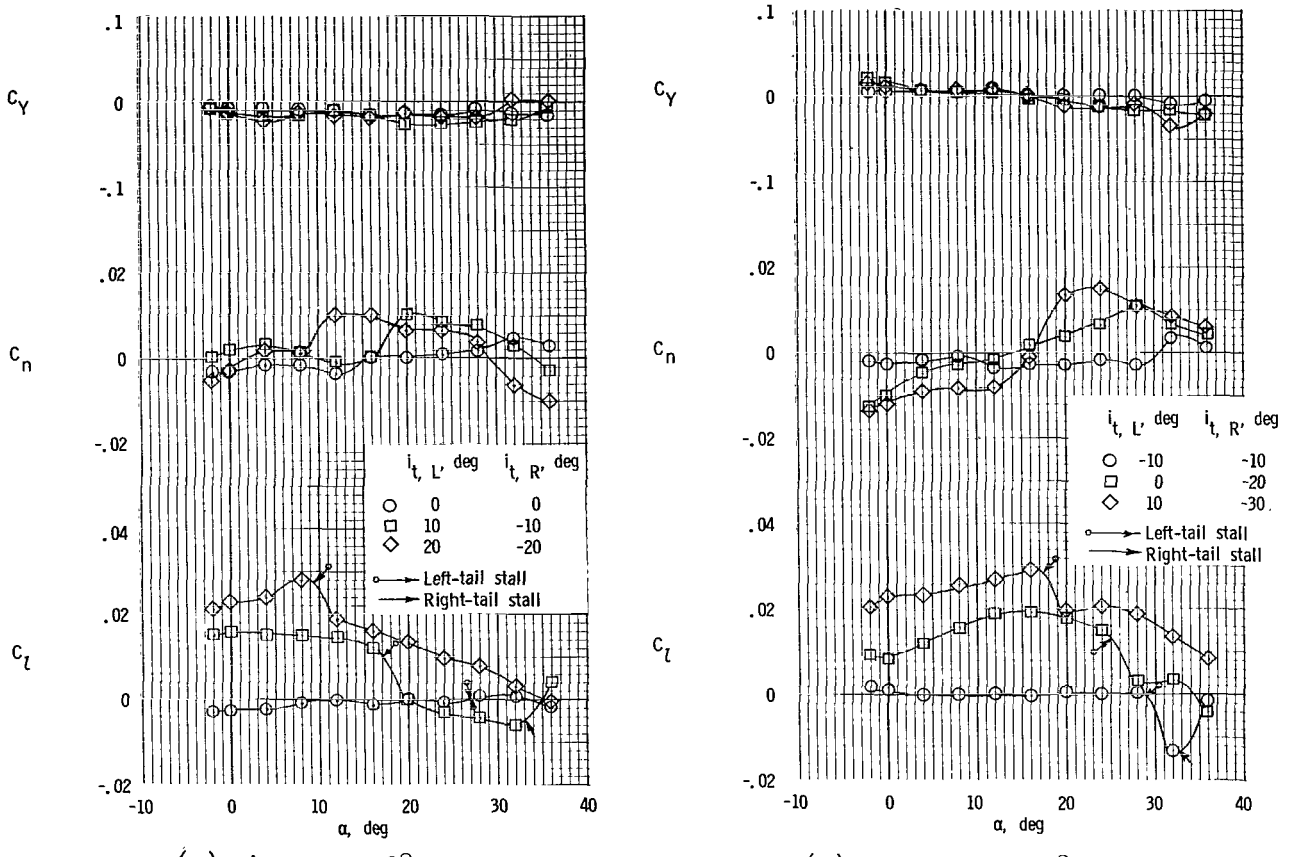

(a) $i_{t,mean} = 0^{\circ}$.

(b) $i_{t,mean} = -10^{\circ}$.

Figure 55.- Lateral-control characteristics with horizontal tail used for control. Twin vertical tails; horizontal tail at center fuselage; $\Theta = 0^{\circ}$; rotor/wing 2.

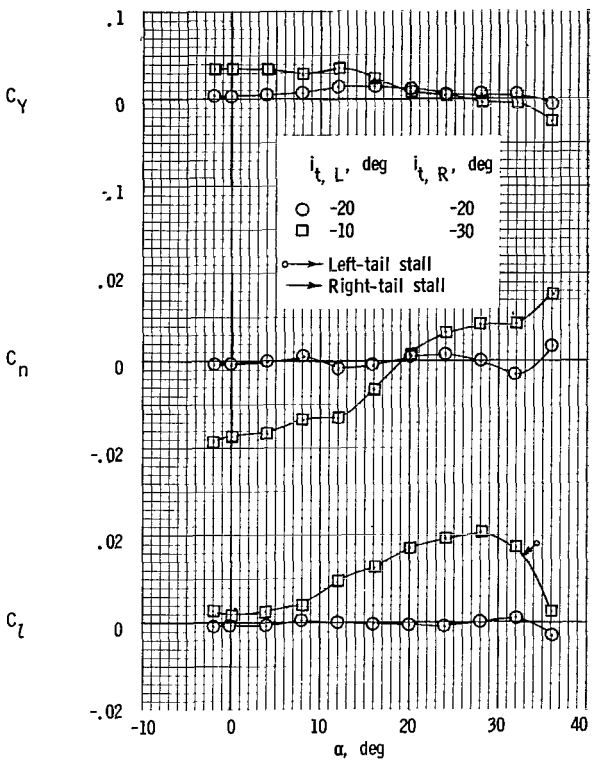

(c) $i_{t,mean} = -20^{\circ}$.

Figure 55.- Concluded.

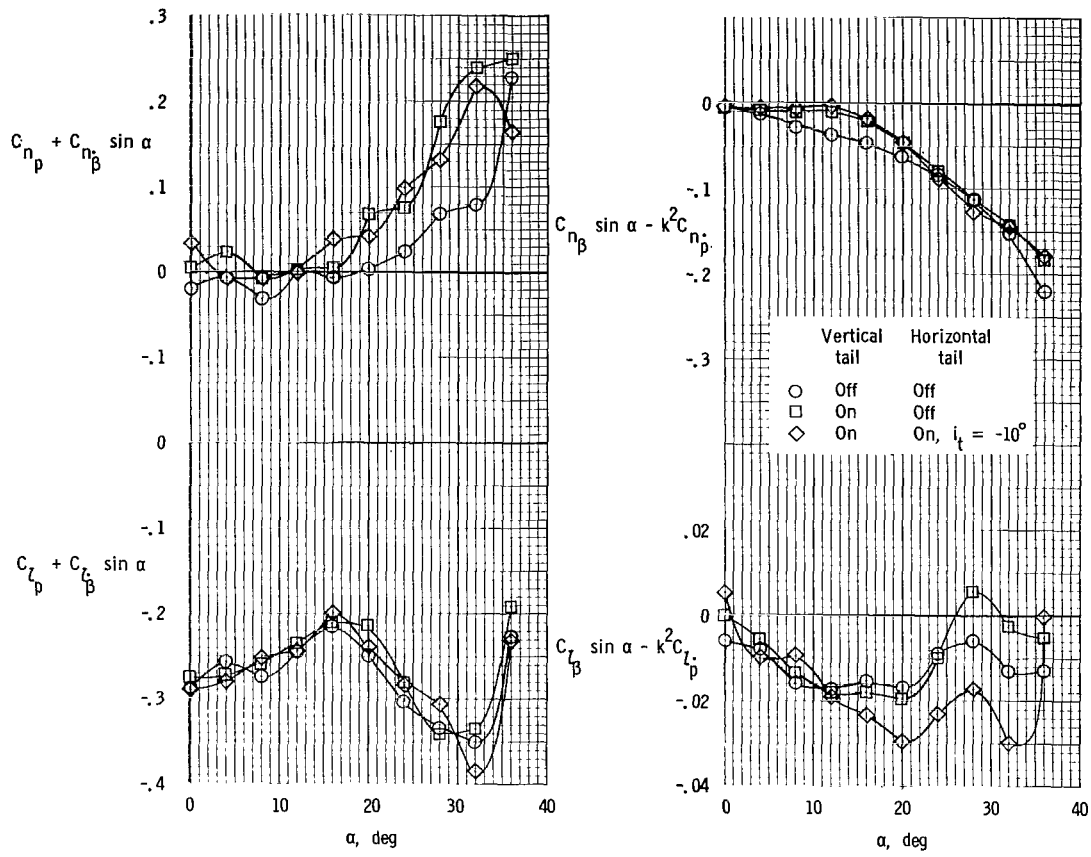

(a) Out-of-phase derivatives.

(b) In-phase derivatives.

Figure 56.- Effect of tails on dynamic-stability derivatives measured in rolling-oscillation tests. Center vertical tail; mid horizontal tail; $\Theta = 0^\circ$; rotor/wing 2.

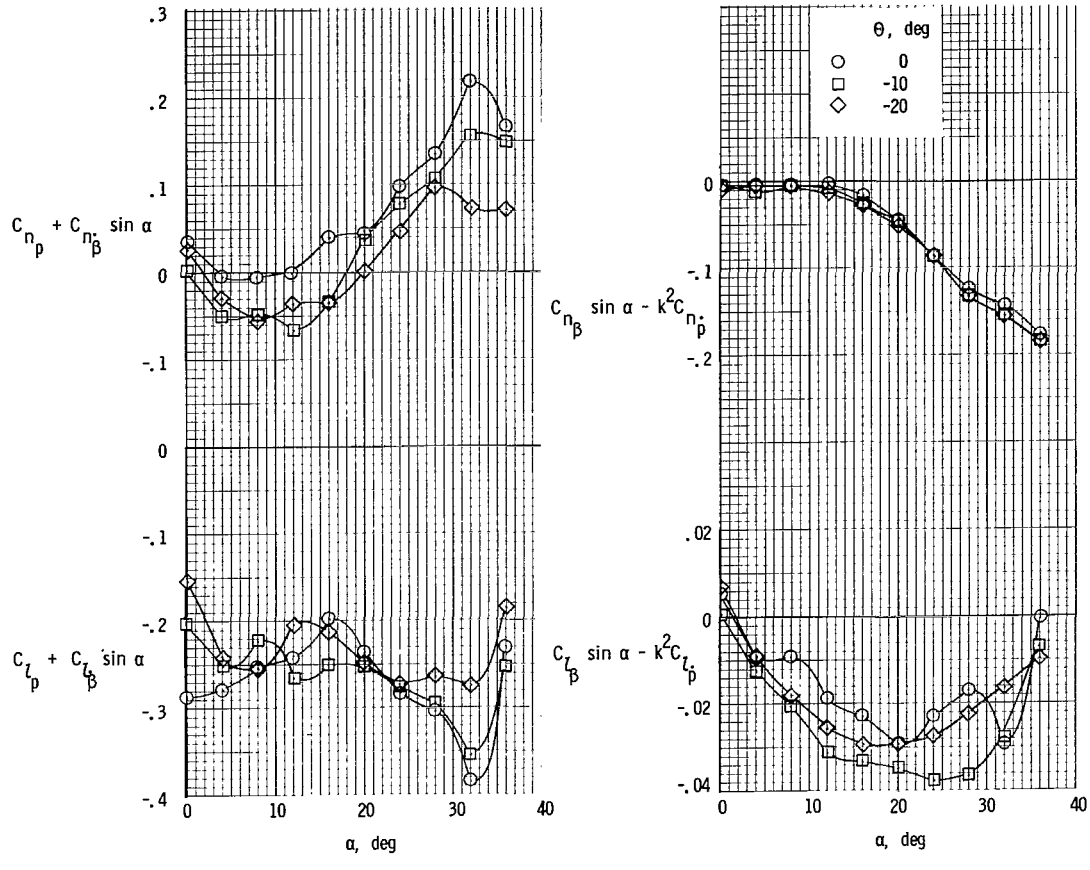

(a) Out-of-phase derivatives.

(b) In-phase derivatives.

Figure 57.- Effect of rotor-blade incidence on dynamic-stability derivatives measured in rolling-oscillation tests. Center vertical tail; mid horizontal tail; $i_t = -10^\circ$; rotor/wing 2.

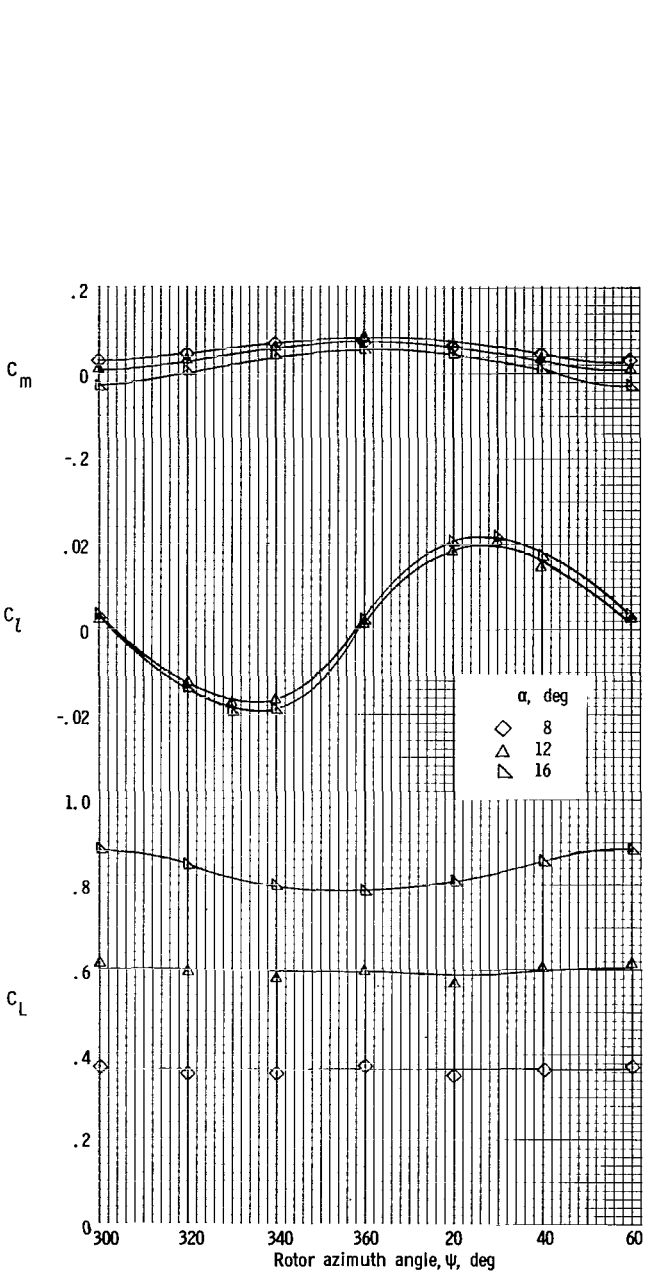

(a) Hub alone; $i_t = 0^o$.

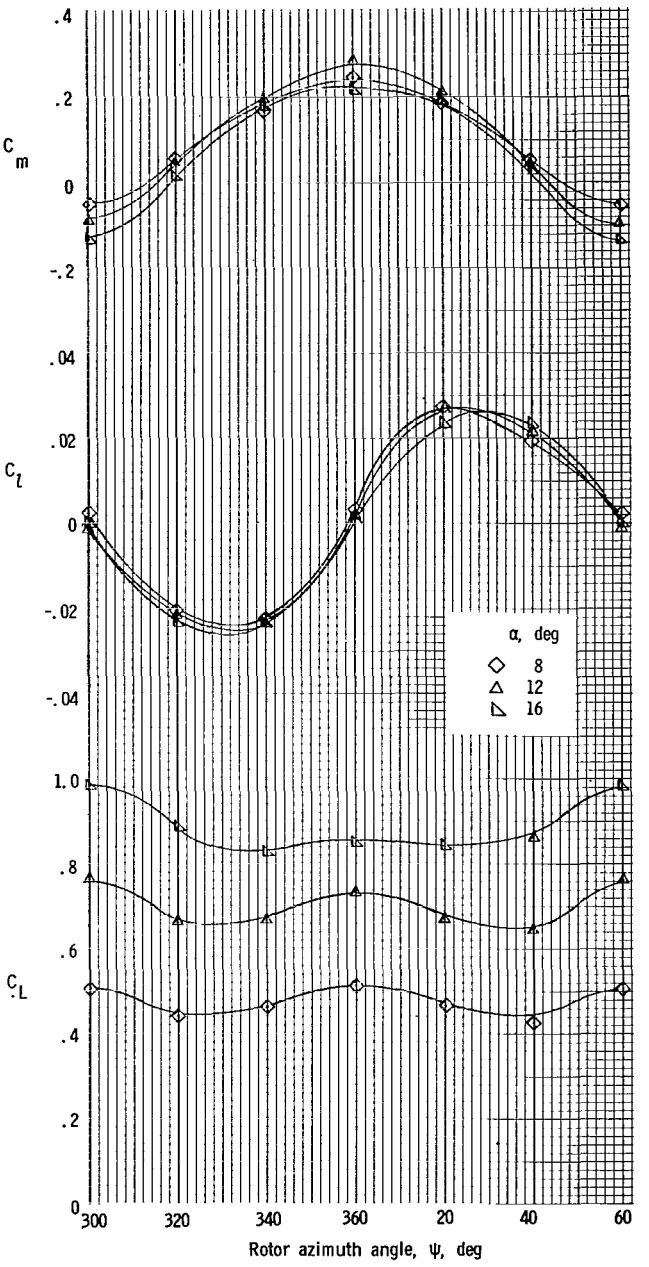

(b) $\Theta = 0^o$; $i_t = 0^o$.

Figure 58.- Effect of azimuth position on lift coefficient and rolling and pitching-moment coefficients for changes in model angle of attack. Rotor/wing 2.

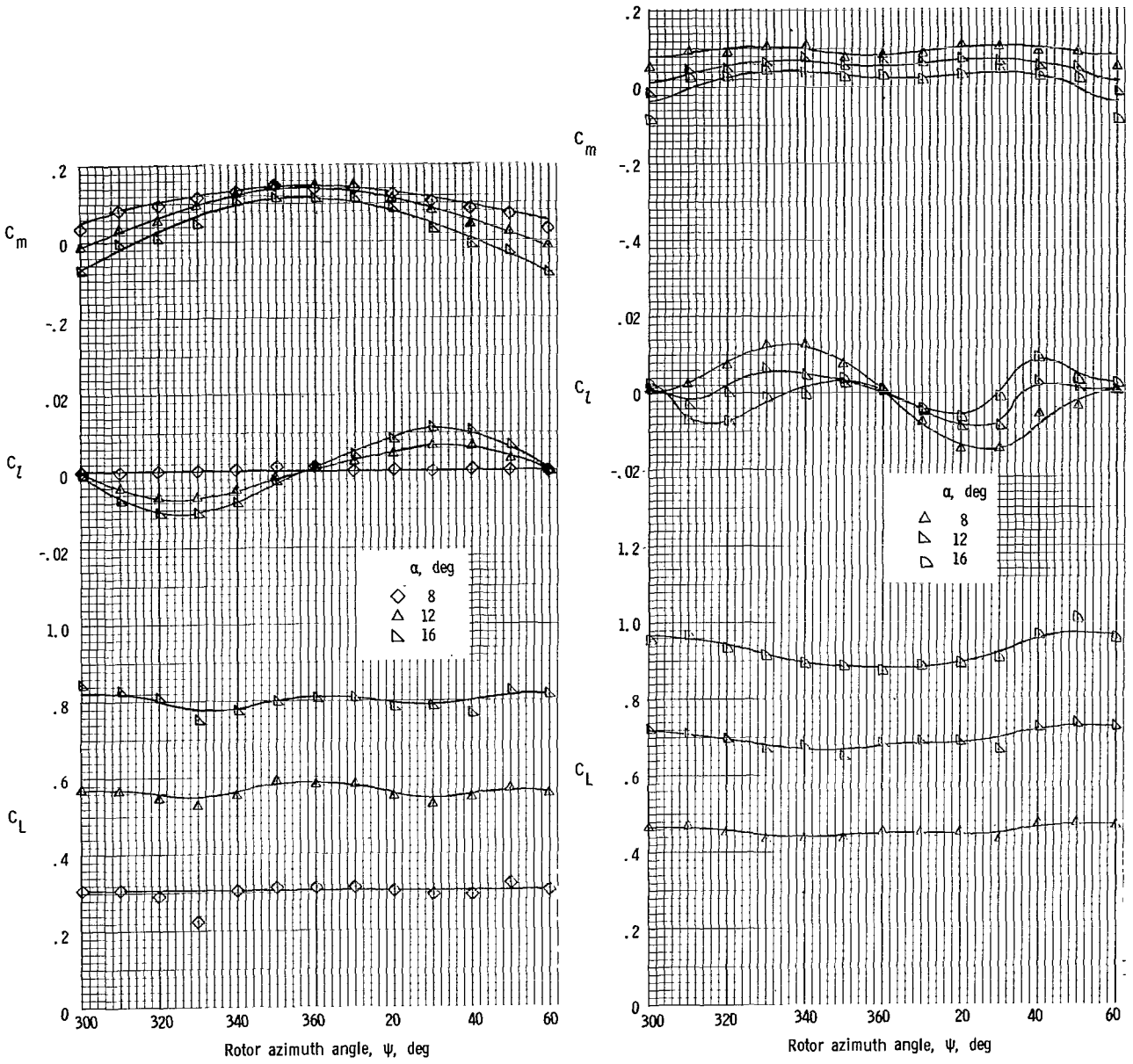

(c) $\Theta = -15^{\circ} \sin \psi$; $i_t = -10^{\circ}$.

(d) $\Theta = -30^{\circ} \sin \psi$; $i_t = 0^{\circ}$.

Figure 58.- Concluded.

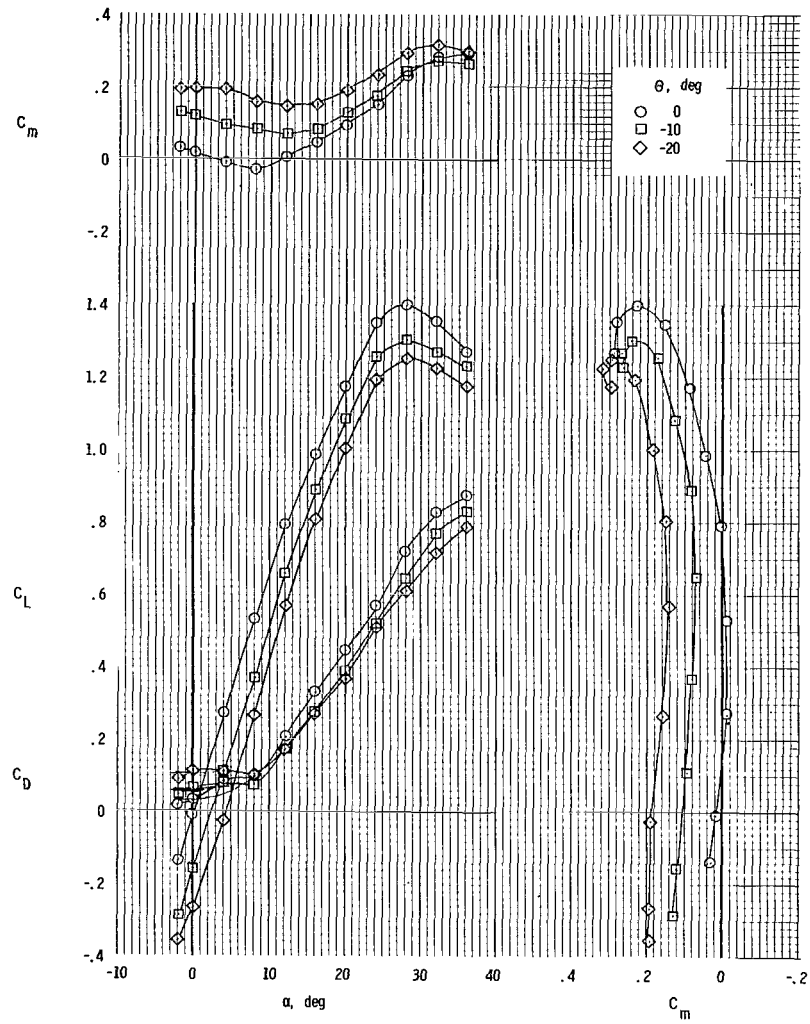

Figure 59.- Longitudinal aerodynamic characteristics. Horizontal tail off; center vertical tail; rotor/wing 3.

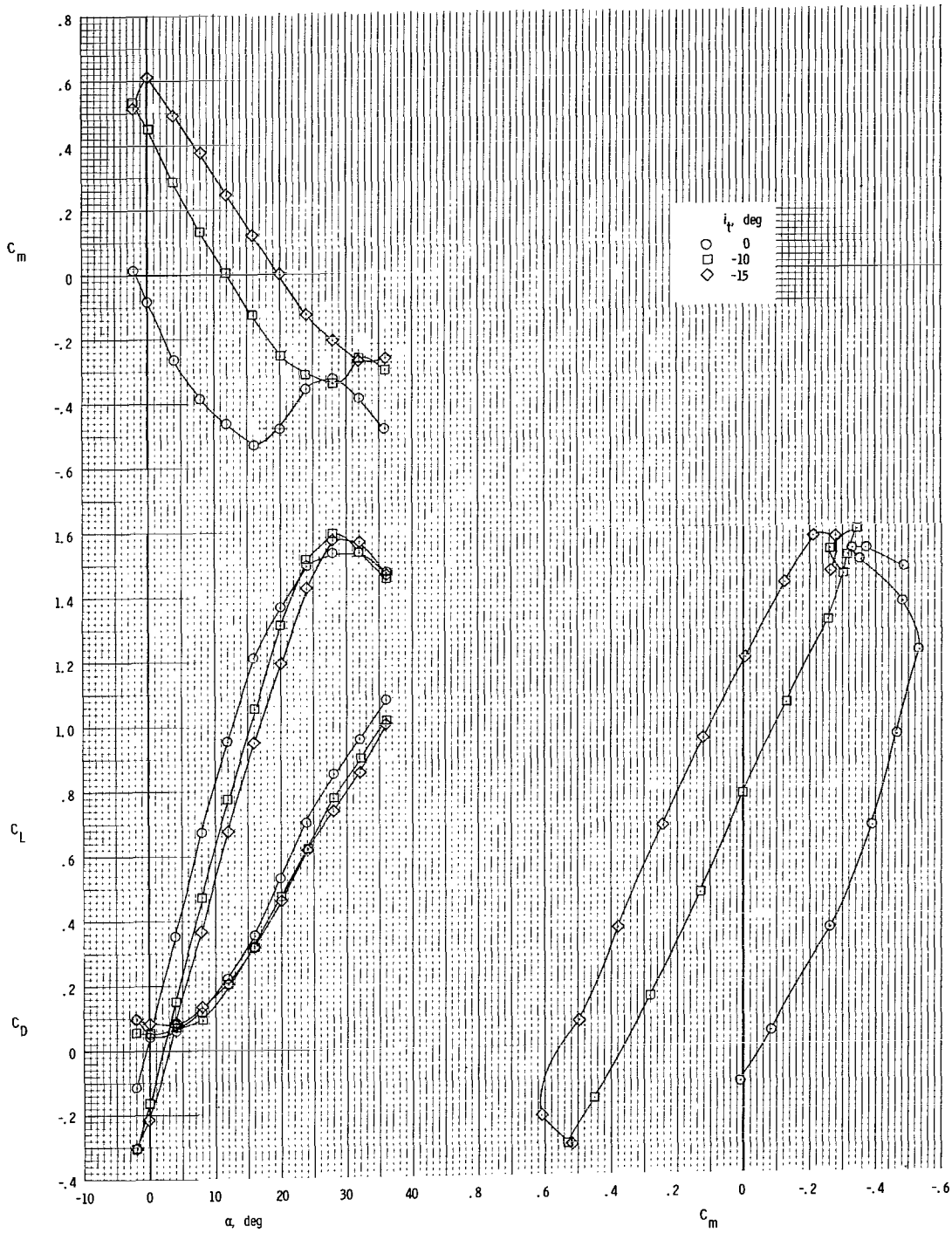

(a) $\Theta = 0^{\circ}$.

Figure 60.- Longitudinal aerodynamic characteristics. Low horizontal tail; center vertical tail; rotor/wing 3.

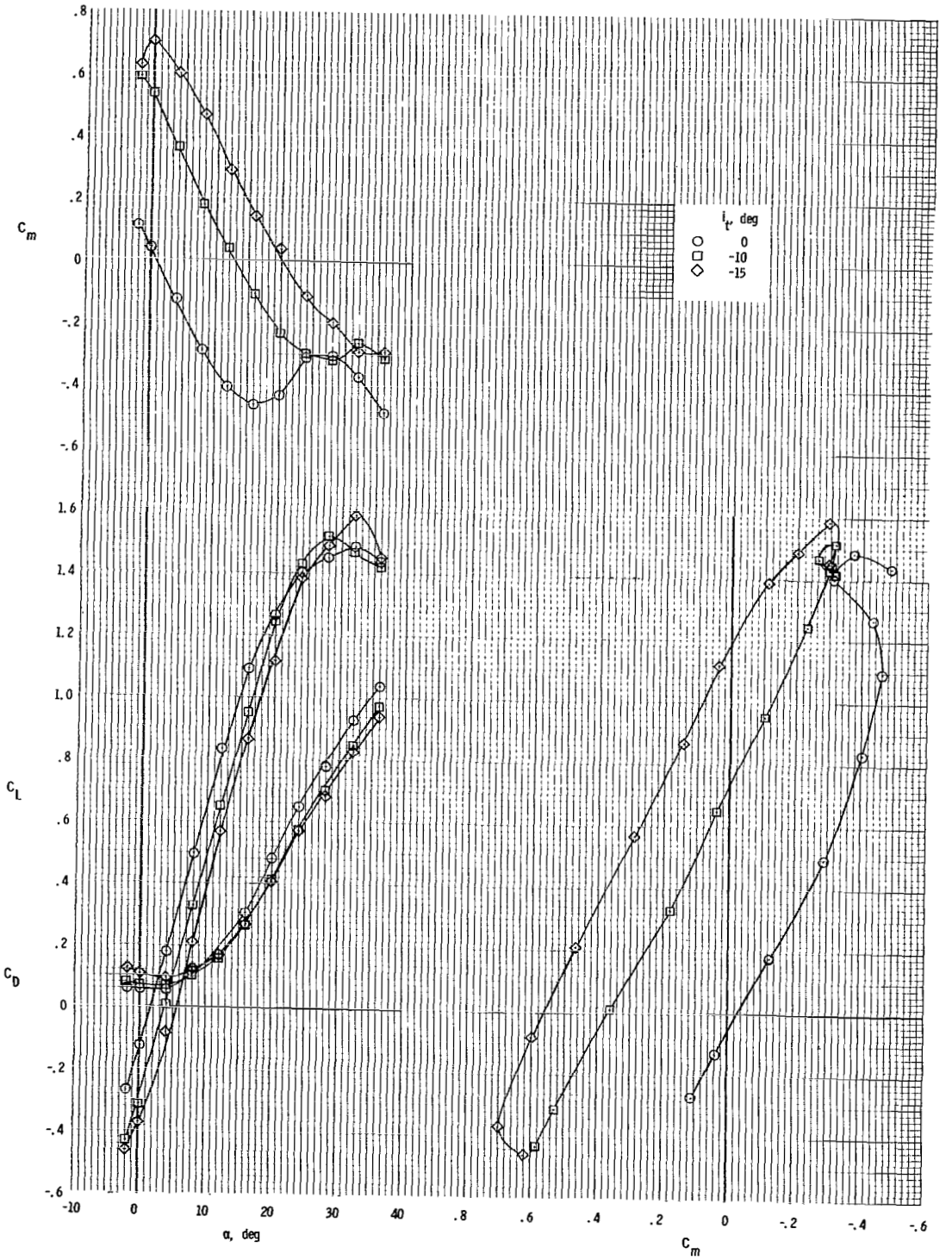

(b) $\Theta = -10^{\circ}$.

Figure 60.- Continued.

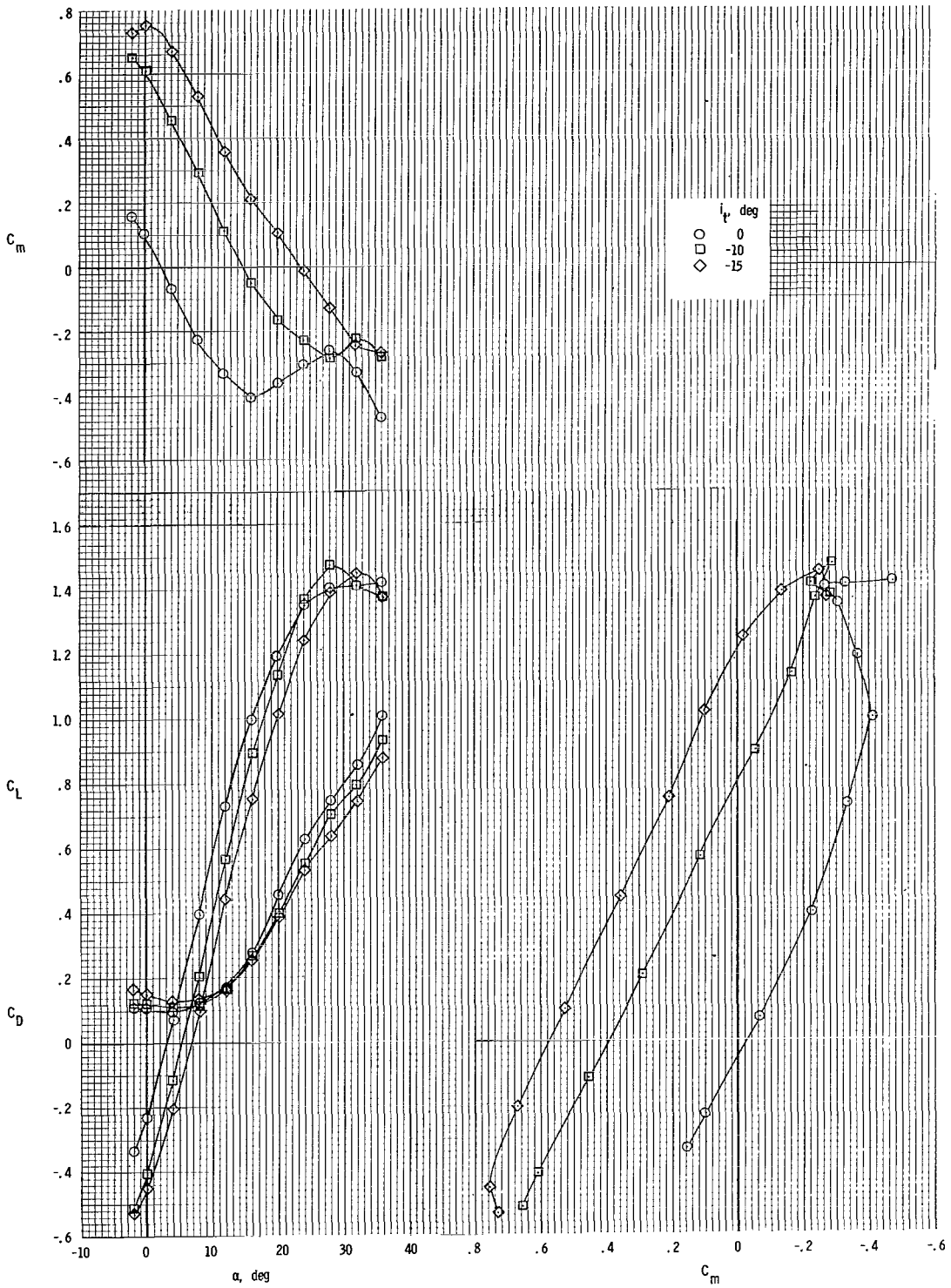

(c) $\Theta = -20^{\circ}$.

Figure 60.- Concluded.

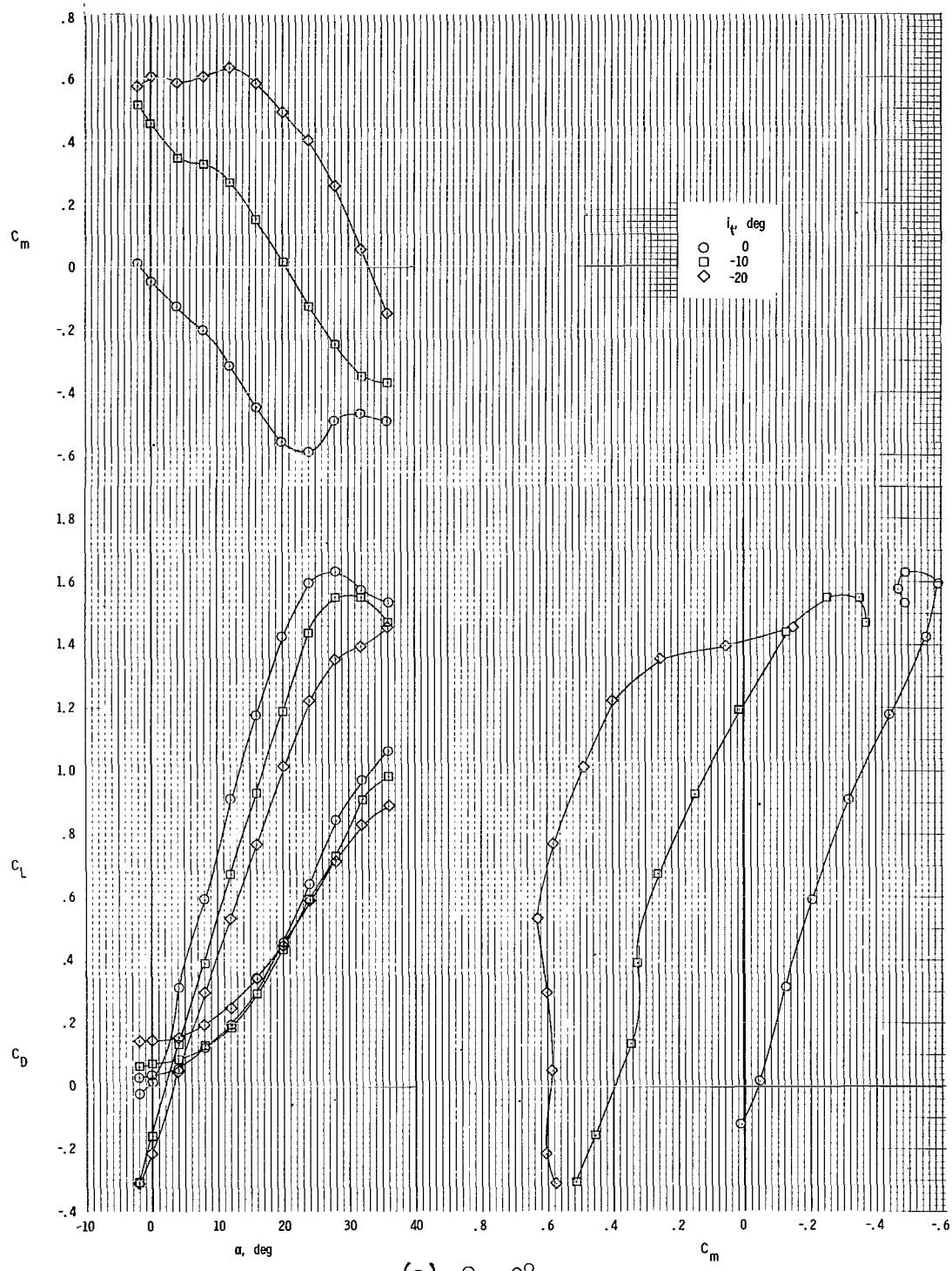

(a) $\Theta = 0^{\circ}$.

Figure 61.- Longitudinal aerodynamic characteristics. Mid horizontal tail; center vertical tail; rotor/wing 3.

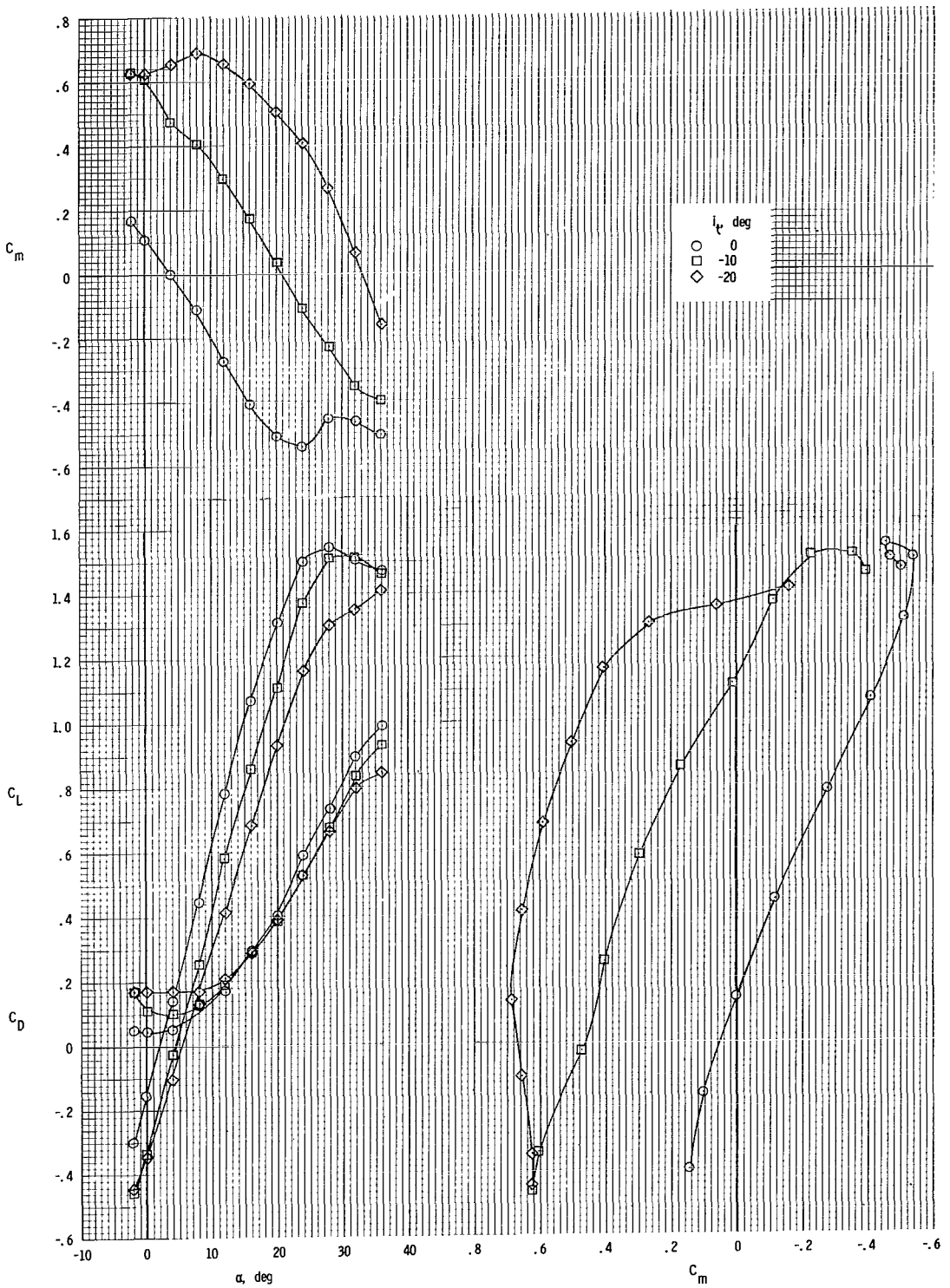

(b) $\Theta = -10^{\circ}$.

Figure 61.- Continued.

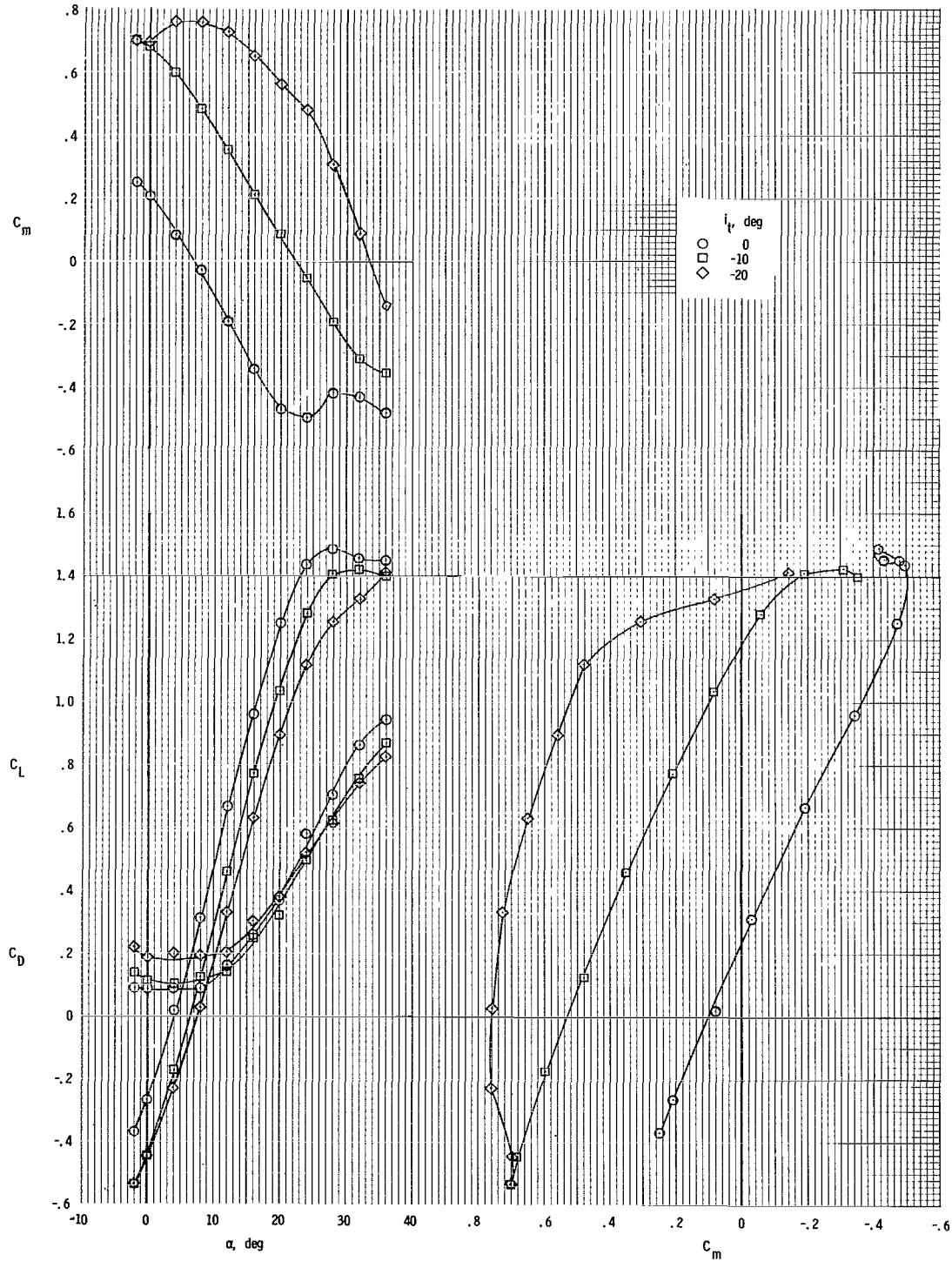

(c) $\Theta = -20^{\circ}$.

Figure 61.- Concluded.

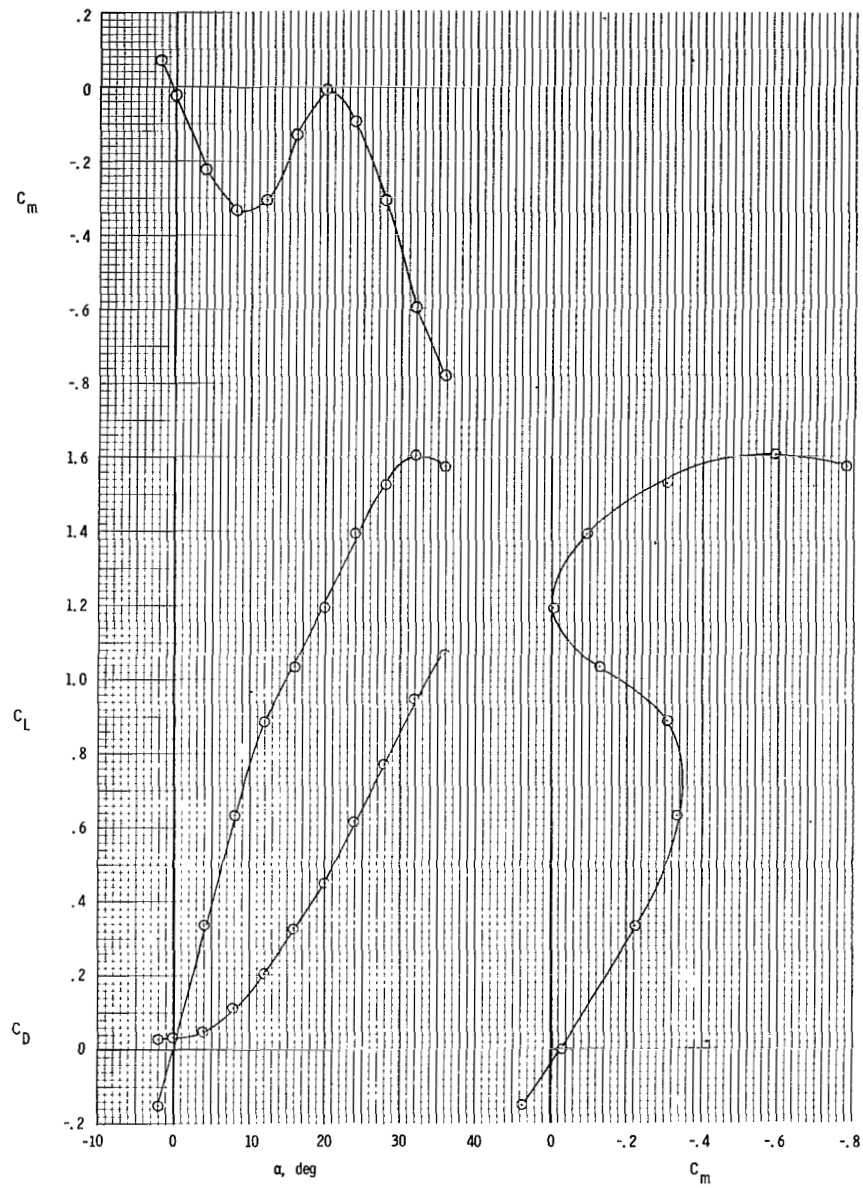

Figure 62.- Longitudinal aerodynamic characteristics. Center vertical tail; horizontal tail in high position; $i_t = 0^o$; $\Theta = 0^o$; rotor/wing 3.

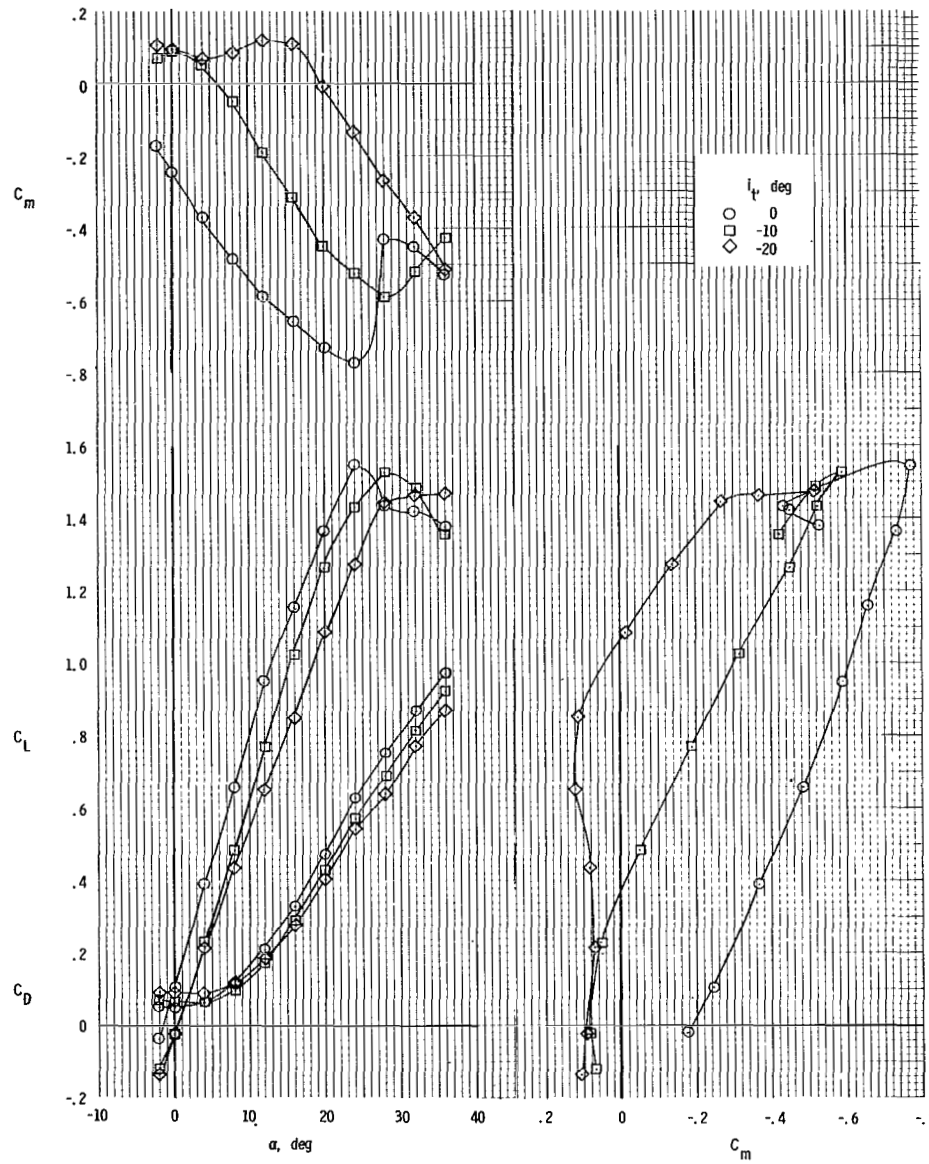

(a) $\Theta = 0^{\circ}$.

Figure 63.- Longitudinal aerodynamic characteristics. Horizontal tail at center fuselage; twin vertical tails; rotor/wing 3.

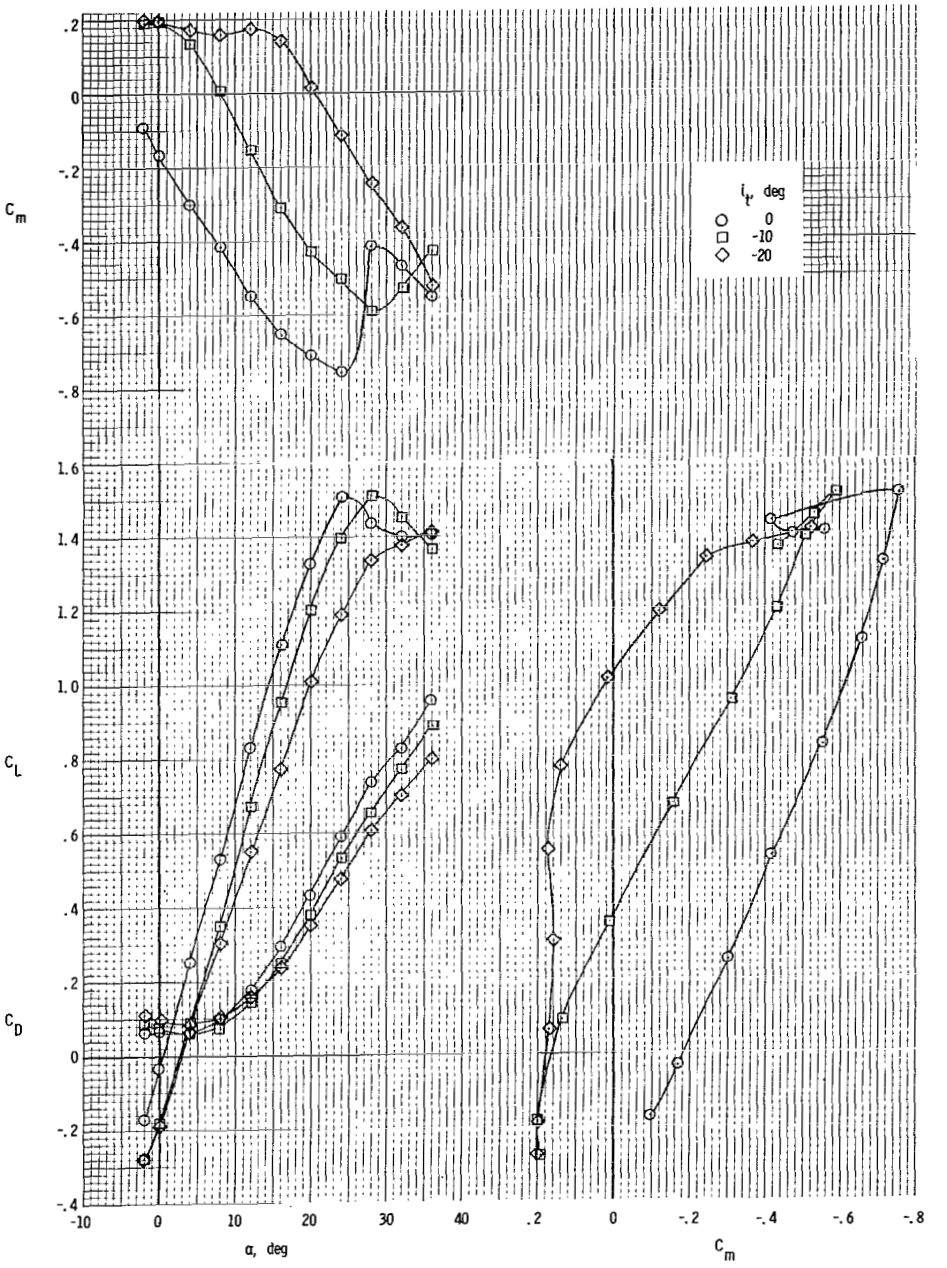

(b) $\Theta = -10^{\circ}$.

Figure 63.- Continued.

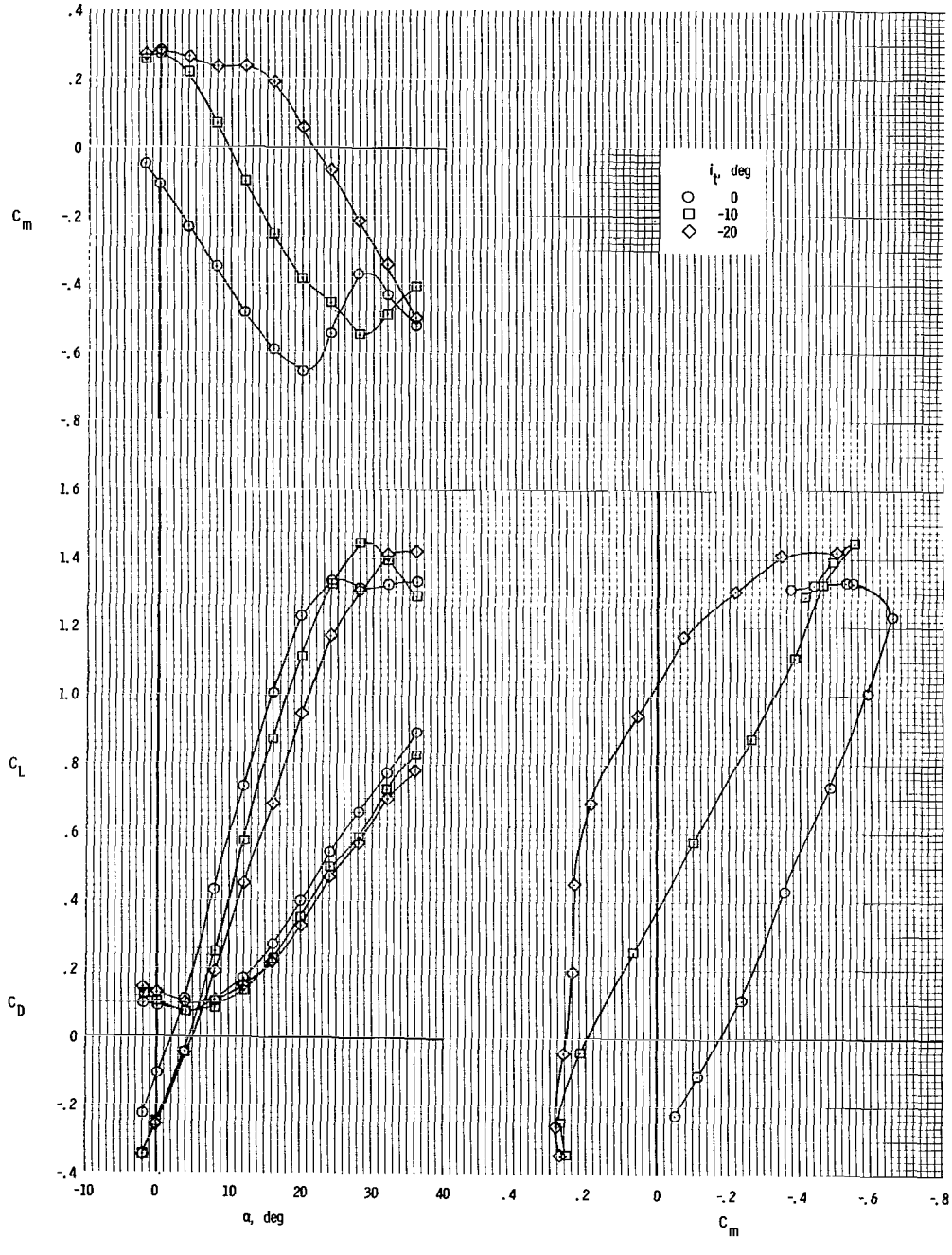

(c) $\Theta = -20°$.

Figure 63.- Concluded.

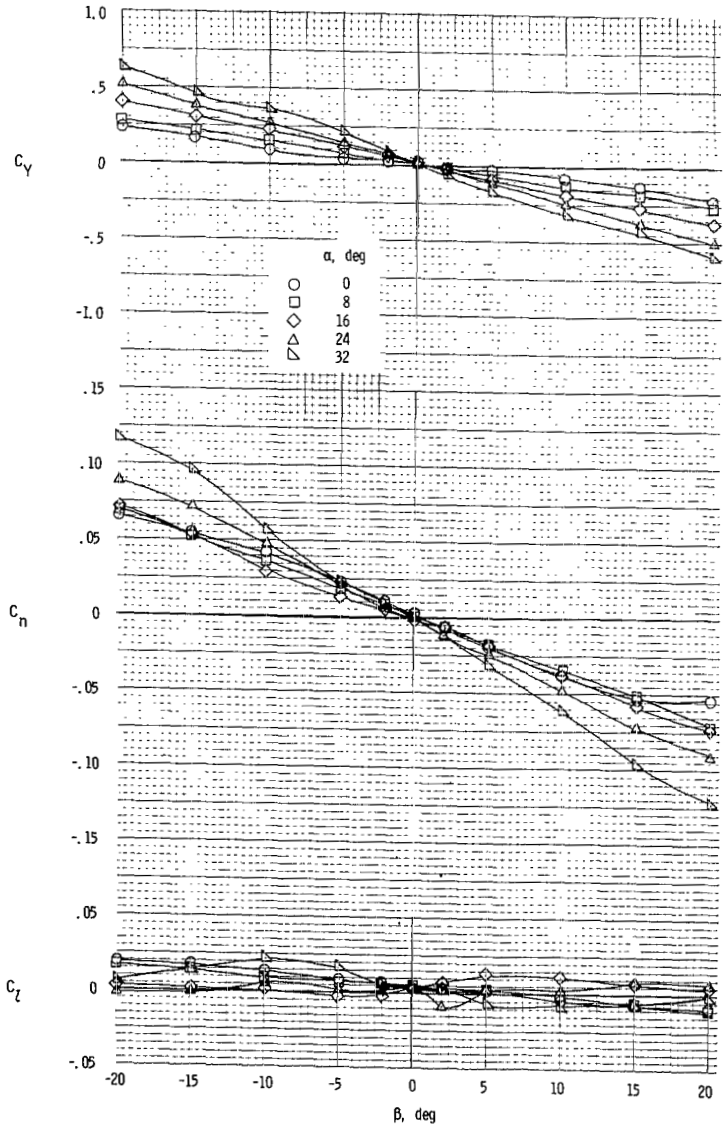

Figure 64.- Sideslip characteristics. Tails off; $\Theta = -10^{\circ}$; rotor/wing 3.

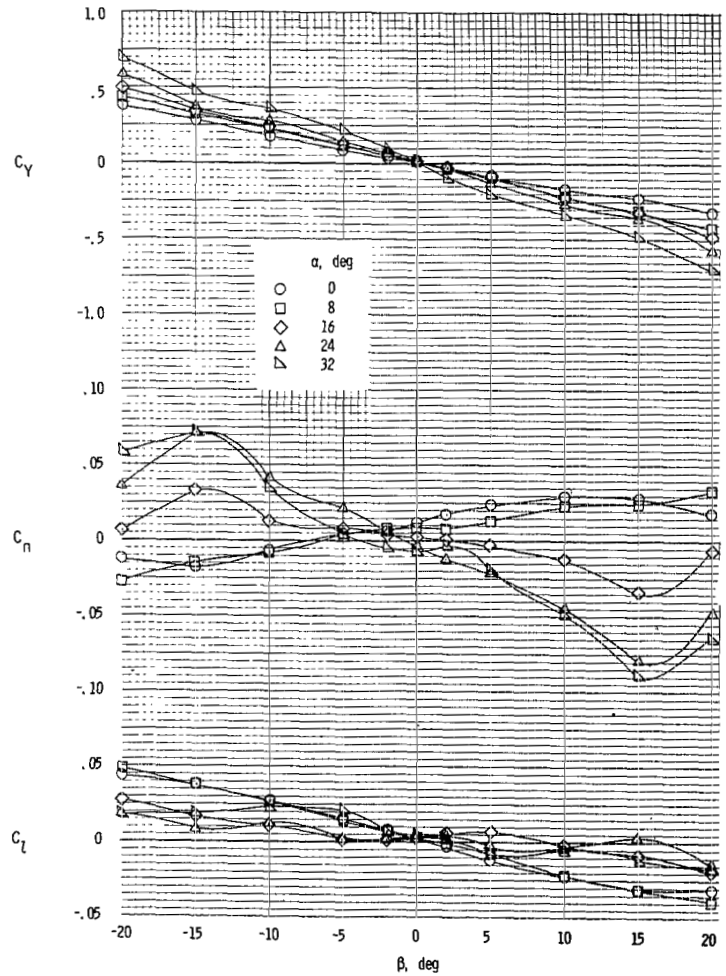

Figure 65.- Sideslip characteristics. Center vertical tail; horizontal tail at mid position; $i_t = -10^{\circ}$; $\Theta = -10^{\circ}$; rotor/wing 3.

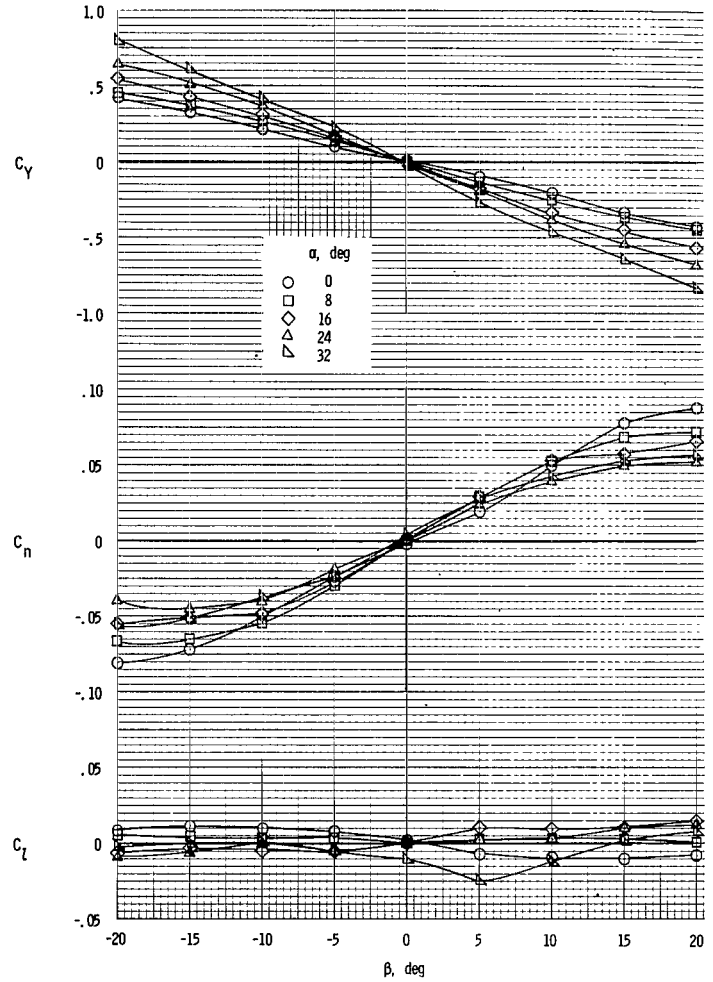

Figure 66.- Sideslip characteristics. Twin vertical tails; horizontal tail at center fuselage; $i_t = -10^\circ$; $\Theta = -10^\circ$; rotor/wing 3.

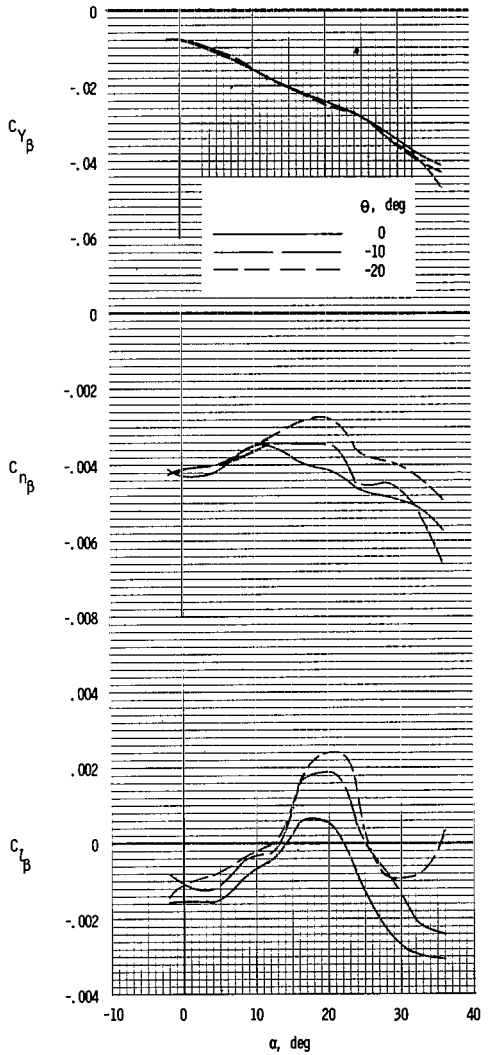

Figure 67.- Static lateral-stability derivatives. Tails off; rotor/wing 3.

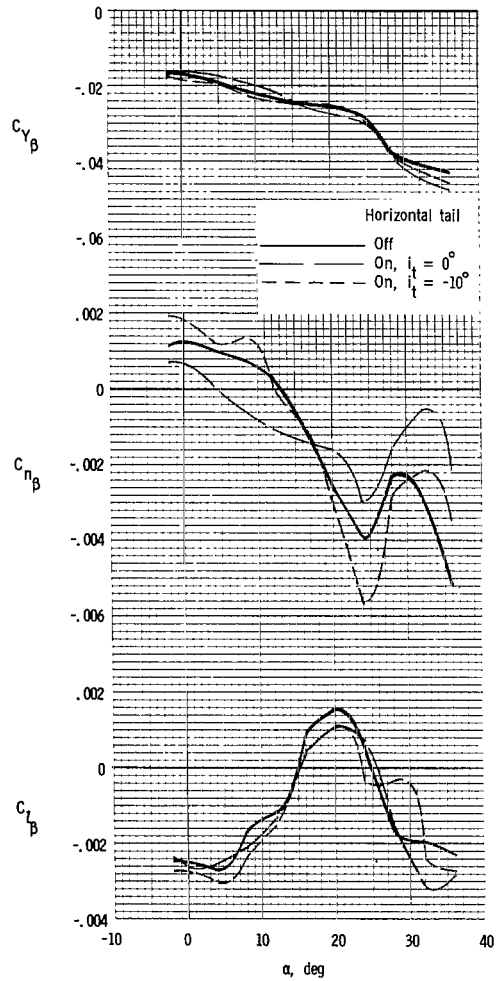

Figure 68.- Effect of horizontal tail on static lateral-stability derivatives. Center vertical tail; mid horizontal tail; $\Theta = -10^\circ$; rotor/wing 3.

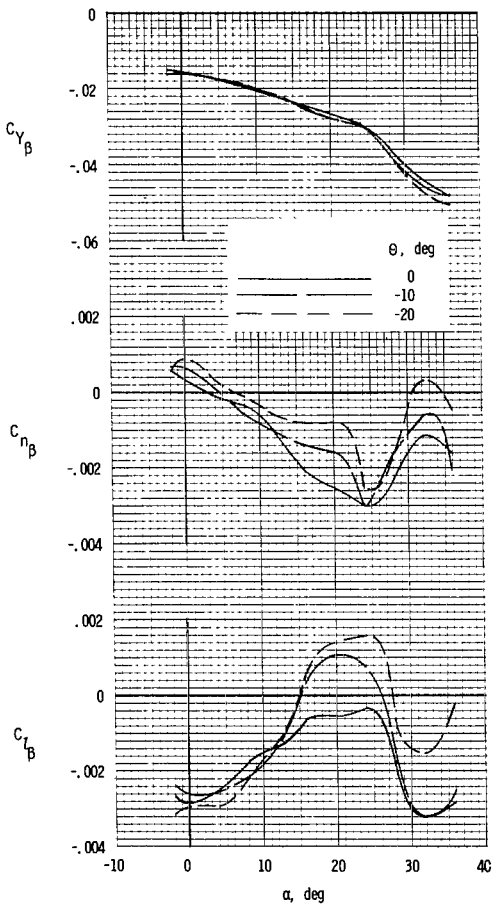

Figure 69.- Static lateral-stability derivatives. Center vertical tail; mid horizontal tail; $i_t = 0^\circ$; rotor/wing 3.

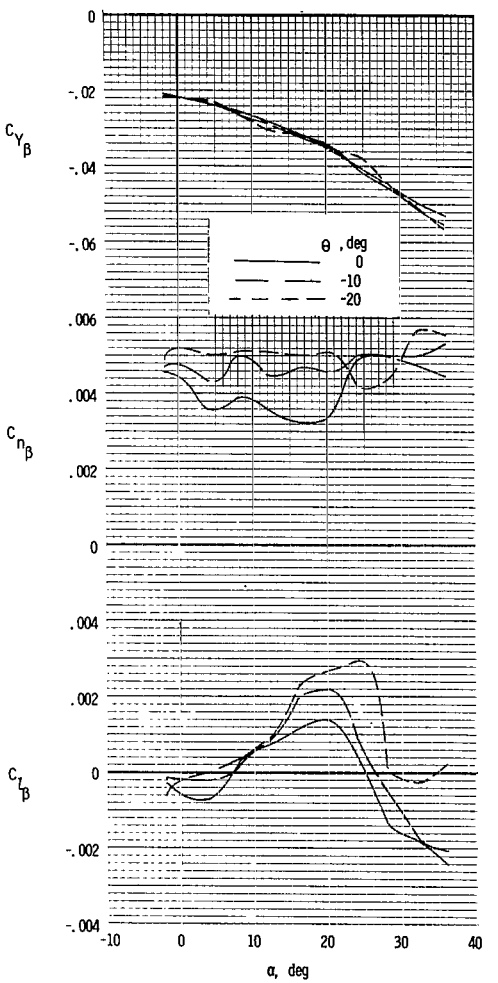

Figure 70.- Static lateral-stability derivatives. Twin vertical tails; horizontal tail at center fuselage; $i_t = 0^\circ$; rotor/wing 3.

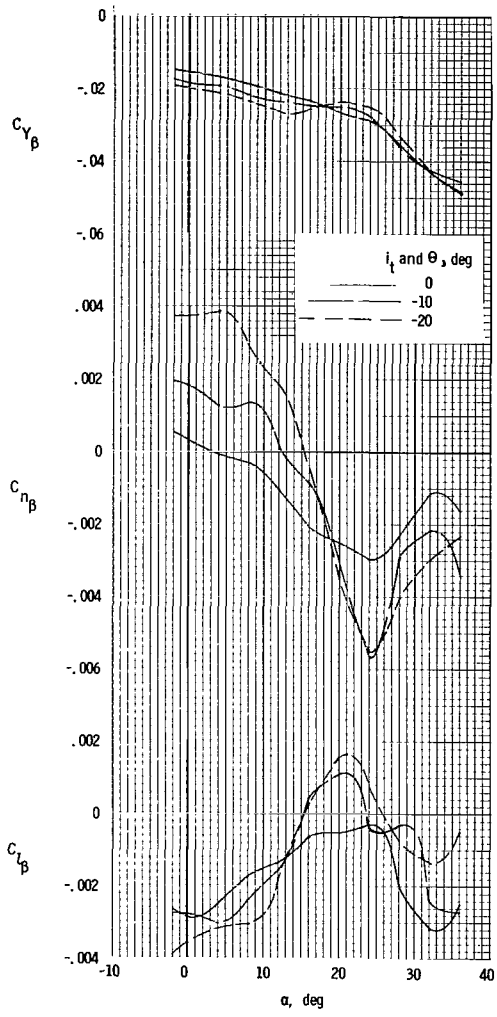

Figure 71.- Static lateral-stability derivatives for combinations of Θ and i_t. Center vertical tail; mid horizontal tail; rotor/wing 3.

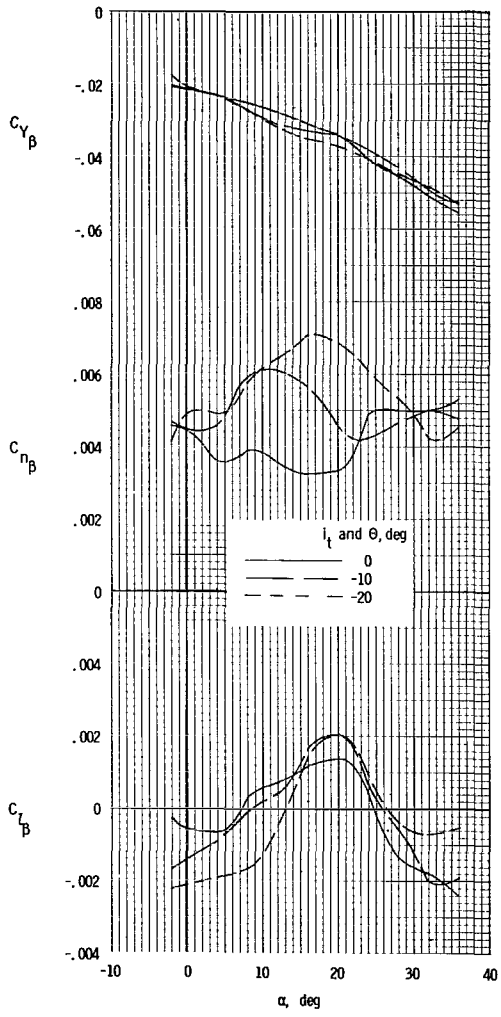

Figure 72.- Static lateral-stability derivatives for combinations of Θ and i_t. Twin vertical tails; horizontal tail at center fuselage; rotor/wing 3.

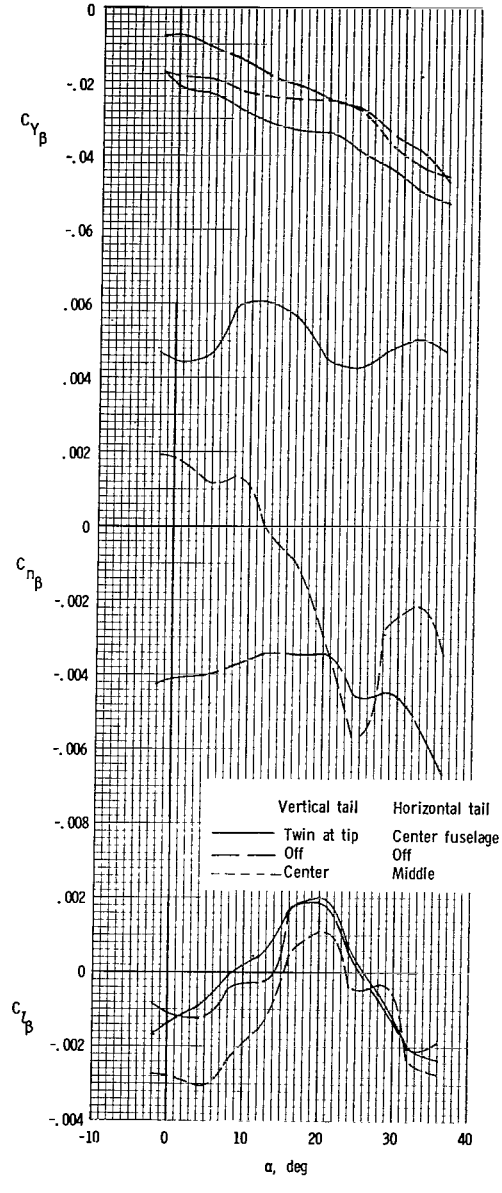

Figure 73.- Effect of vertical-tail configuration on static lateral-stability derivatives. $\Theta = -10^\circ$; $i_t = -10^\circ$; rotor/wing 3.

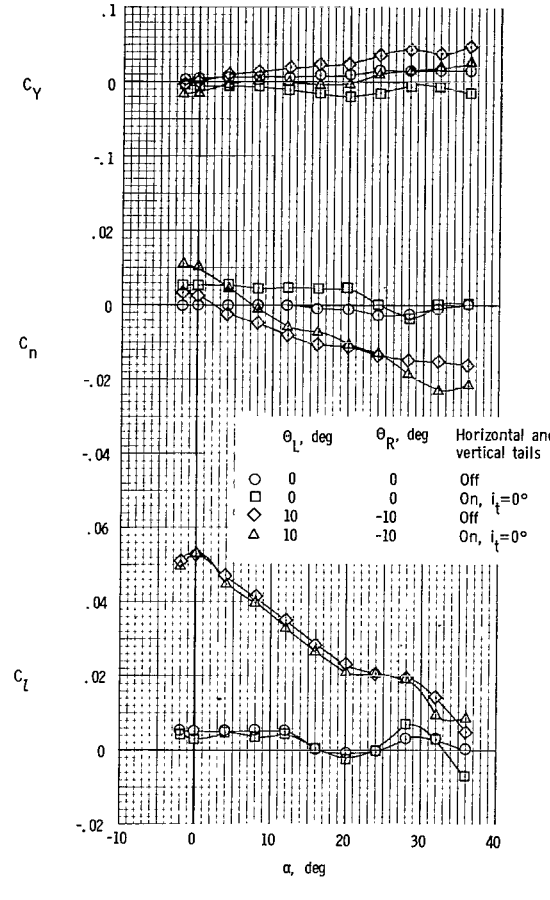

Figure 74.- Effect of tails on lateral-control characteristics with rotor blades used for control. Center vertical tail; mid horizontal tail; $\Theta_{mean} = 0^\circ$; rotor/wing 3.

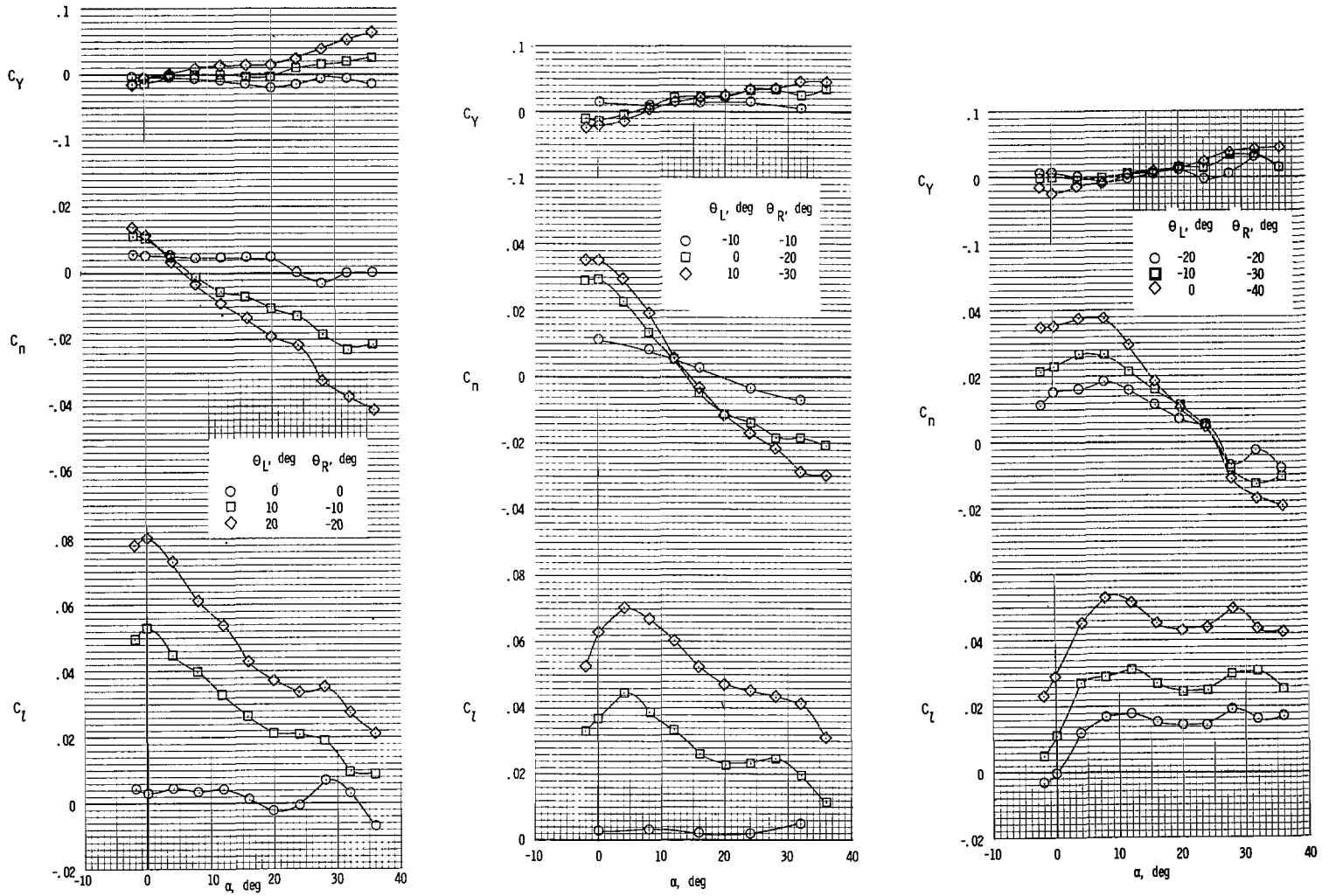

(a) $\Theta_{mean} = 0^o$; $i_t = 0^o$.

(b) $\Theta_{mean} = -10^o$.

(c) $\Theta_{mean} = -20^o$.

Figure 75.- Lateral-control characteristics with rotor blades used for control. Center vertical tail; mid horizontal tail; rotor/wing 3.

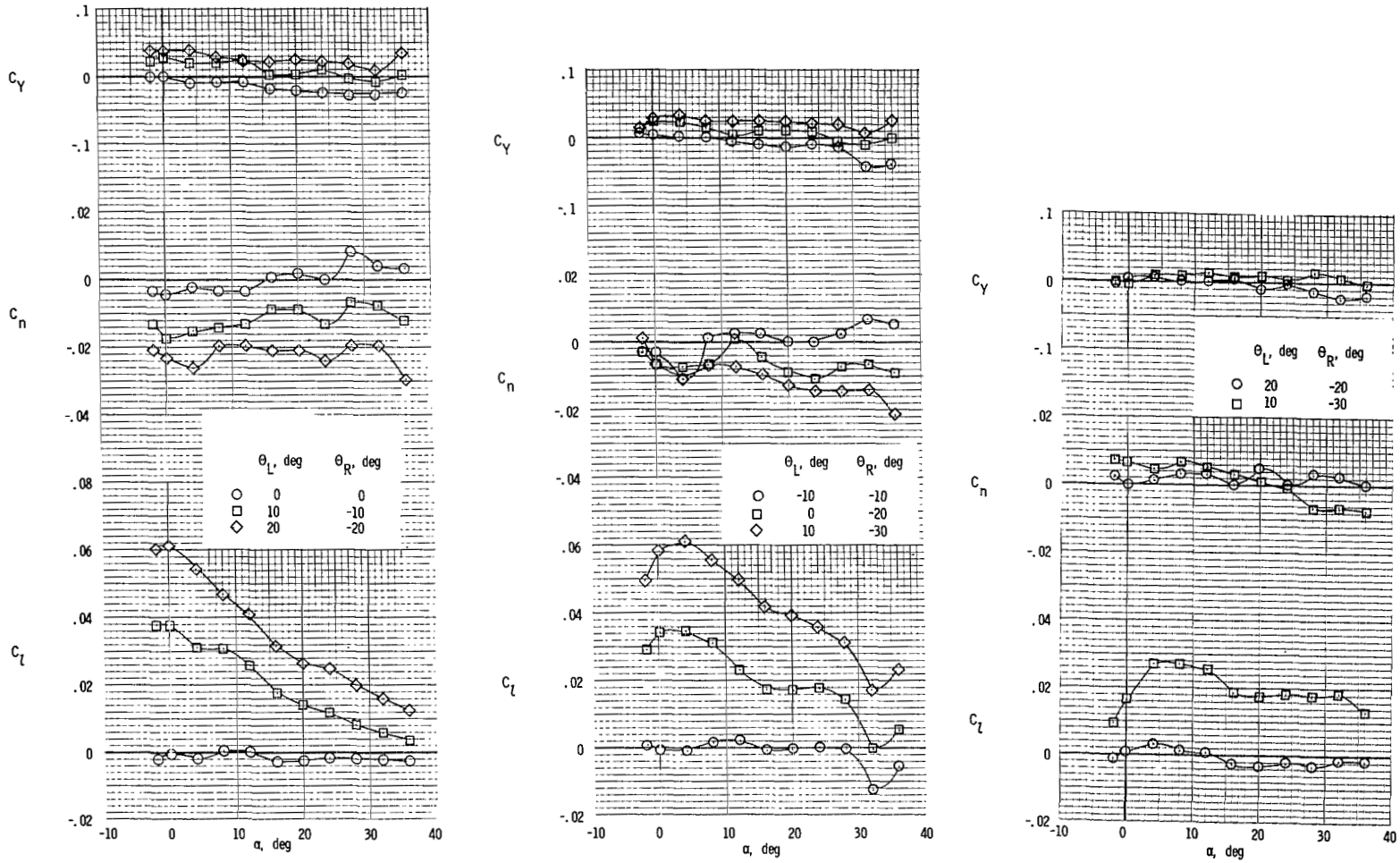

(a) $i_t = 0^o$; $\Theta_{mean} = 0^o$. (b) $i_t = -10^o$; $\Theta_{mean} = -10^o$. (c) $i_t = -20^o$; $\Theta_{mean} = -20^o$.

Figure 76.- Lateral-control characteristics with the rotor blades used for control. Twin vertical tails; horizontal tail at center fuselage; rotor/wing 3.

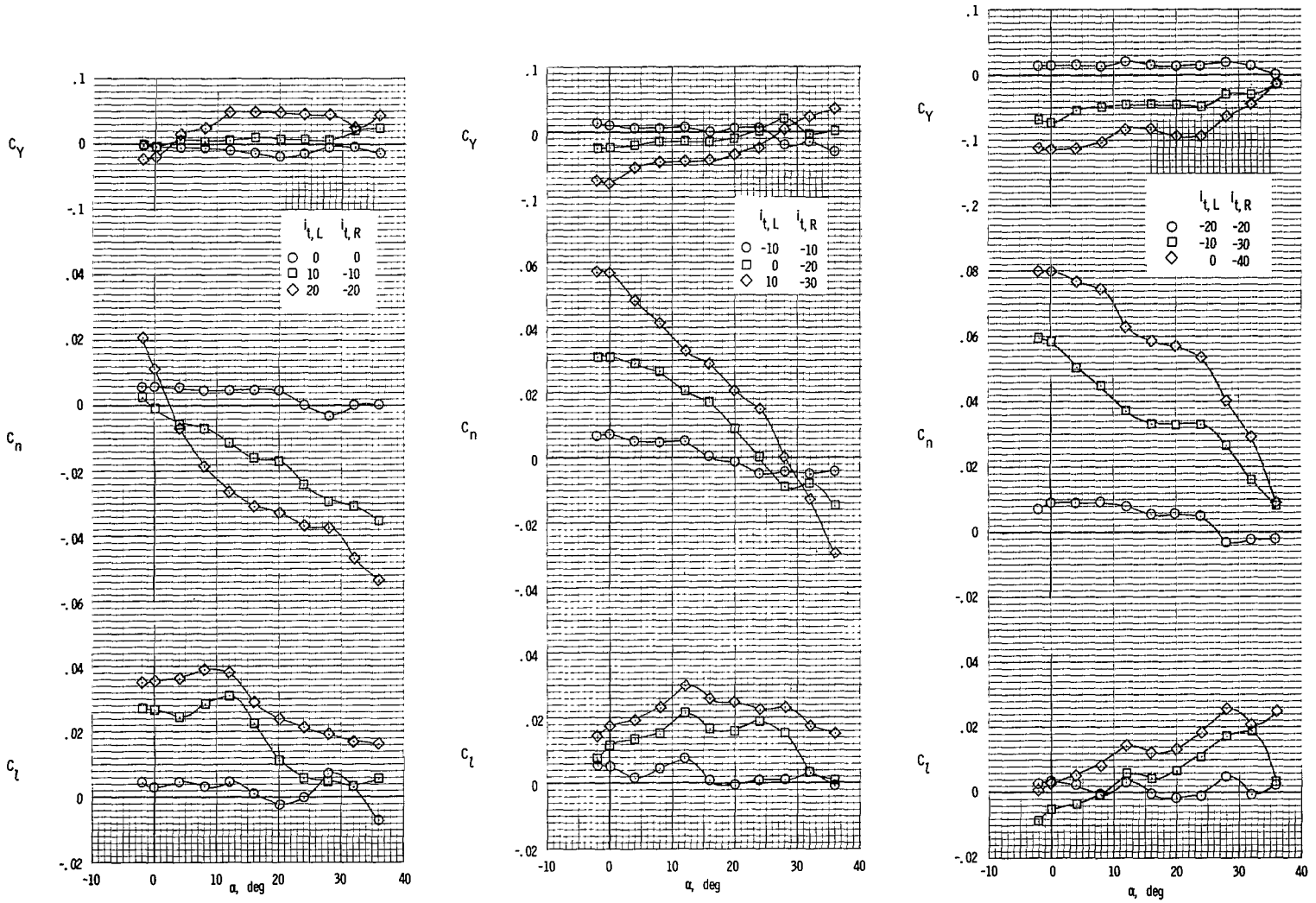

(a) $i_{t,mean} = 0°$. (b) $i_{t,mean} = -10°$. (c) $i_{t,mean} = -20°$.

Figure 77.- Lateral-control characteristics with horizontal tail used for control. Center vertical tail; mid horizontal tail; $\Theta = 0°$; rotor/wing 3.

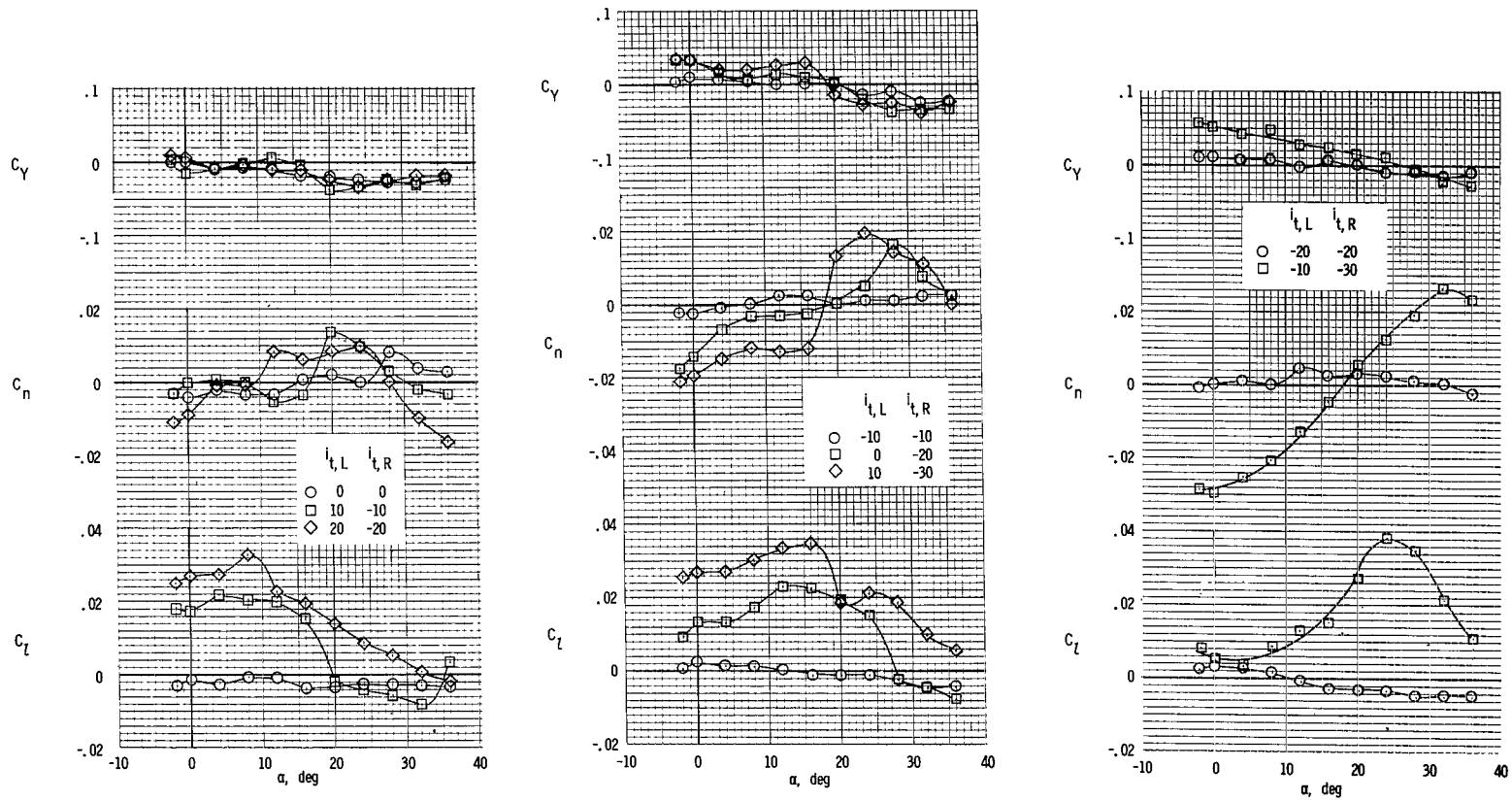

(a) $i_{t,mean} = 0^o$. (b) $i_{t,mean} = -10^o$. (c) $i_{t,mean} = -20^o$.

Figure 78.- Lateral-control characteristics with horizontal tail used for control. Twin vertical tails; horizontal tail at center fuselage; $\Theta = 0^o$; rotor/wing 3.

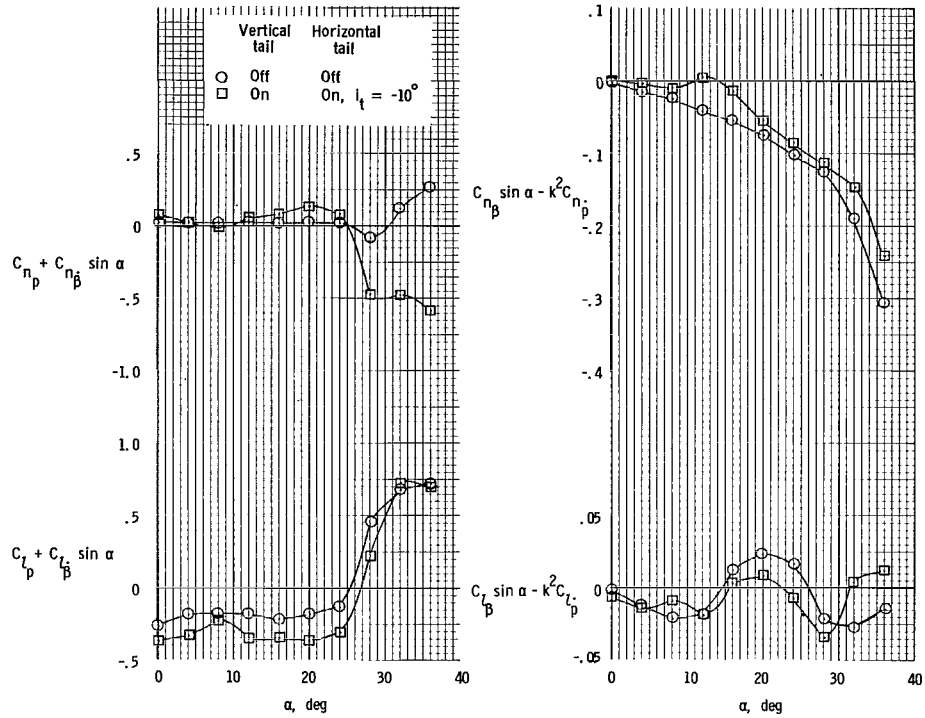

(a) Out-of-phase derivatives. (b) In-phase derivatives.

Figure 79.- Effect of tails on dynamic stability derivatives measured in rolling-oscillation tests. Center vertical tail; mid horizontal tail; $\Theta = 0^\circ$; rotor/wing 3.

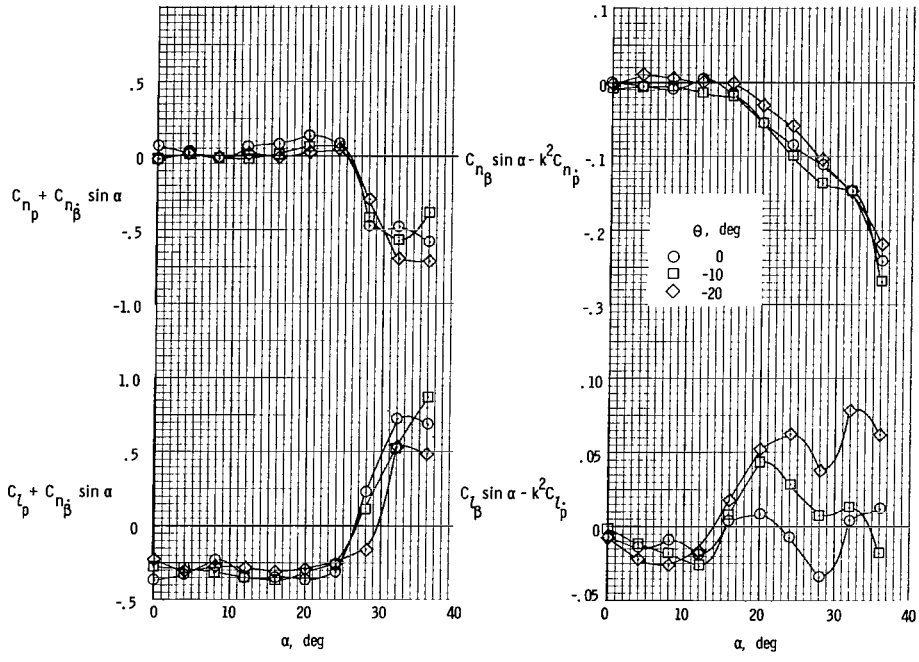

(a) Out-of-phase derivatives. (b) In-phase derivatives.

Figure 80.- Effect of rotor-blade incidence on dynamic-stability derivatives measured in rolling-oscillation tests. Center vertical tail; mid horizontal tail; $i_t = -10^\circ$; rotor/wing 3.

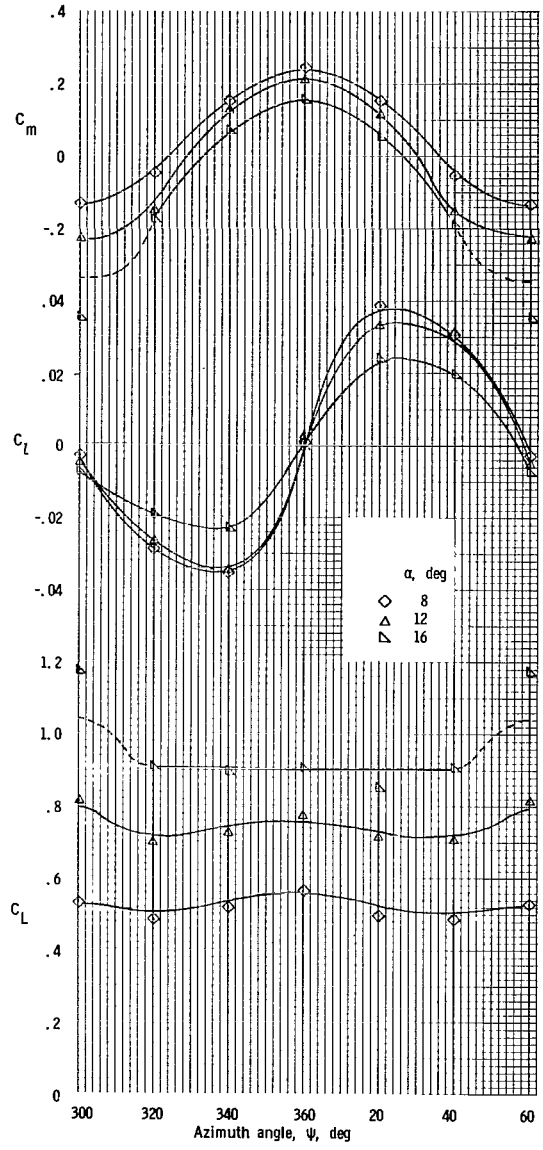

Figure 81.- Effect of azimuth on lift coefficient and rolling- and pitching-moment coefficients for changes in model angle of attack. $i_t = 0^\circ$; $\Theta = 0^\circ$; rotor/wing 3.

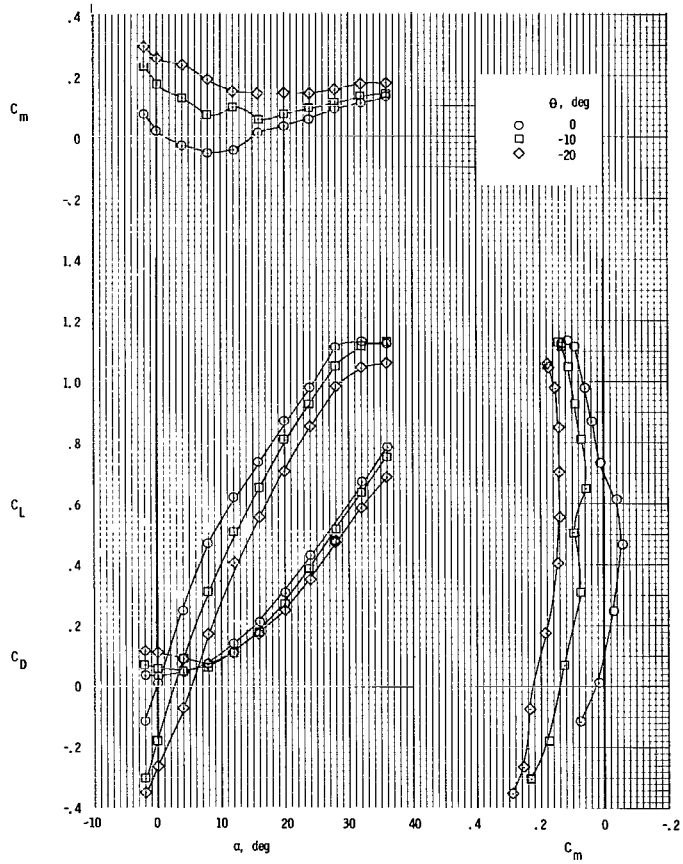

Figure 82.- Longitudinal aerodynamic characteristics. Tails off; rotor/wing 4.

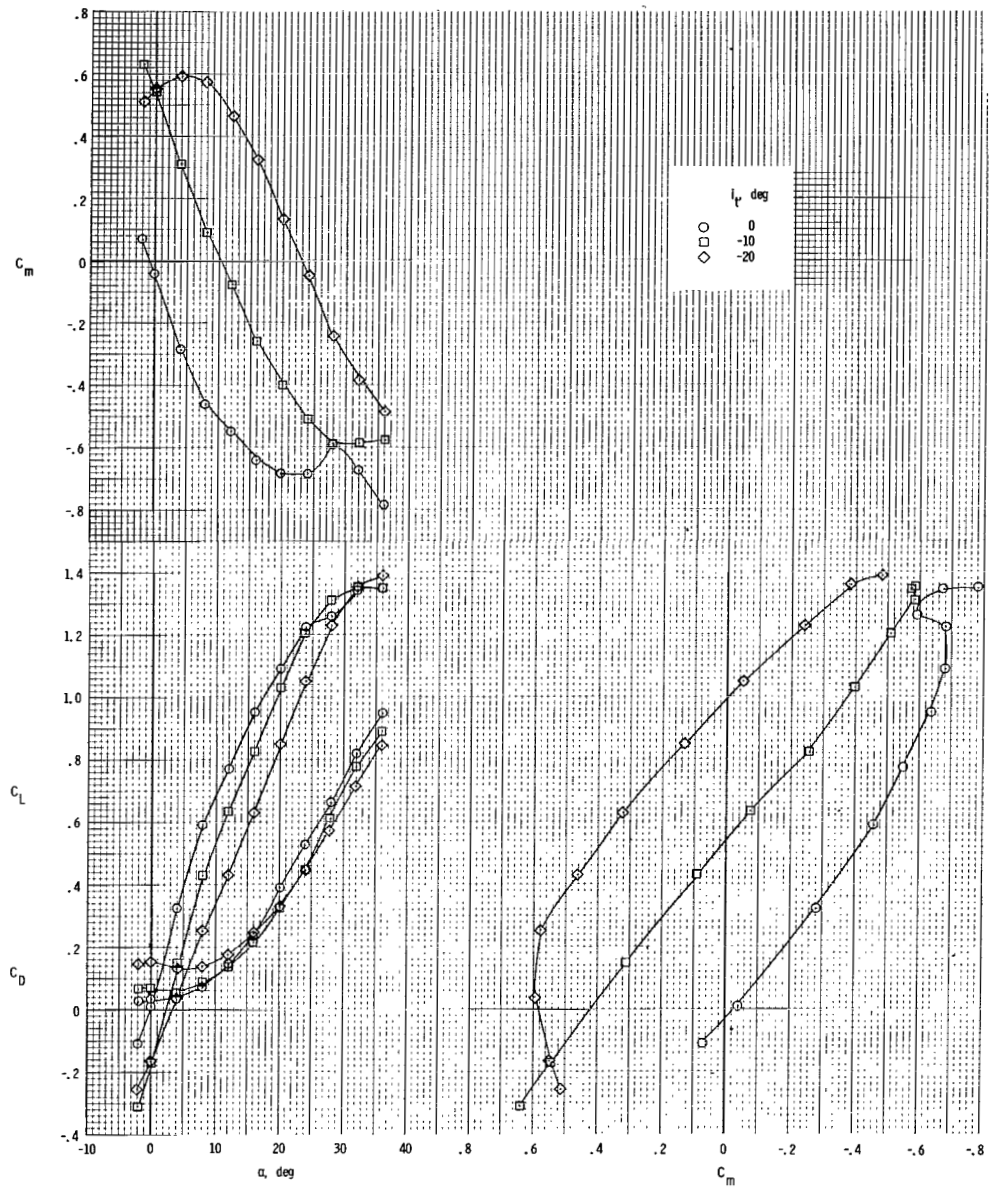

(a) $\Theta = 0^{\circ}$.

Figure 83.- Longitudinal aerodynamic characteristics. Low horizontal tail; center vertical tail; rotor/wing 4.

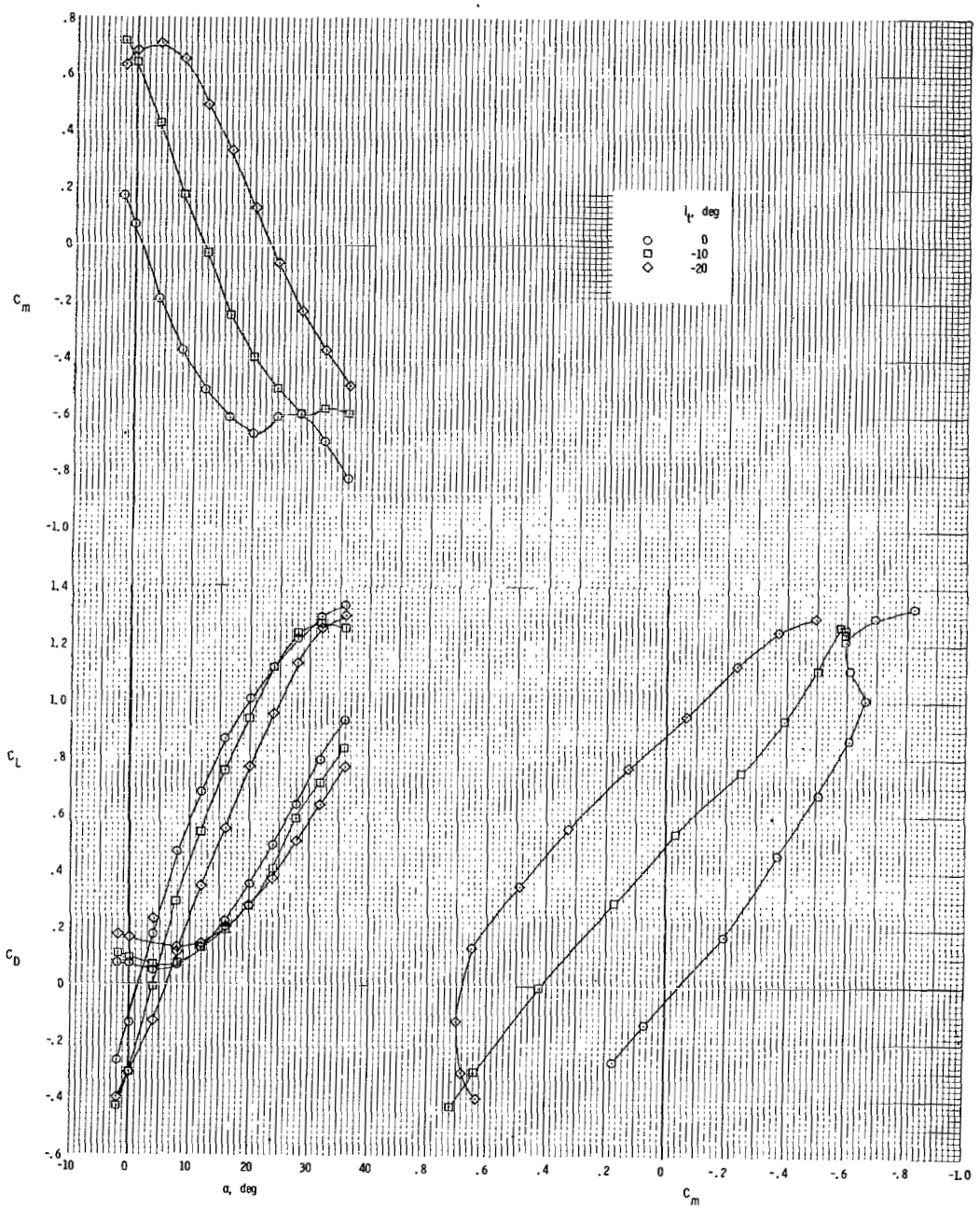

(b) $\Theta = -10^{\circ}$.

Figure 83.- Continued.

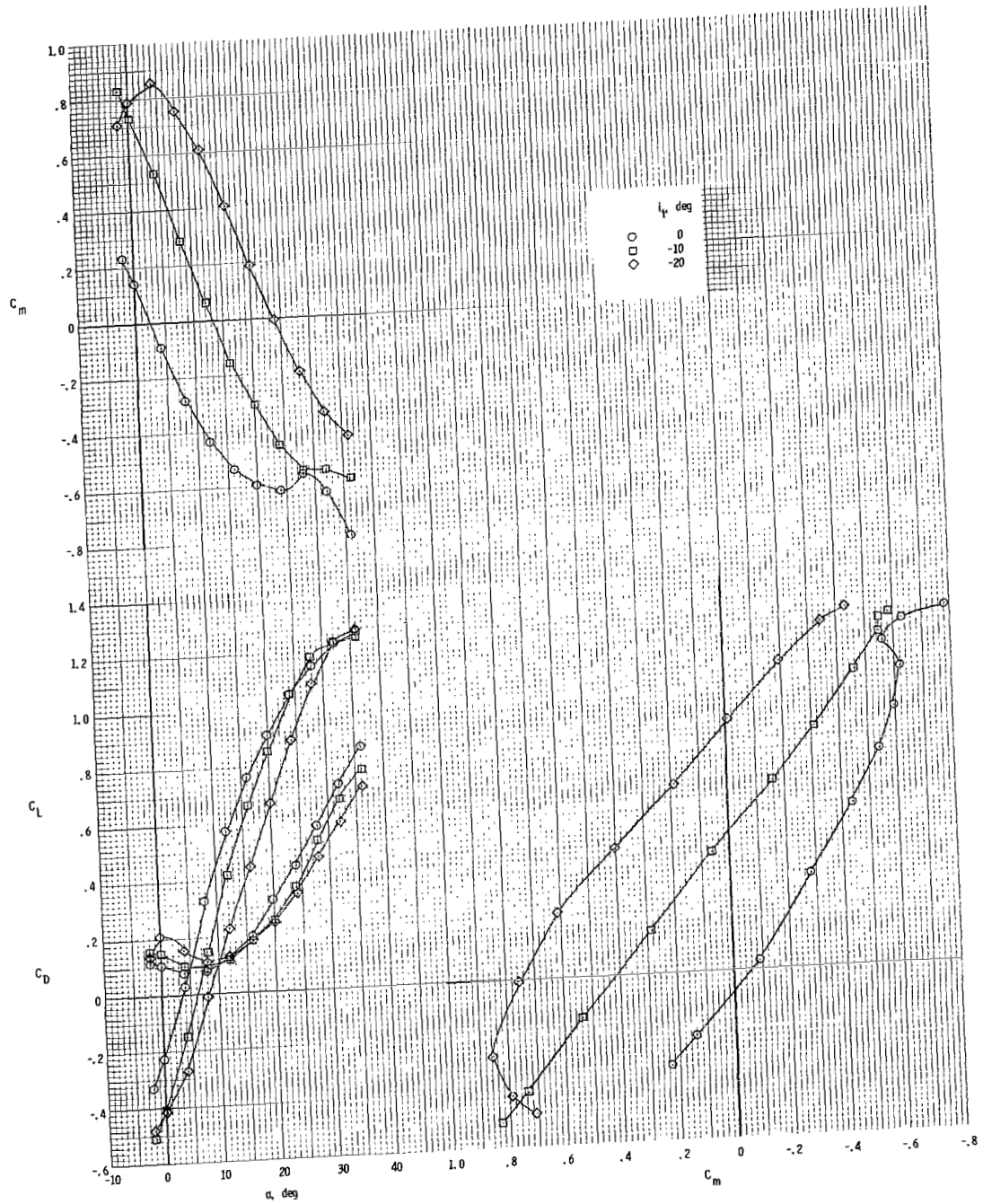

(c) $\Theta = -20^\circ$.

Figure 83.- Concluded.

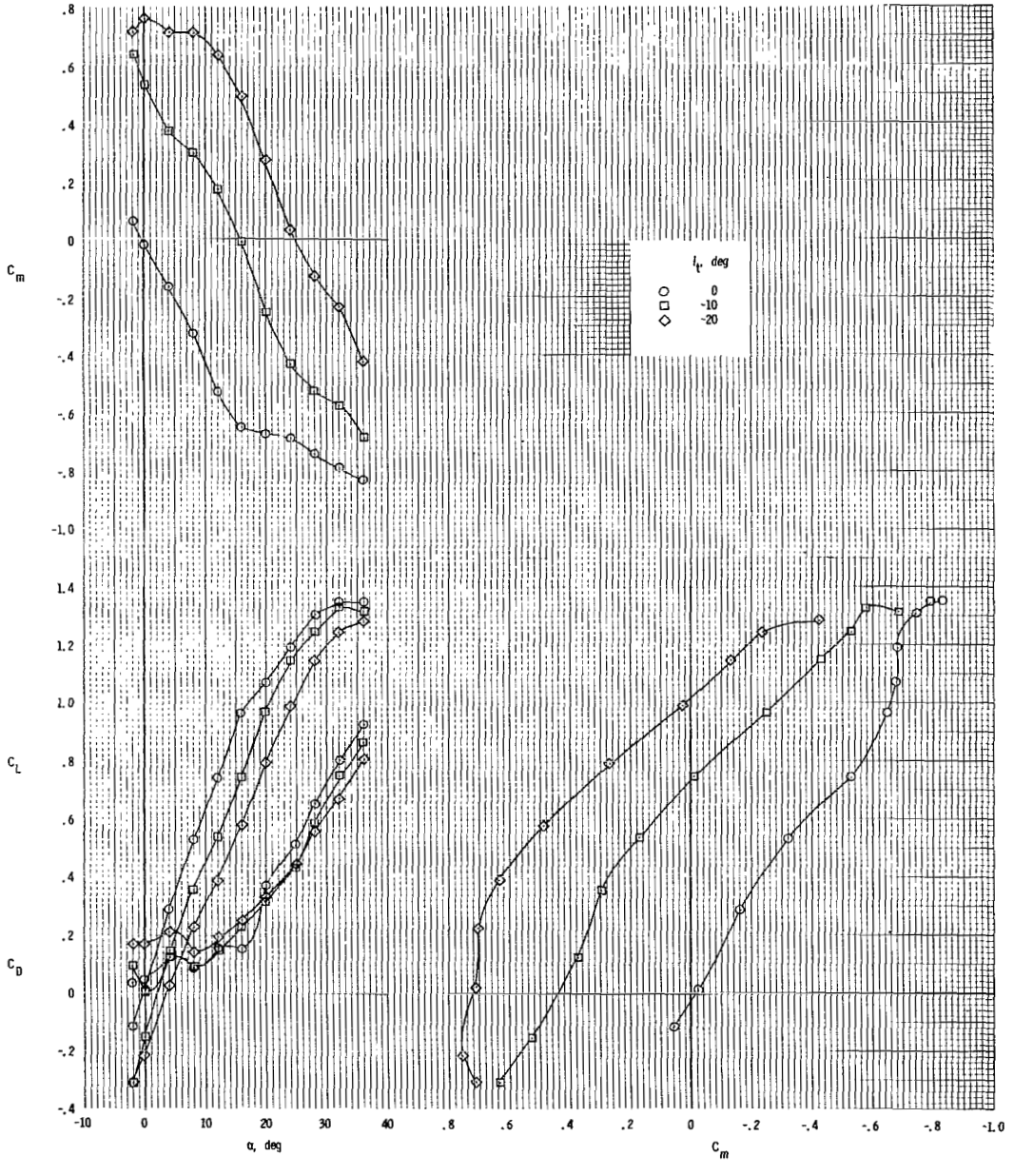

(a) $\Theta = 0^{\circ}$.

Figure 84.- Longitudinal aerodynamic characteristics. Mid horizontal tail; center vertical tail; rotor/wing 4.

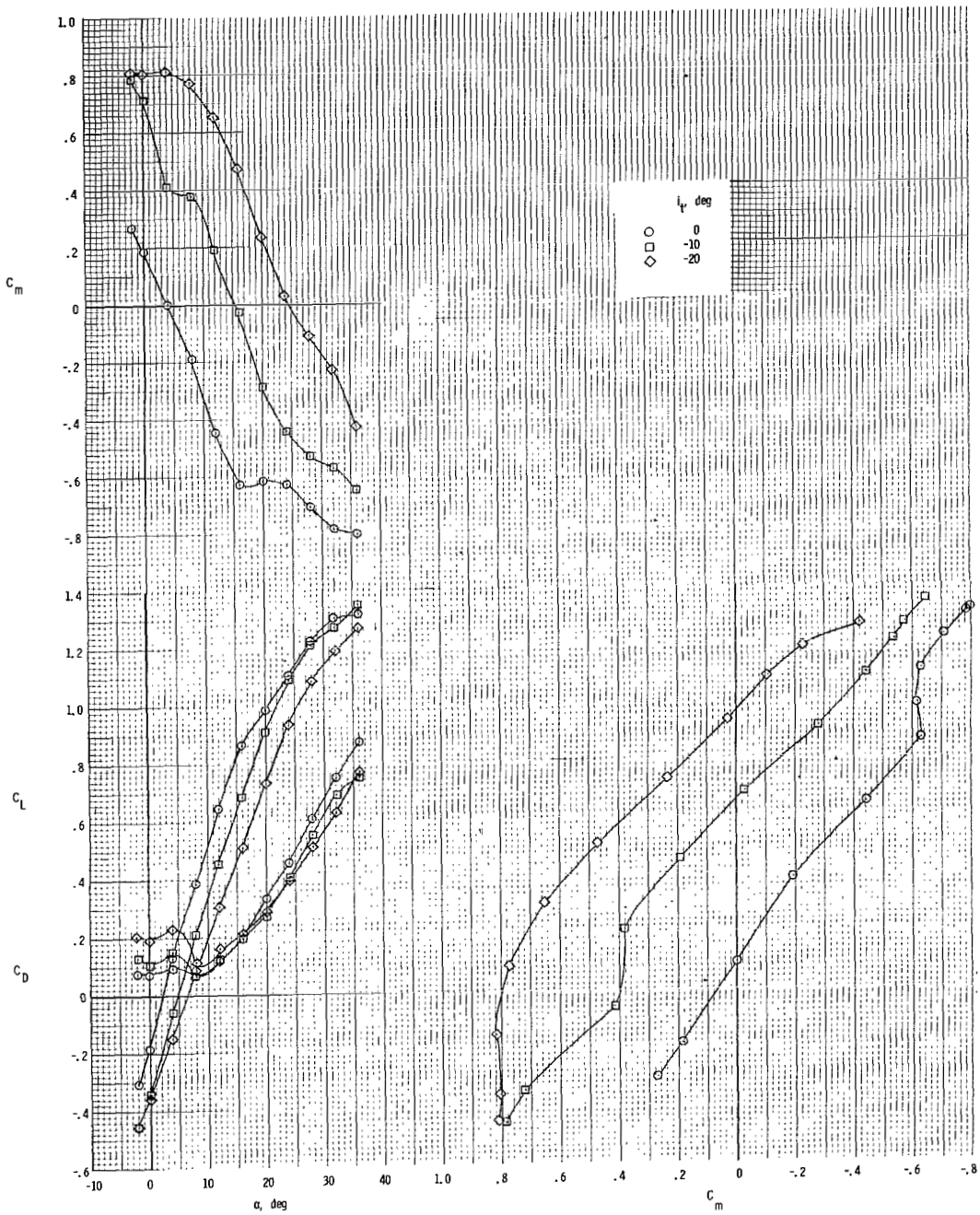

(b) $\Theta = -10^{\circ}$.

Figure 84.- Continued.

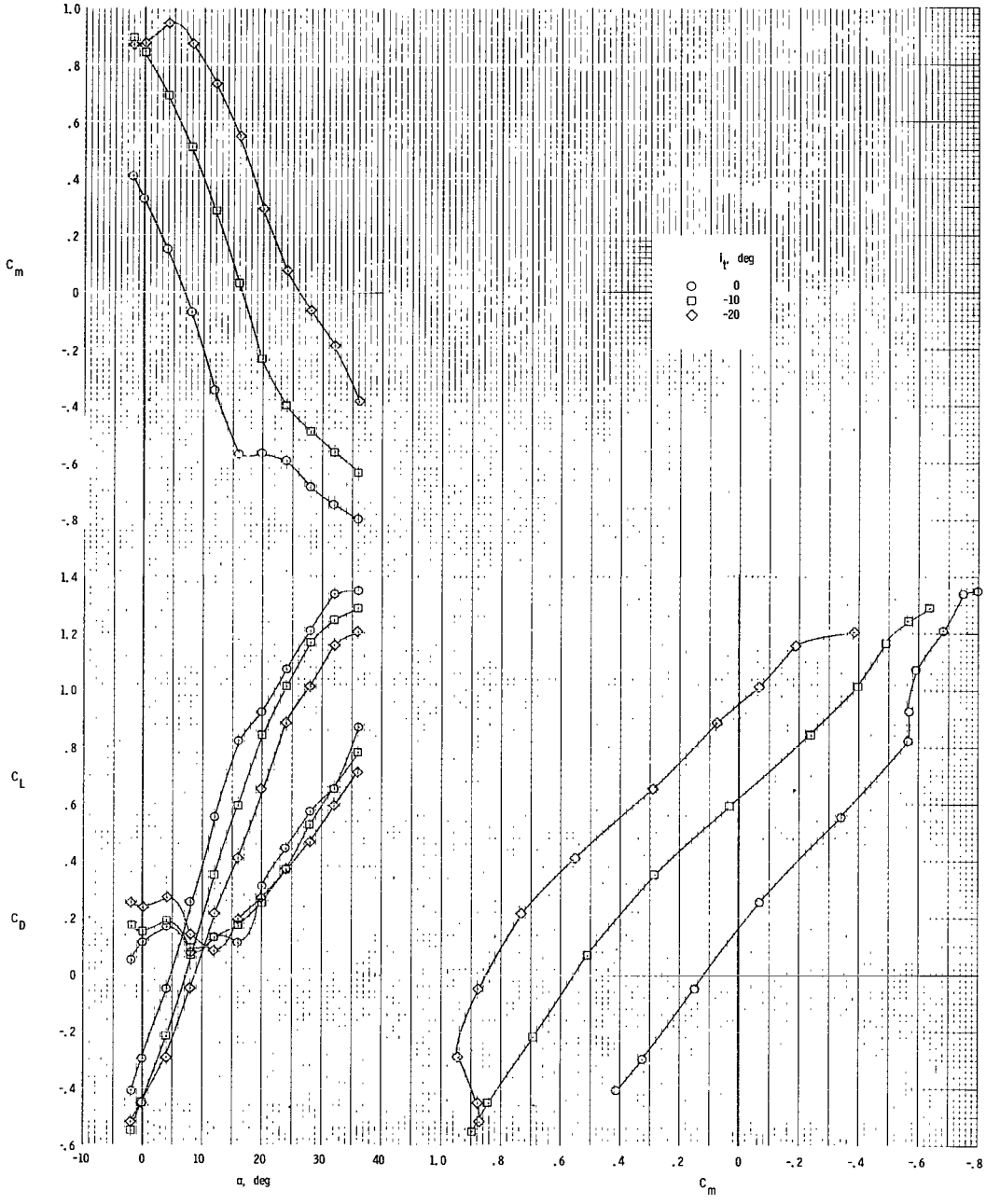

(c) $\Theta = -20^{\circ}$.

Figure 84.- Concluded.

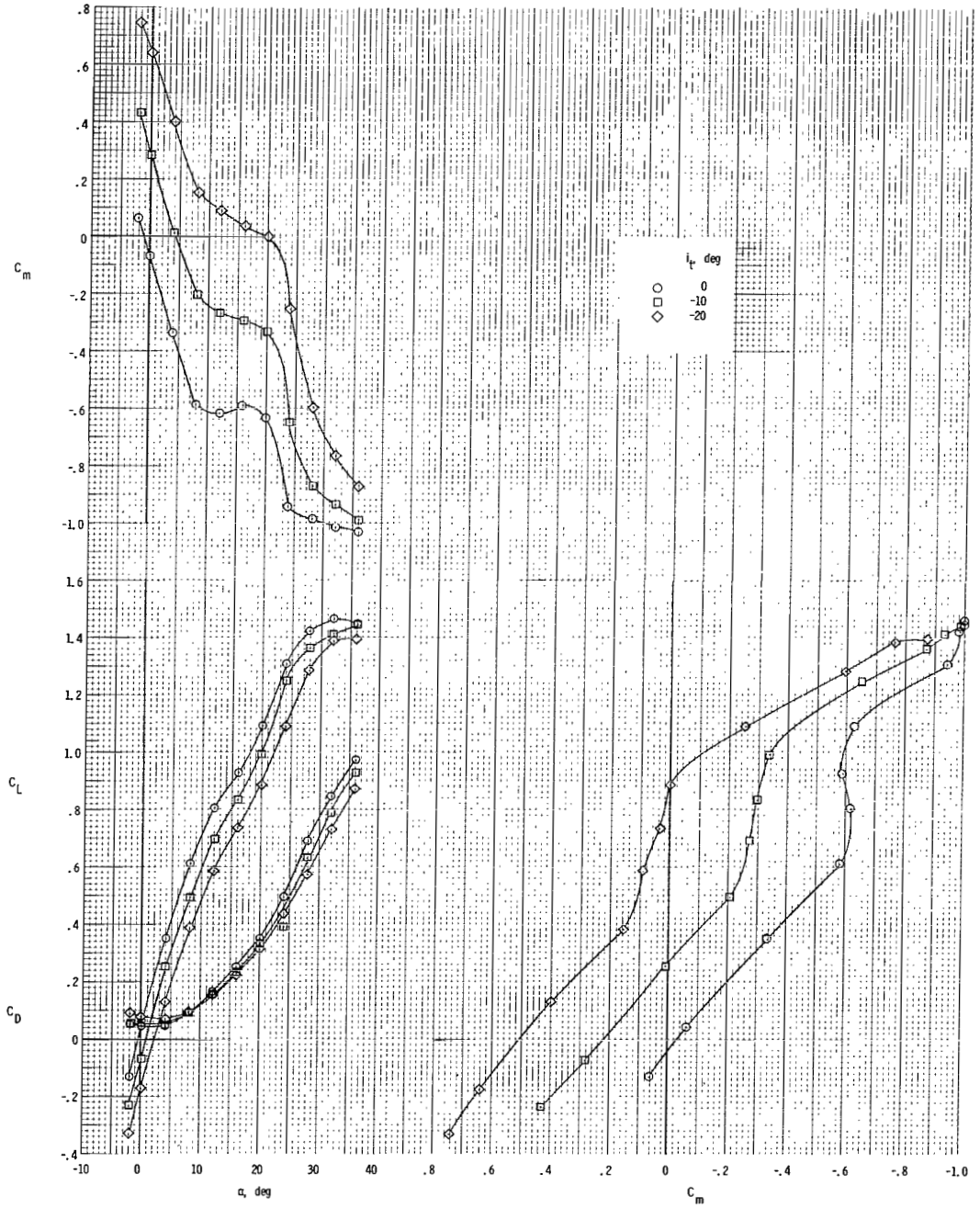

(a) $\Theta = 0^{\circ}$.

Figure 85.- Longitudinal aerodynamic characteristics. High horizontal tail; center vertical tail; rotor/wing 4.

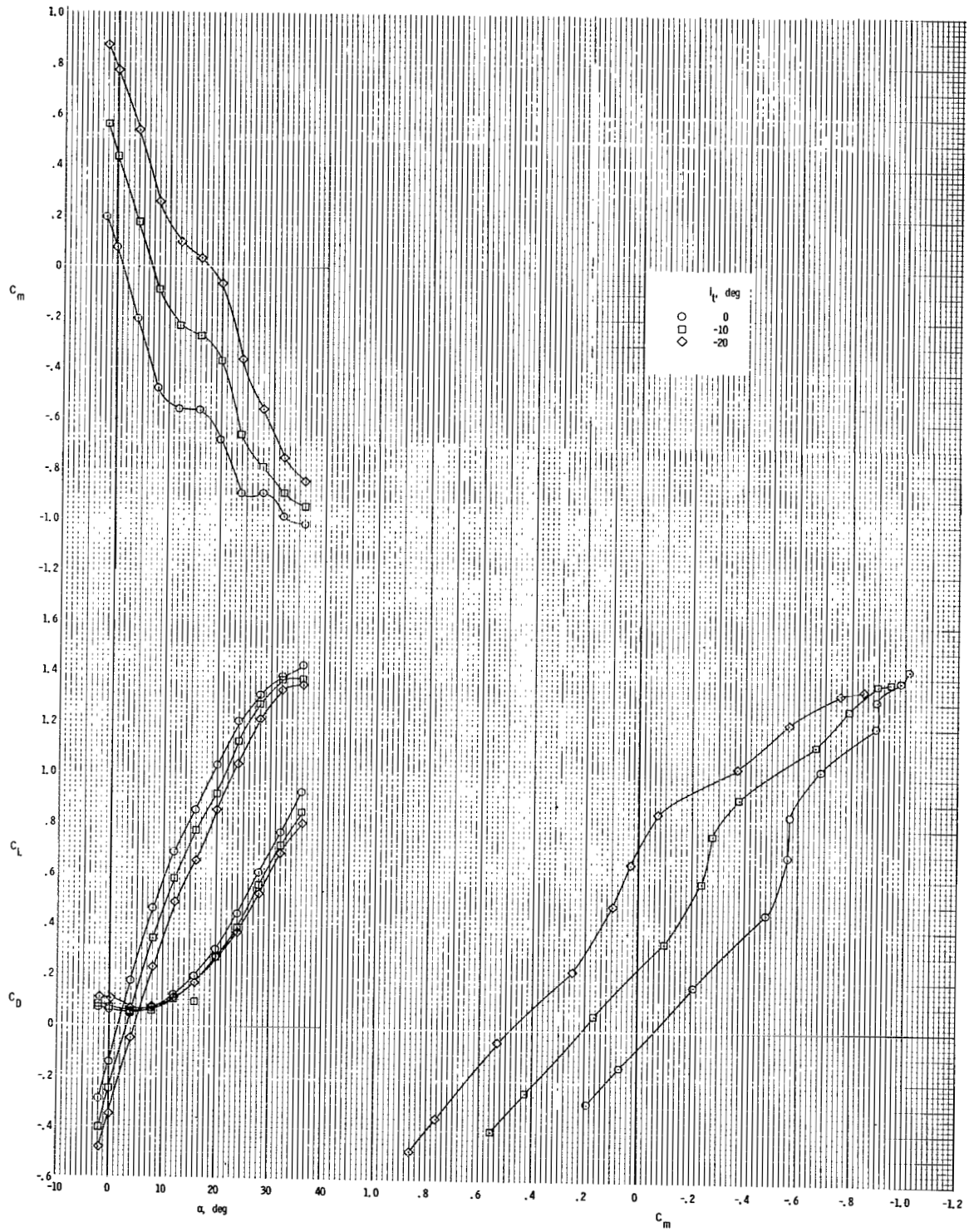

(b) $\Theta = -10^{\circ}$.

Figure 85.- Continued.

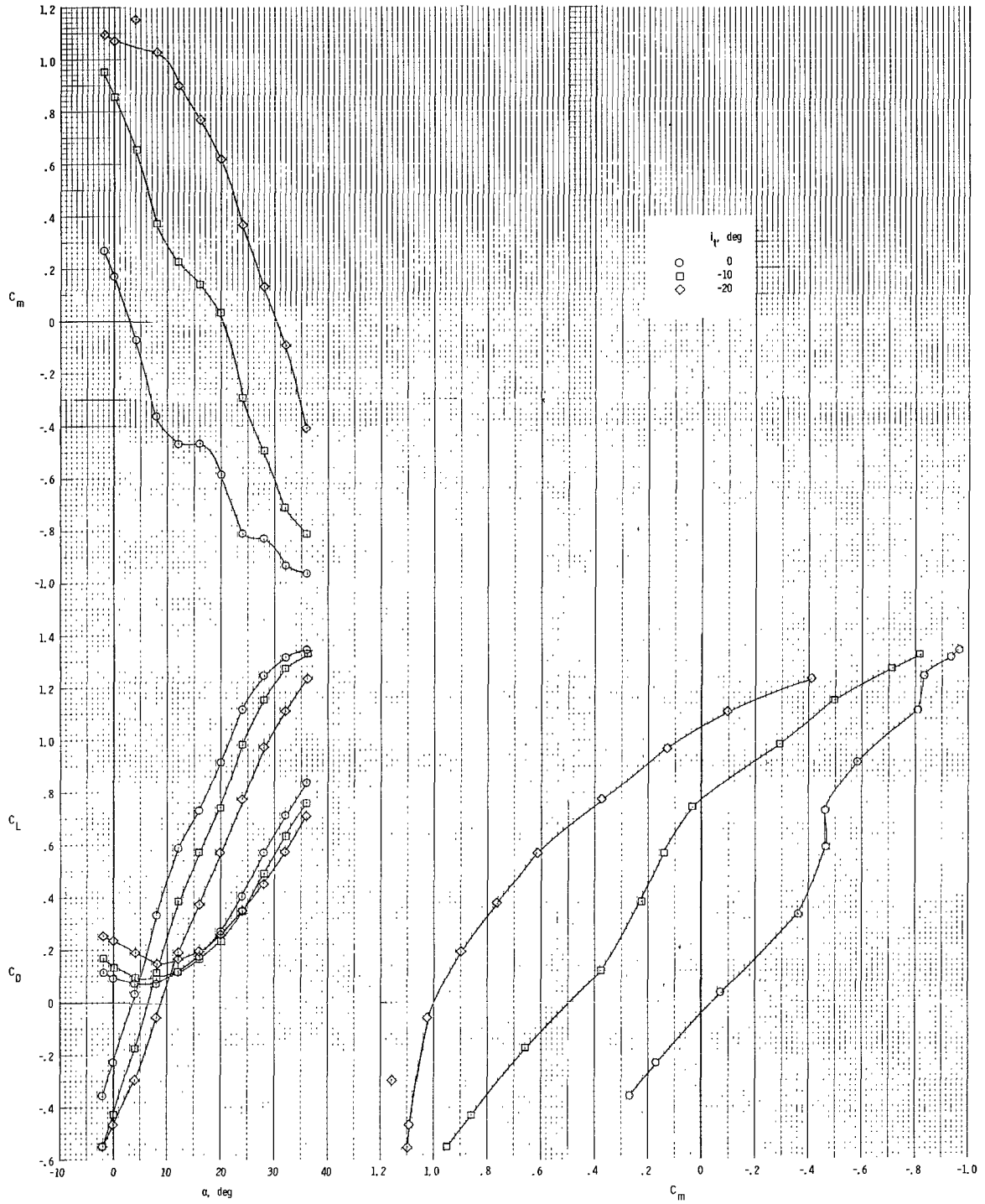

(c) $\Theta = -20^{\circ}$.

Figure 85.- Concluded.

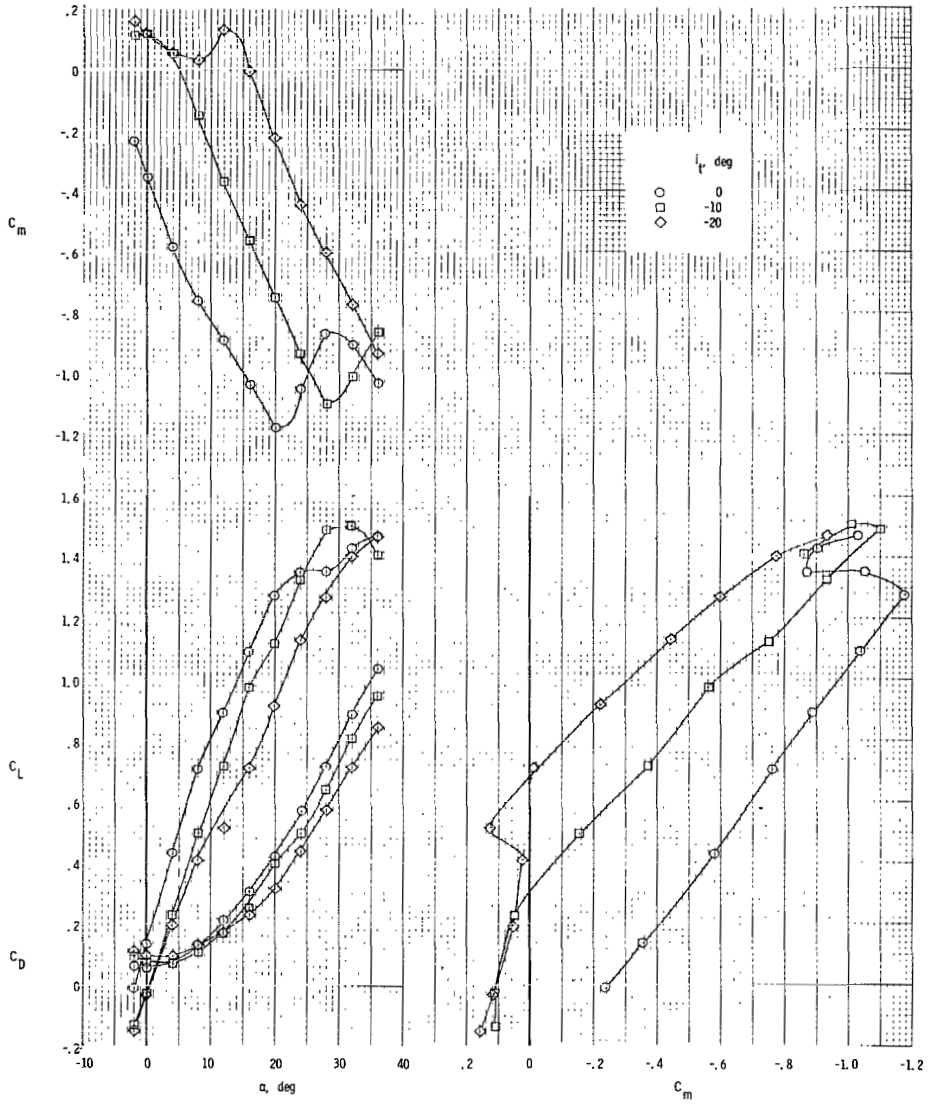

(a) $\Theta = 0^{\circ}$.

Figure 86.- Longitudinal aerodynamic characteristics. Horizontal tail at center fuselage; twin vertical tails; rotor/wing 4.

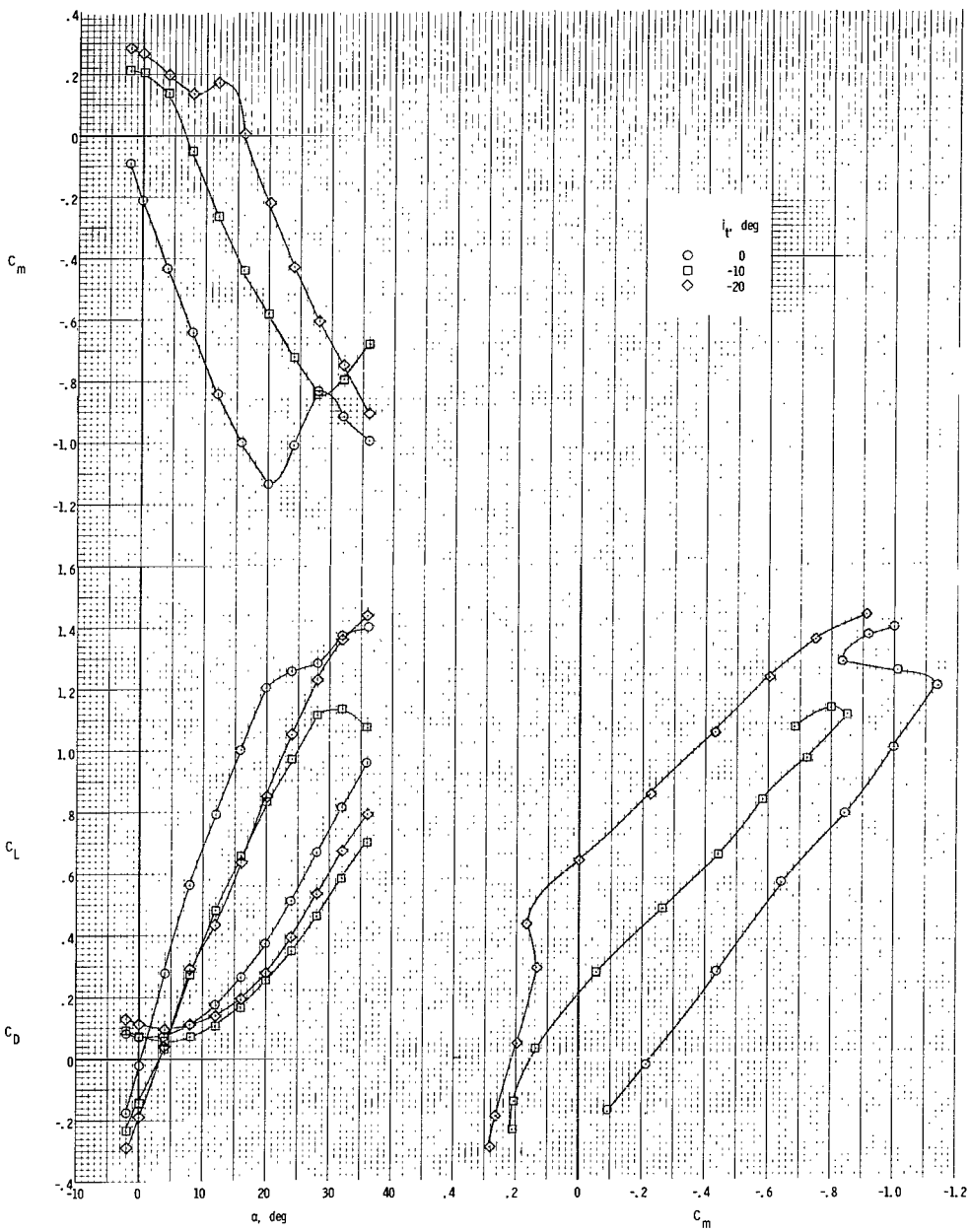

(b) $\Theta = -10^{\circ}$.

Figure 86.- Continued.

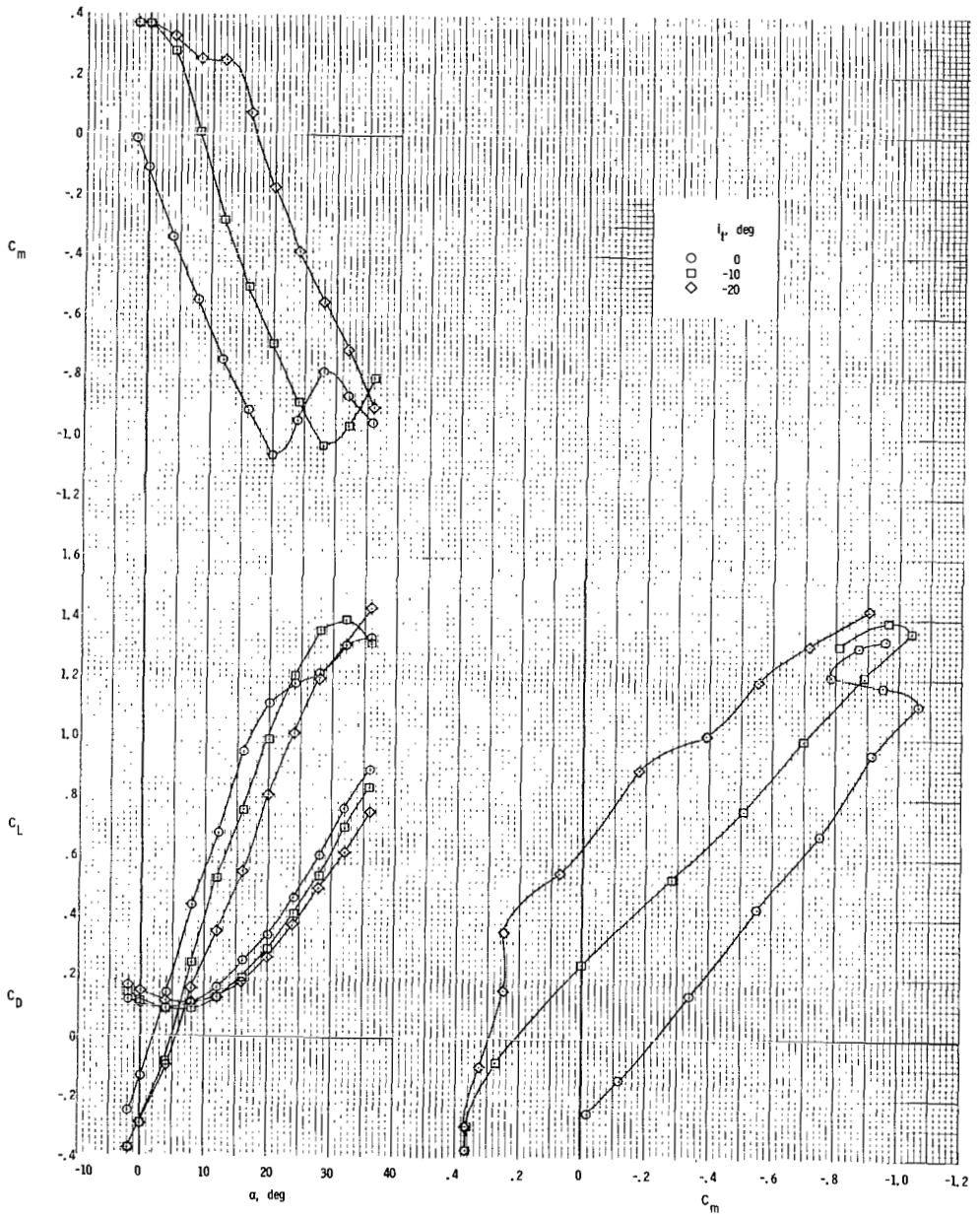

(c) $\Theta = -20^{\circ}$.

Figure 86.- Concluded.

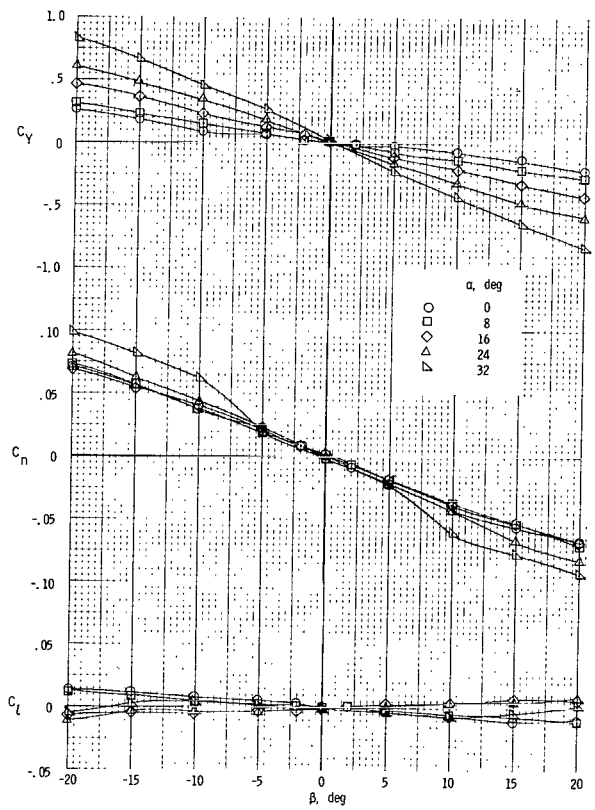

Figure 87.- Sideslip characteristics. Tails off; $\Theta = -10^{\circ}$; rotor/wing 4.

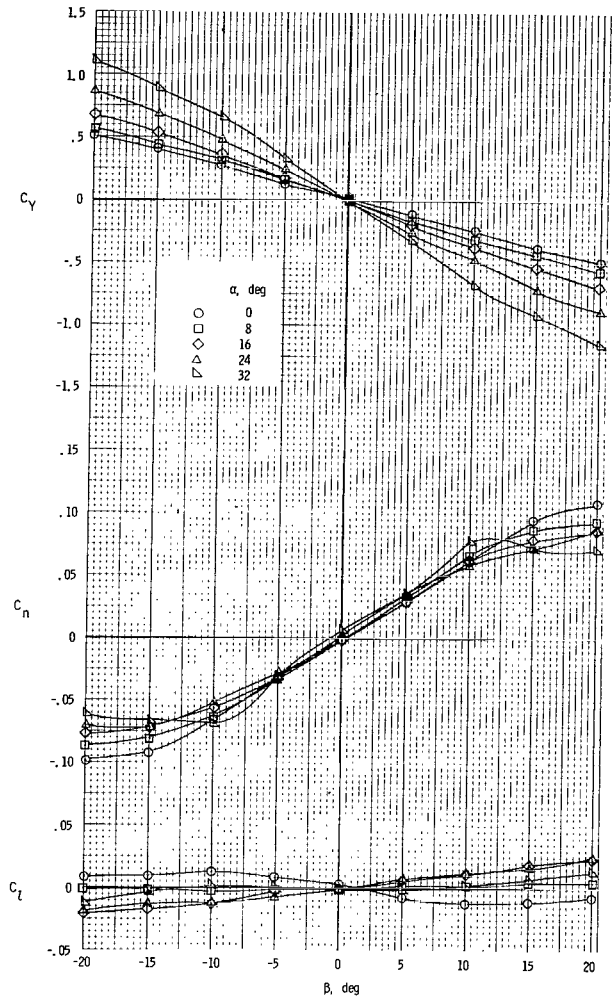

Figure 88.- Sideslip characteristics. Twin vertical tails; horizontal tail at center fuselage; $i_t = -10^{\circ}$; $\Theta = -10^{\circ}$; rotor/wing 4.

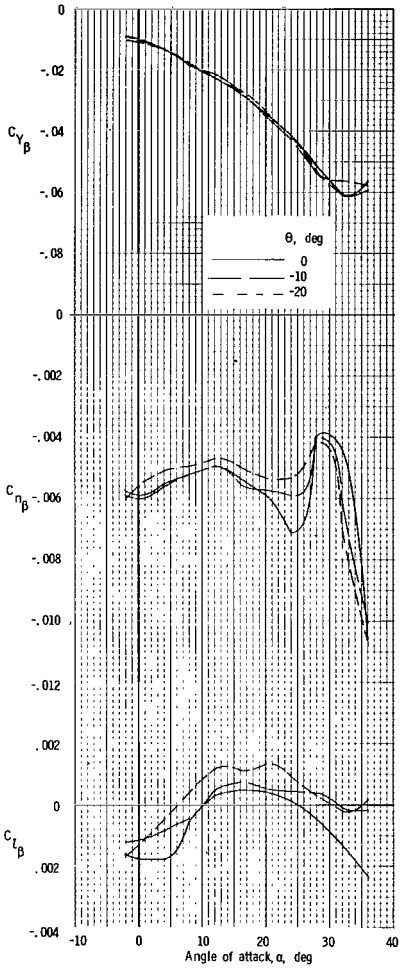

Figure 89.- Static lateral-stability derivatives. Tails off; rotor/wing 4.

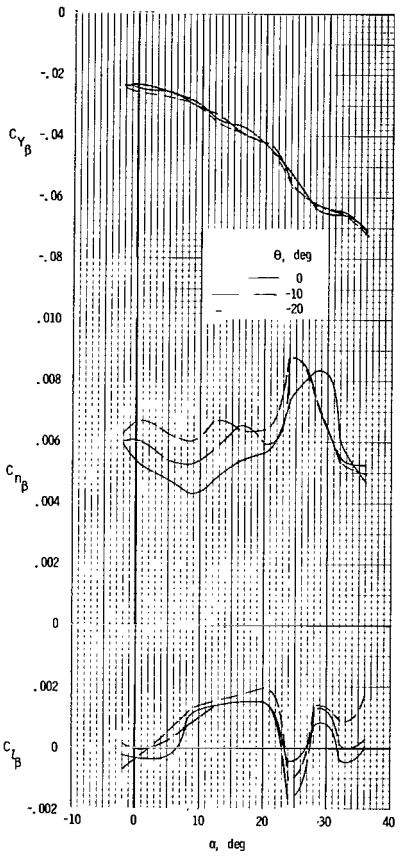

Figure 90.- Static lateral-stability derivatives. Twin vertical tails; horizontal tail at center fuselage; $i_t = 0^o$; rotor/wing 4.

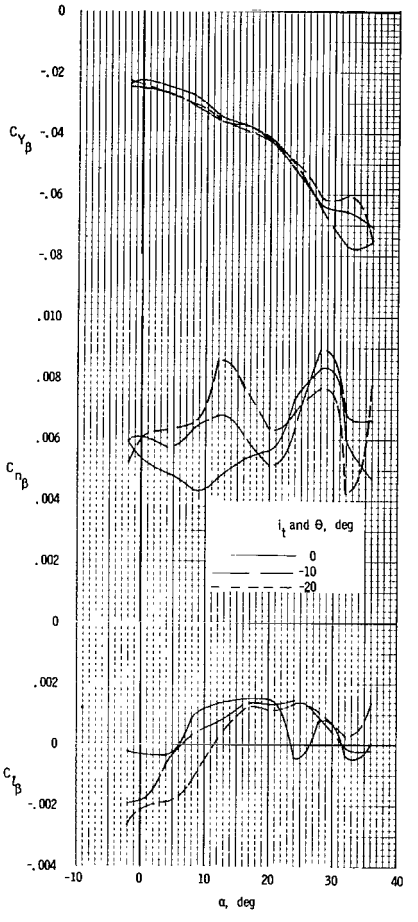

Figure 91.- Static lateral-stability derivatives for combinations of Θ and i_t. Twin vertical tails; horizontal tail at center fuselage; rotor/wing 4.

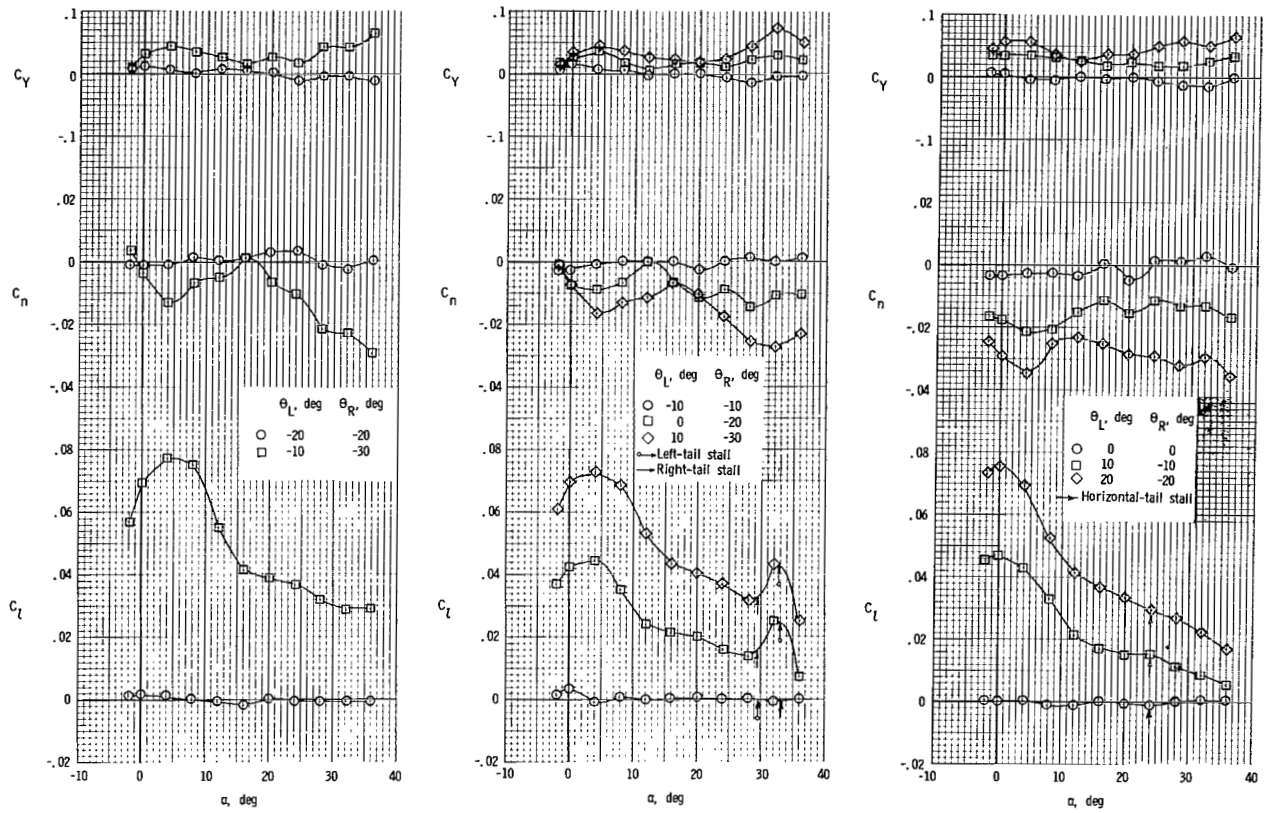

(a) $i_t = 0°$; $\Theta_{mean} = 0°$.

(b) $i_t = -10°$; $\Theta_{mean} = -10°$.

(c) $i_t = -20°$; $\Theta_{mean} = -20°$.

Figure 92.- Lateral-control characteristics with rotor blades used for control. Twin vertical tails; horizontal tail at center fuselage; rotor/wing 4.

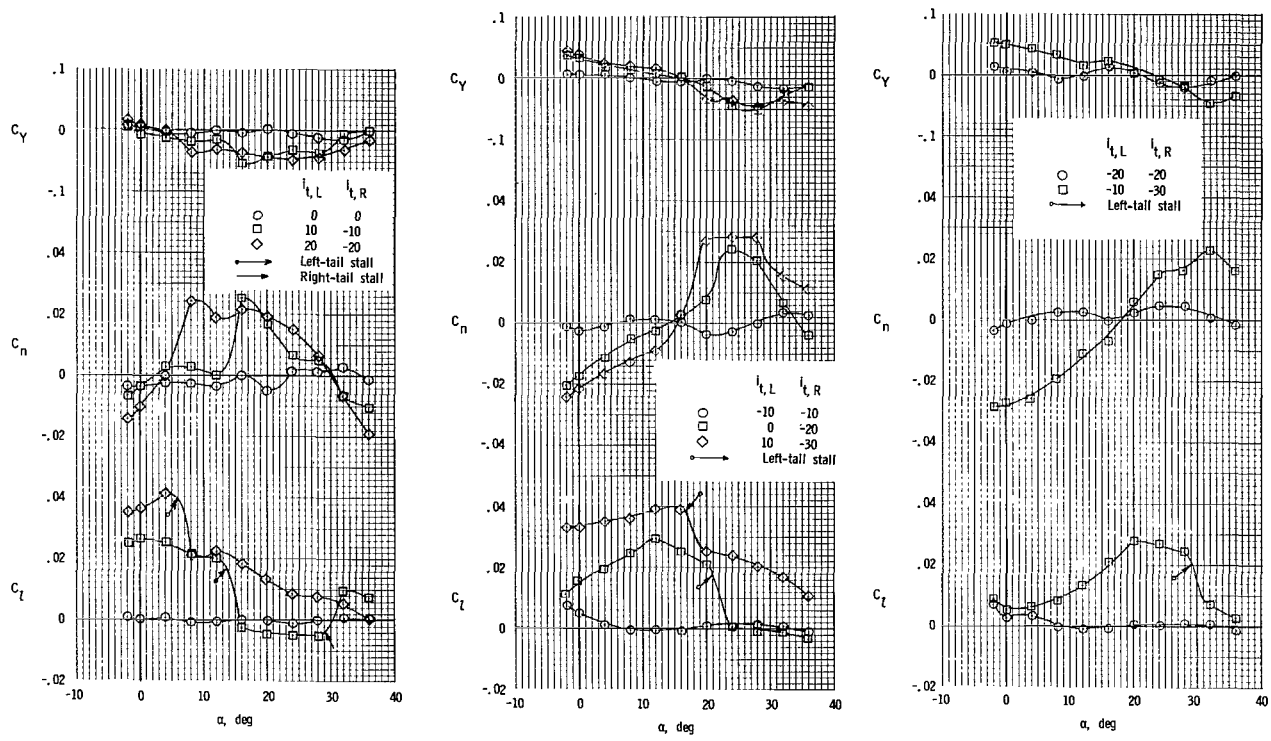

(a) $i_{t,mean} = 0^{\circ}$. (b) $i_{t,mean} = -10^{\circ}$. (c) $i_{t,mean} = -20^{\circ}$.

Figure 93.- Lateral-control characteristics with horizontal tail used for control. Twin vertical tails; horizontal tail at center fuselage; $\Theta = 0^{\circ}$; rotor/wing 4.

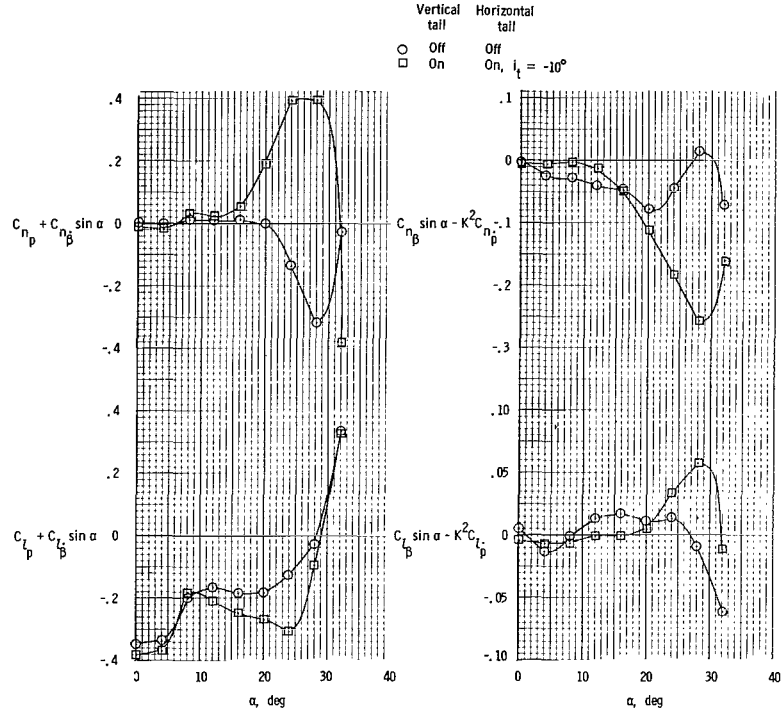

(a) Out-of-phase derivatives.

(b) In-phase derivatives.

Figure 94.- Effect of tails on dynamic-stability derivatives measured in rolling-oscillation tests. Center vertical tail; mid horizontal tail; $\Theta = 0^\circ$; rotor/wing 4.

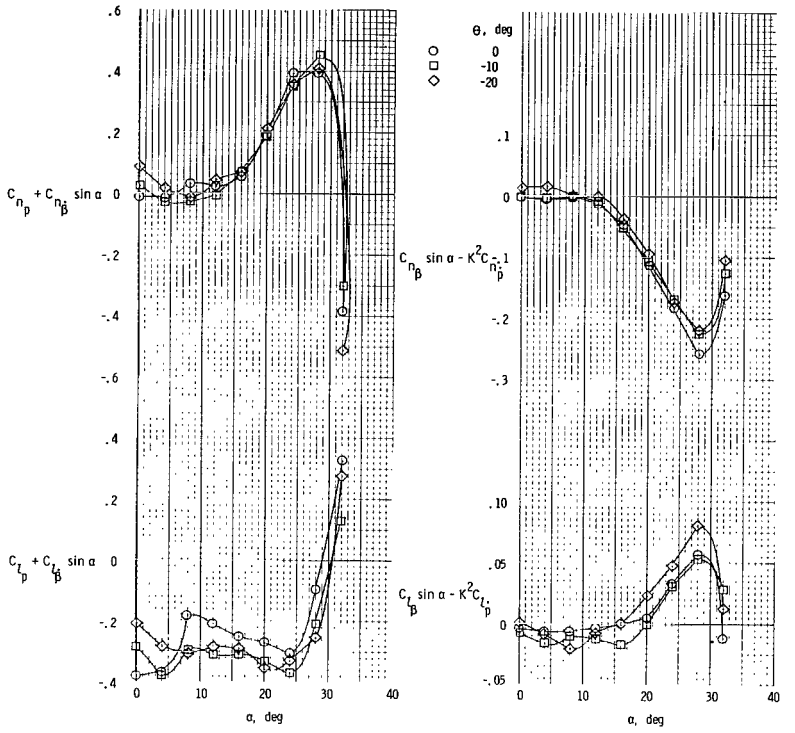

(a) Out-of-phase derivatives.

(b) In-phase derivatives.

Figure 95.- Effect of rotor-blade incidence on dynamic-stability derivatives measured in rolling-oscillation tests. Center vertical tail; mid horizontal tail; $i_t = -10^\circ$; rotor/wing 4.

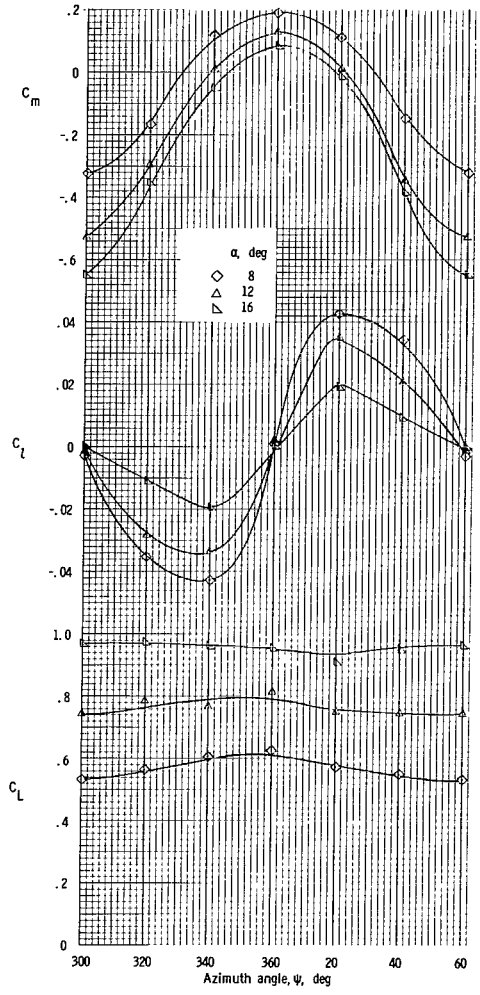

Figure 96.- Effect of azimuth position on lift coefficient and rolling- and pitching-moment coefficients for changes in model angle of attack. $i_t = 0^\circ$; $\Theta = 0^\circ$; rotor/wing 4.

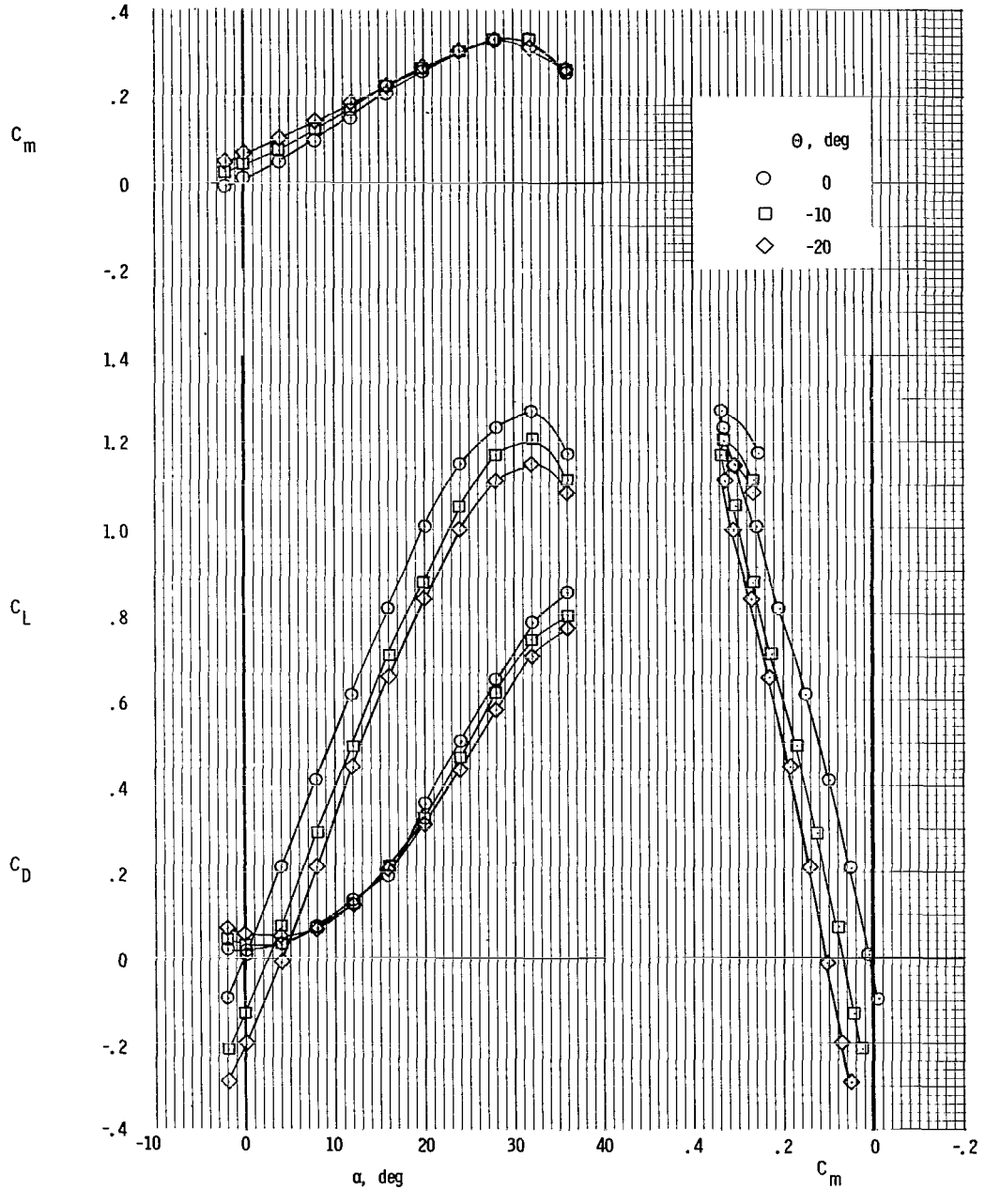

Figure 97.- Longitudinal aerodynamic characteristics. Tails off; rotor/wing 5.

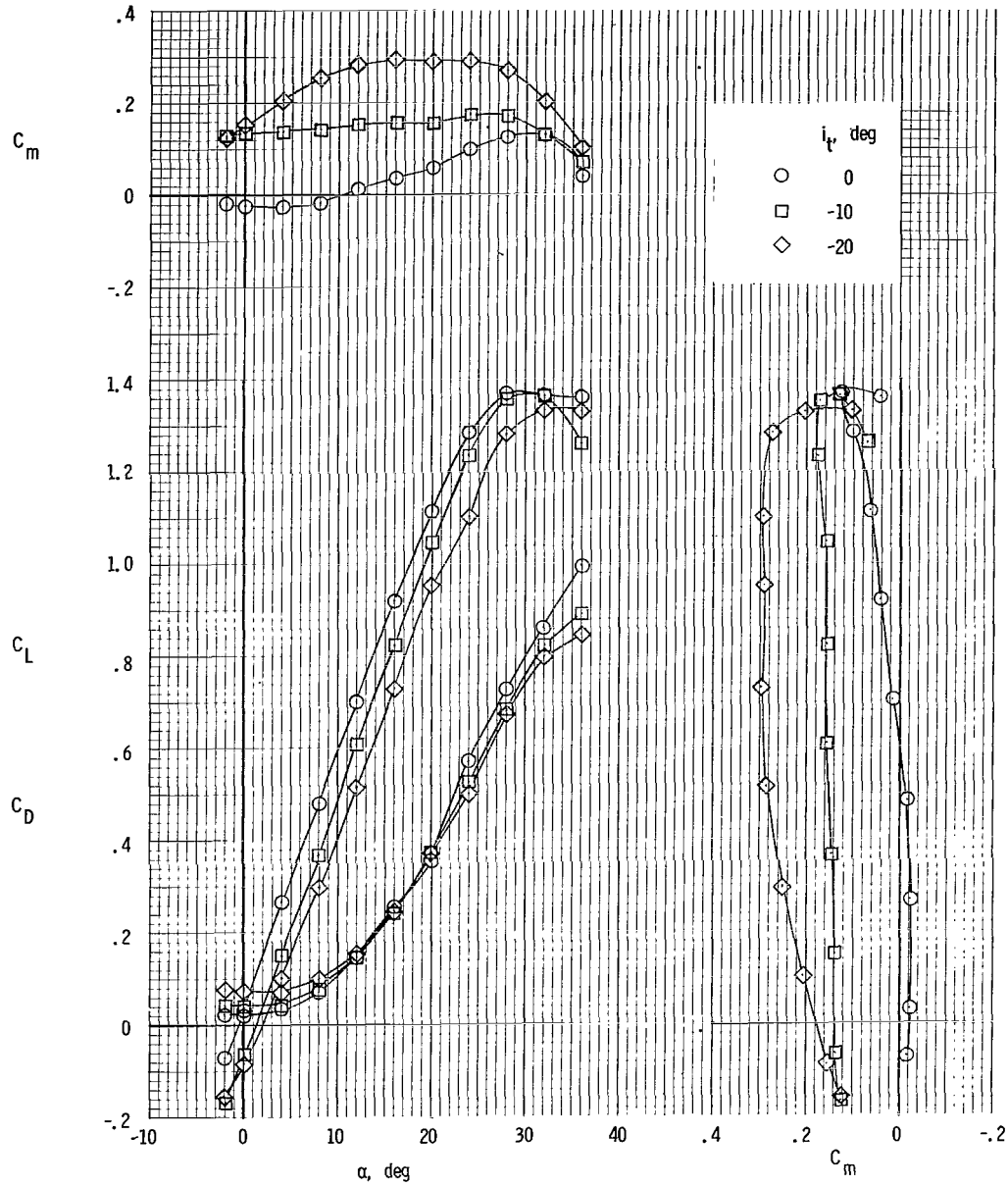

(a) $\Theta = 0^{\circ}$.

Figure 98.- Longitudinal aerodynamic characteristics. Low horizontal tail; center vertical tail; rotor/wing 5.

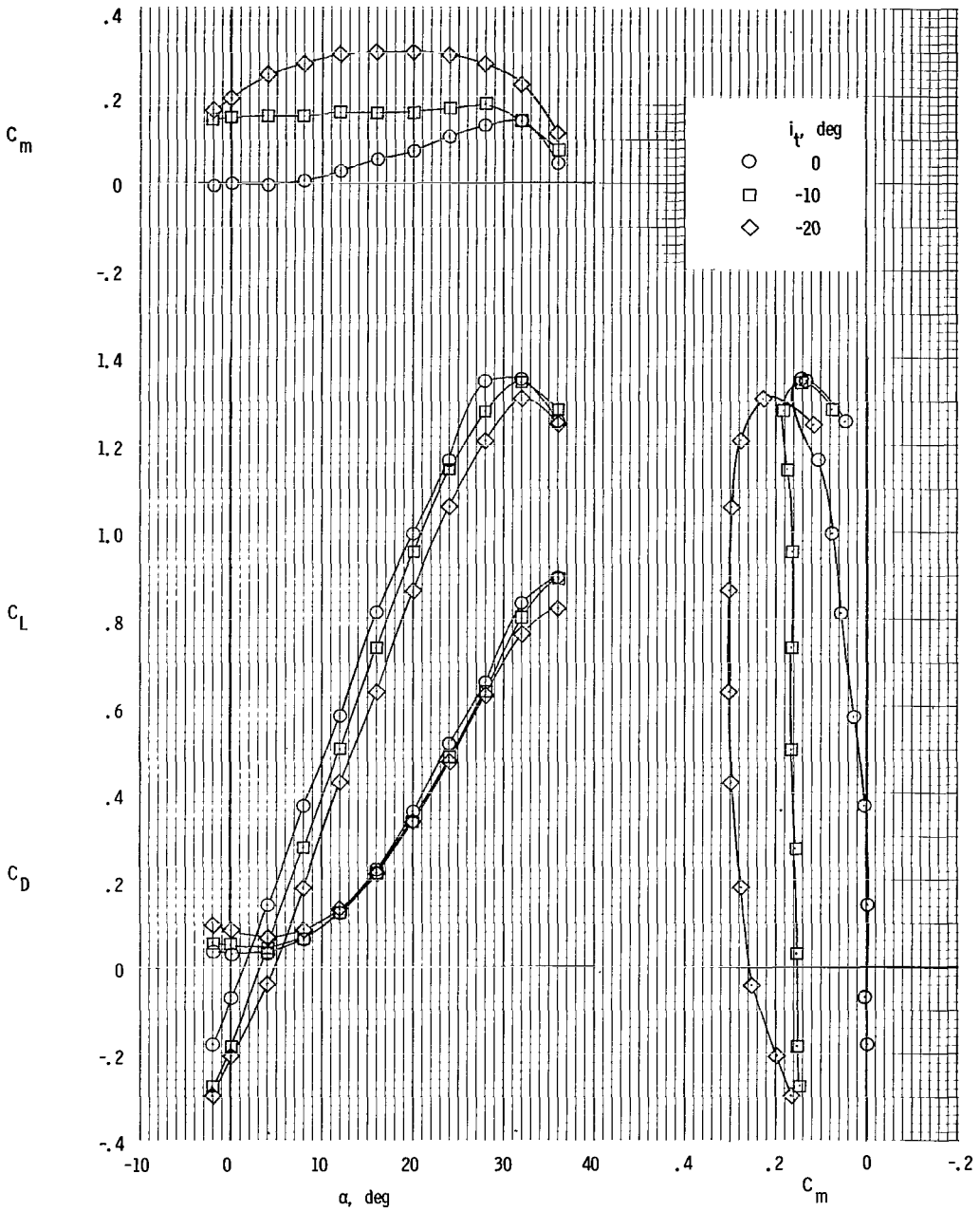

(b) $\Theta = -10^{\circ}$.

Figure 98.- Continued.

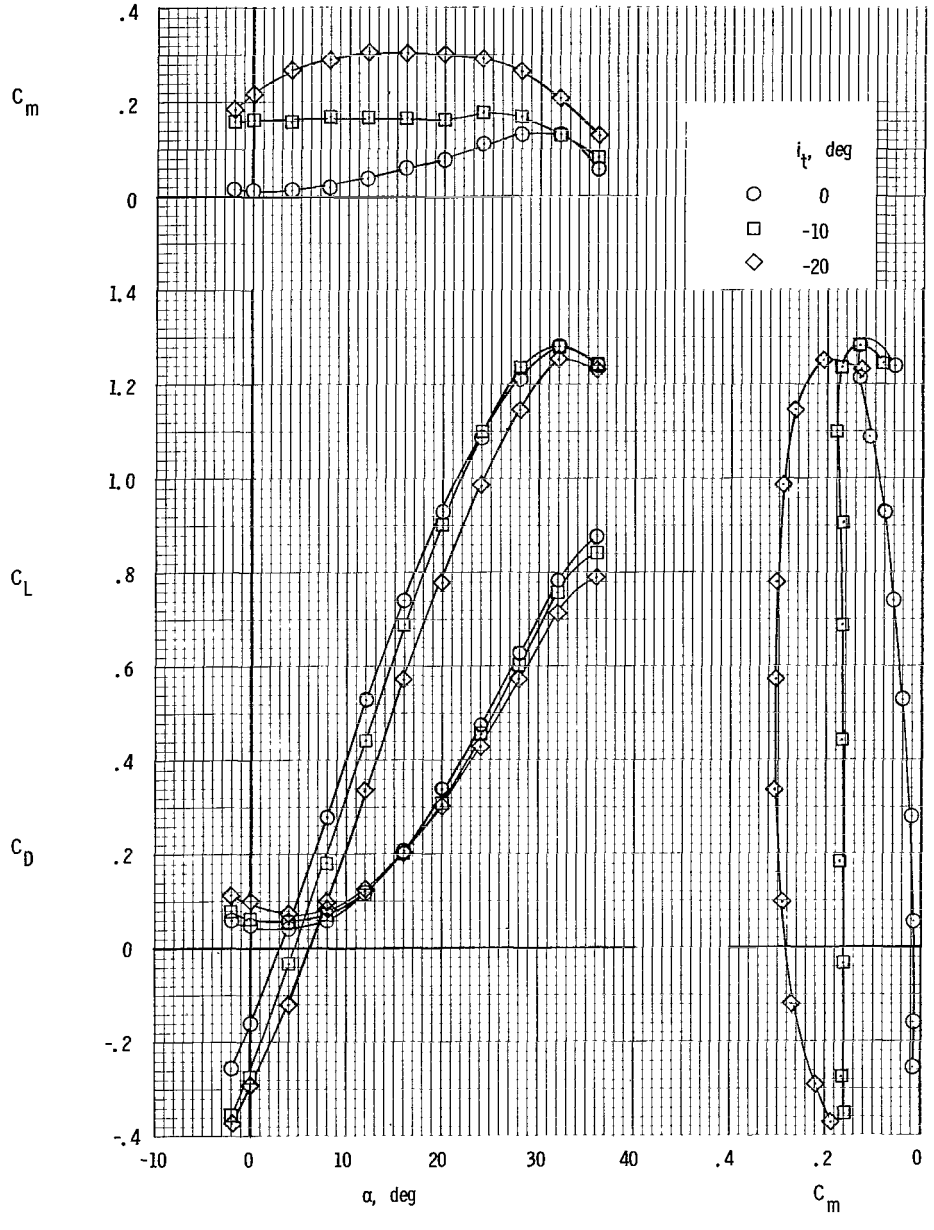

(c) $\Theta = -20^{\circ}$.

Figure 98.- Concluded.

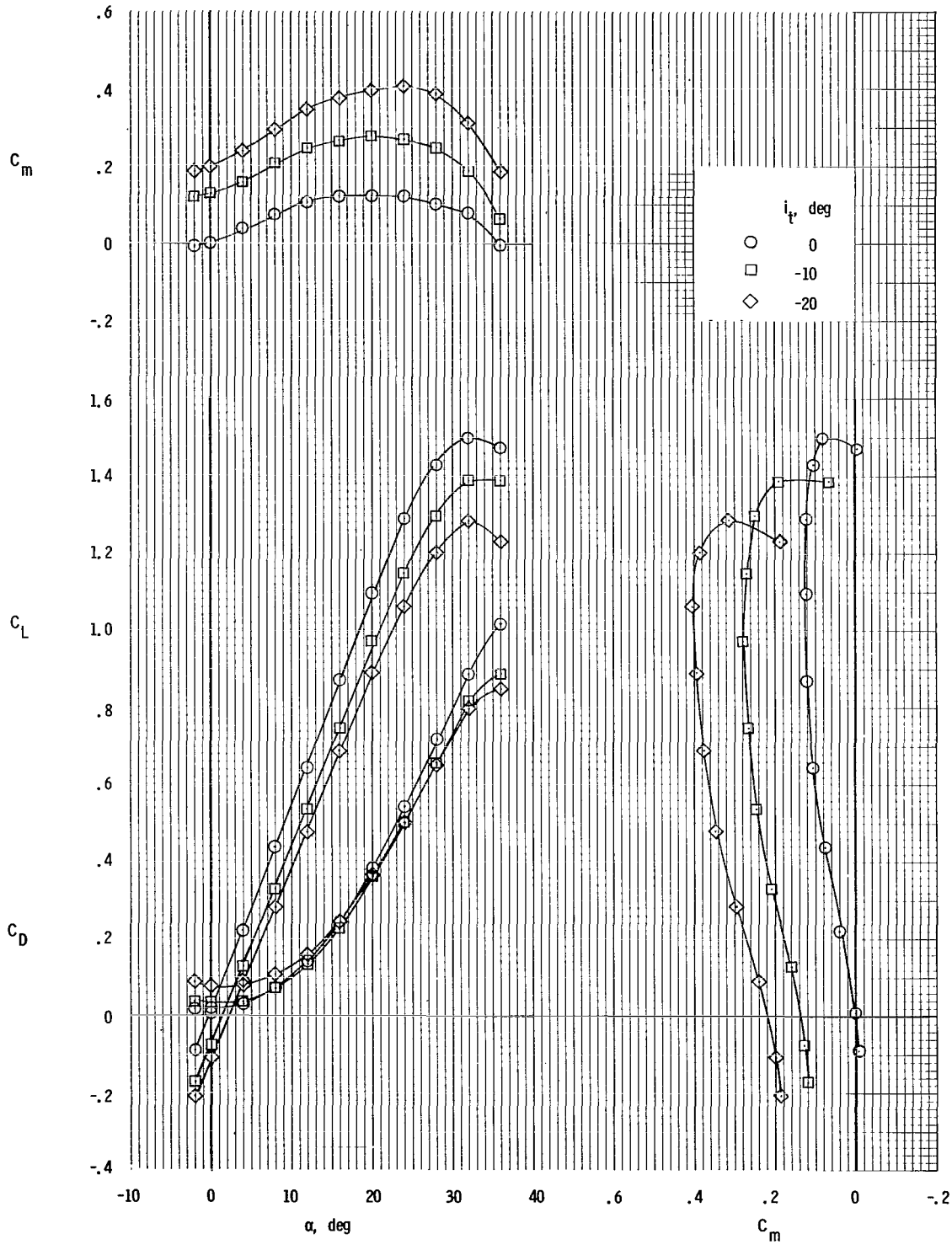

(a) $\Theta = 0^{\circ}$.

Figure 99.- Longitudinal aerodynamic characteristics. Mid horizontal tail; center vertical tail; rotor/wing 5.

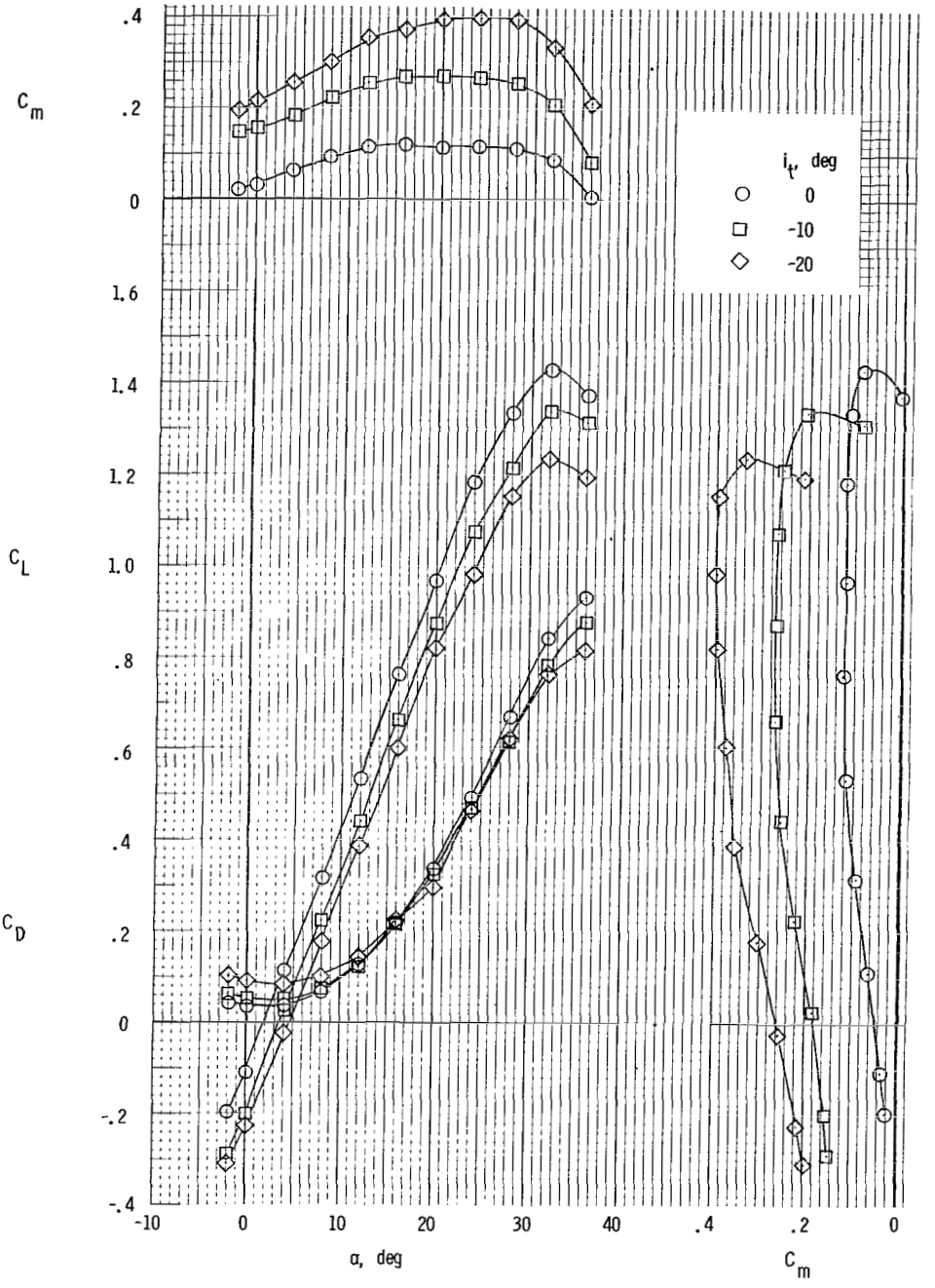

(b) $\Theta = -10^{\circ}$.

Figure 99.- Continued.

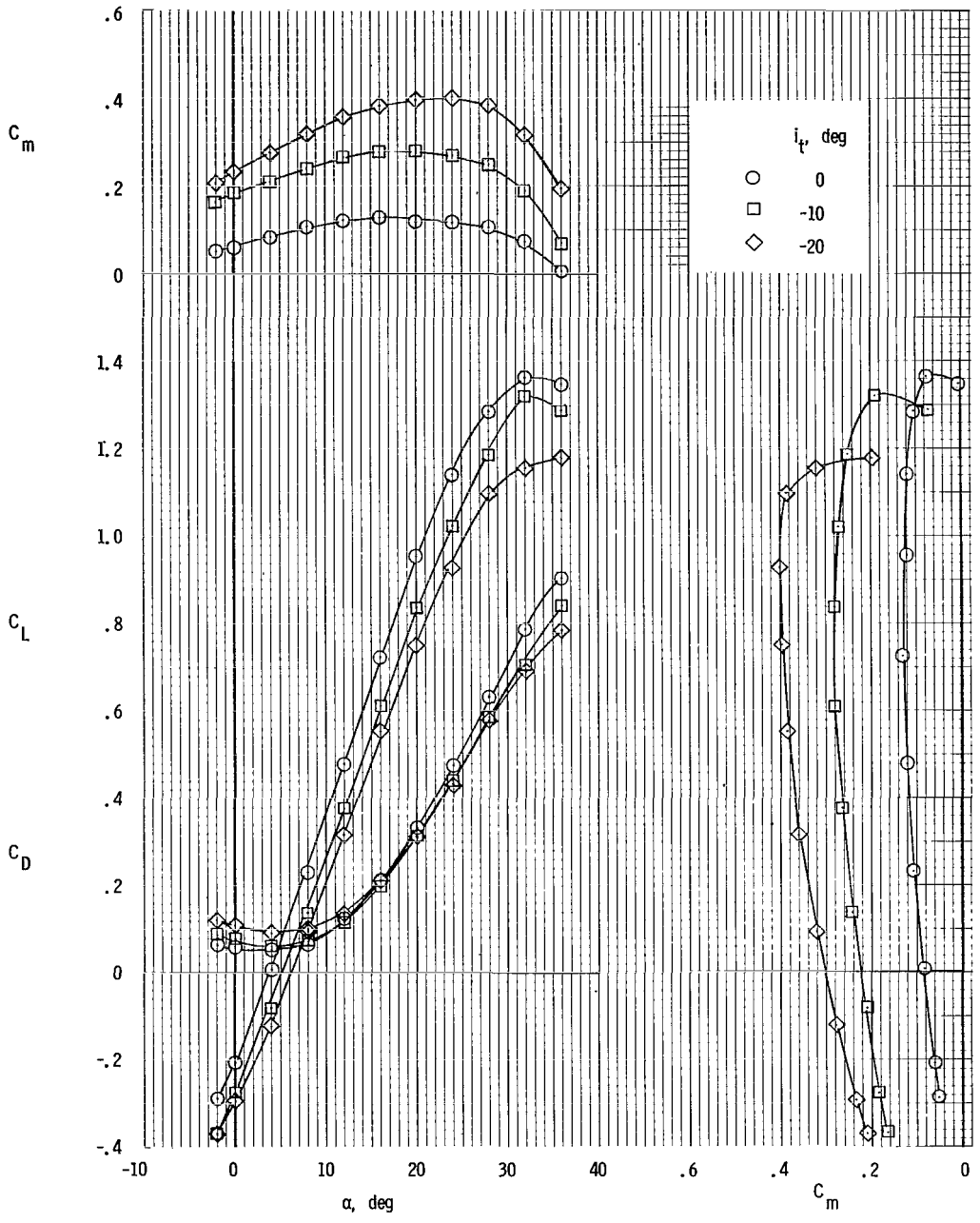

(c) $\Theta = -20^{\circ}$.

Figure 99.- Concluded.

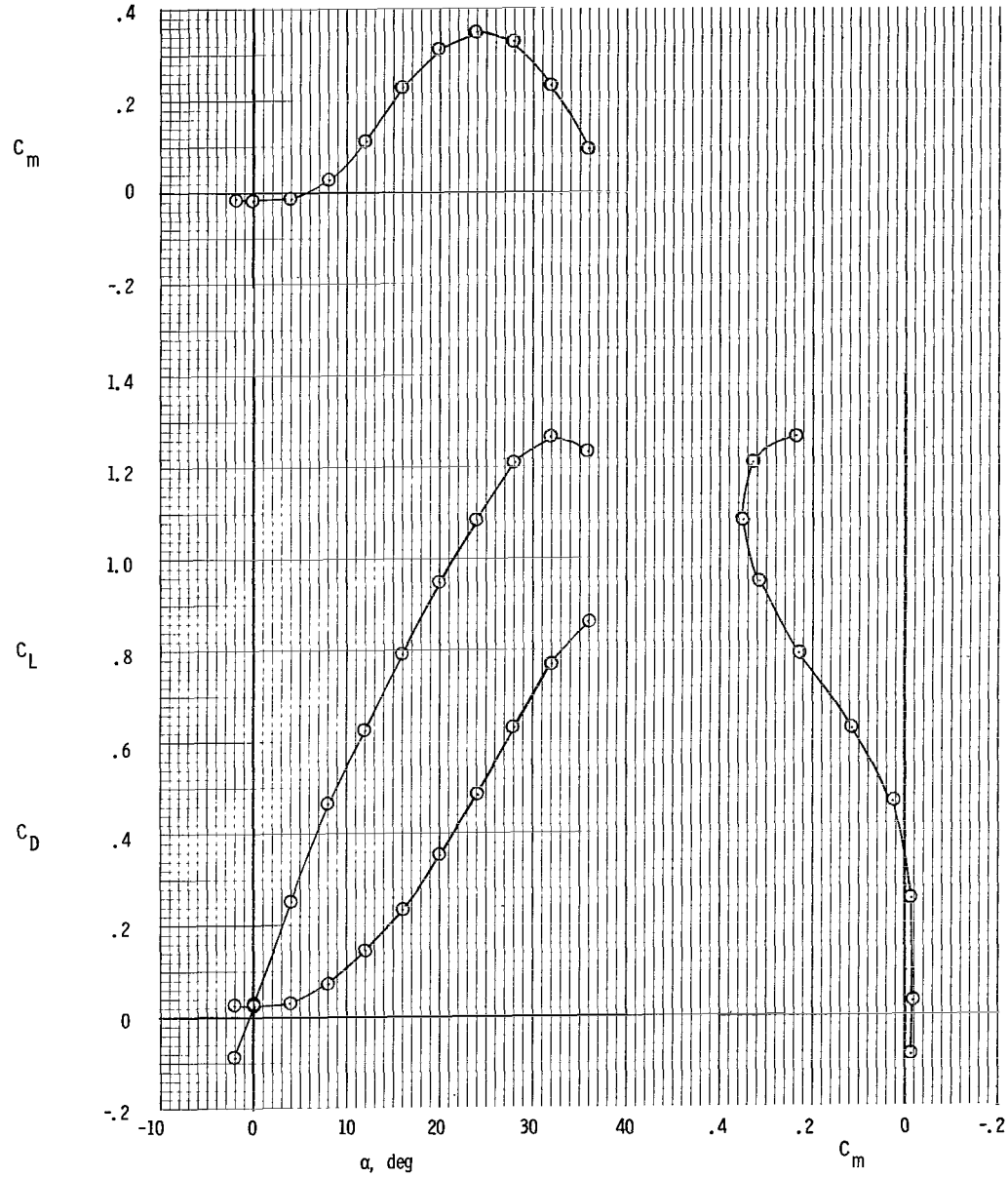

Figure 100.- Longitudinal aerodynamic characteristics. High horizontal tail; center vertical tail; $\Theta = 0^{\circ}$; $i_t = 0^{\circ}$; rotor/wing 5.

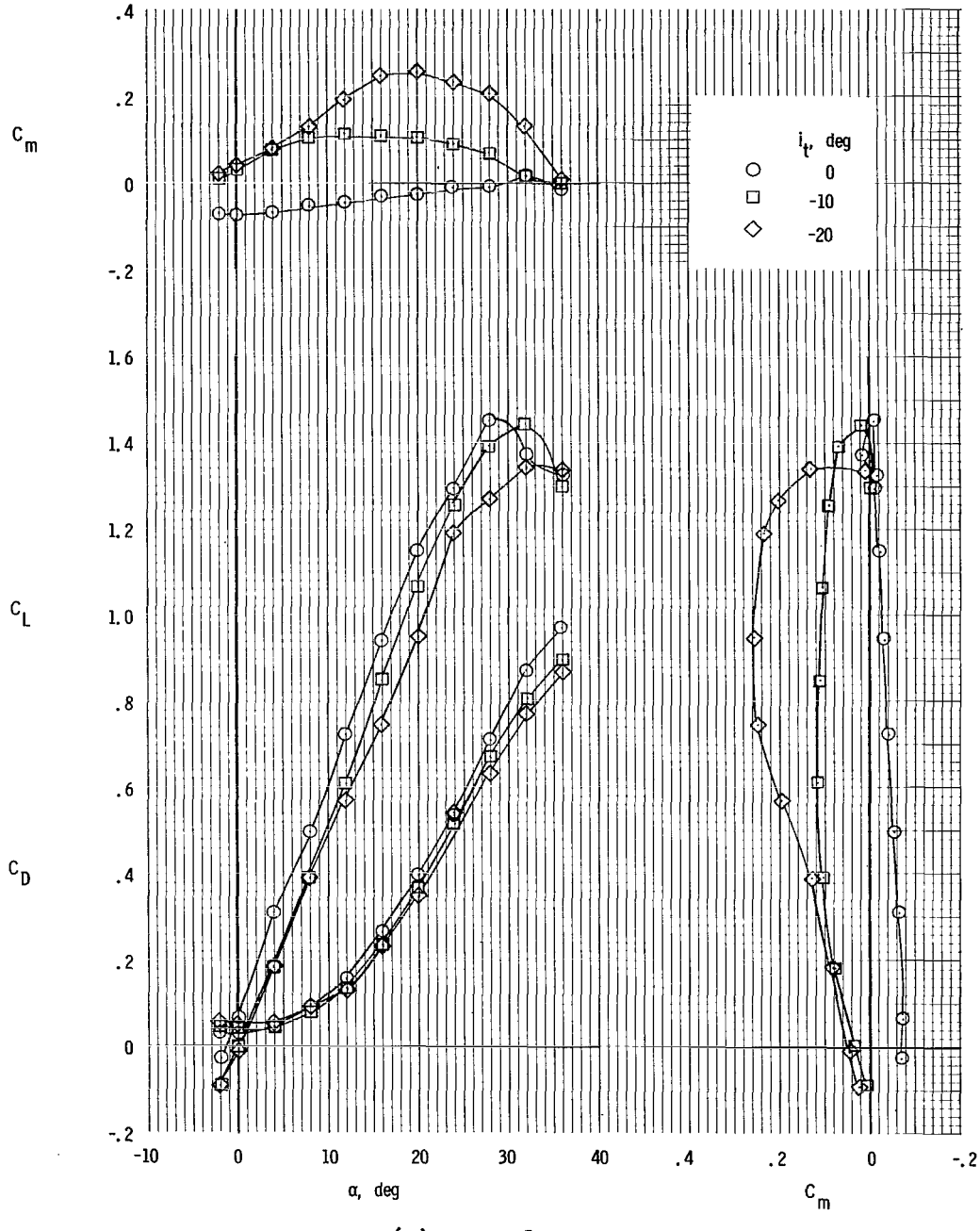

(a) $\Theta = 0^{\circ}$.

Figure 101.- Longitudinal aerodynamic characteristics. Twin vertical tails; horizontal tail at center fuselage; rotor/wing 5.

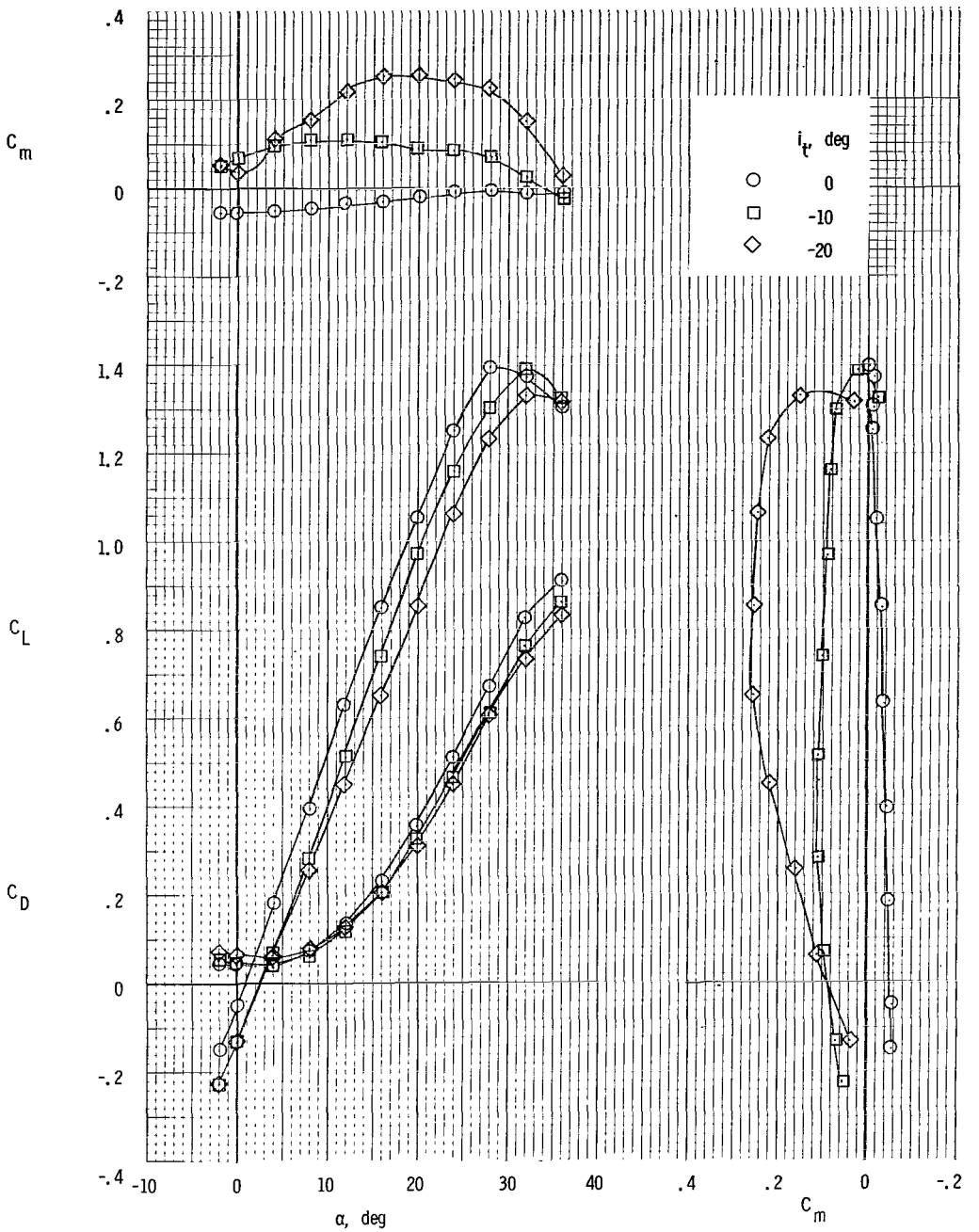

(b) $\Theta = -10^{\circ}$.

Figure 101.- Continued.

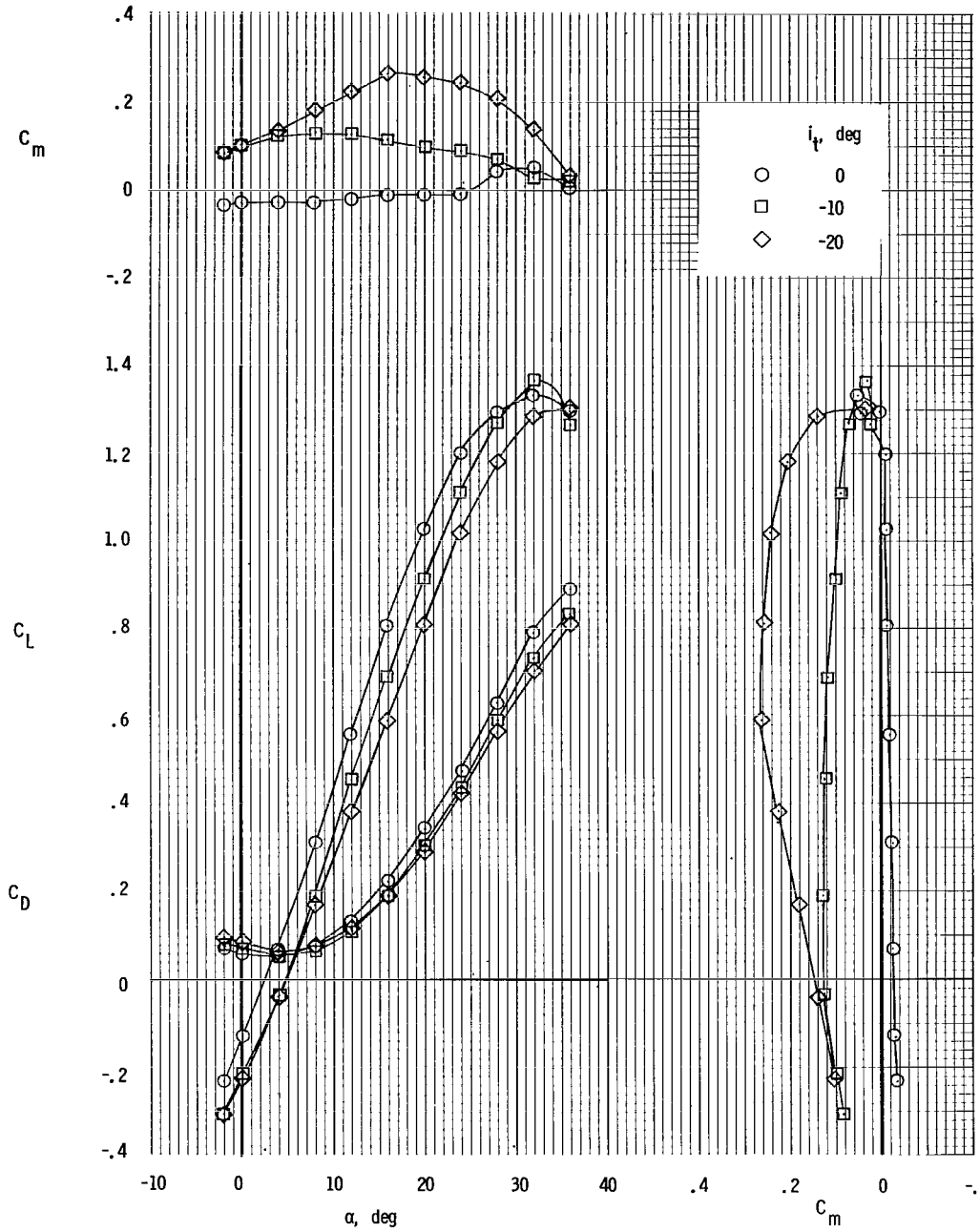

(c) $\Theta = -20^{\circ}$.

Figure 101.- Concluded.

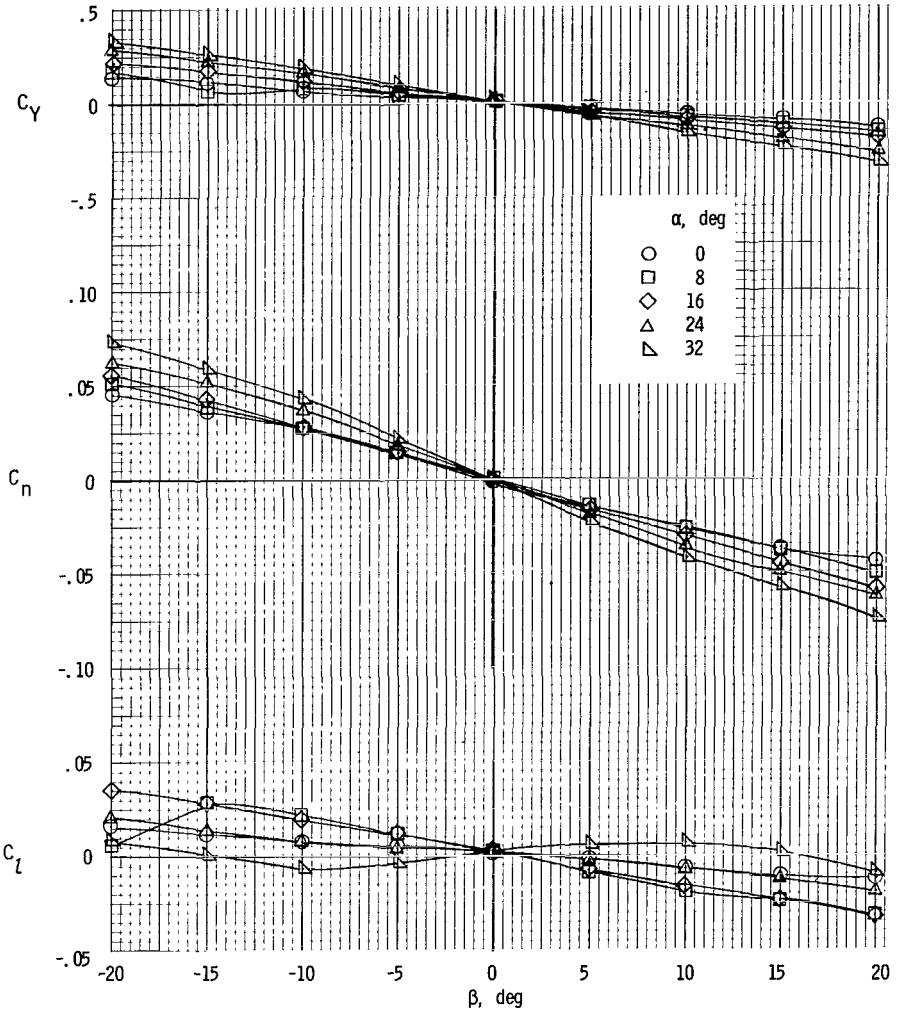

Figure 102.- Sideslip characteristics. Tails off; $\Theta = -10^{\circ}$; rotor/wing 5.

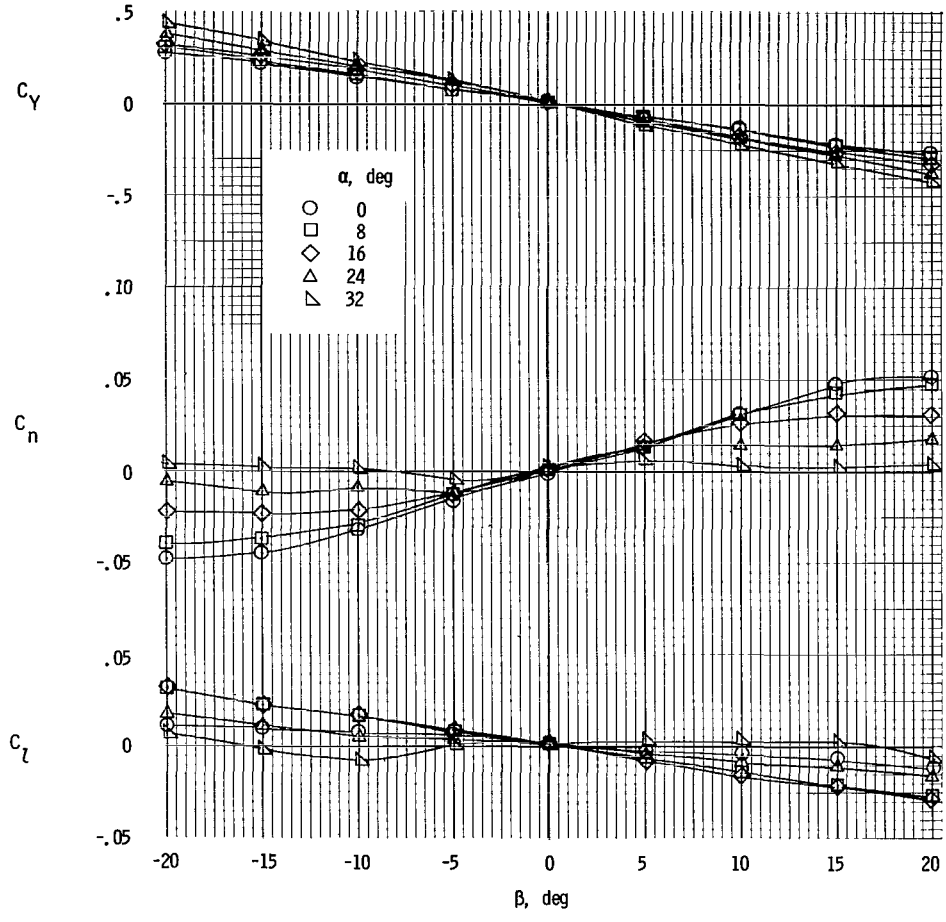

Figure 103.- Sideslip characteristics. Twin vertical tails; horizontal tail at center fuselage; $i_t = -10^\circ$; $\Theta = -10^\circ$; rotor/wing 5.

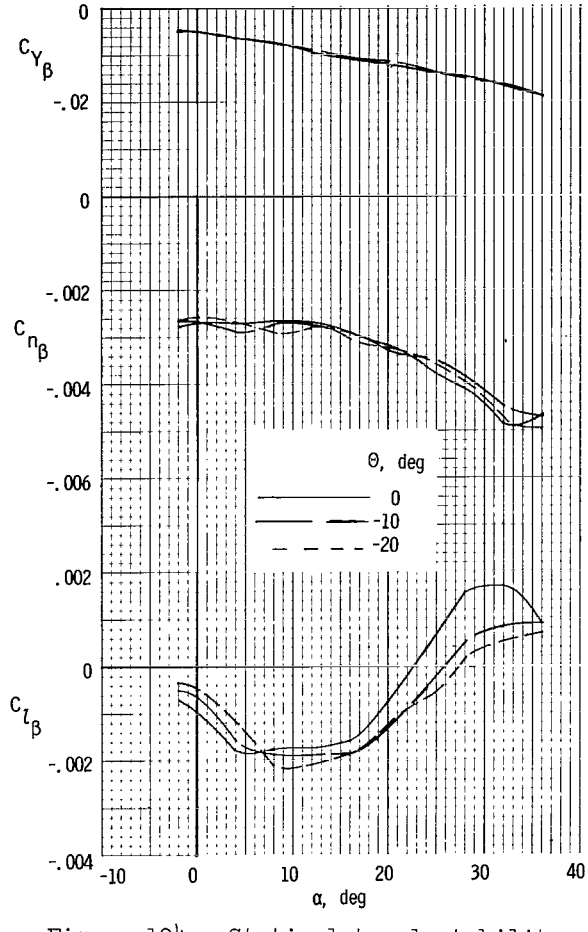

Figure 104.- Static lateral-stability derivatives. Tails off; rotor/wing 5.

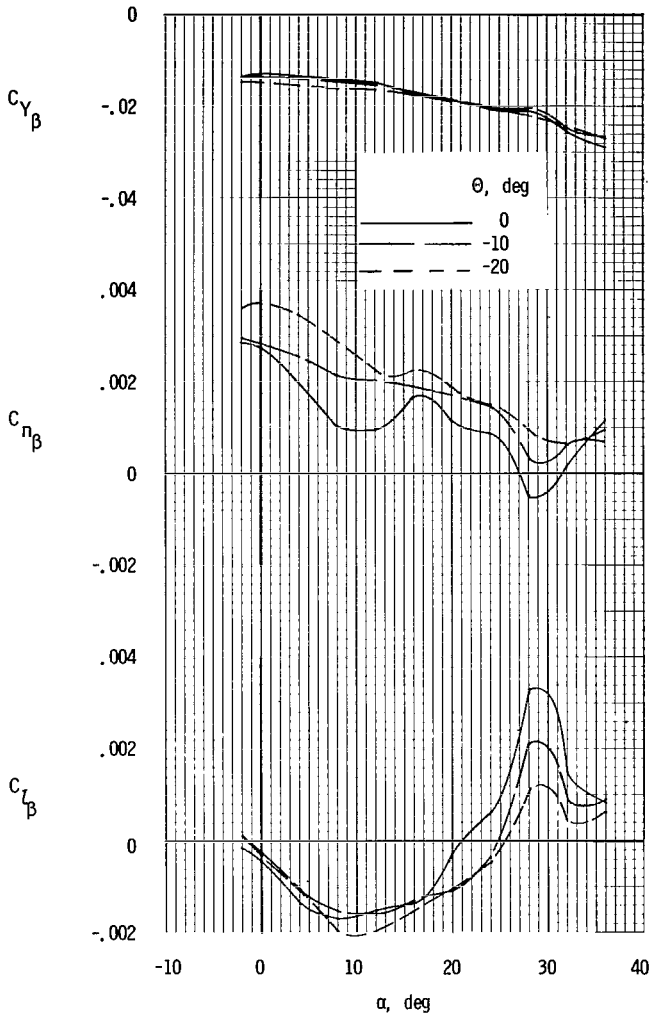

Figure 105.- Static lateral-stability derivatives. Twin vertical tails; horizontal tail at center fuselage; $i_t = 0^o$; rotor/wing 5.

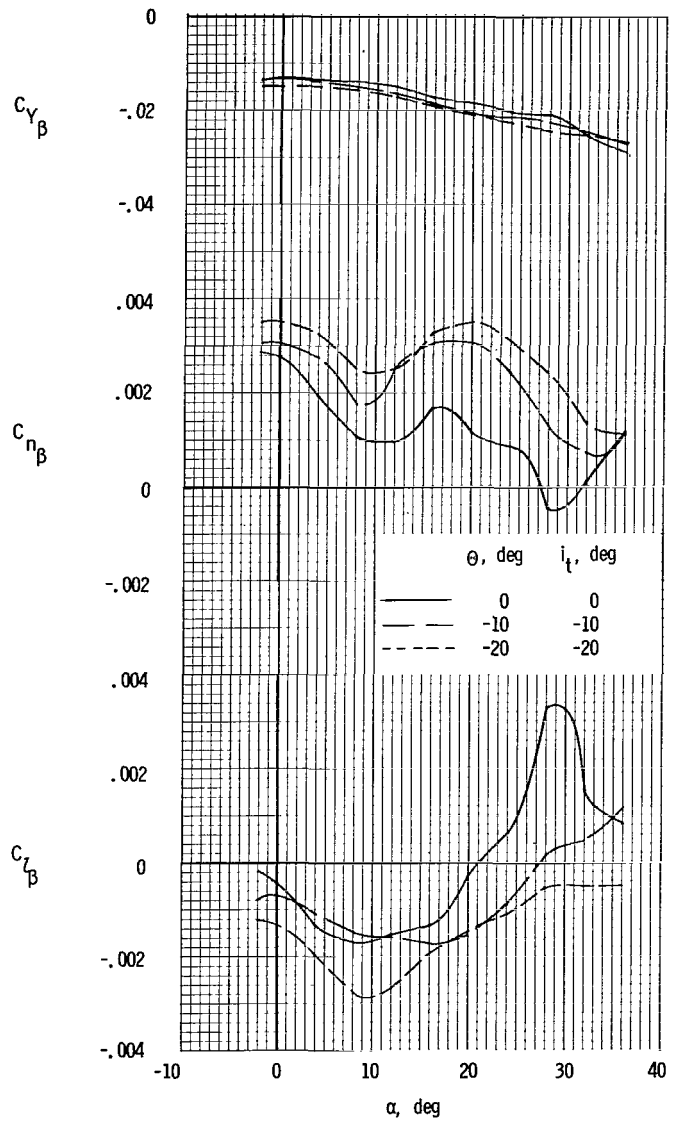

Figure 106.- Static lateral-stability derivatives for combinations of Θ and i_t. Twin vertical tails; horizontal tail at center fuselage; rotor/wing 5.

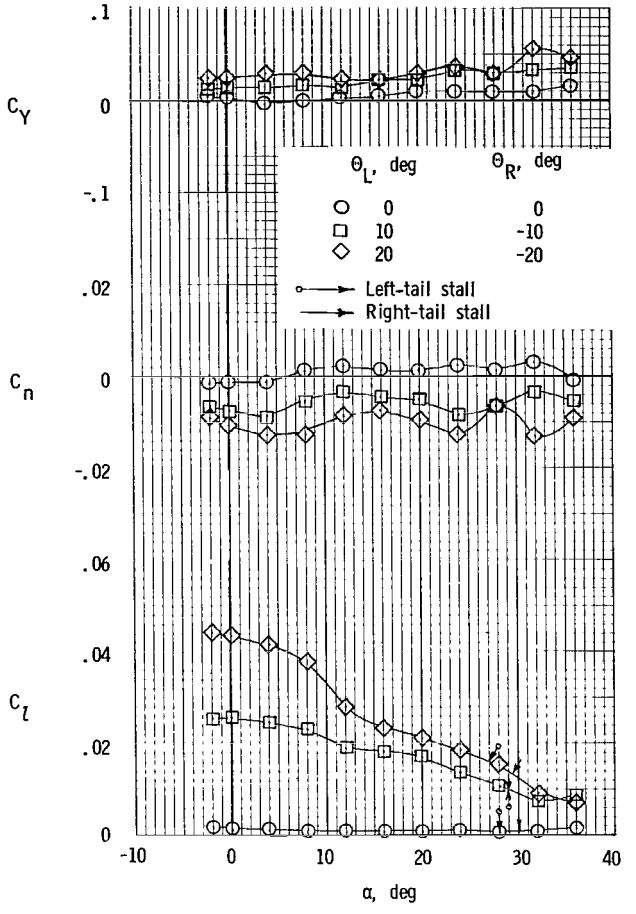

(a) $i_t = 0^\circ$; $\Theta_{mean} = 0^\circ$.

Figure 107.- Lateral-control characteristics with rotor blades used for control. Twin vertical tails; horizontal tail at center fuselage; rotor/wing 5.

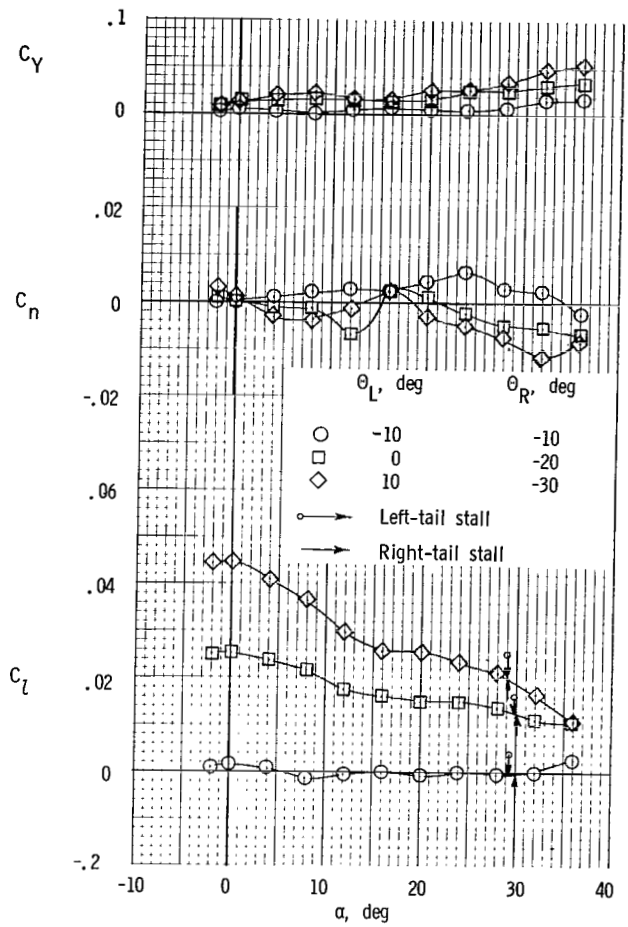

(b) $i_t = -10^\circ$; $\Theta_{mean} = -10^\circ$.

Figure 107.- Continued.

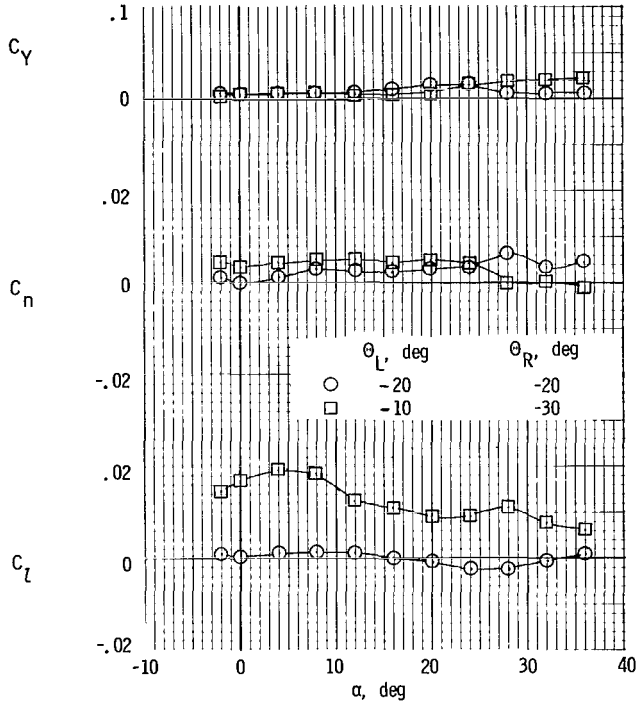

(c) $i_t = -20^\circ$; $\Theta_{mean} = -20^\circ$.

Figure 107.- Concluded.

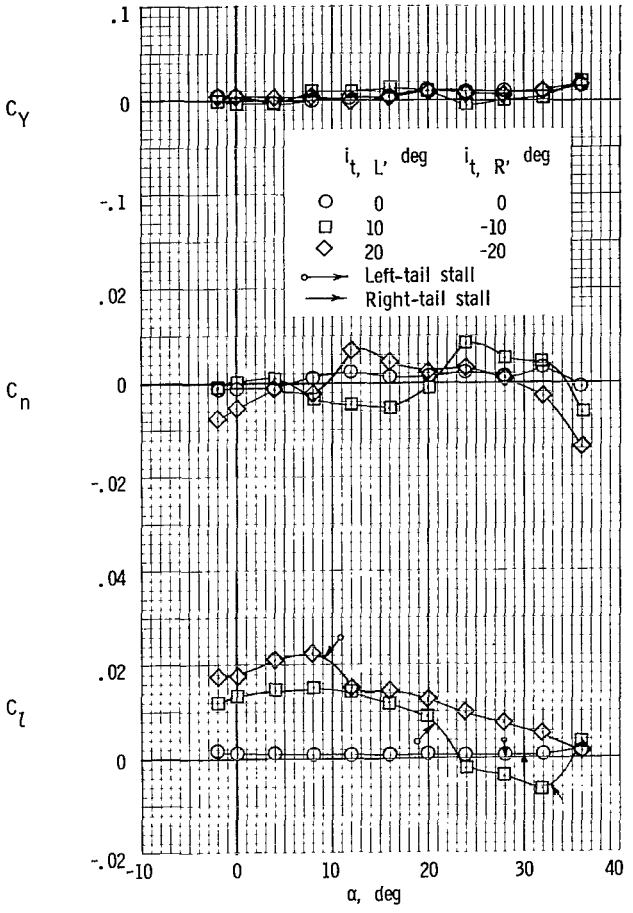

(a) $i_{t,mean} = 0^\circ$.

Figure 108.- Lateral-control characteristics with horizontal tail used for control. Twin vertical tails; horizontal tail at center fuselage; $\Theta = 0^\circ$; rotor/wing 5.

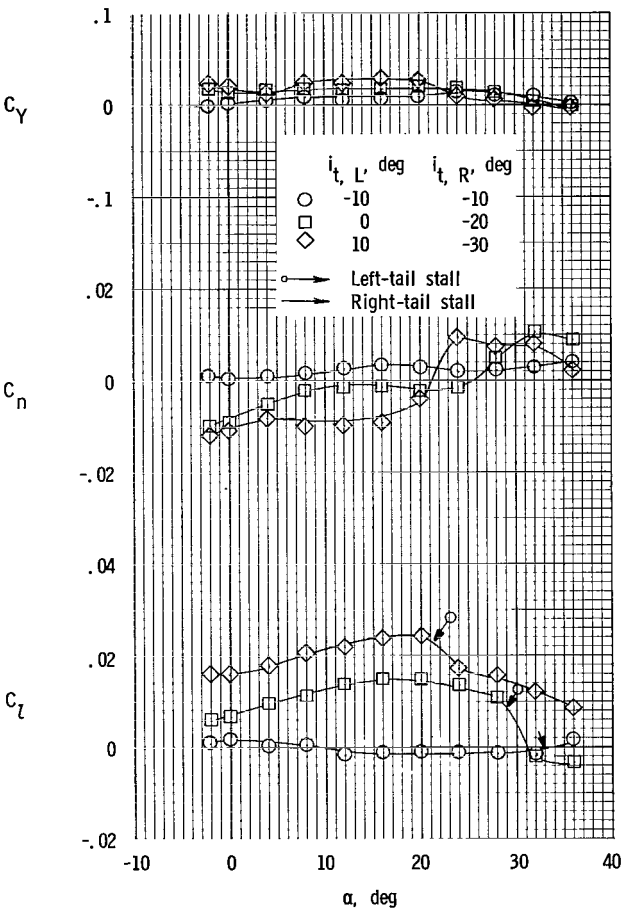

(b) $i_{t,mean} = -10^{\circ}$.

Figure 108.- Continued.

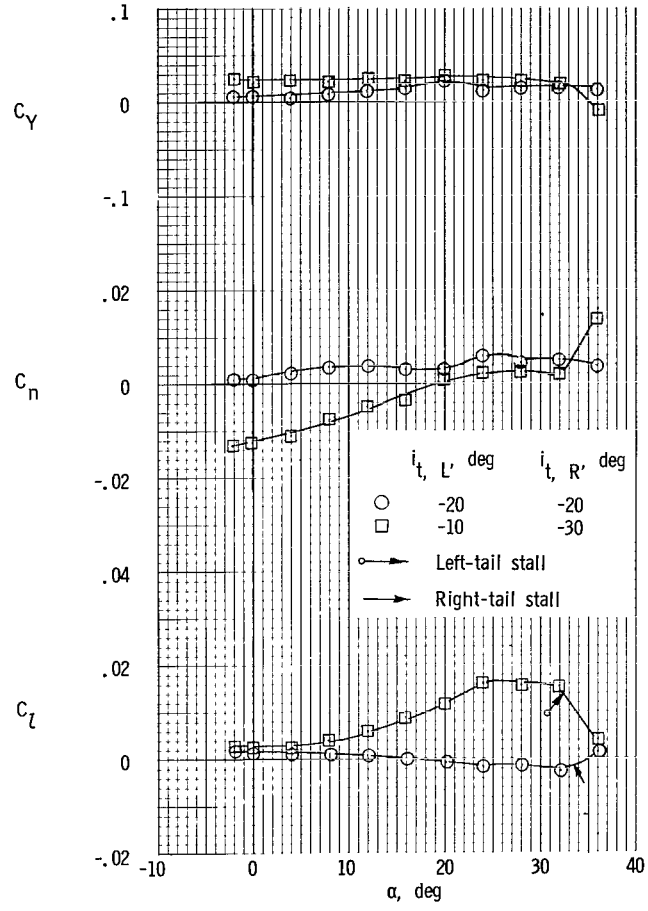

(c) $i_{t,mean} = -20°$.

Figure 108.- Concluded.

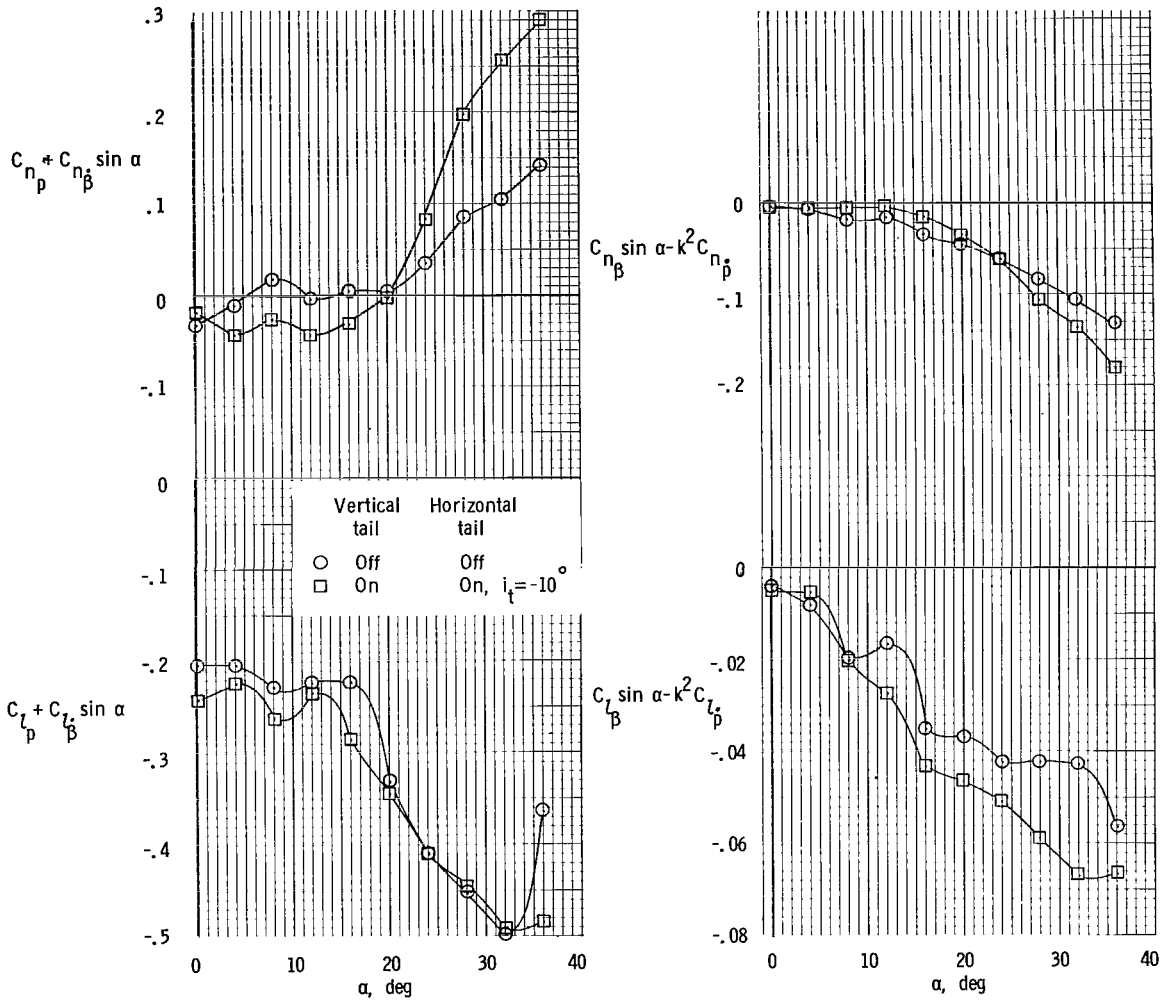

(a) Out-of-phase derivatives.

(b) In-phase derivatives.

Figure 109.- Effect of tails on dynamic-stability derivatives measured in rolling-oscillation tests. Center vertical tail; mid horizontal tail; $\Theta = 0°$; rotor/wing 5.

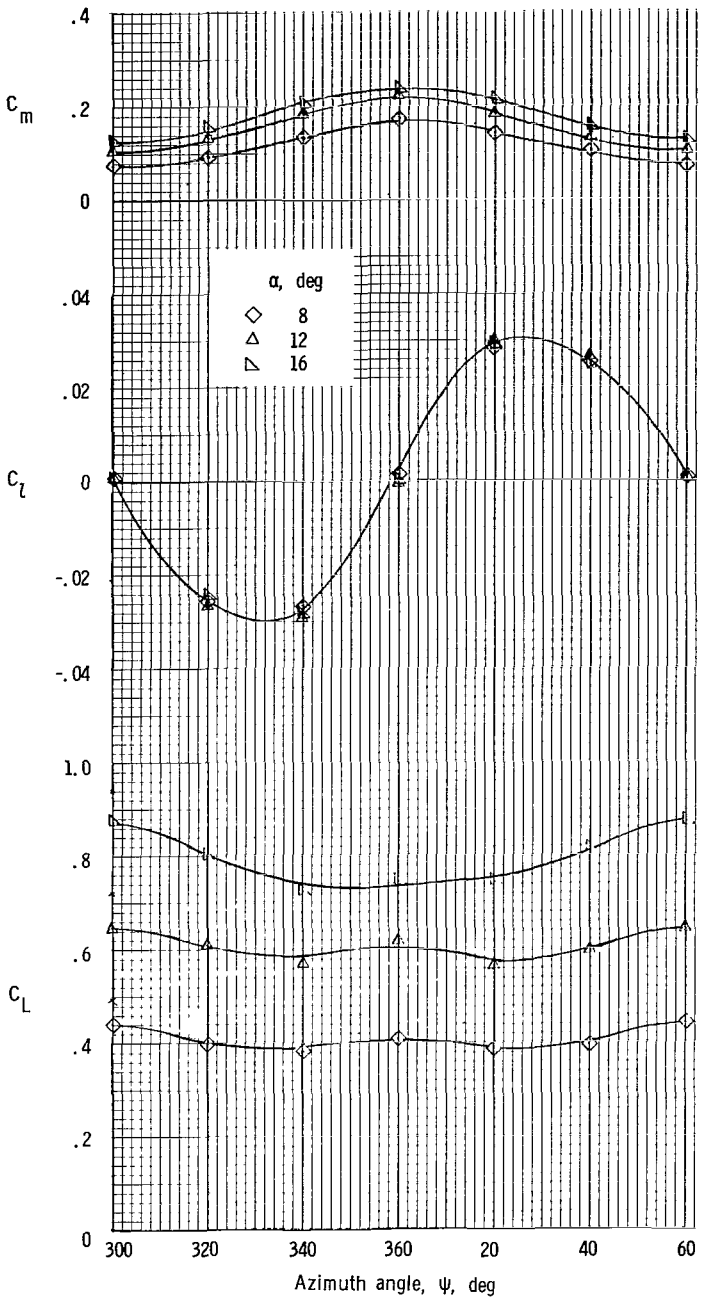

Figure 110.- Effect of azimuth location on lift coefficient and rolling- and pitching-moment coefficients for changes in model angle of attack. $i_t = 0^o$; $\Theta = 0^o$; rotor/wing 5.

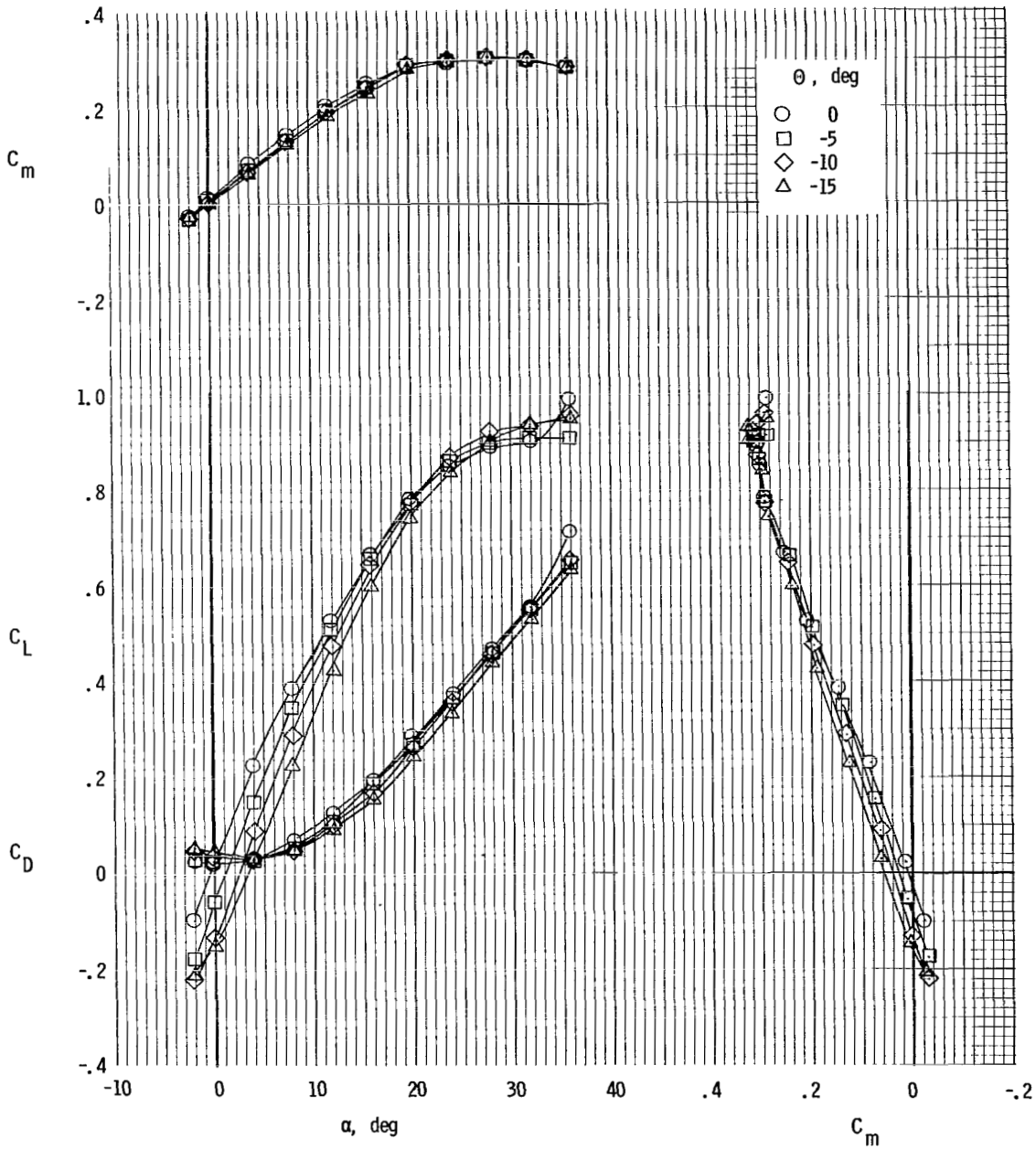

Figure 111.- Longitudinal aerodynamic characteristics. Tails off; rotor/wing 6.

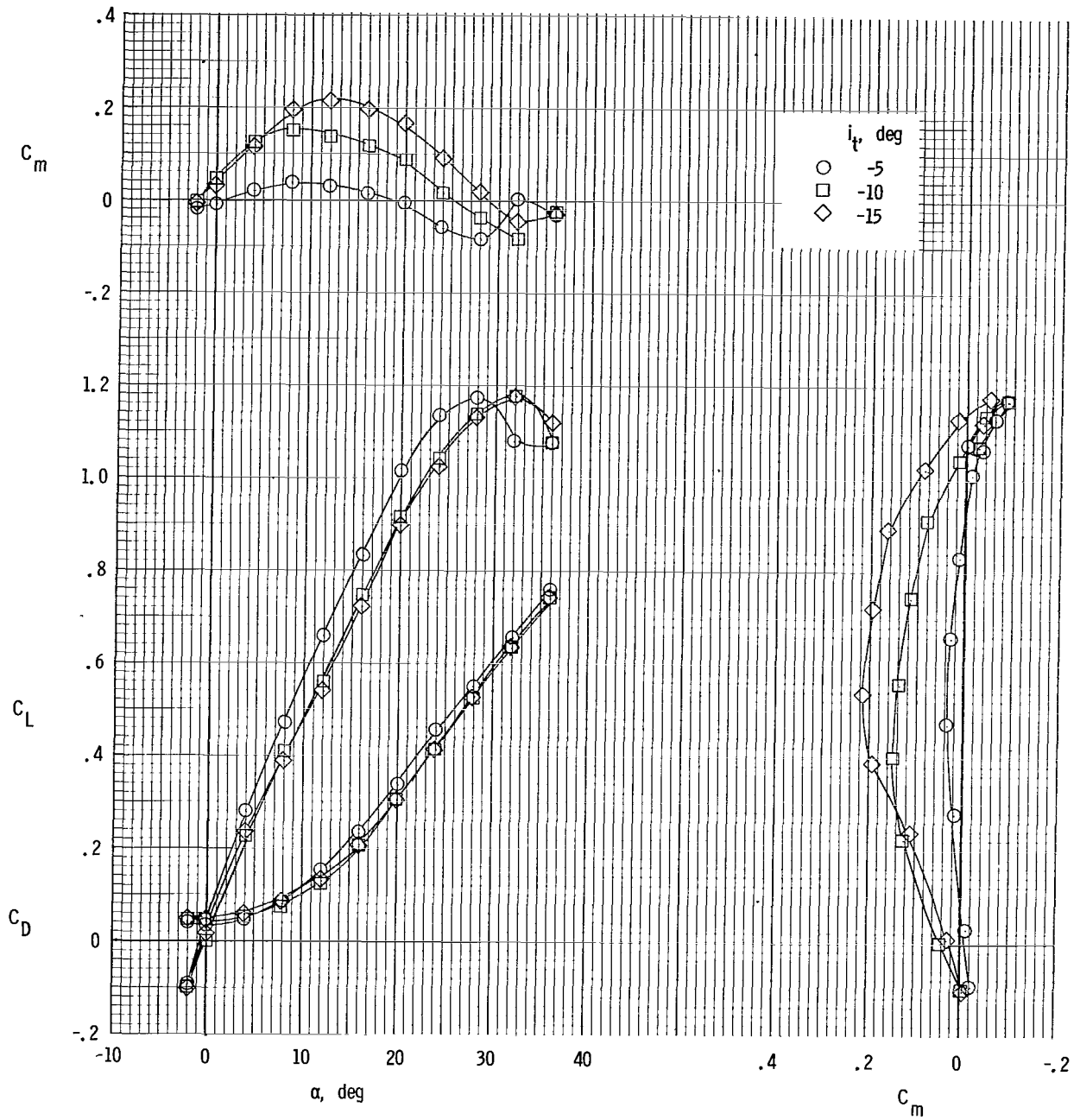

(a) $\Theta = 0^{\circ}$.

Figure 112.- Longitudinal aerodynamic characteristics. Twin vertical tails; horizontal tail at center fuselage; rotor/wing 6.

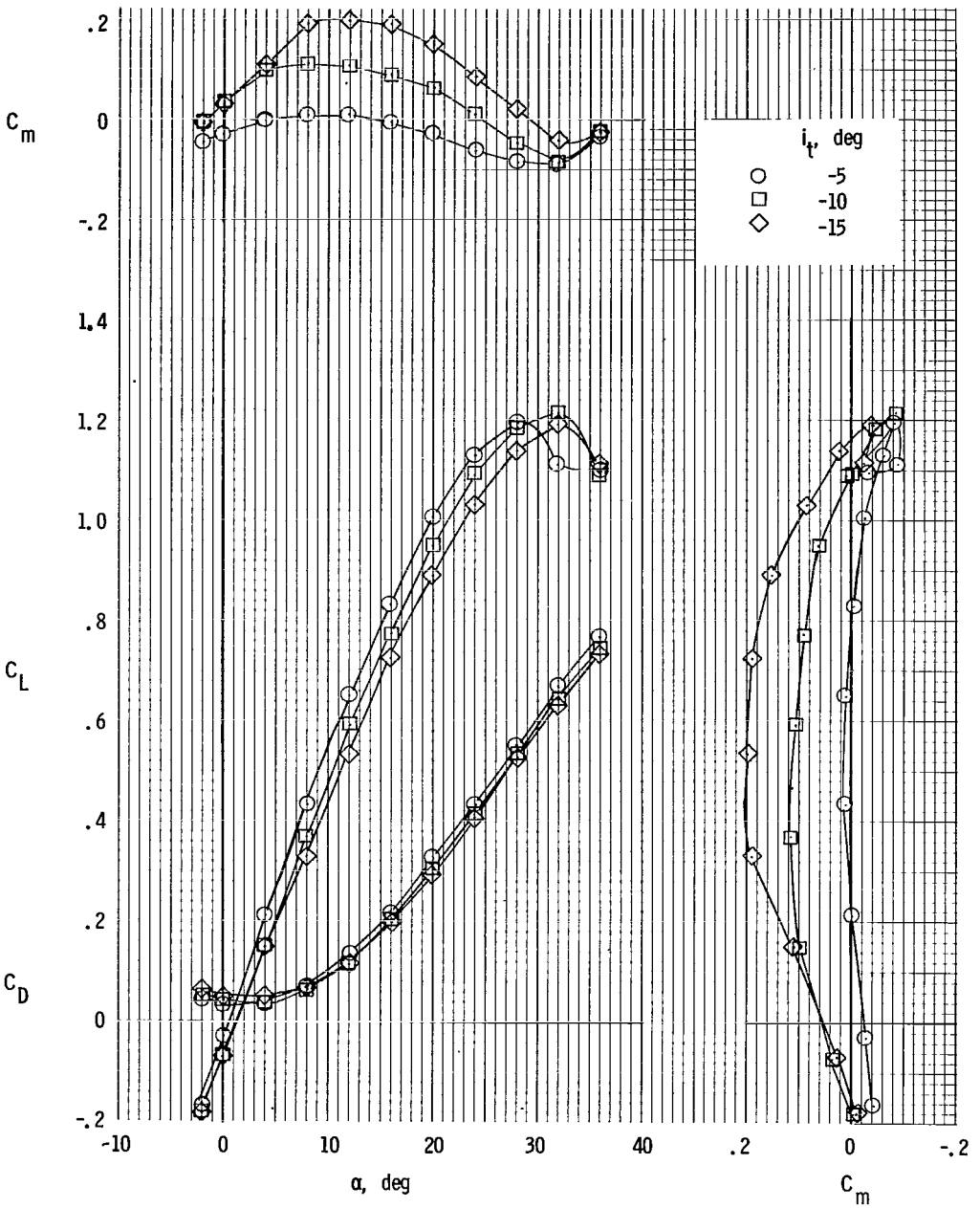

(b) $\Theta = -5^{\circ}$.

Figure 112.- Continued.

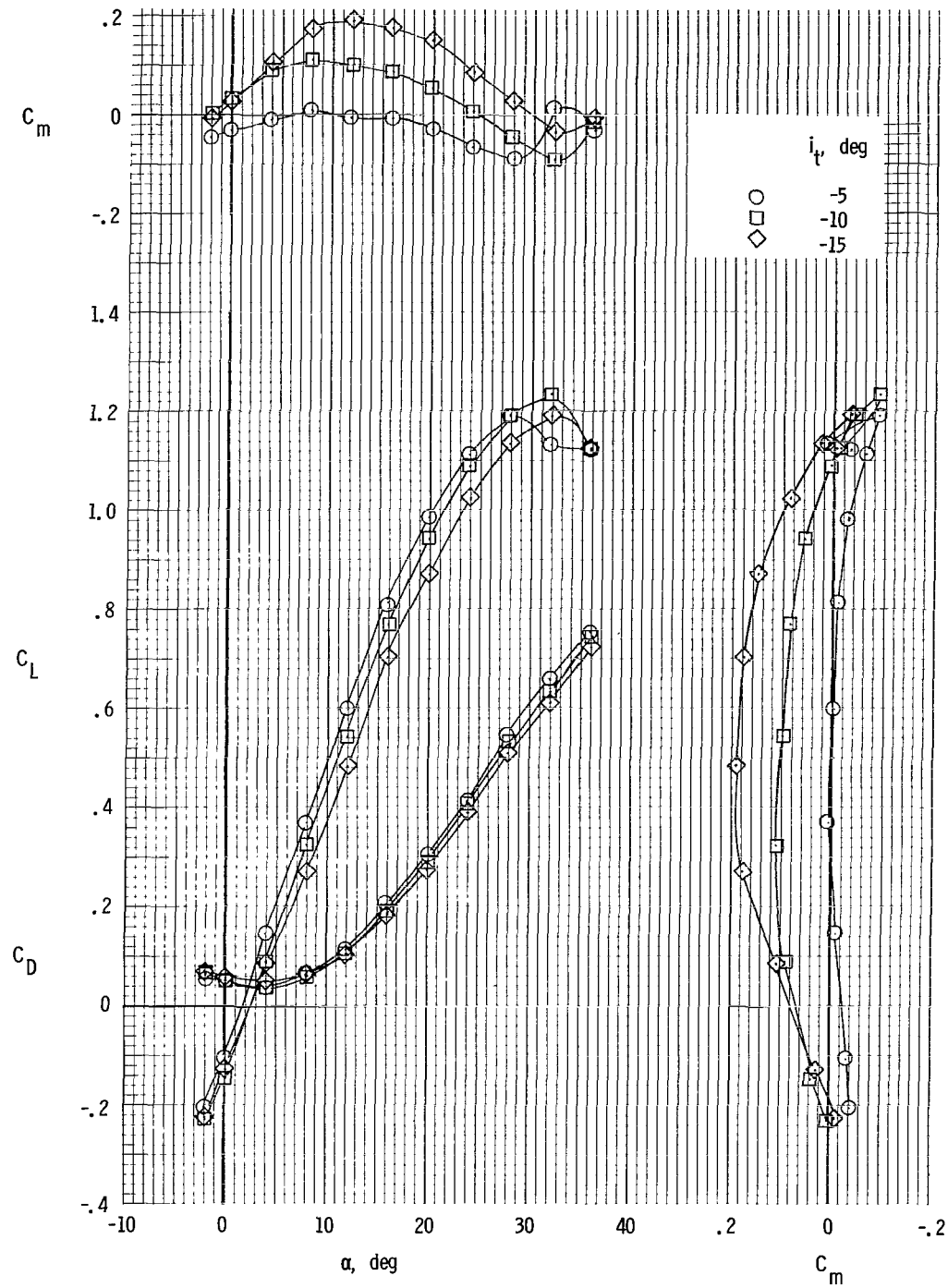

(c) $\Theta = -10^{\circ}$.

Figure 112.- Continued.

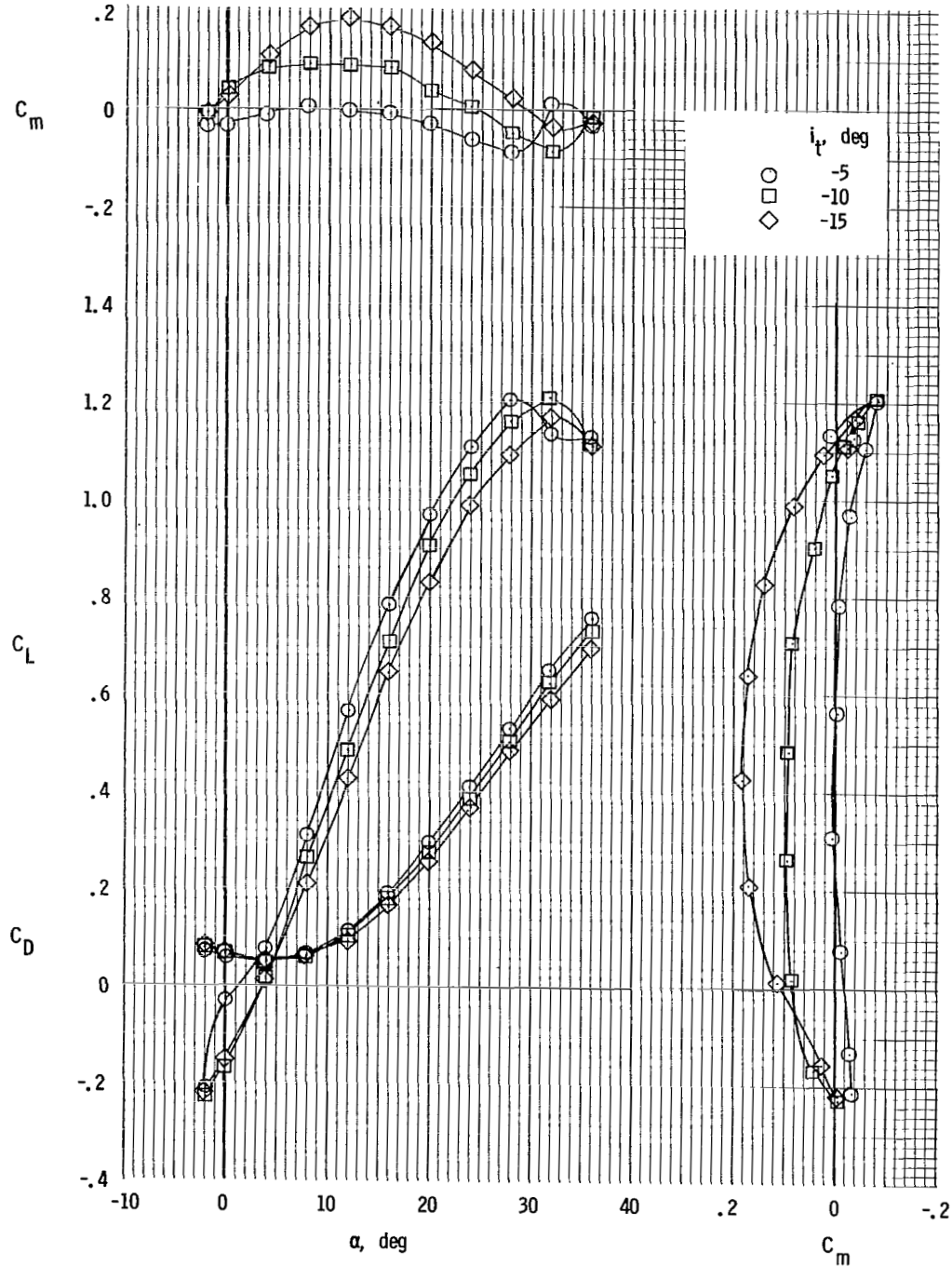

(d) $\Theta = -15^\circ$.

Figure 112.- Concluded.

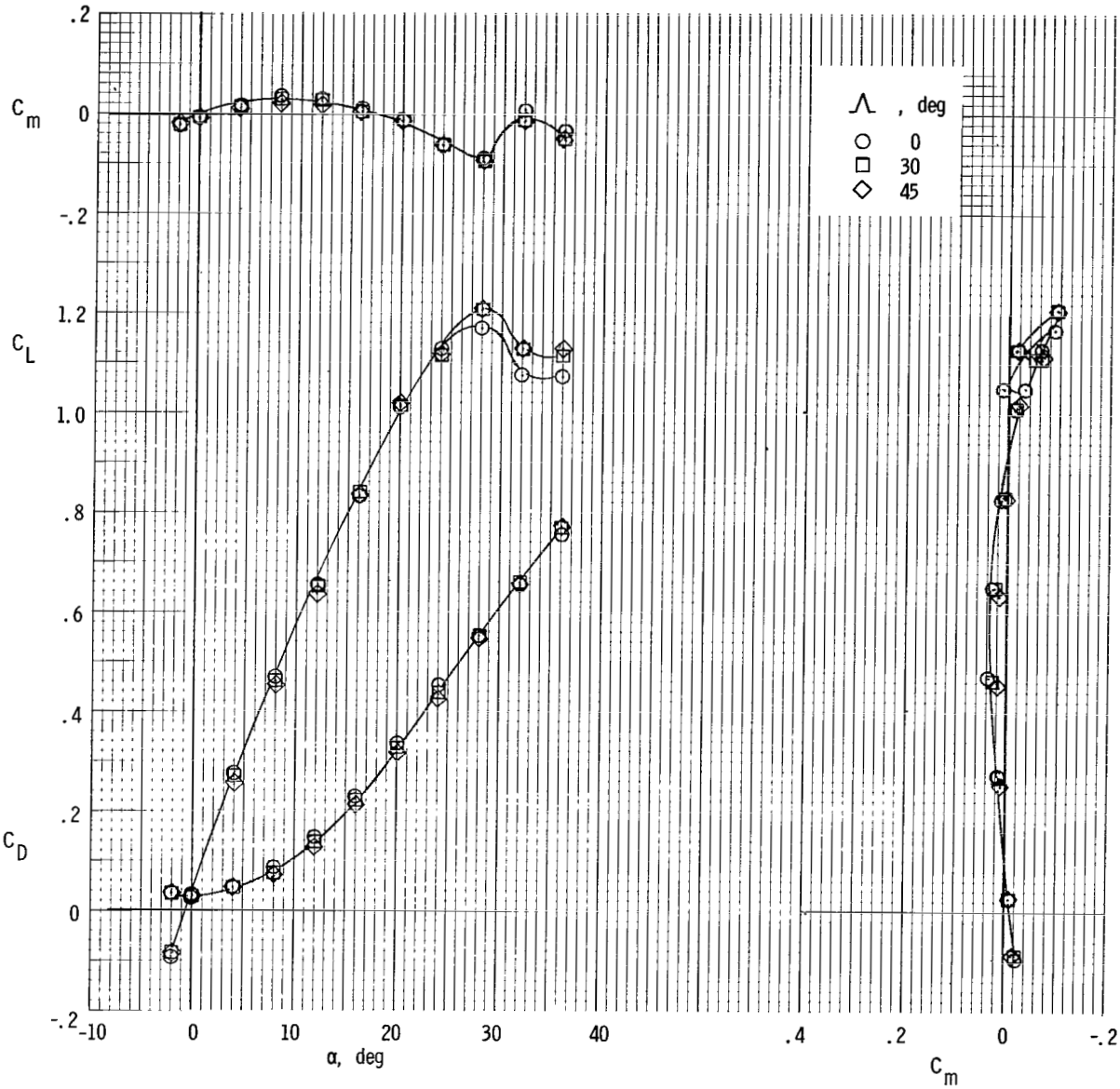

Figure 113.- Effect of blade sweep on the longitudinal aerodynamic characteristics. Twin vertical tail; horizontal tail at center fuselage; $\Theta = 0^\circ$; $i_t = -5^\circ$; rotor/wing 6.

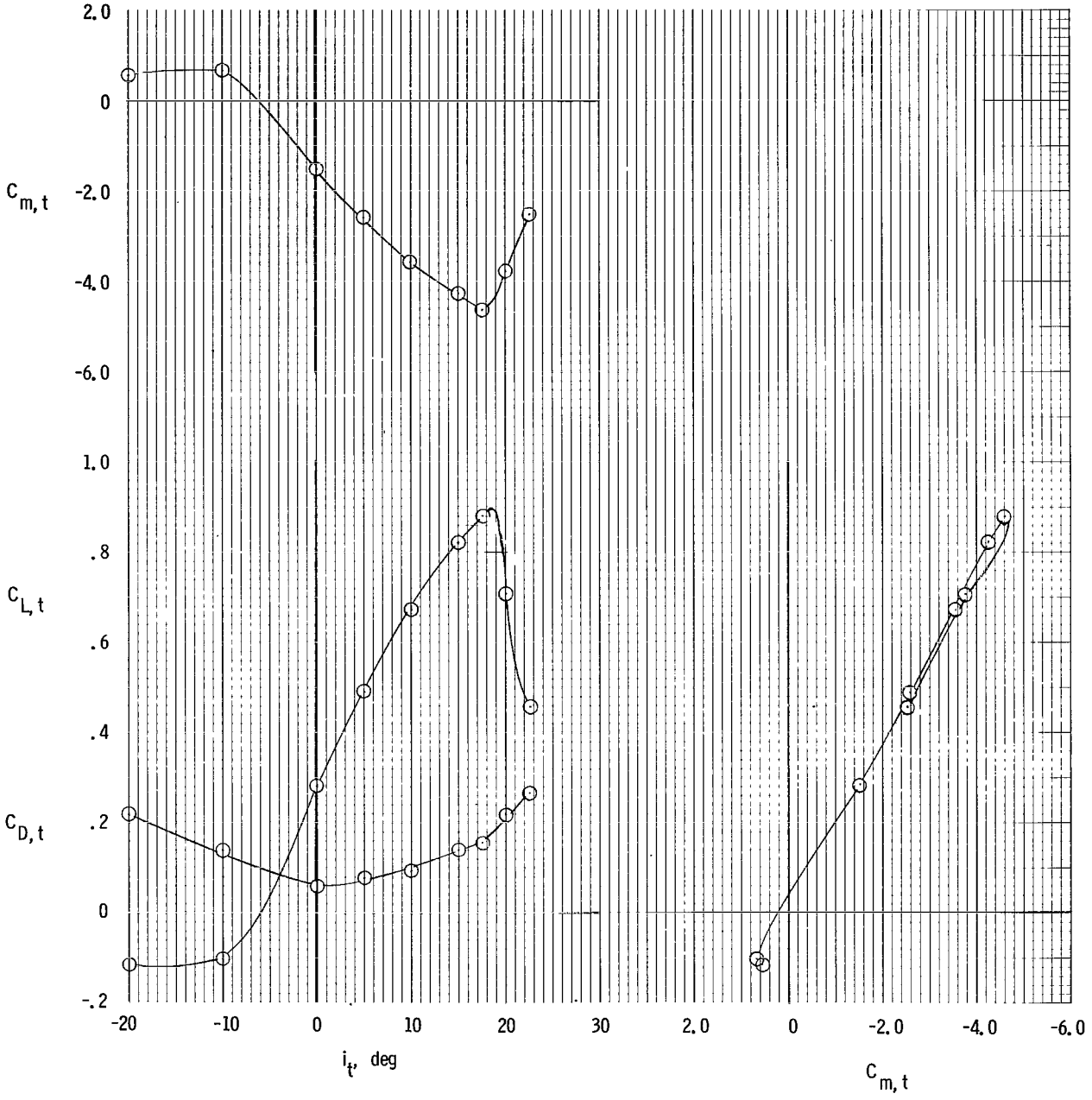

Figure 114.- Lift and drag characteristics of the horizontal tail (with cambered airfoil section) based on tail area. Twin vertical tail; horizontal tail at center fuselage; $\Theta = 0^{\circ}$; $\alpha = 0^{\circ}$; rotor/wing 6.

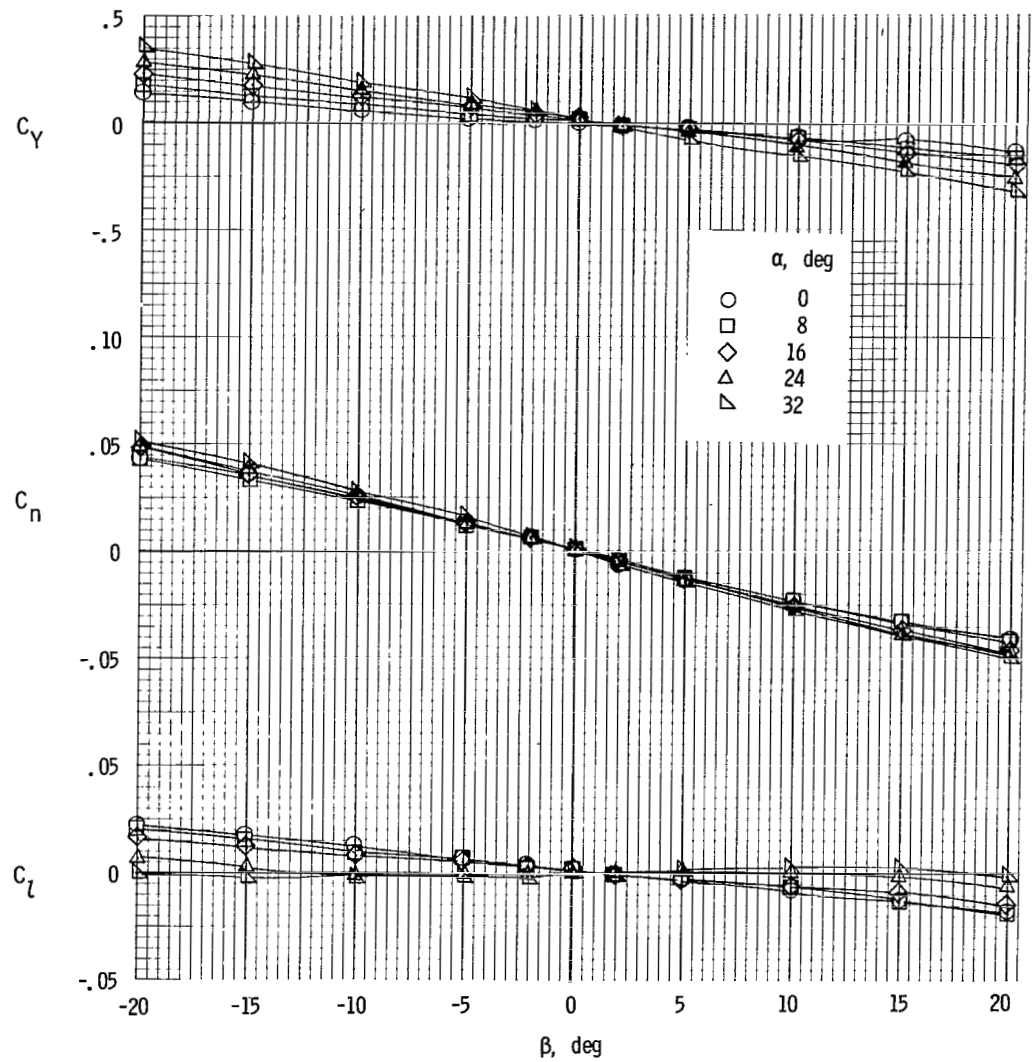

Figure 115.- Sideslip characteristics. Tails off; $\Theta = -10^{\circ}$; rotor/wing 6.

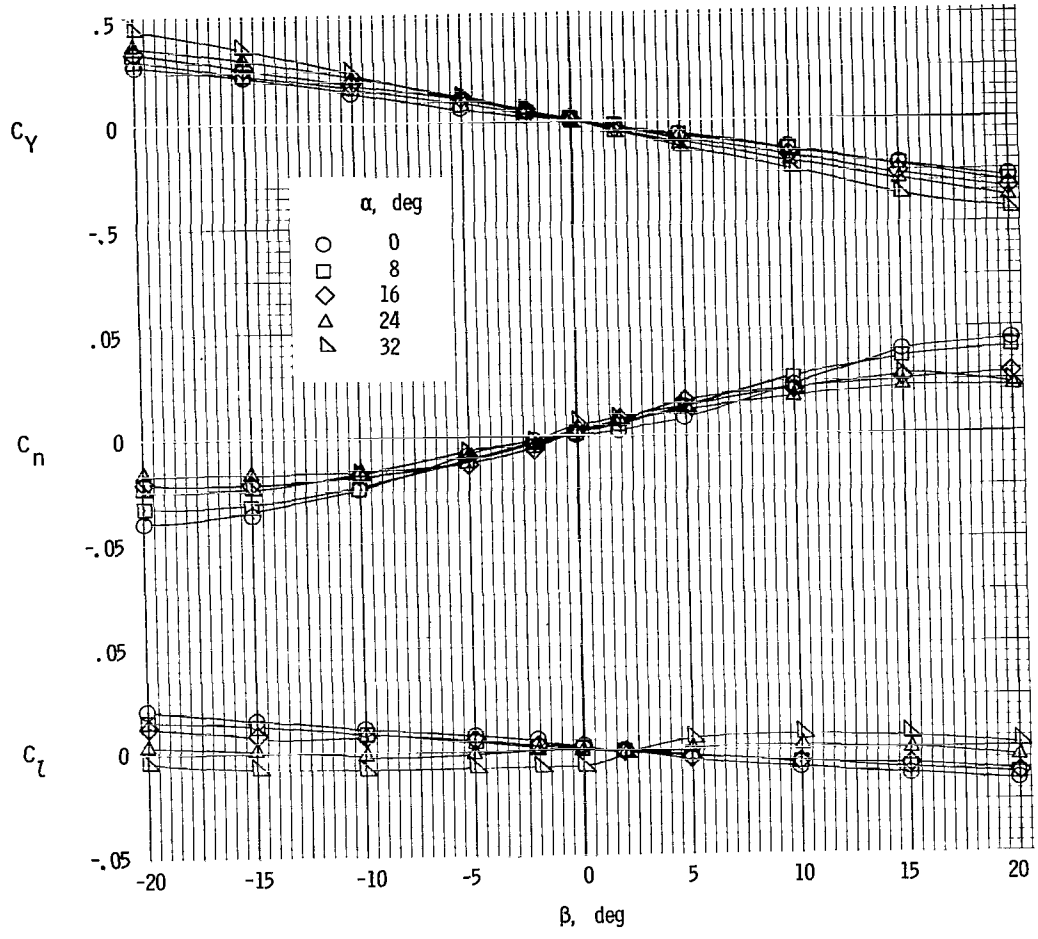

Figure 116.- Sideslip characteristics. Twin vertical tails on; horizontal tail at center fuselage; $i_t = -10^\circ$; $\Theta = -10^\circ$; rotor/wing 6.

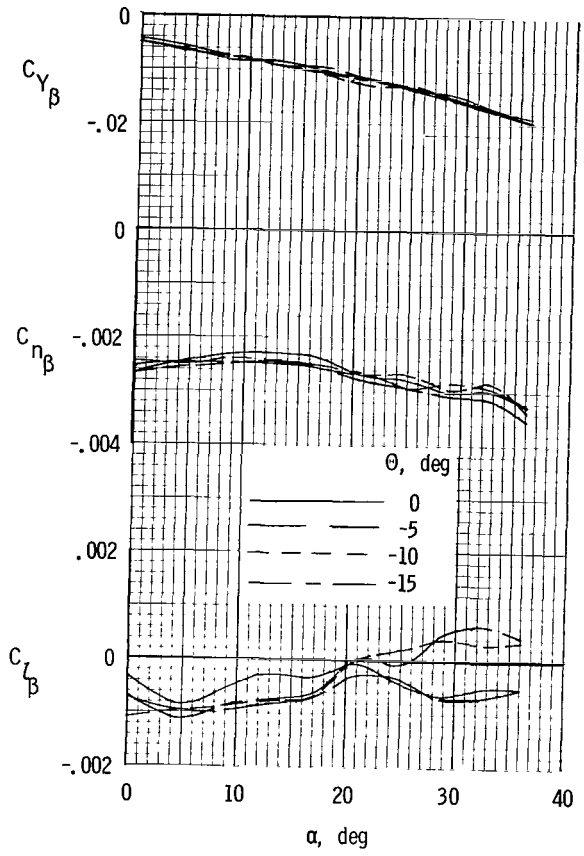

Figure 117.- Static lateral-stability derivatives. Tails off; rotor/wing 6.

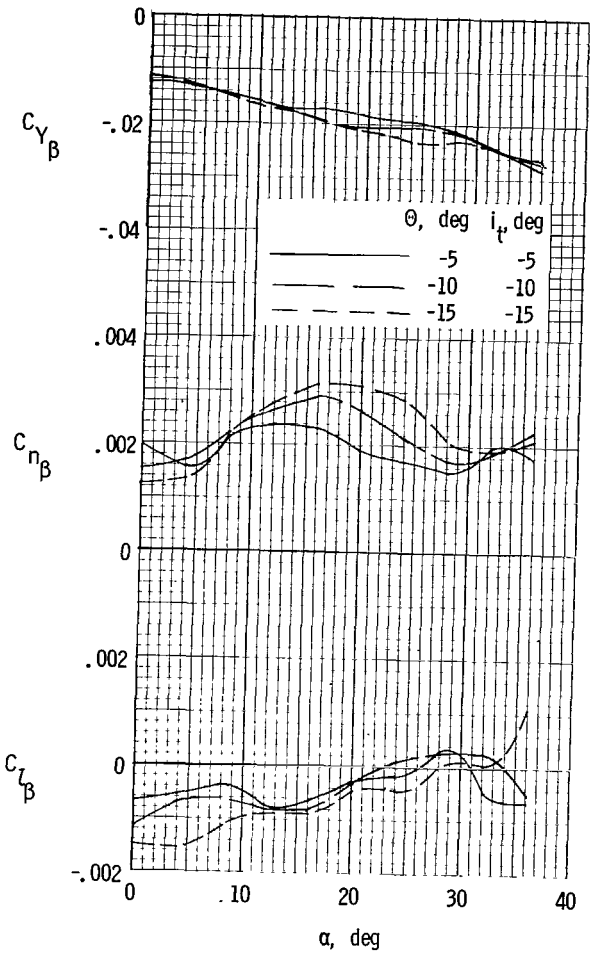

Figure 118.- Static lateral-stability derivatives for combinations of Θ and i_t. Twin vertical tails; horizontal tail at center fuselage; rotor/wing 6.

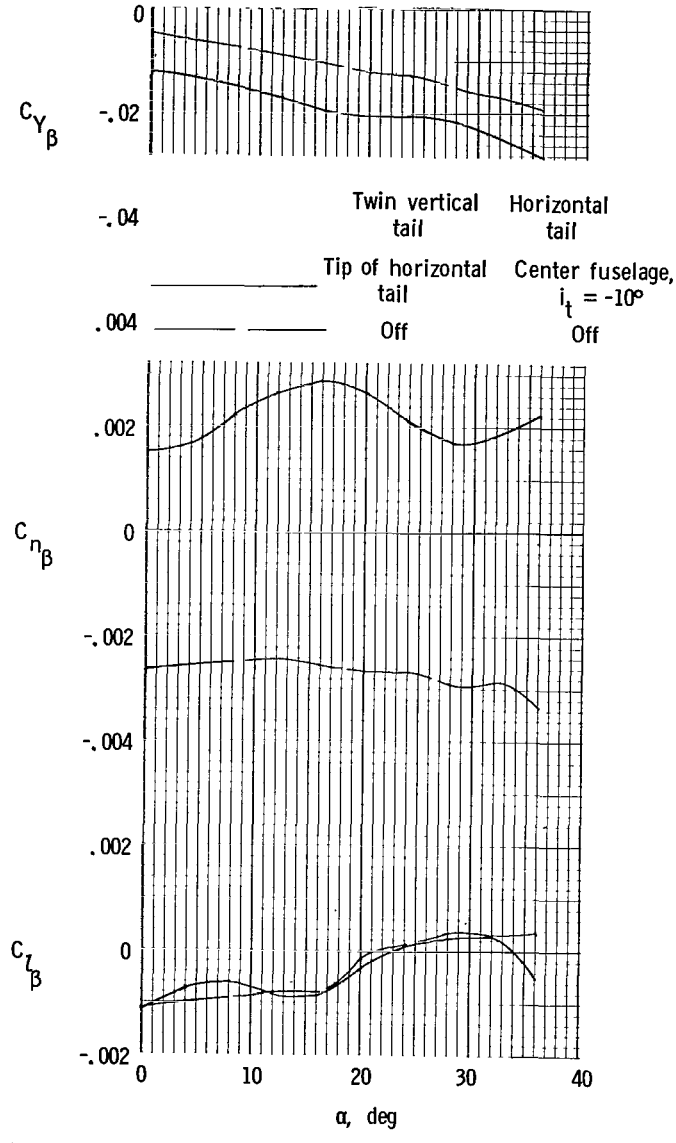

Figure 119.- Effect of vertical-tail configuration on static lateral-stability derivatives. $\Theta = -10°$; rotor/wing 6.

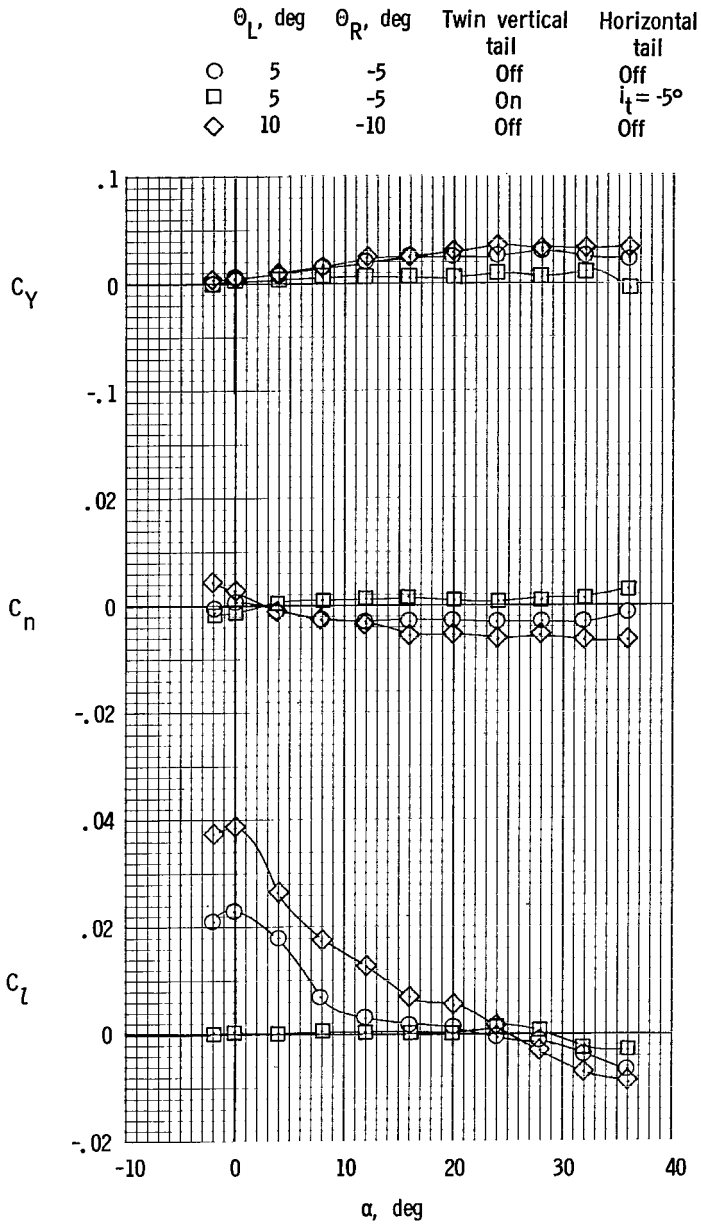

Figure 120.- Effect of tails on lateral-control characteristics with rotor blades used for control. Twin vertical tails; horizontal tail at center fuselage; Θ_{mean} = 0°; rotor/wing 6.

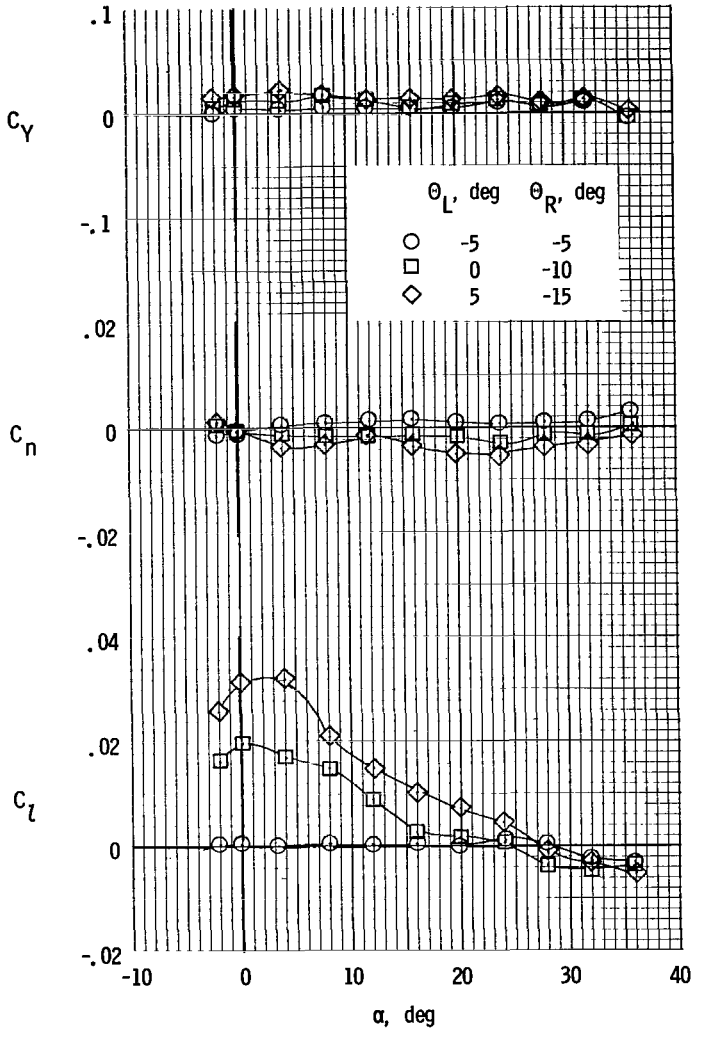

(a) $\Theta_{mean} = -5^\circ$; $i_t = -5^\circ$.

Figure 121.- Lateral-control characteristics with rotor blades used for control. Twin vertical tails; horizontal tail at center fuselage; rotor/wing 6.

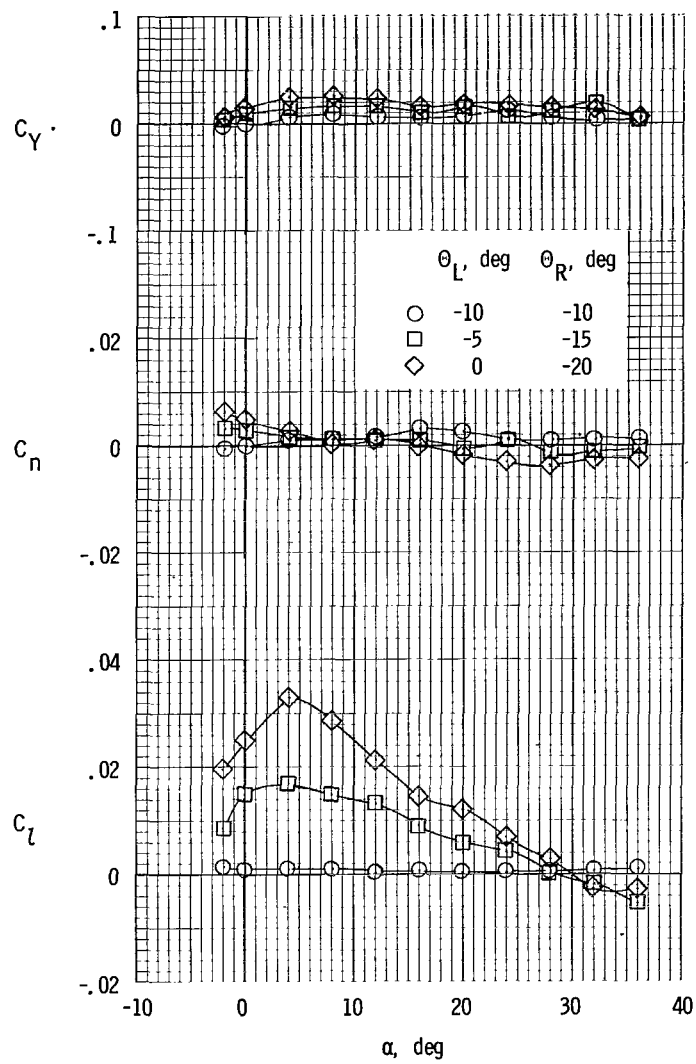

(b) $\Theta_{mean} = -10^{\circ}$; $i_t = -10^{\circ}$.

Figure 121.- Continued.

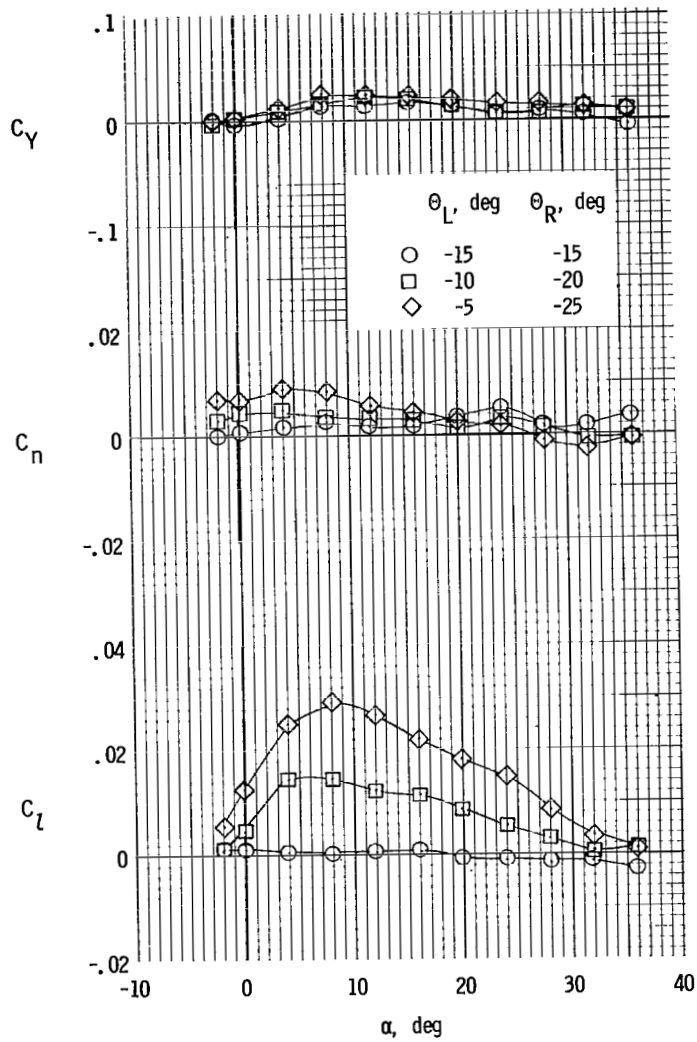

(c) $\Theta_{mean} = -15^\circ$; $i_t = -15^\circ$.

Figure 121.- Concluded.

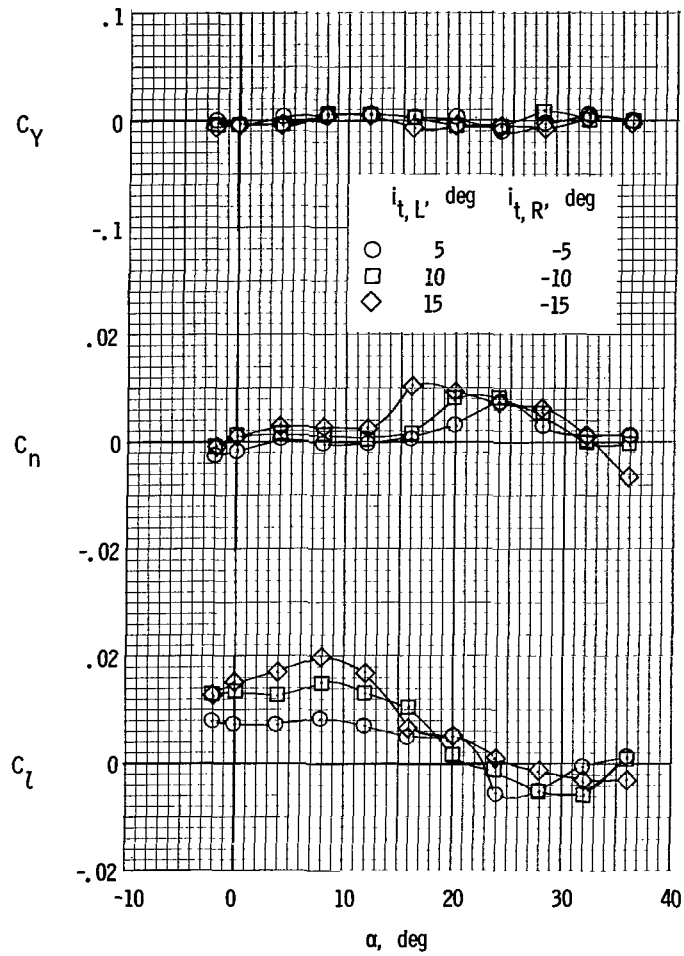

(a) $i_{t,mean} = 0^{\circ}$.

Figure 122.- Lateral-control characteristics with horizontal tail for control. Twin vertical tails; horizontal tail at center fuselage; $\Theta = 0^{\circ}$; rotor/wing 6.

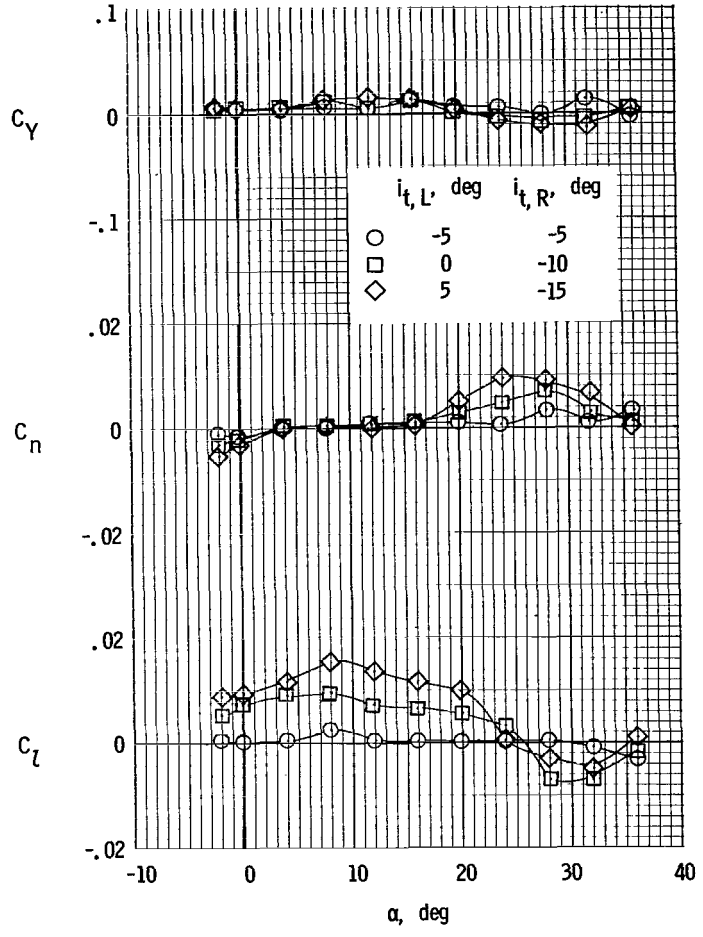

(b) $i_{t,mean} = -5°$.

Figure 122.- Continued.

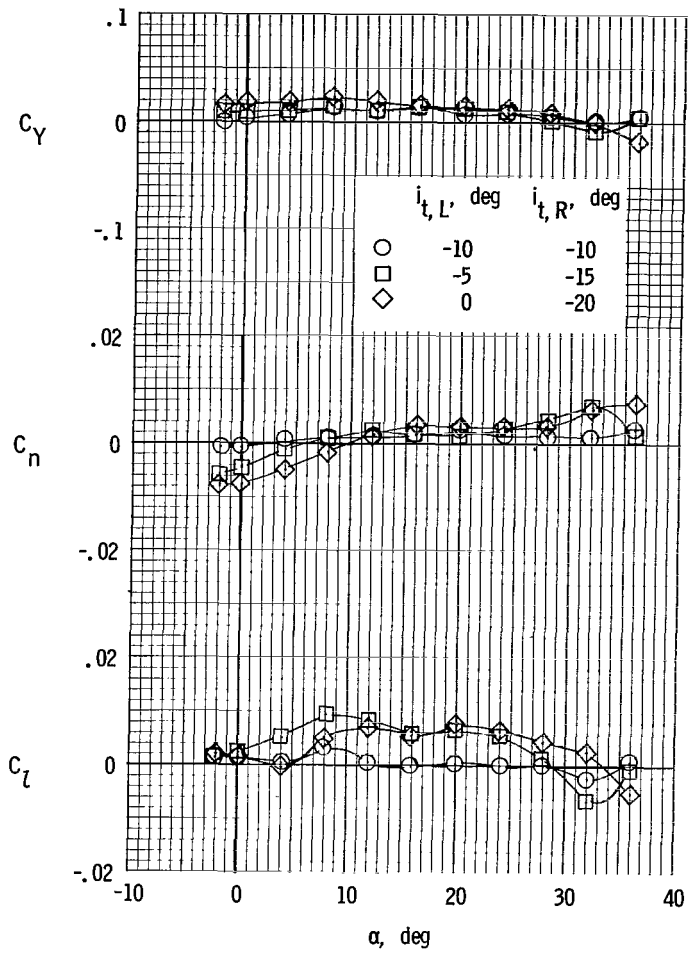

(c) $i_{t,mean} = -10^{\circ}$.

Figure 122.- Continued.

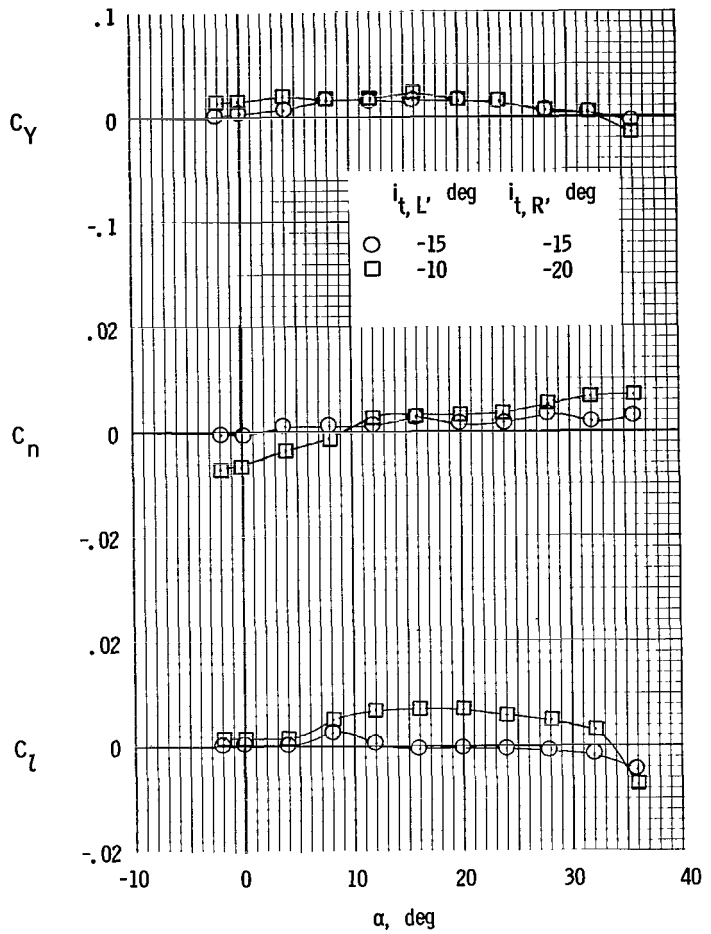

(d) $i_{t,mean} = -15^{\circ}$.

Figure 122.- Concluded.

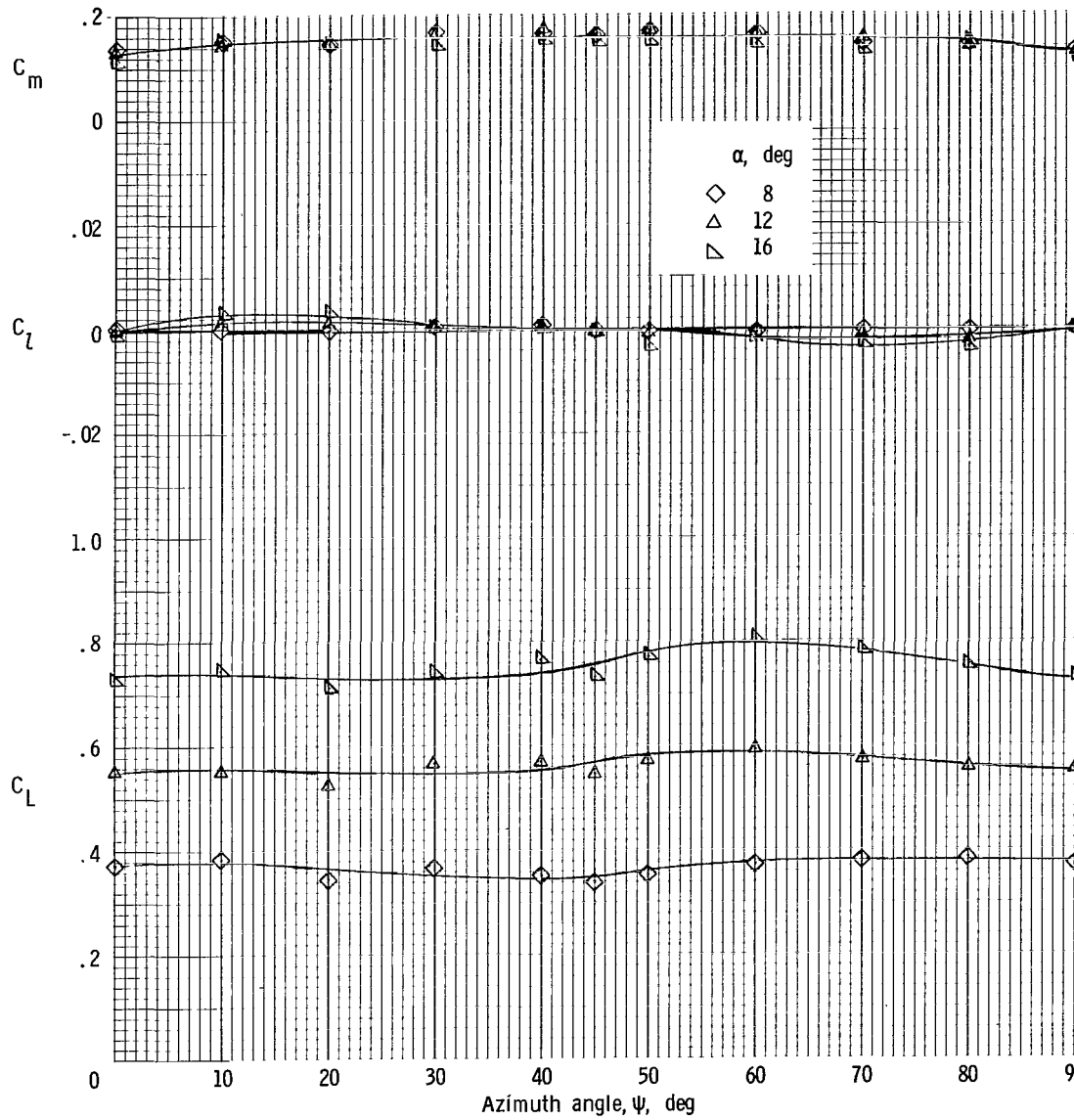

Figure 123.- Effect of azimuth position on lift coefficient and rolling- and pitching-moment coefficients for changes in model angle of attack. $i_t = -10^\circ$; $\Theta = 0^\circ$; rotor/wing 6.

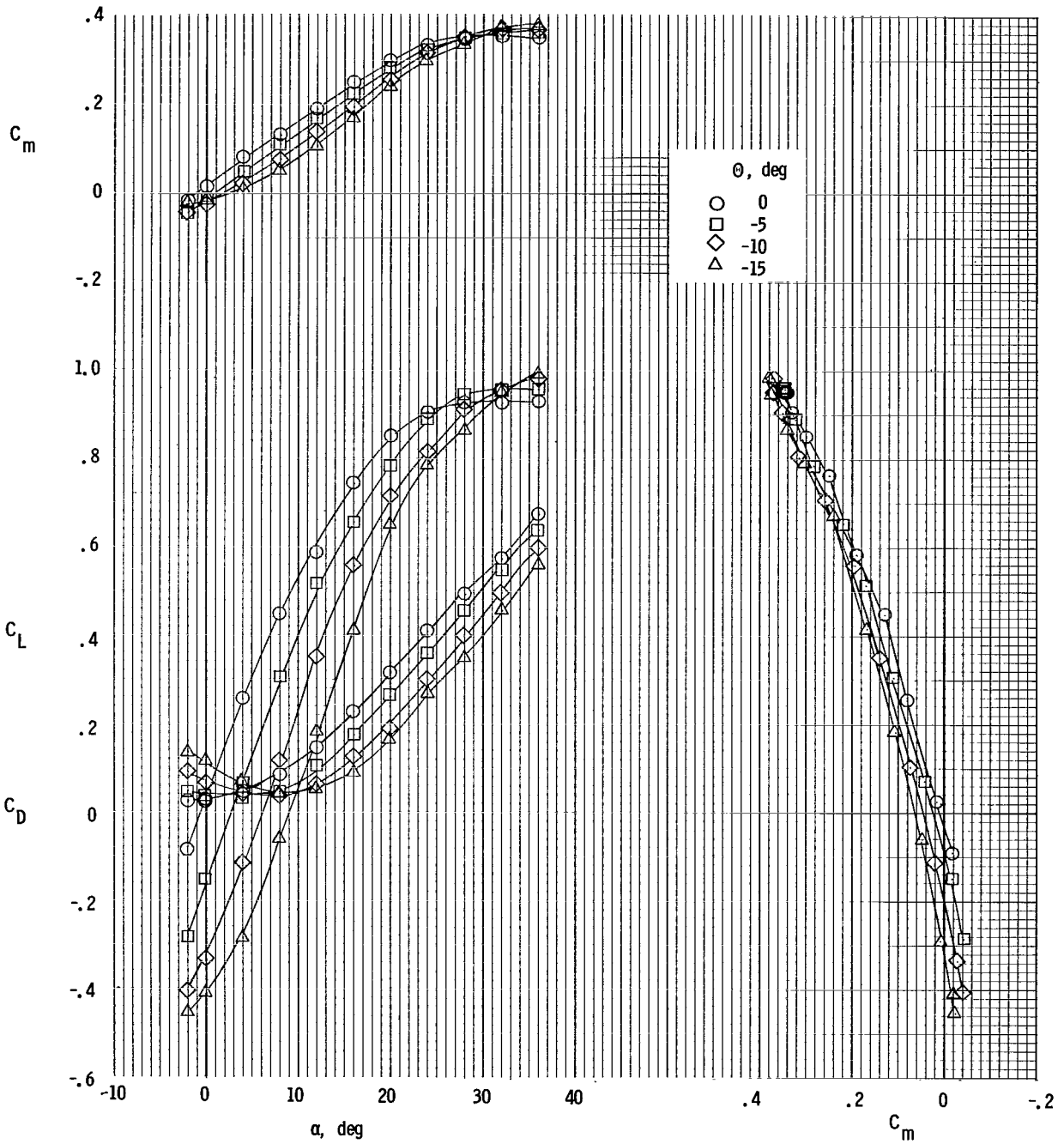

Figure 124.- Longitudinal aerodynamic characteristics. Tails off; rotor/wing 7.

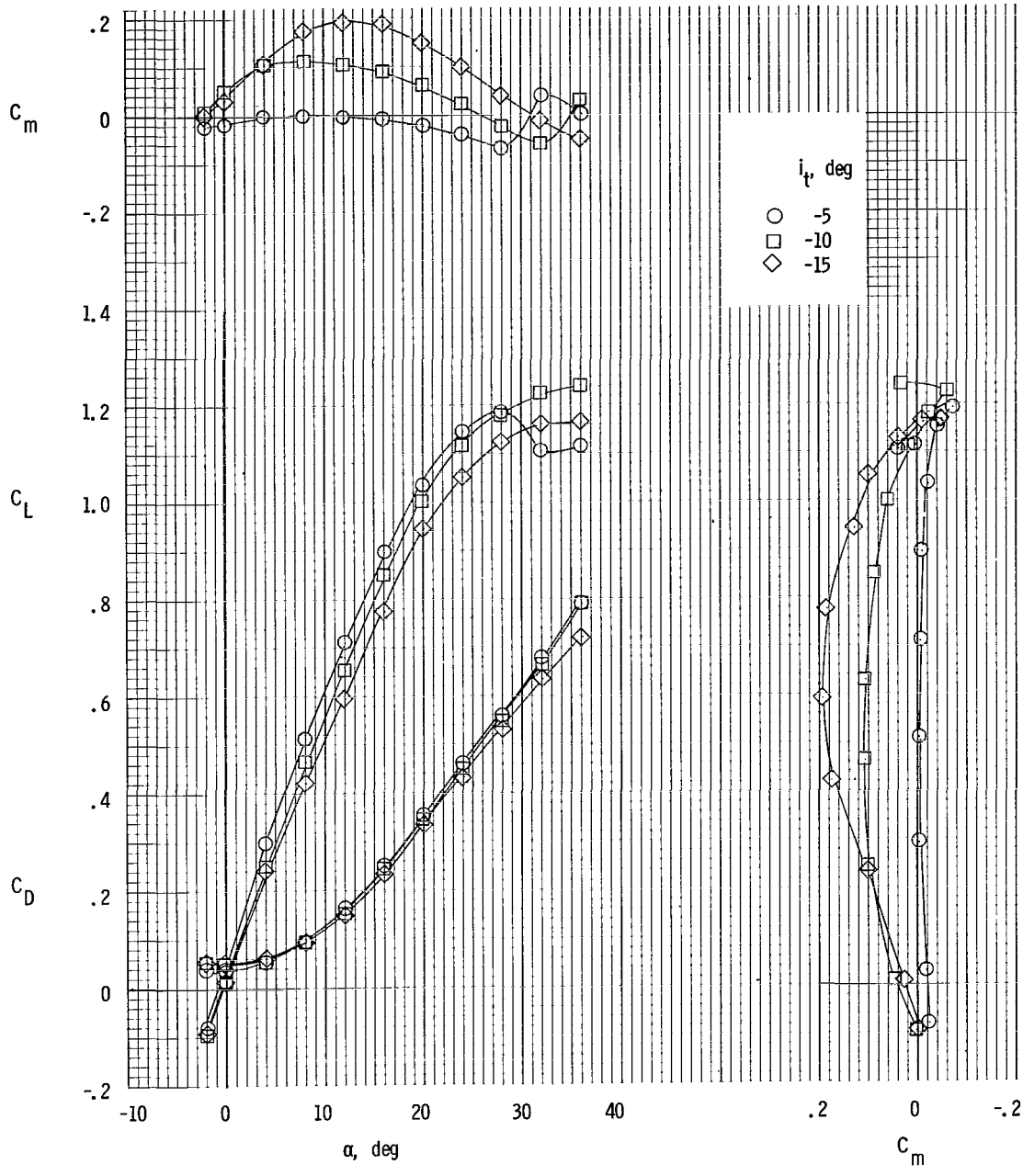

(a) $\Theta = 0^{\circ}$.

Figure 125.- Longitudinal aerodynamic characteristics. Twin vertical tails; horizontal tail at center fuselage; rotor/wing 7.

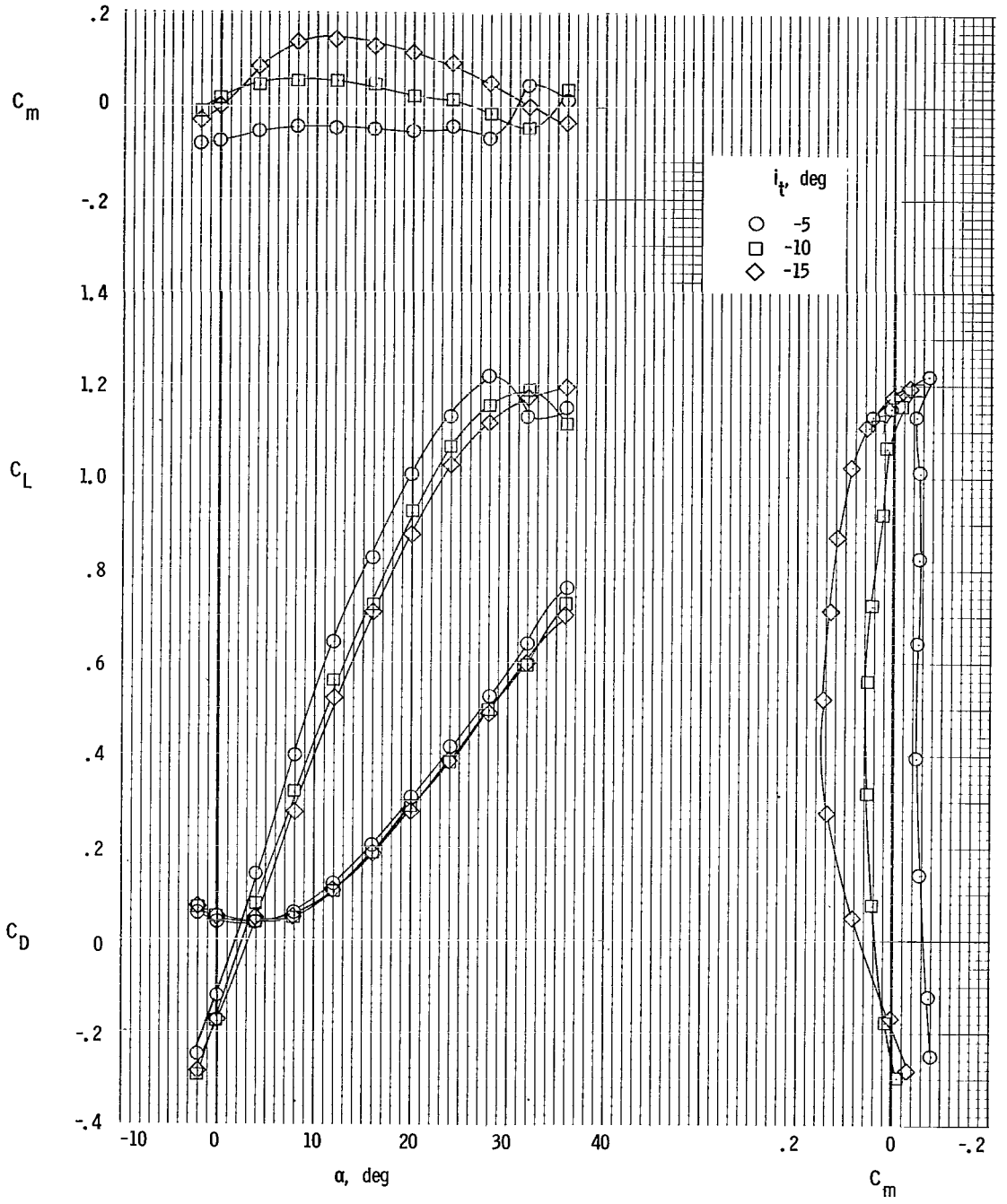

(b) $\Theta = -5^\circ$.

Figure 125.- Continued.

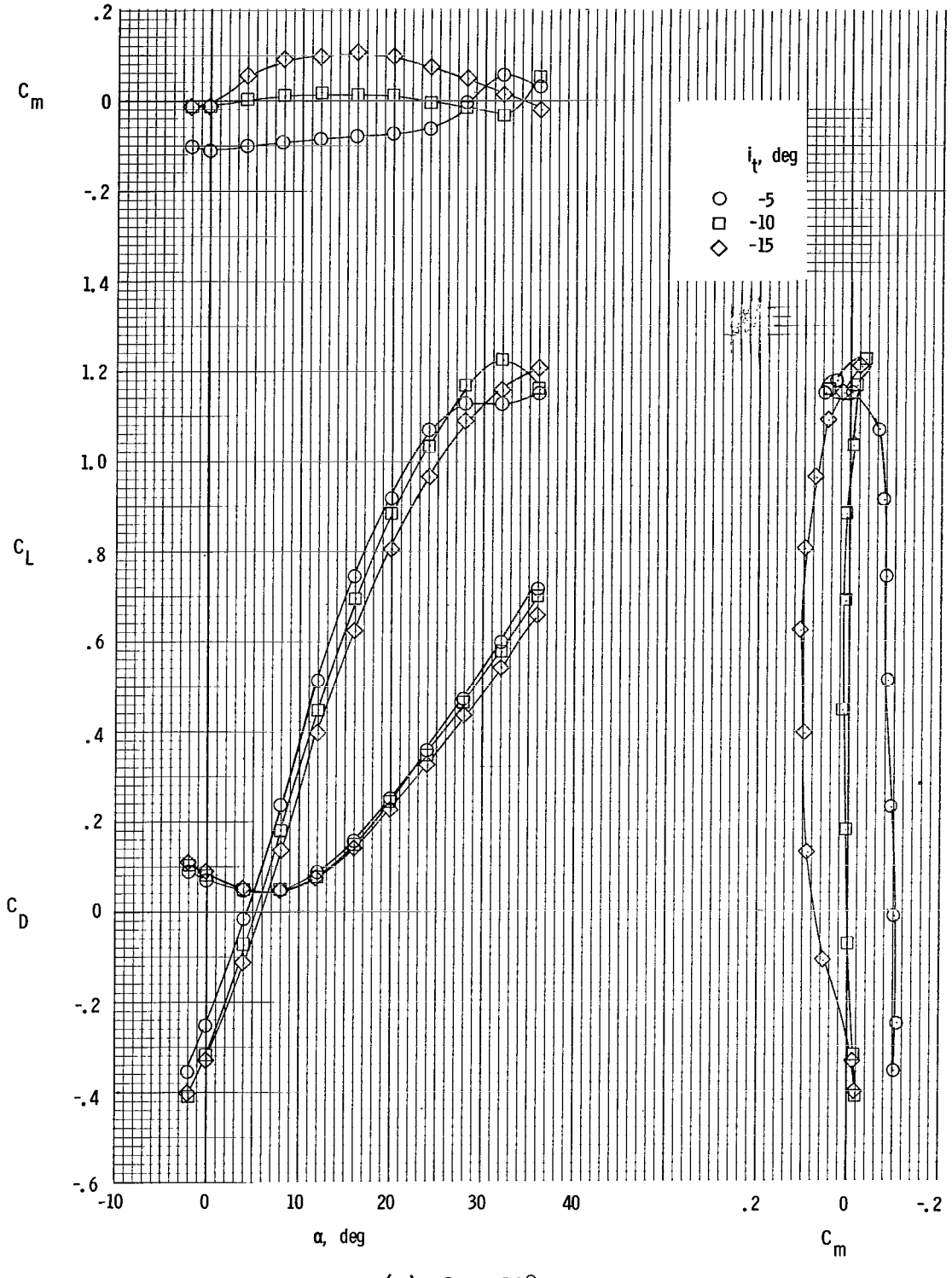

(c) $\Theta = -10^{\circ}$.

Figure 125.- Continued.

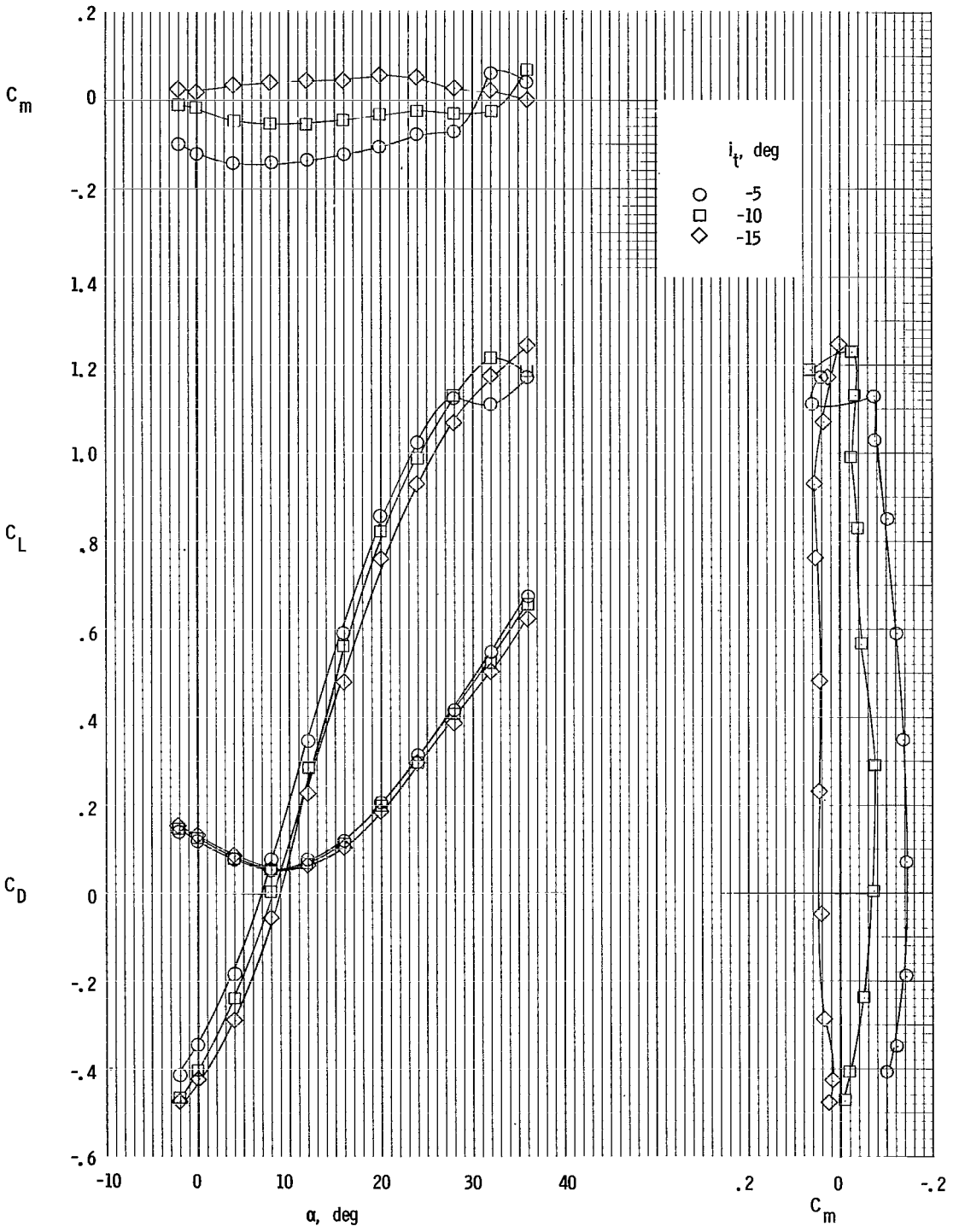

(d) $\Theta = -15^{\circ}$.

Figure 125.- Concluded.

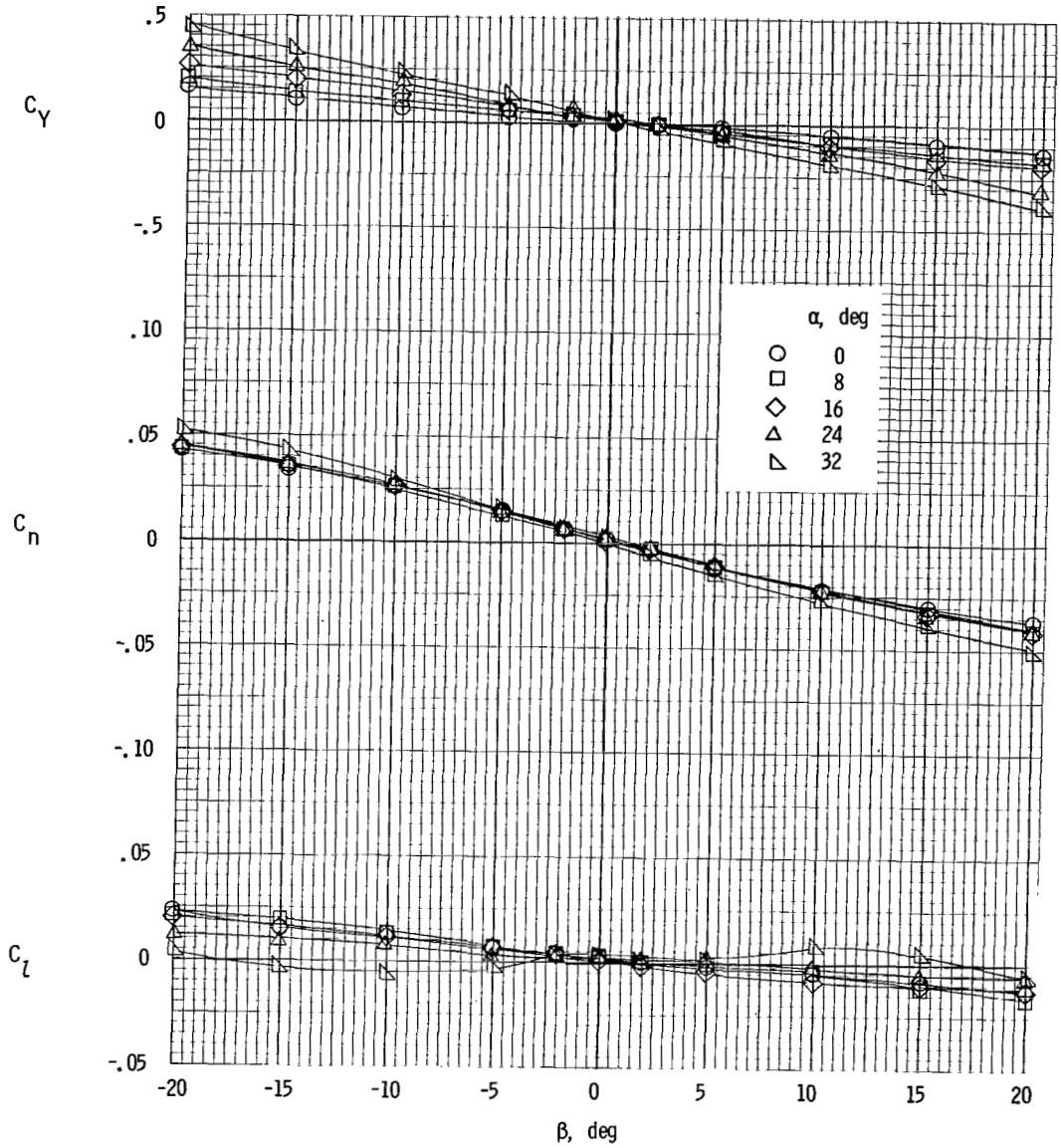

Figure 126.- Sideslip characteristics. Tails off; $\Theta = -10^{\circ}$; rotor/wing 7.

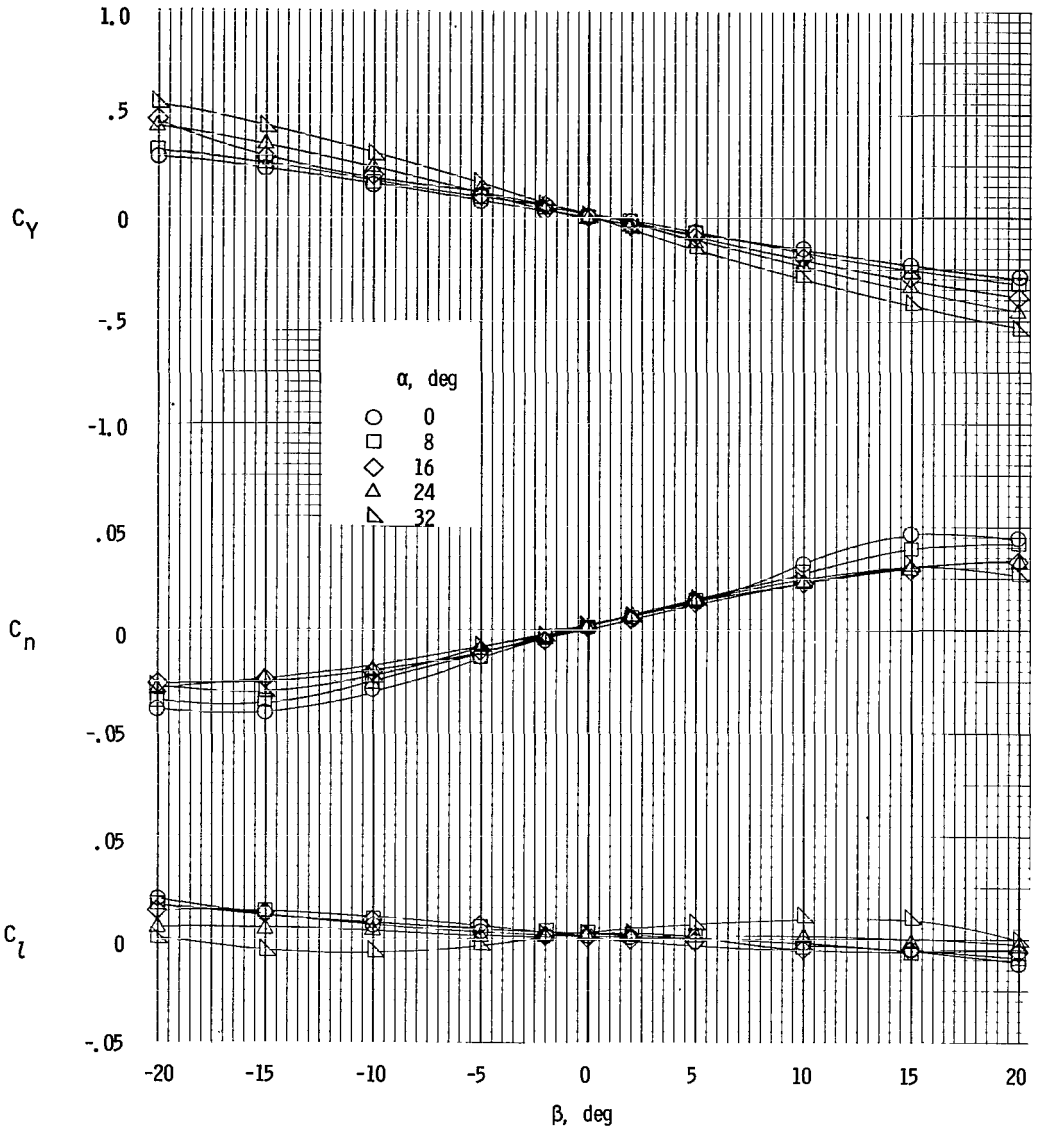

Figure 127.- Sideslip characteristics. Twin vertical tails; horizontal tail at center fuselage; $i_t = -10^o$; $\Theta = -10^o$; rotor/wing 7.

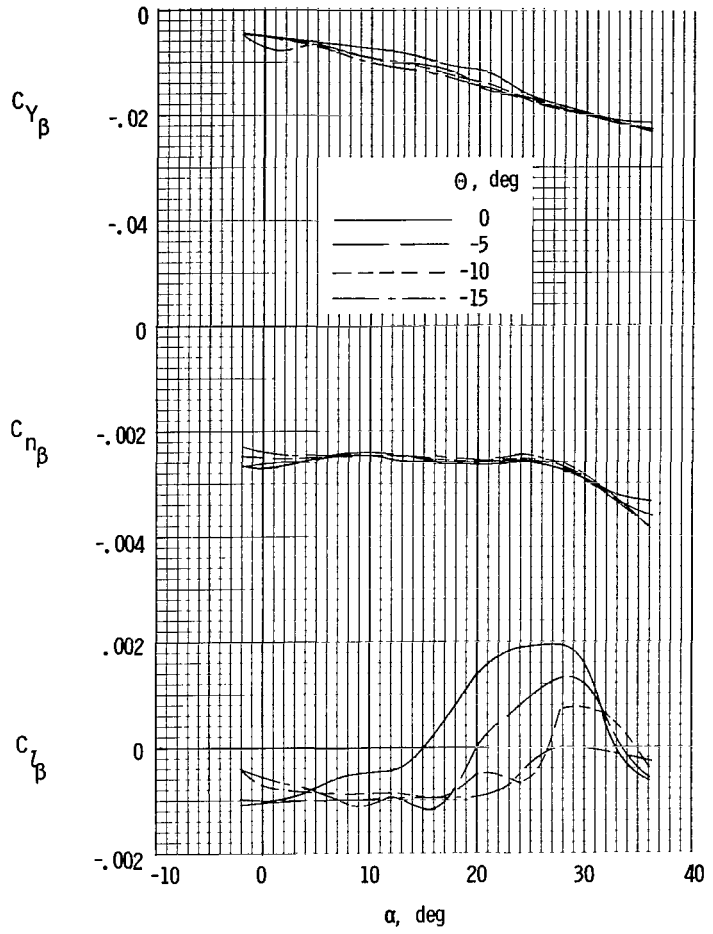

Figure 128.- Static lateral-stability derivatives. Tails off; rotor/wing 7.

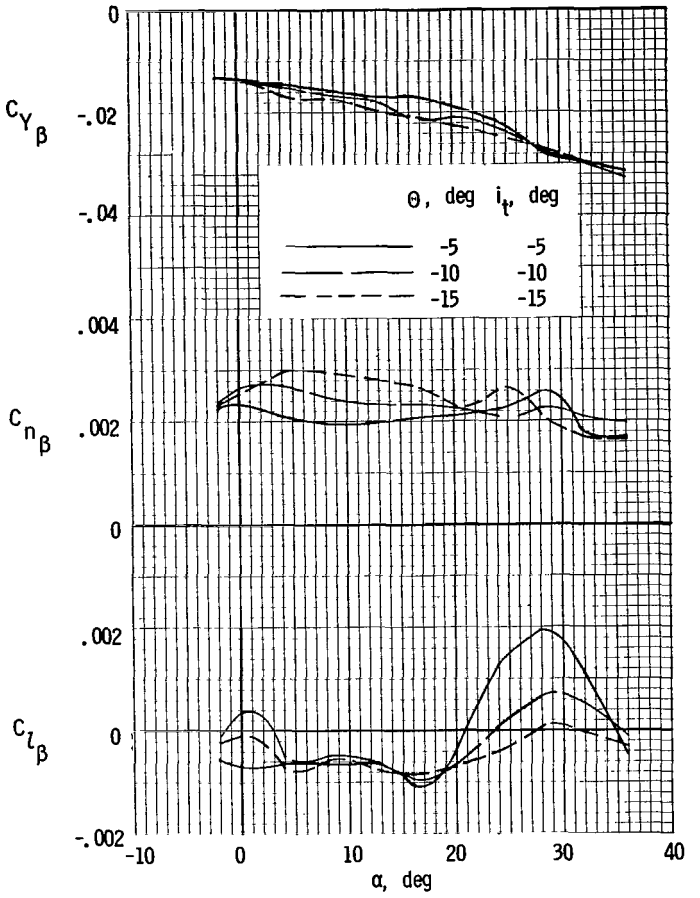

Figure 129.- Static lateral-stability derivatives for combinations of Θ and i_t. Twin vertical tails; horizontal tail at center fuselage; rotor/wing 7.

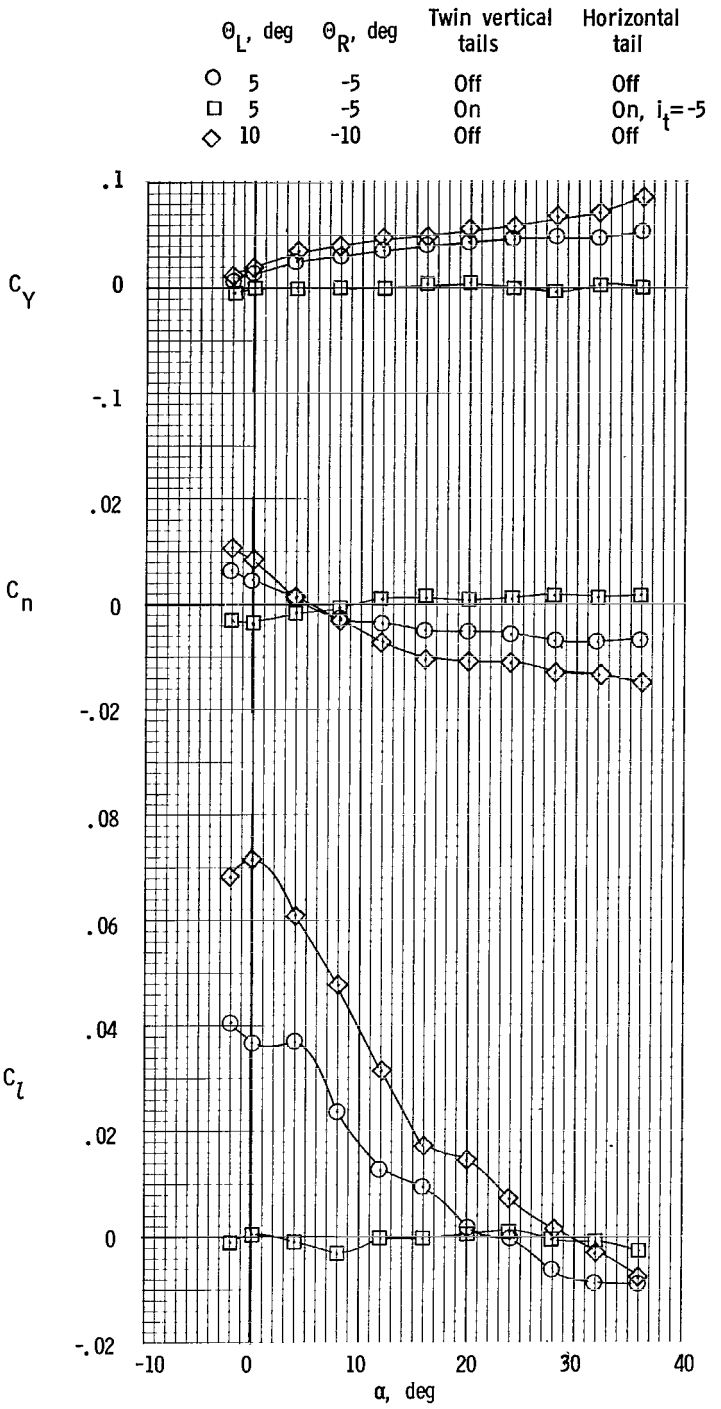

Figure 130.- Effect of tails on lateral-control characteristics with rotor blades used for control. Twin vertical tails; horizontal tail at center fuselage; $\Theta_{mean} = 0^{\circ}$; rotor/wing 7.

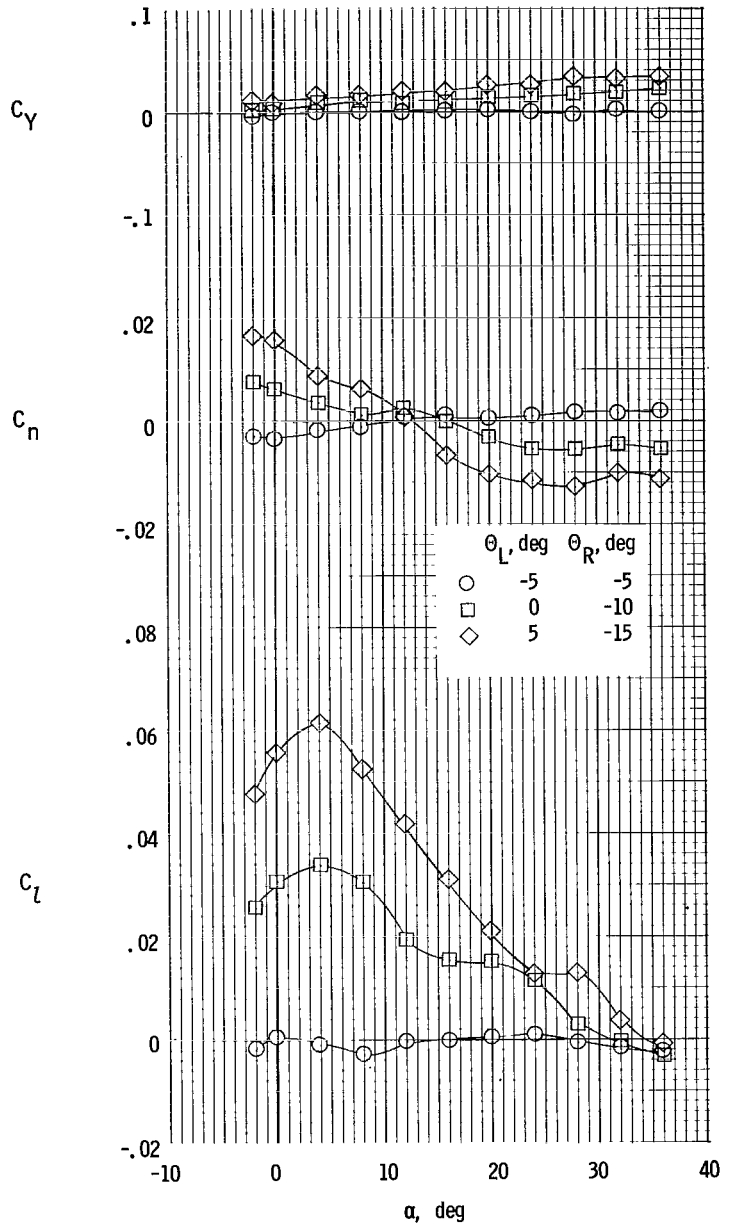

(a) $i_t = -5^\circ$; $\Theta_{mean} = -5^\circ$.

Figure 131.- Lateral-control characteristics with rotor blades used for control. Twin vertical tails; horizontal tail at center fuselage; rotor/wing 7.

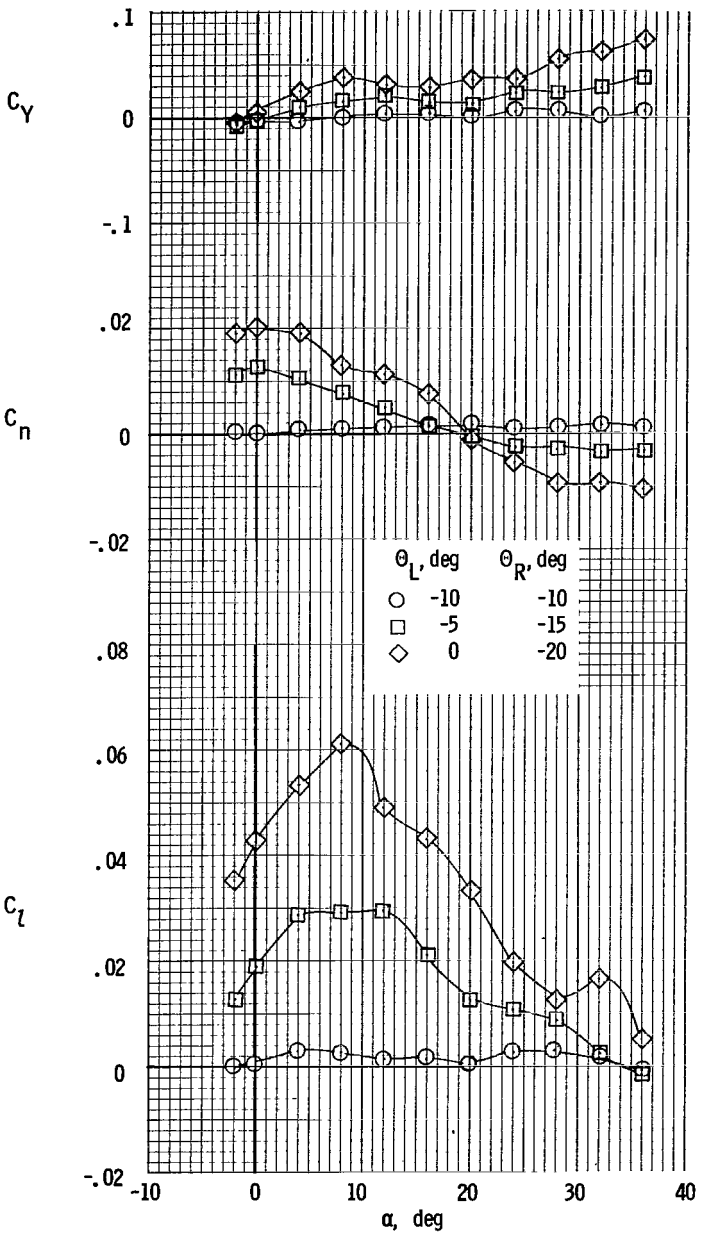

(b) $i_t = -10°$; $\Theta_{mean} = -10°$.

Figure 131.- Continued.

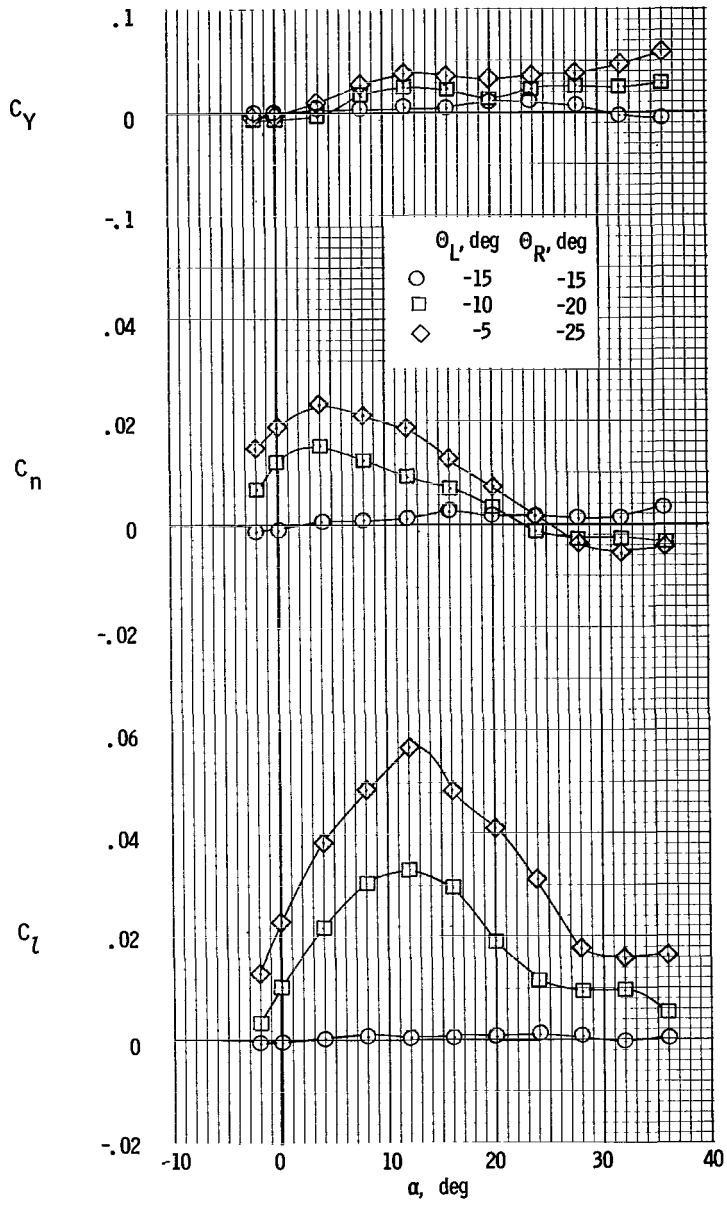

(c) $i_t = -15°$; $\Theta_{mean} = -15°$.

Figure 131.- Concluded.

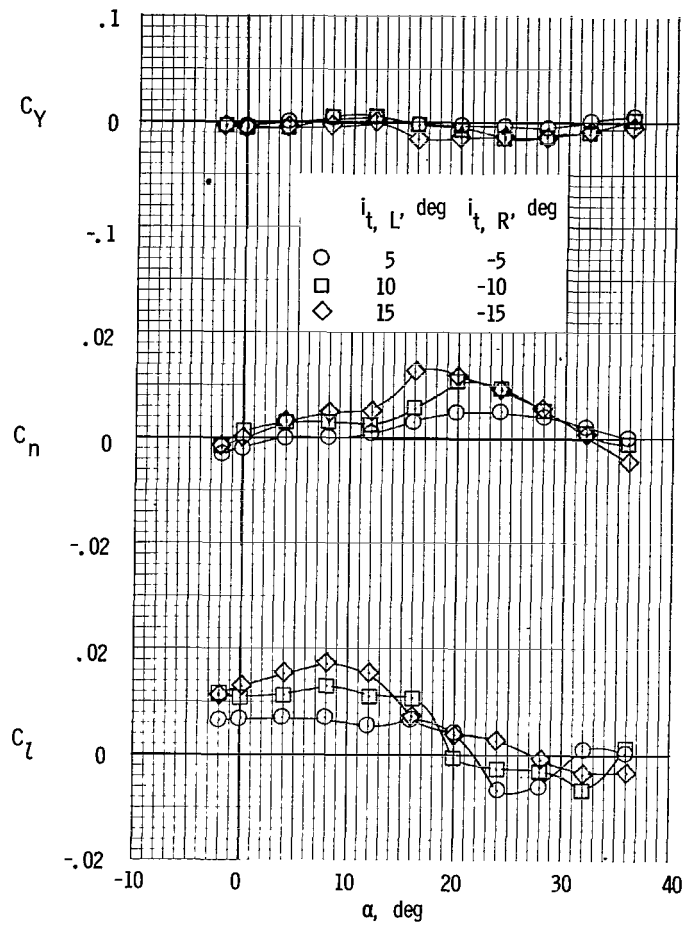

(a) $i_{t,mean} = 0^\circ$.

Figure 132.- Lateral-control characteristics with horizontal tail used for control. Twin vertical tails; horizontal tail at center fuselage; $\Theta = 0^\circ$; rotor/wing 7.

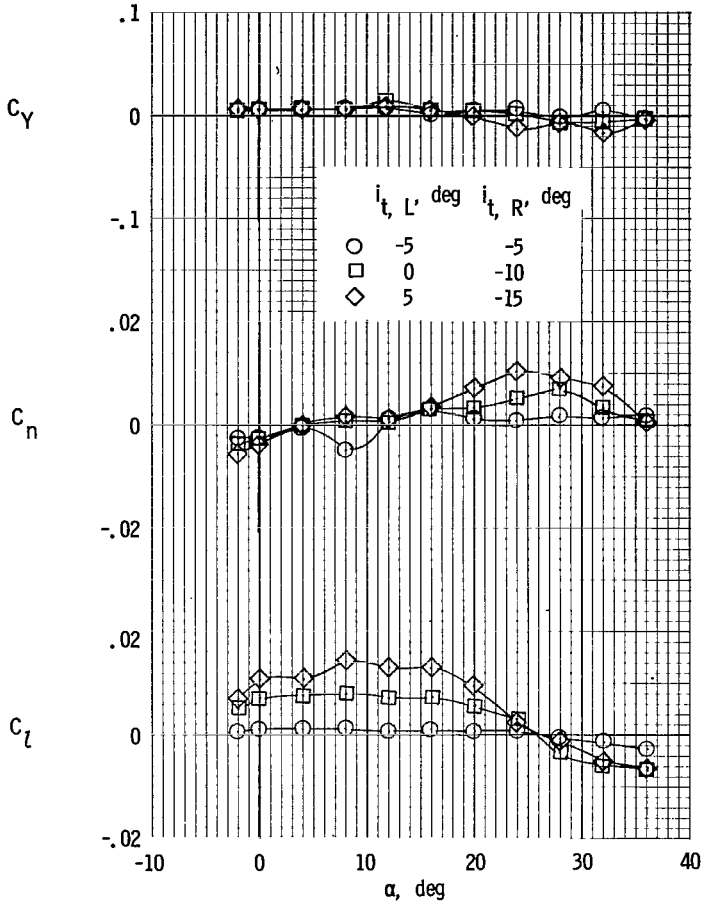

(b) $i_{t,mean} = -5^{\circ}$.

Figure 132.- Continued.

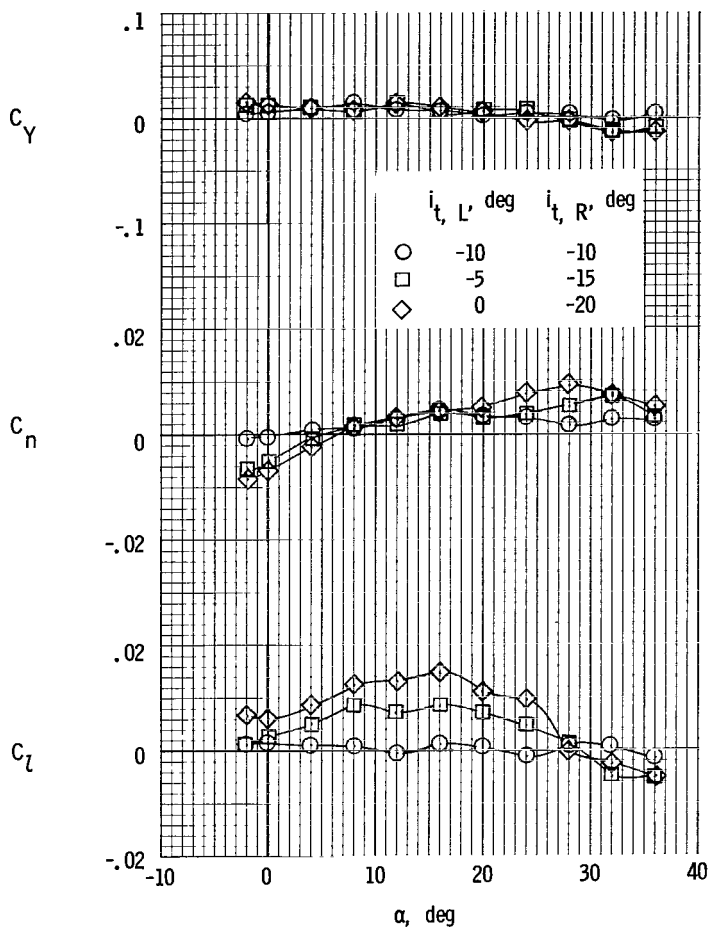

(c) $i_{t,mean} = -10°$.

Figure 132.- Continued.

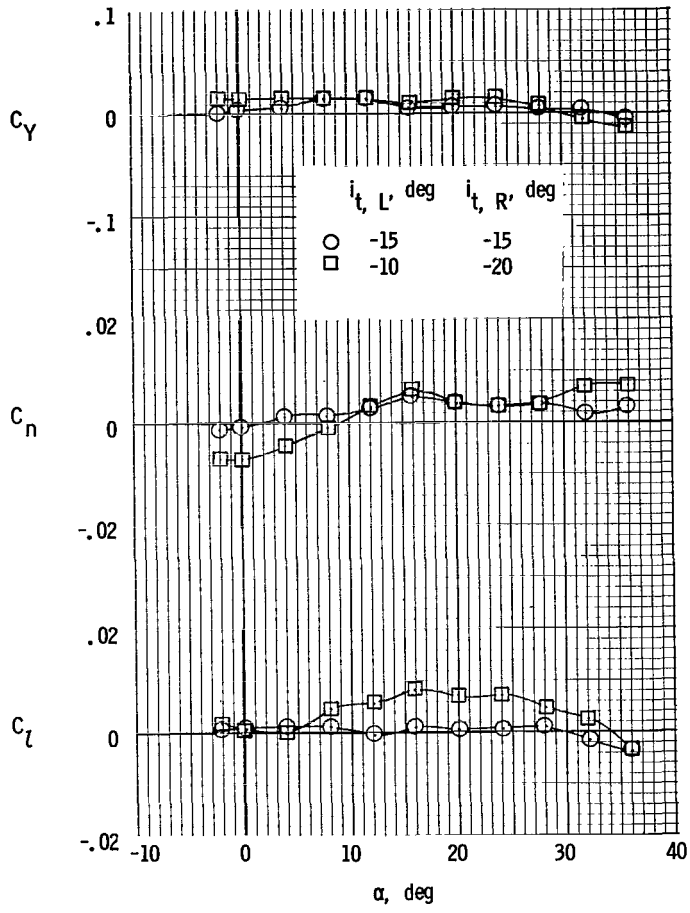

(d) $i_{t,mean} = -15^{\circ}$.

Figure 132.- Concluded.

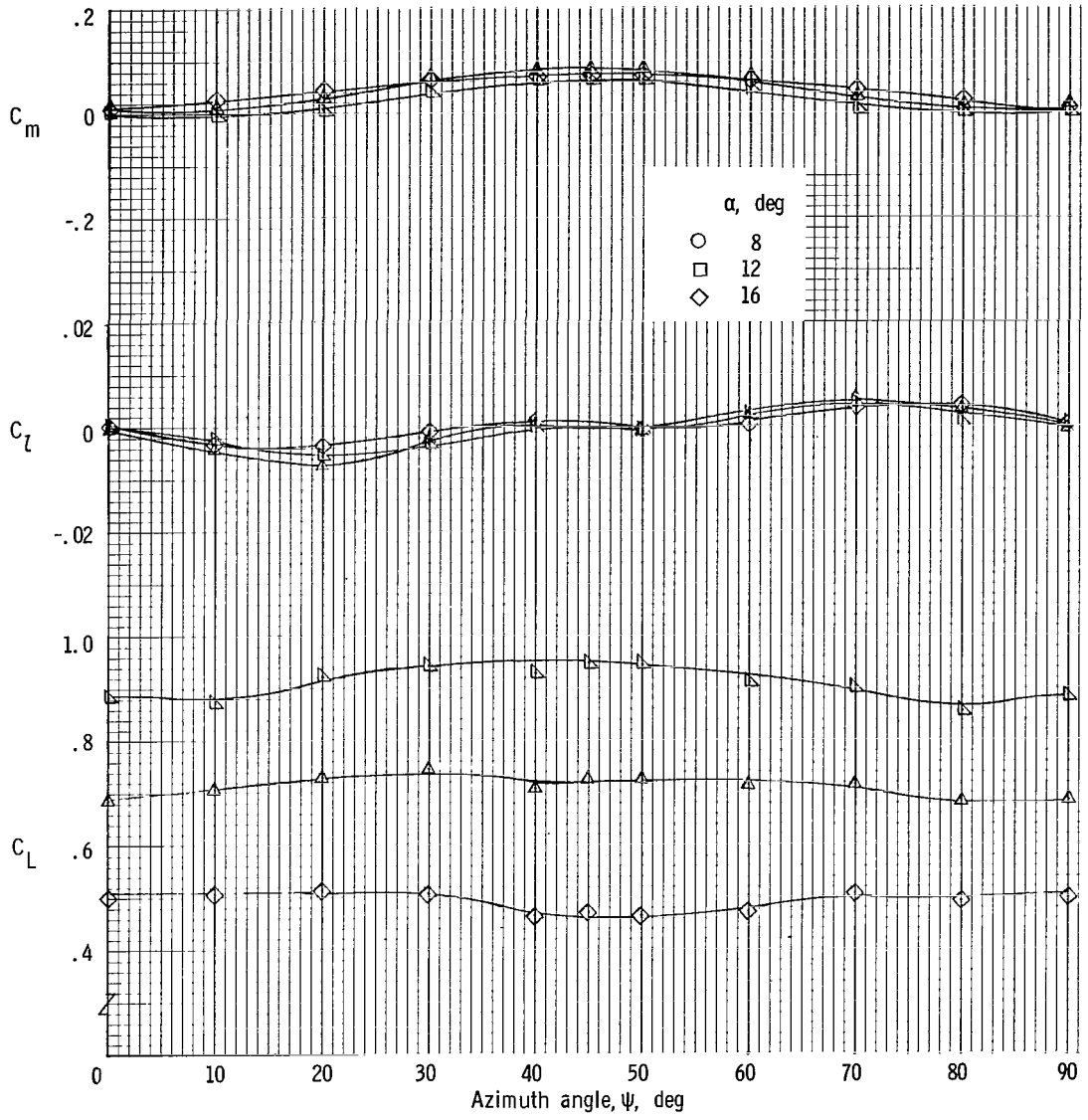

Figure 133.- Effect of azimuth position on lift coefficient and rolling- and pitching-moment coefficients for changes in model angle of attack. $\Theta = 0^\circ$; $i_t = -5^\circ$; rotor/wing 7.

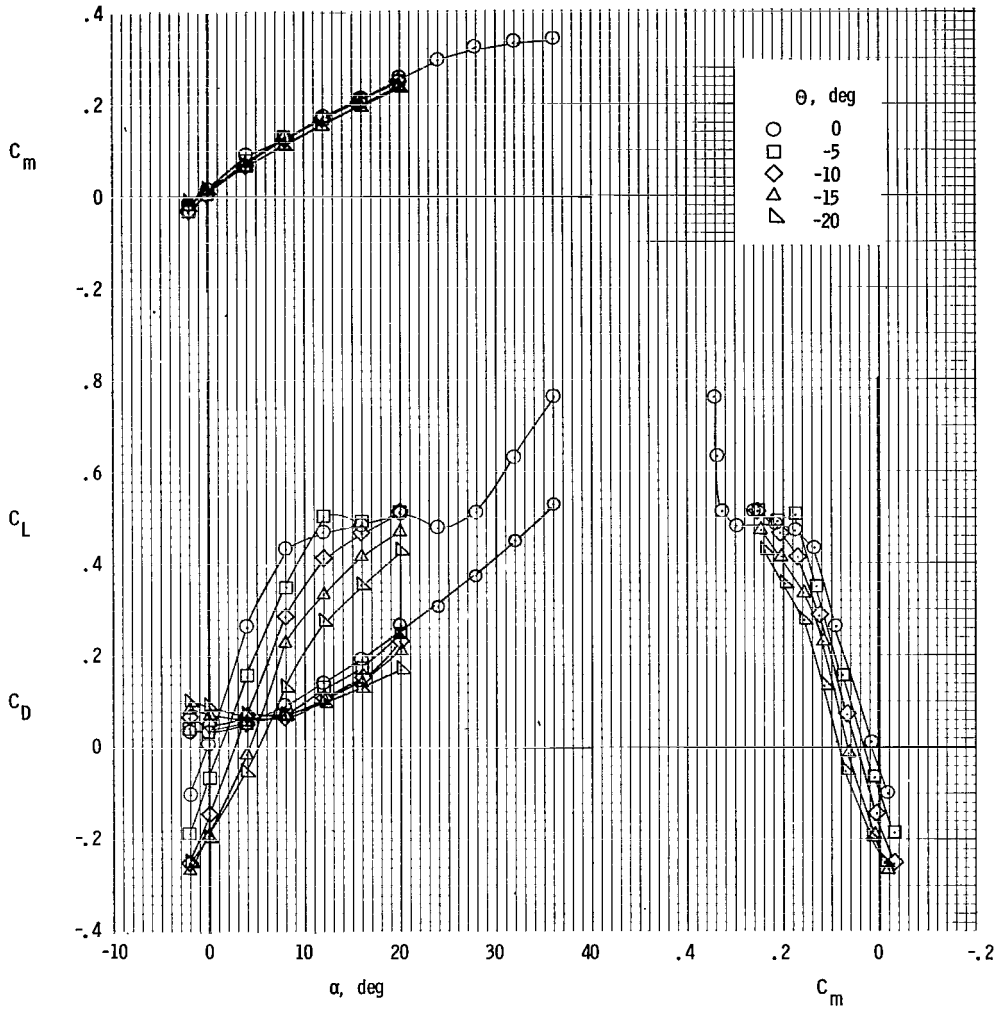

Figure 134.- Longitudinal aerodynamic characteristics. Tails off; rotor/wing 8.

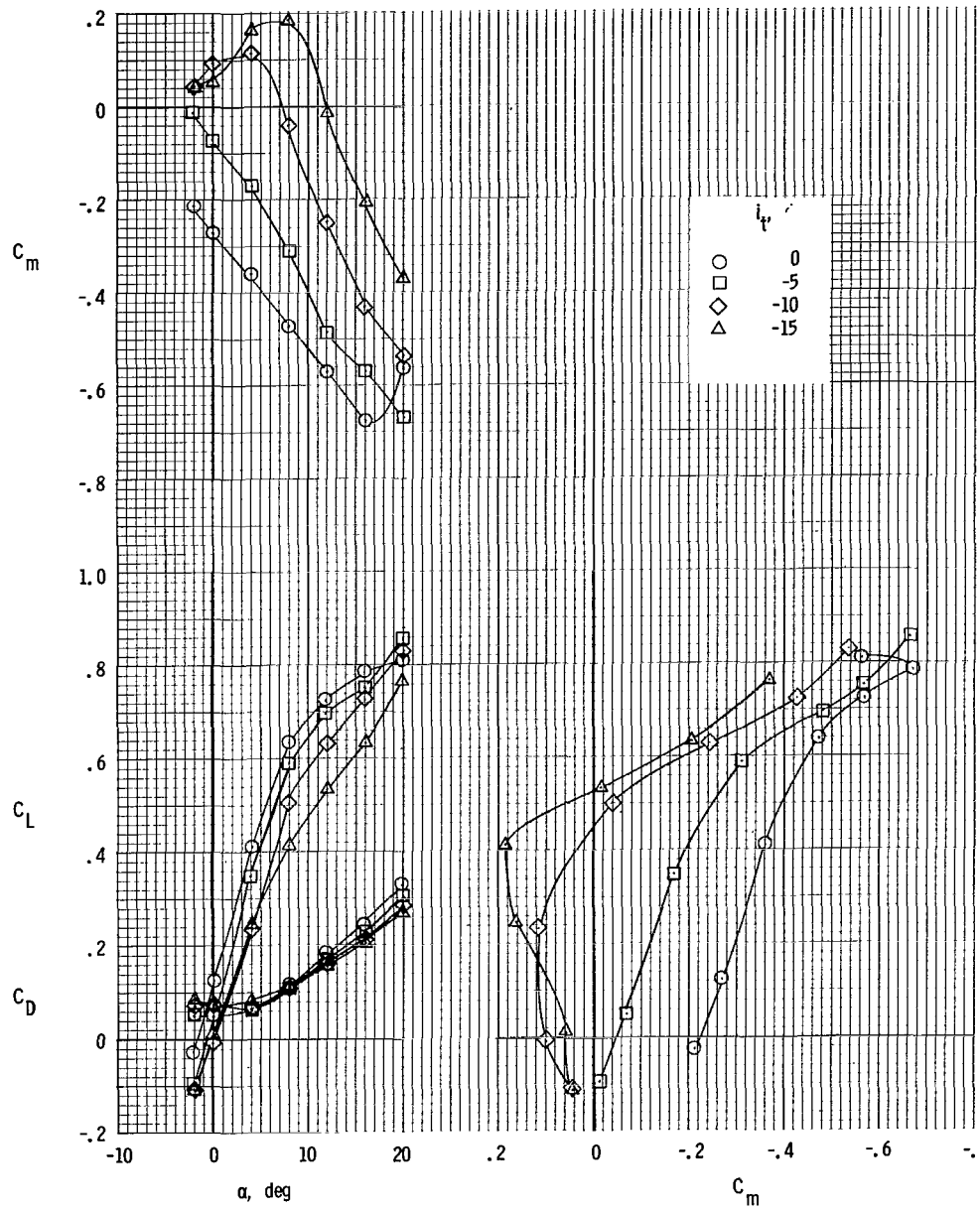

(a) $\Theta = 0^\circ$.

Figure 135.- Longitudinal aerodynamic characteristics. Twin vertical tails; horizontal tail at center fuselage; rotor/wing 8.

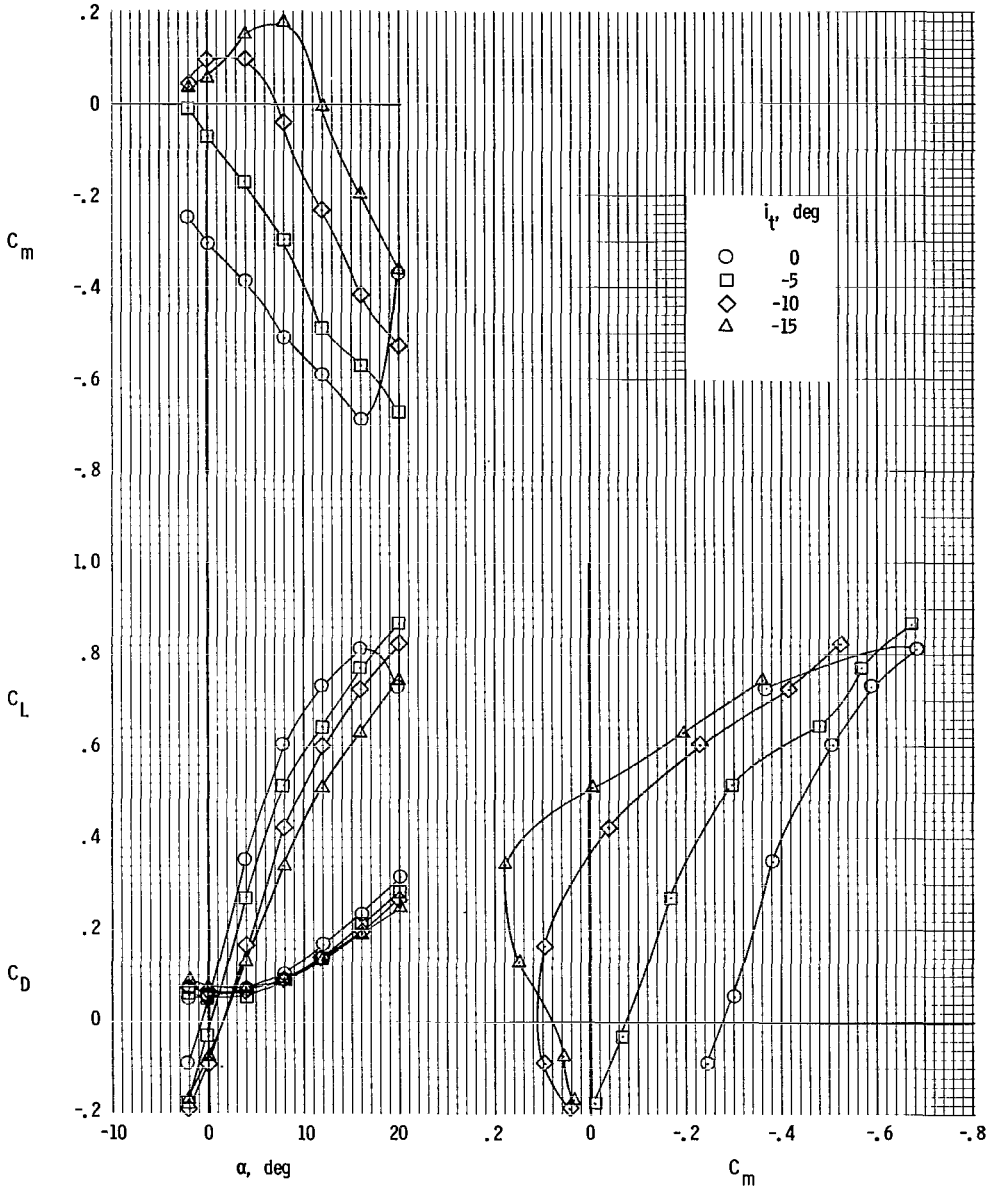

(b) $\Theta = -5^{\circ}$.

Figure 135.- Continued.

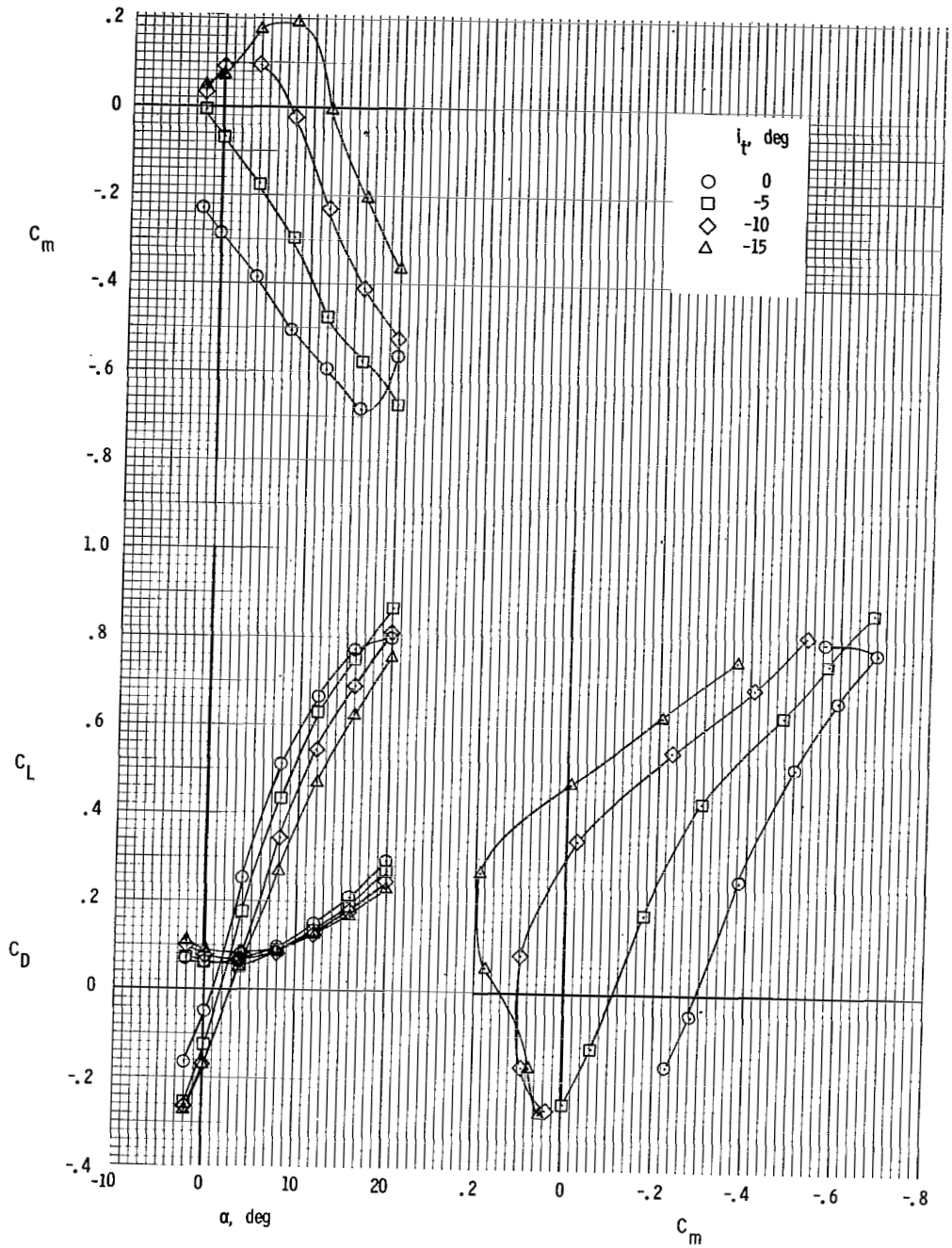

(c) $\Theta = -10^\circ$.

Figure 135.- Continued.

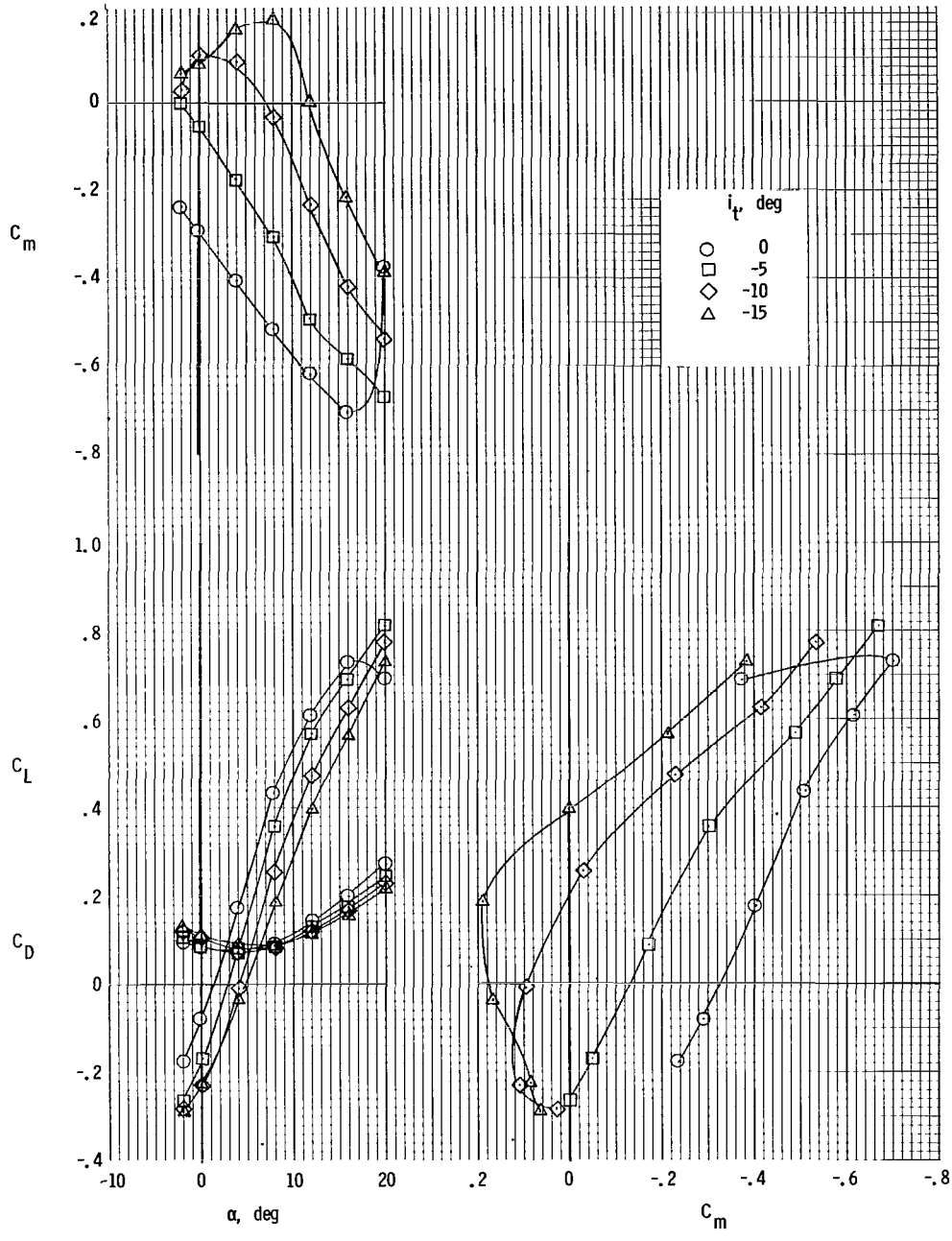

(d) $\Theta = -15^{\circ}$.

Figure 135.- Concluded.

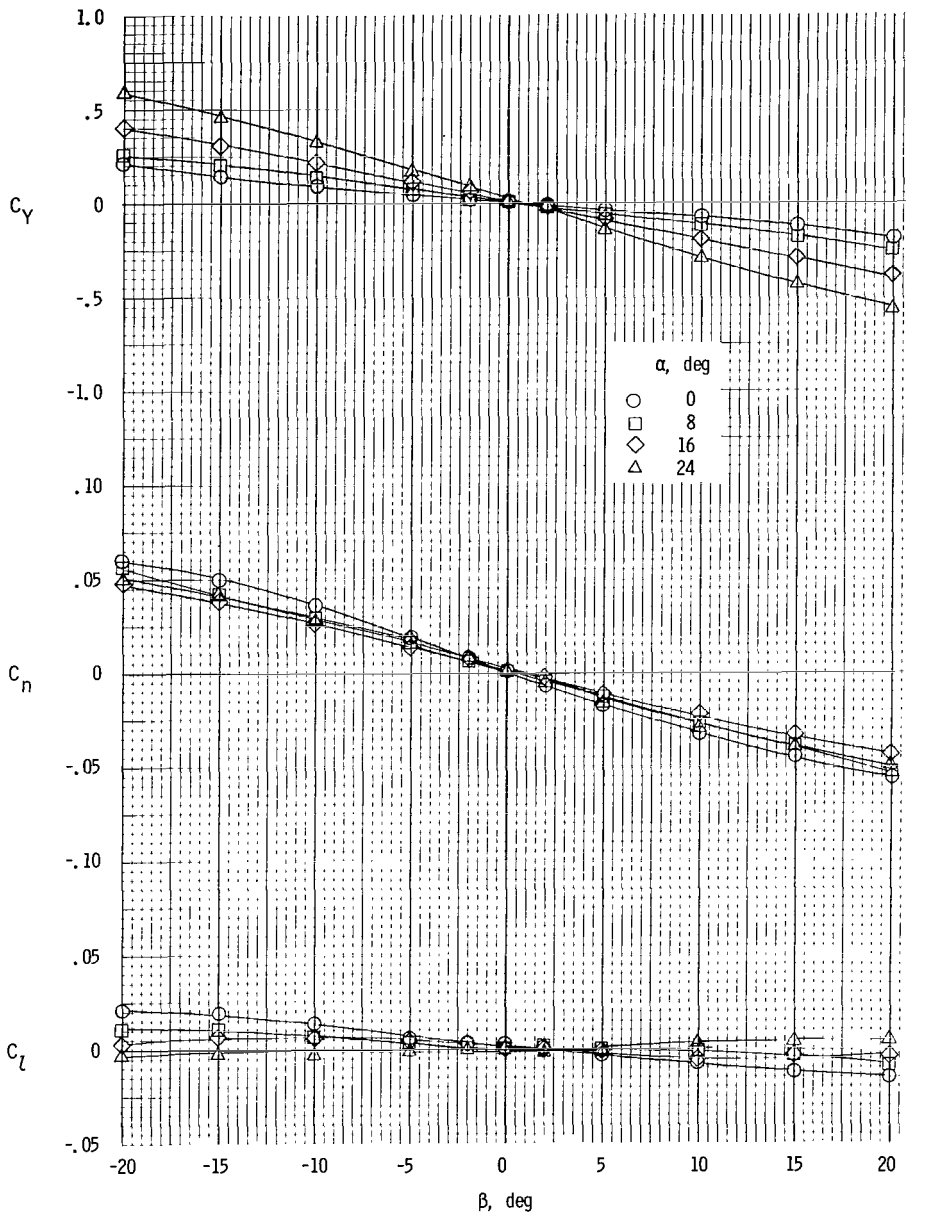

Figure 136.- Sideslip characteristics. Tails off; $\Theta = -10^{\circ}$; rotor/wing 8.

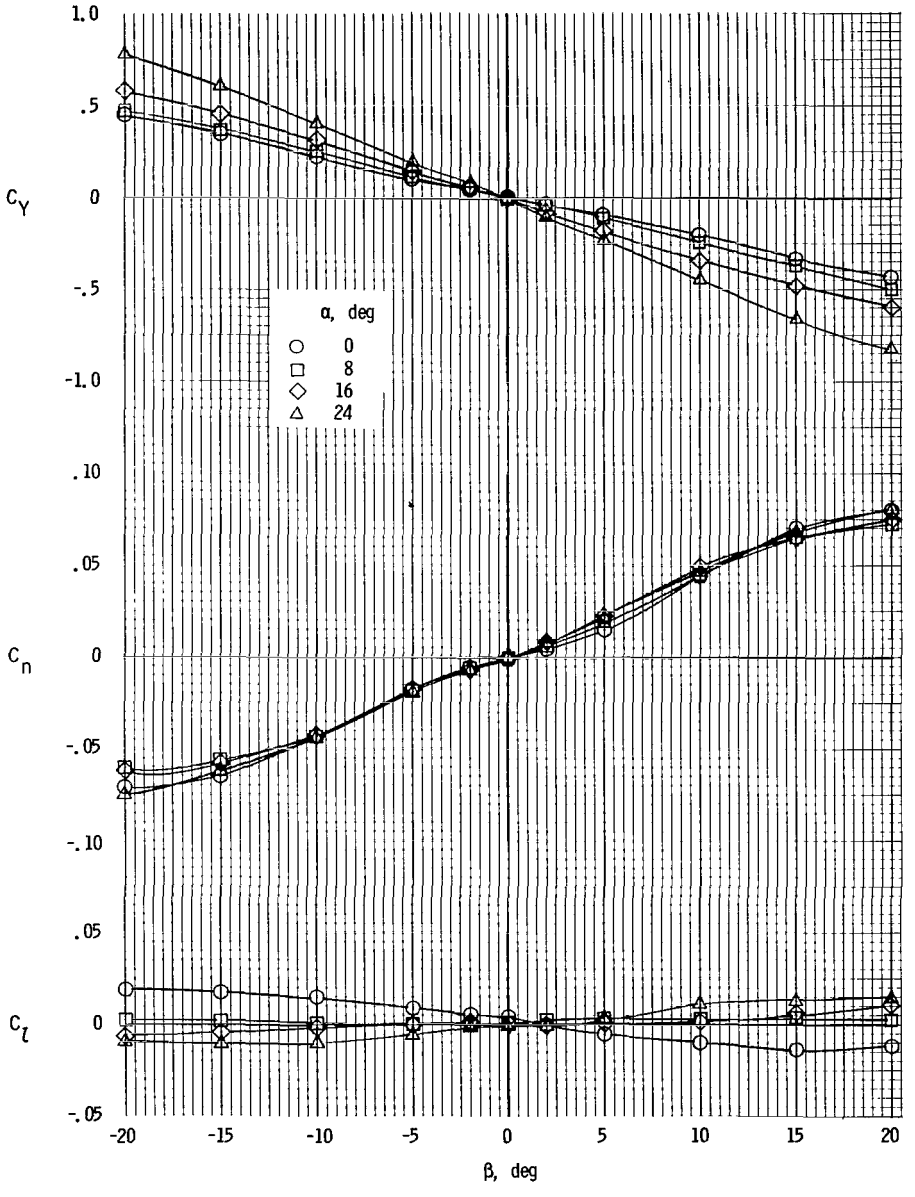

Figure 137.- Sideslip characteristics. Twin vertical tails; horizontal tail at center fuselage; $i_t = -10^\circ$; $\Theta = -10^\circ$; rotor/wing 8.

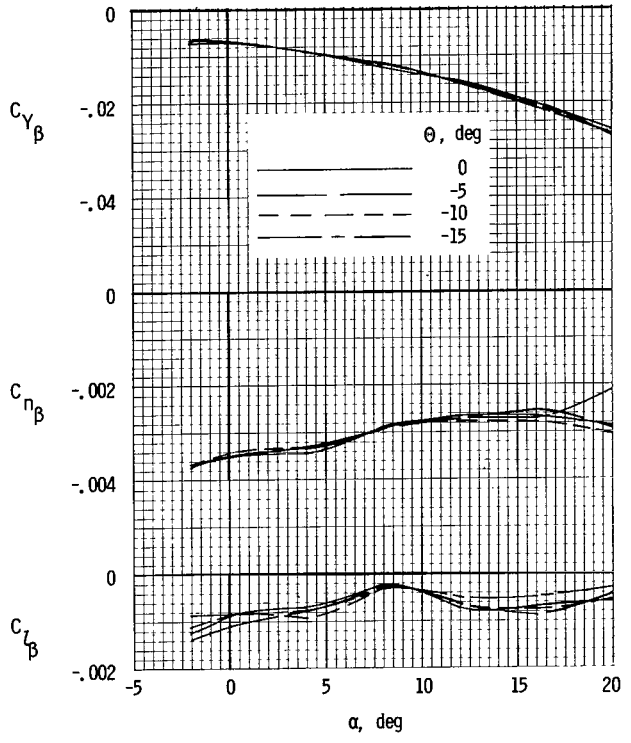

Figure 138.- Static lateral-stability derivatives. Tails off; rotor/wing 8.

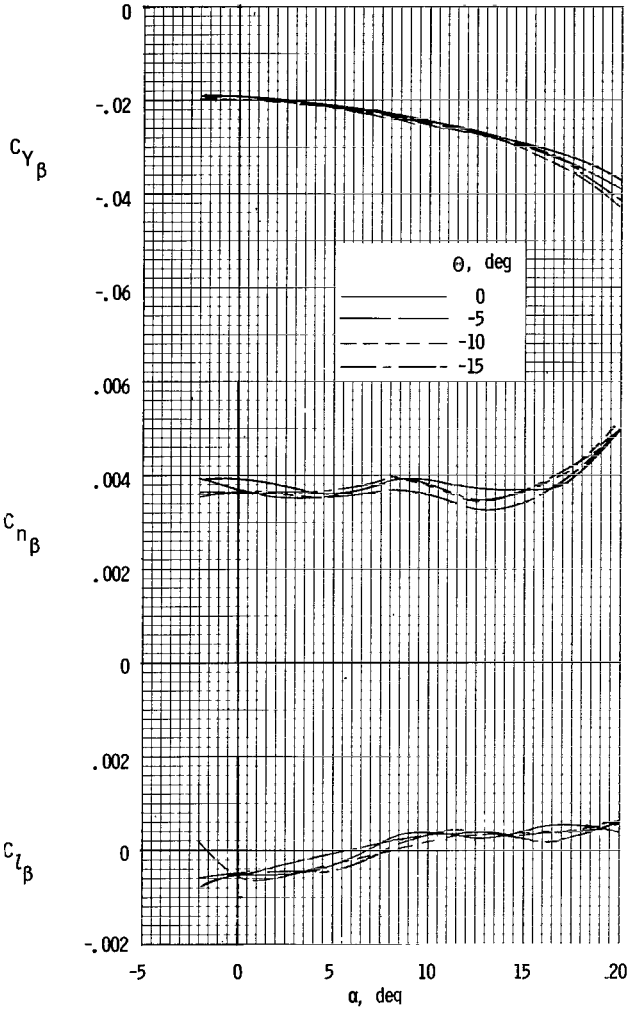

Figure 139.- Static lateral-stability derivatives. Twin vertical tails; horizontal tail at center fuselage; $i_t = -5^\circ$; rotor/wing 8.

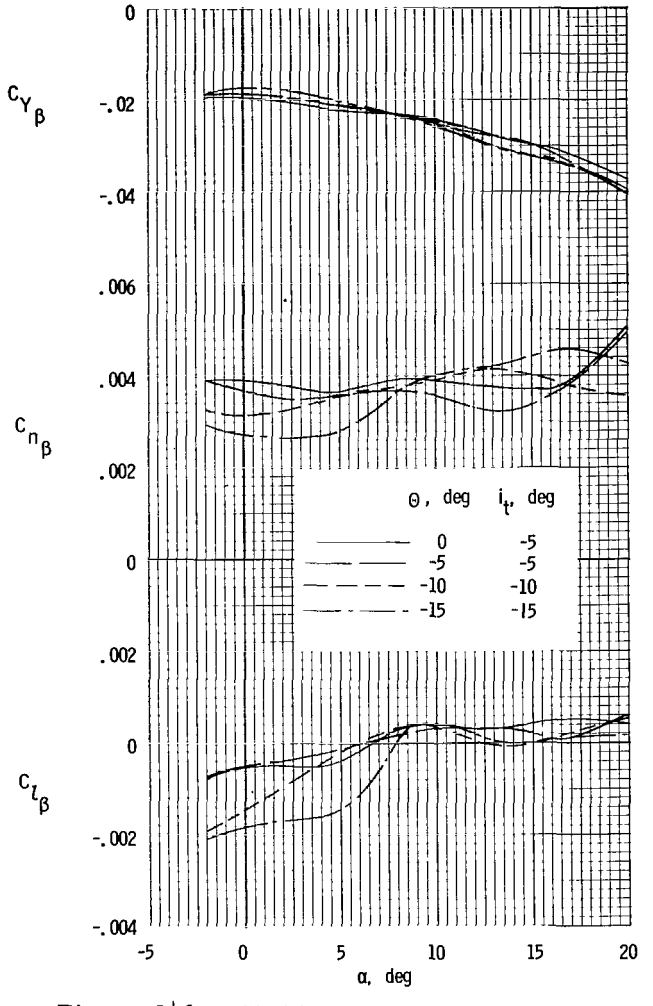

Figure 140.- Static lateral-stability derivatives for combinations of Θ and i_t. Twin vertical tails; horizontal tail at center fuselage; rotor/wing 8.

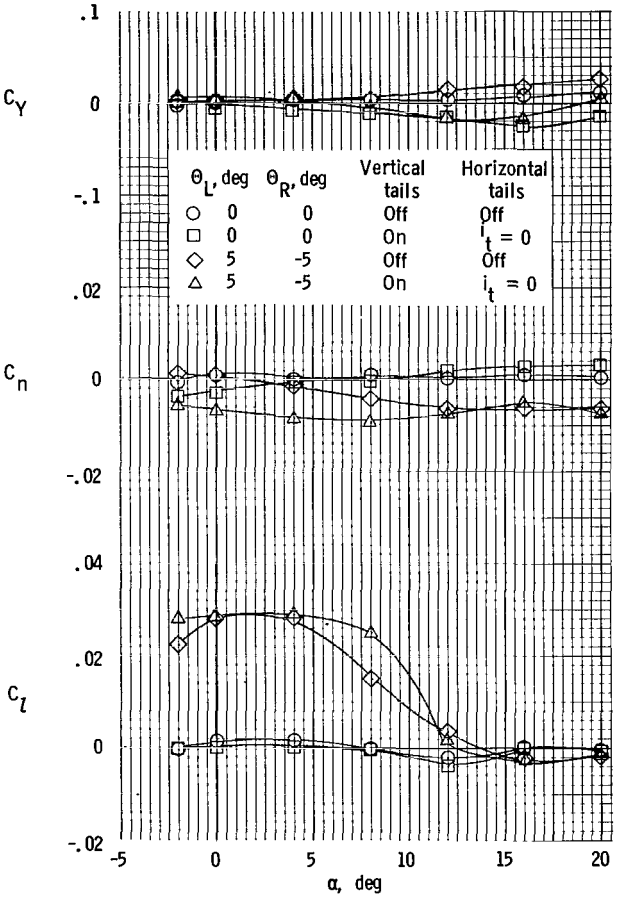

Figure 141.- Effect of tails on lateral-control characteristics with rotor blades used for control. Twin vertical tails; horizontal tail at center fuselage; $\Theta_{mean} = 0^\circ$; rotor/wing 8.

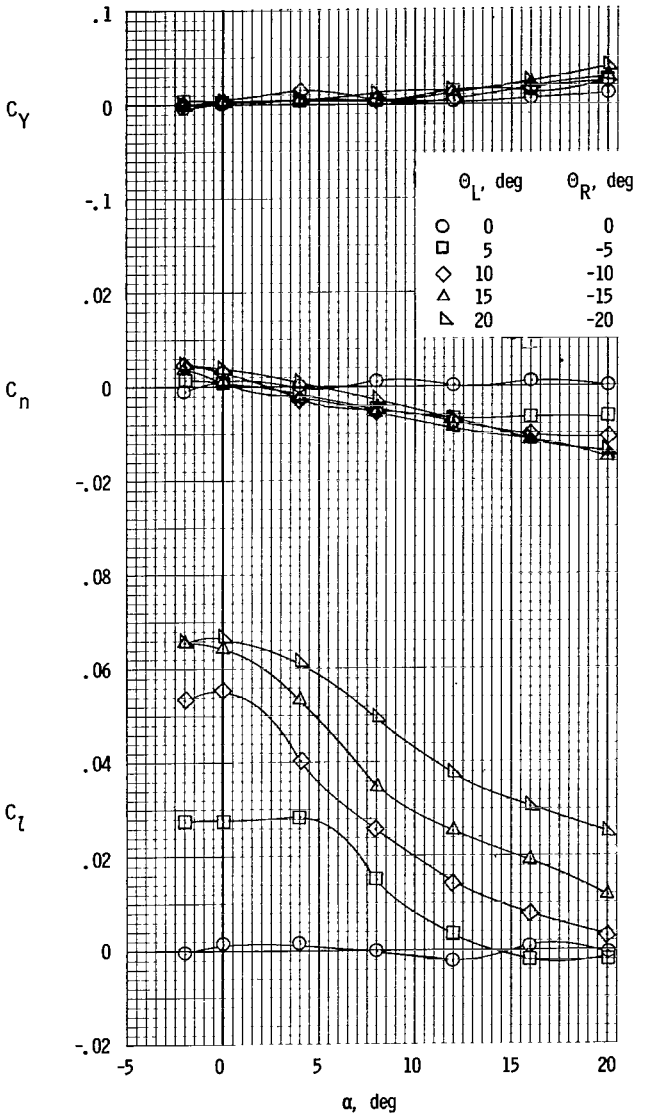

Figure 142.- Lateral-control characteristics with rotor blades used for control. Tails off; $\Theta_{mean} = 0^{\circ}$; rotor/wing 8.

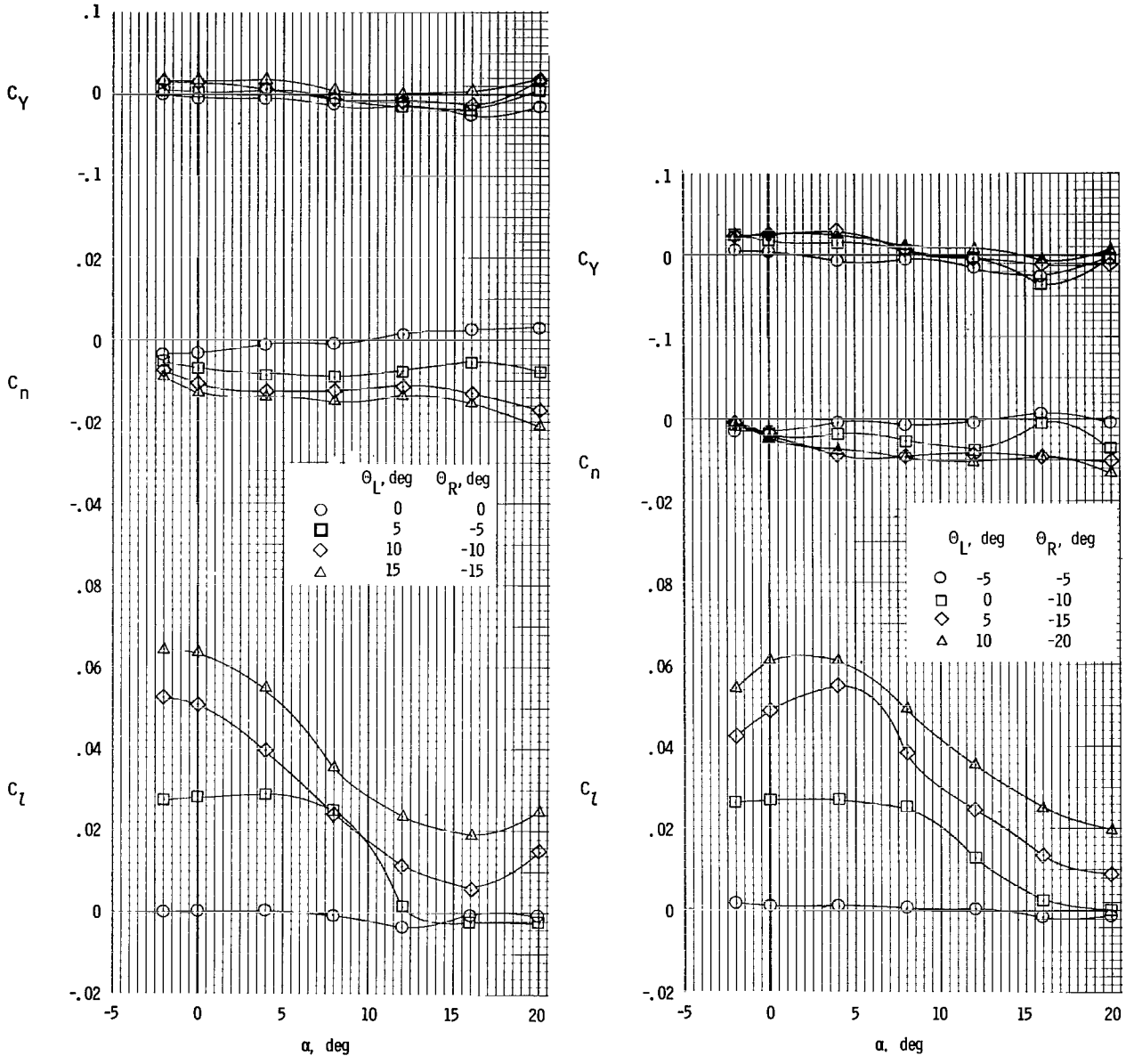

(a) $i_t = 0^\circ$; $\Theta_{mean} = 0^\circ$.

(b) $i_t = -5^\circ$; $\Theta_{mean} = -5^\circ$.

Figure 143.- Lateral-control characteristics with rotor blades used for control. Twin vertical tails; horizontal tail at center fuselage; rotor/wing 8.

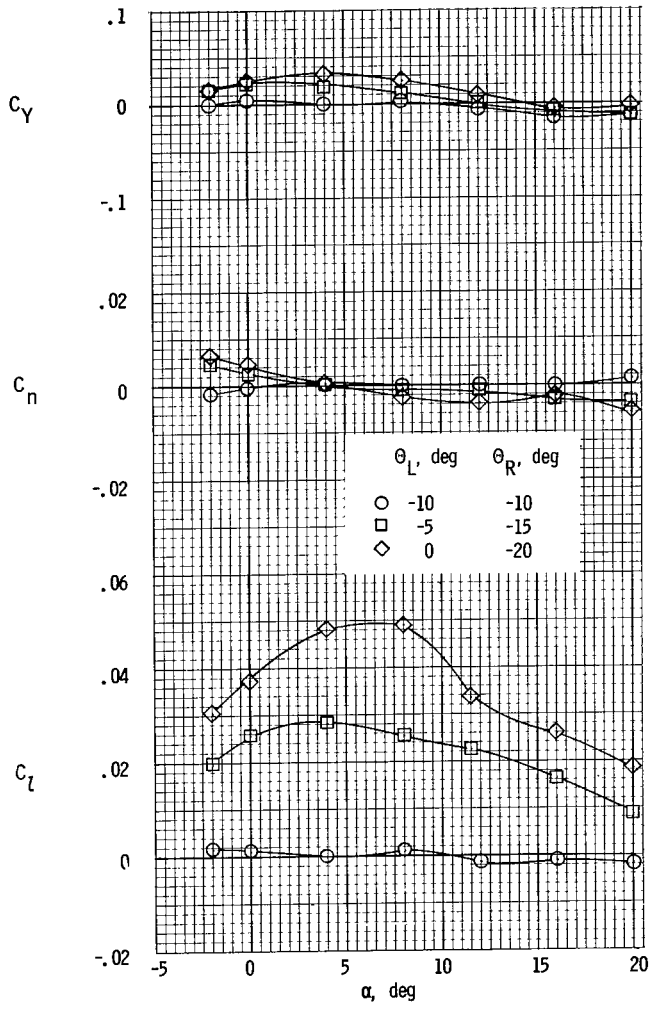

(c) $i_t = -10°$; $\Theta_{mean} = -10°$.

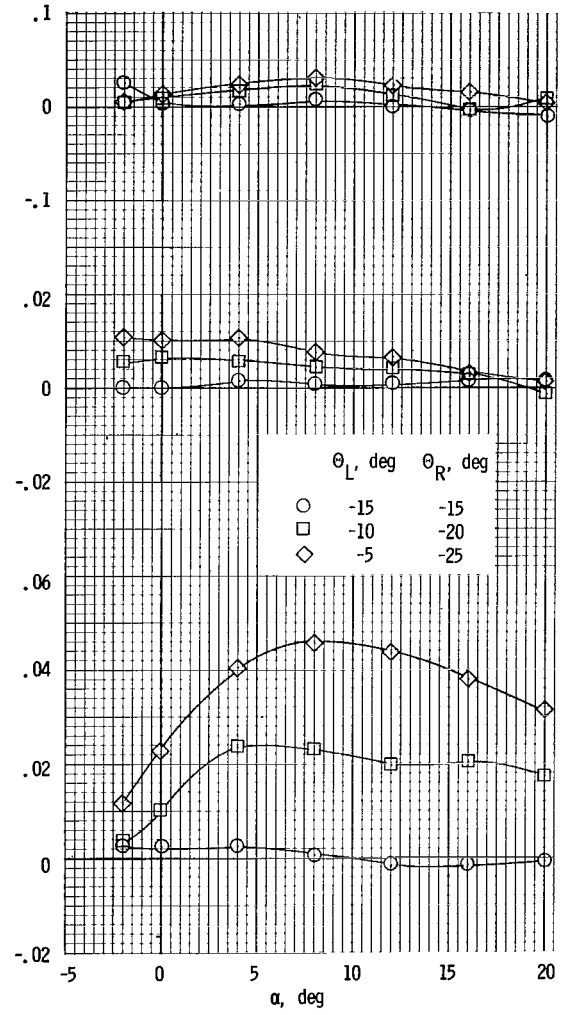

(d) $i_t = -15°$; $\Theta_{mean} = -15°$.

Figure 143.- Concluded.

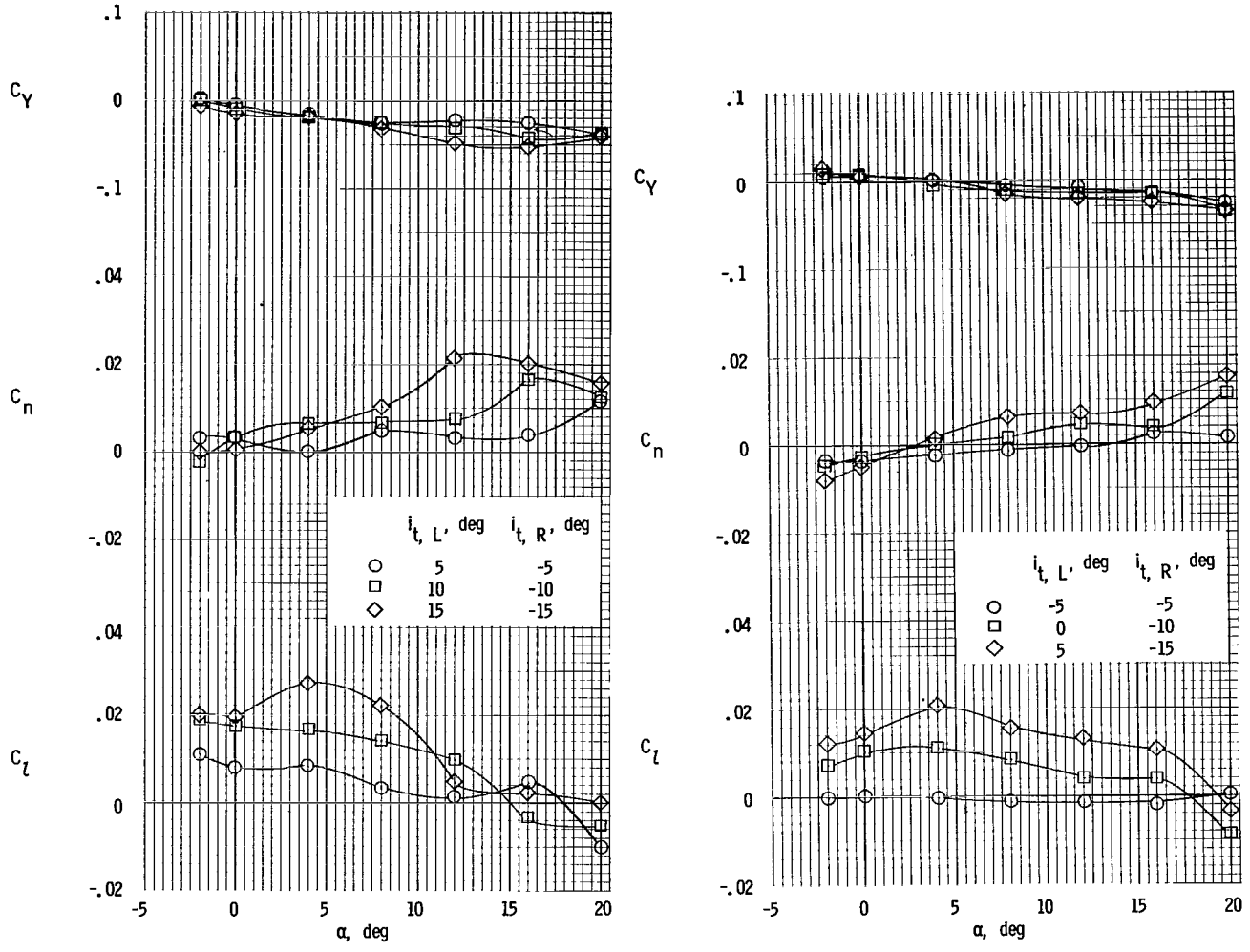

(a) $i_{t,mean} = 0^\circ$.

(b) $i_{t,mean} = -5^\circ$.

Figure 144.- Lateral-control characteristics with horizontal tail used for control. Twin vertical tails; horizontal tail at center fuselage; $\Theta = 0^\circ$; rotor/wing 8.

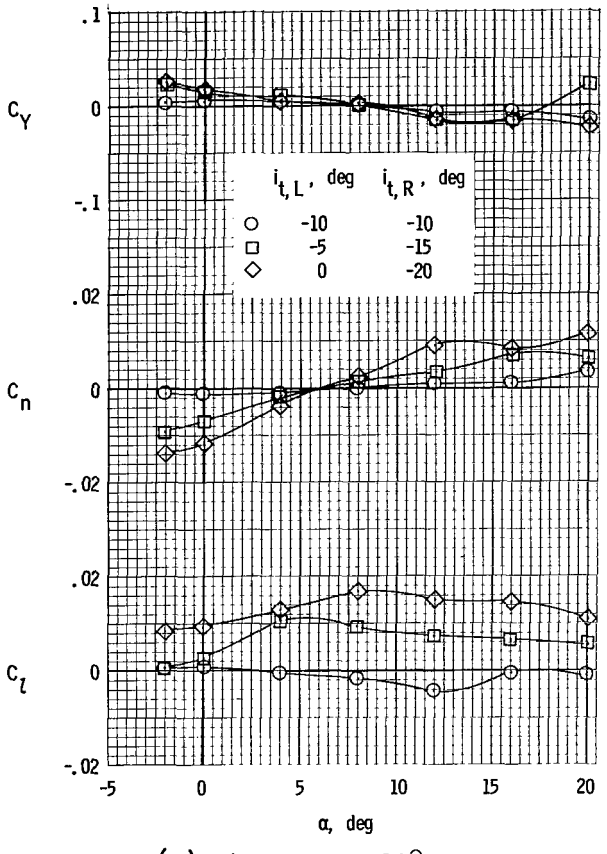

(c) $i_{t,mean} = -10°$.

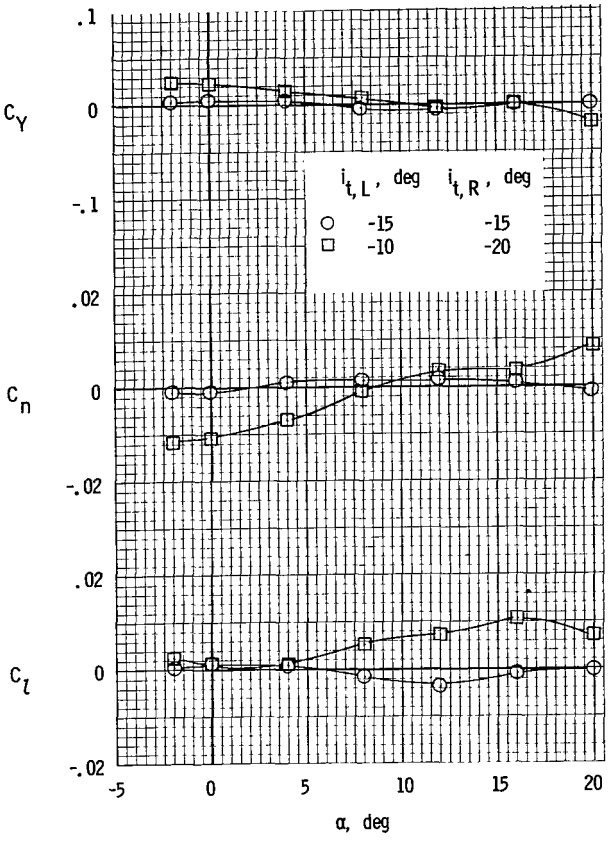

(d) $i_{t,mean} = -15°$.

Figure 144.- Concluded.

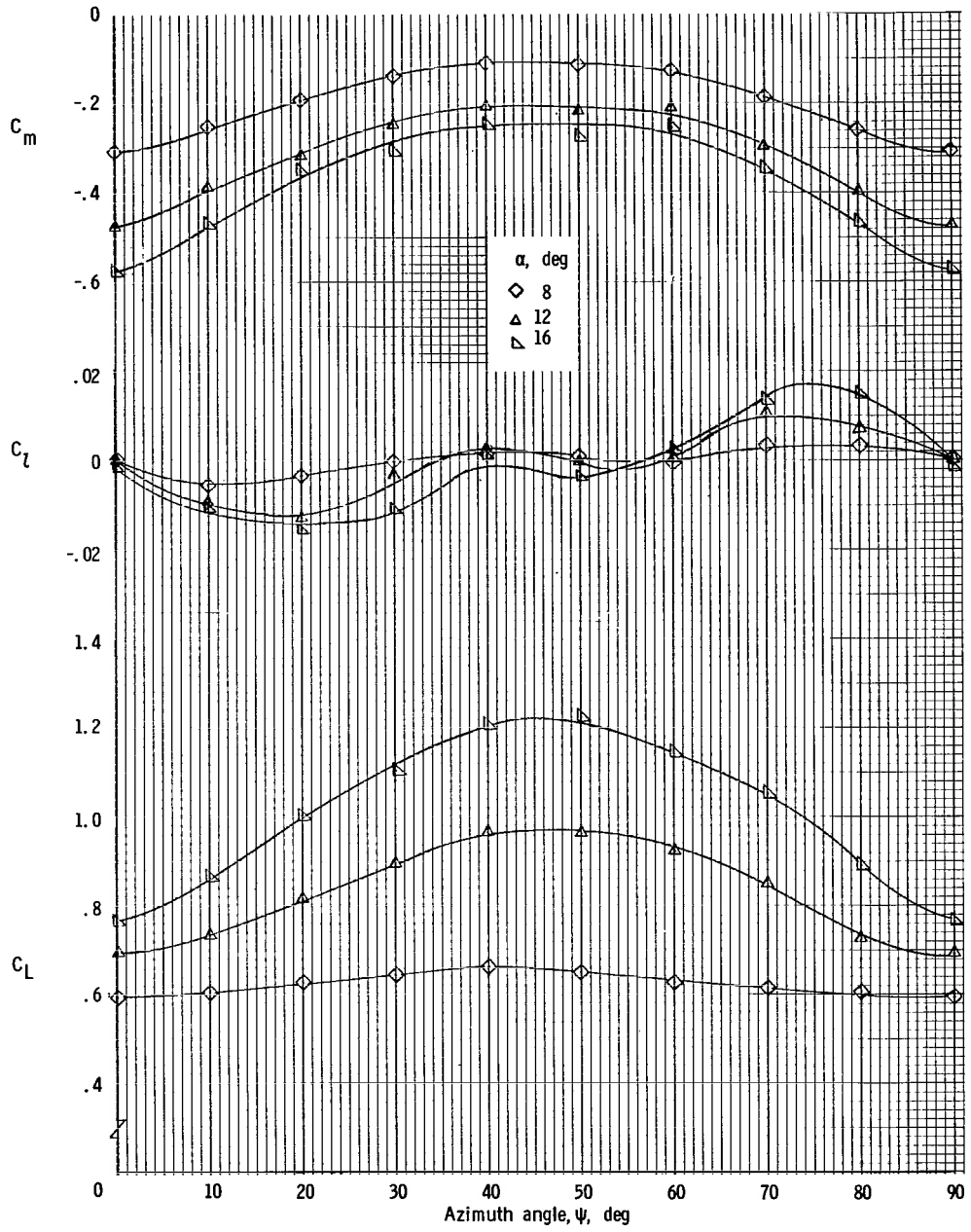

(a) $\Theta = 0^{\circ}$.

Figure 145.- Effect of azimuth position on lift coefficient and rolling- and pitching-moment coefficients for changes in model angle of attack. $i_t = -5^{\circ}$; rotor/wing 8.

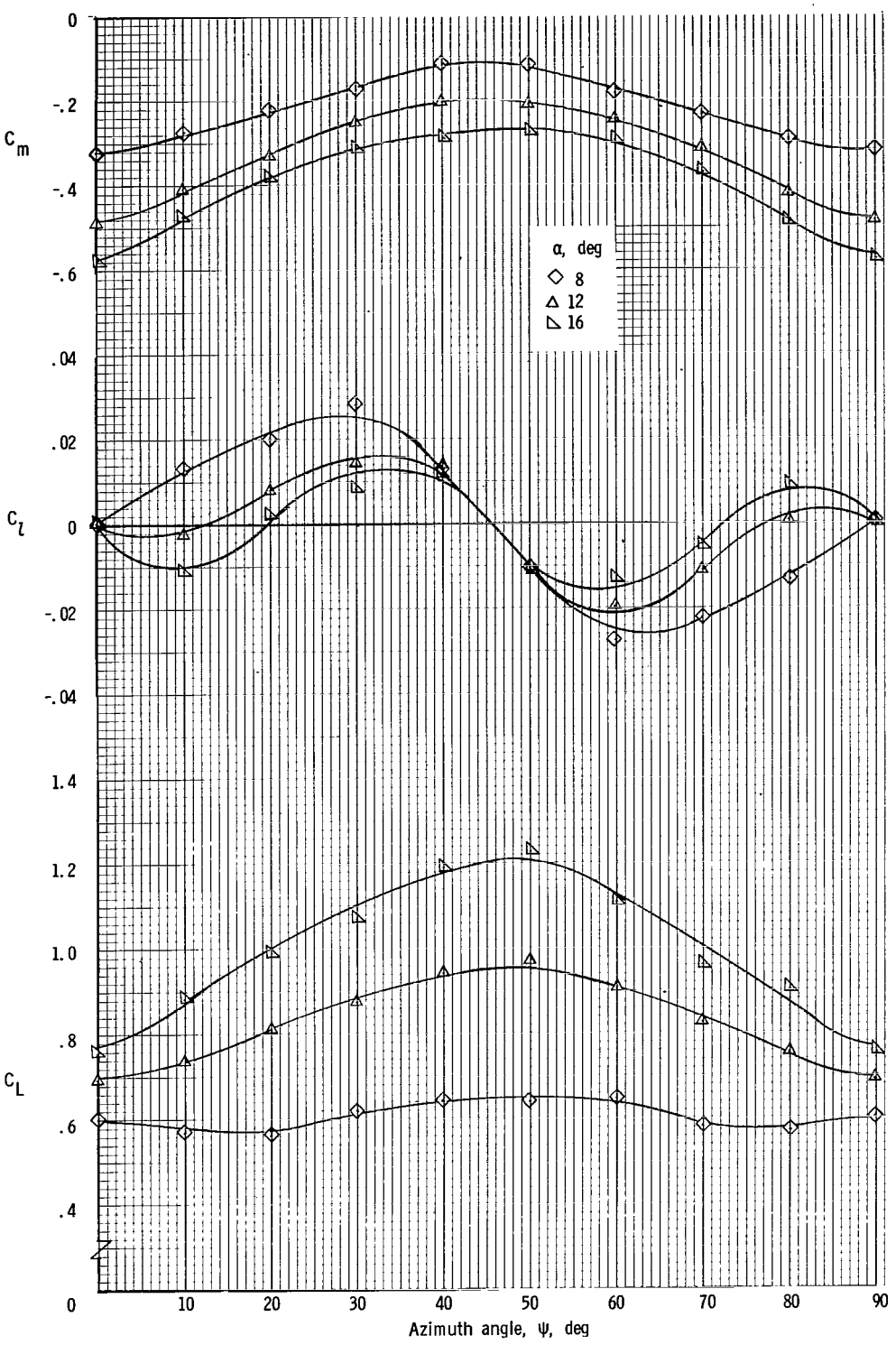

(b) $\Theta = -10^{\circ} \sin 4\psi$.

Figure 145.- Concluded.

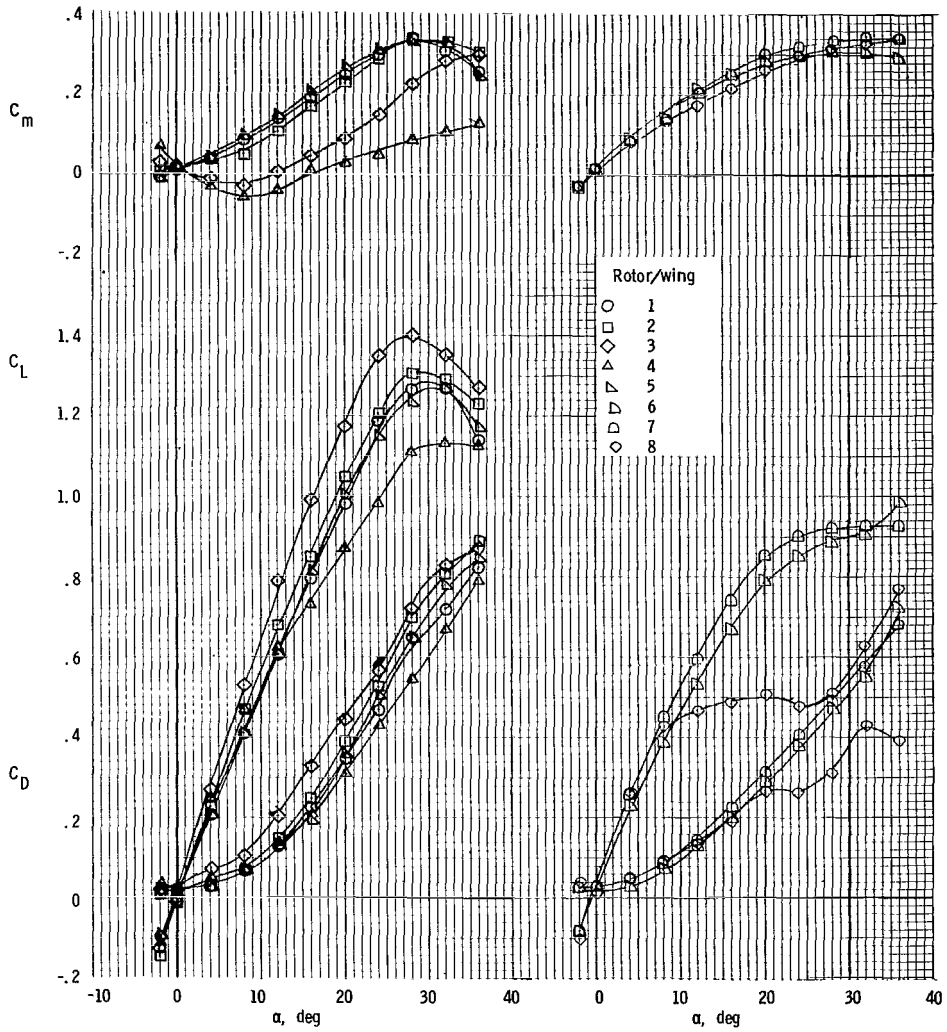

(a) Three-blade rotor/wing. (b) Four-blade rotor/wing.

Figure 146.- Longitudinal aerodynamic characteristics. Tails off; $\Theta = 0^{\circ}$.

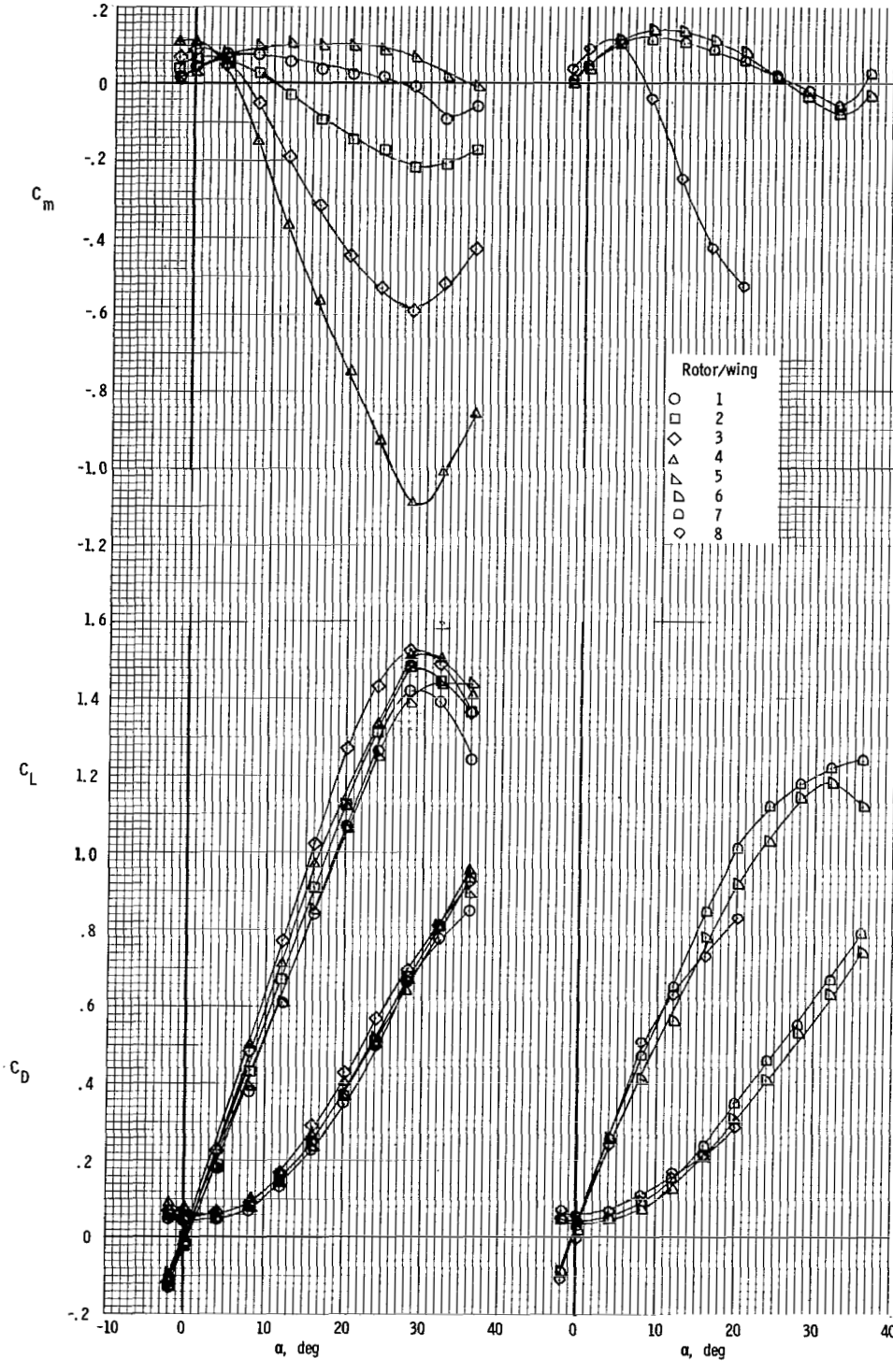

(a) Three-blade rotor/wing. (b) Four-blade rotor/wing.

Figure 147.- Longitudinal aerodynamic characteristics. Horizontal tail at center fuselage; twin vertical tails at tip of horizontal tail; $\Theta = 0^{\circ}$; $i_t = -10^{\circ}$.

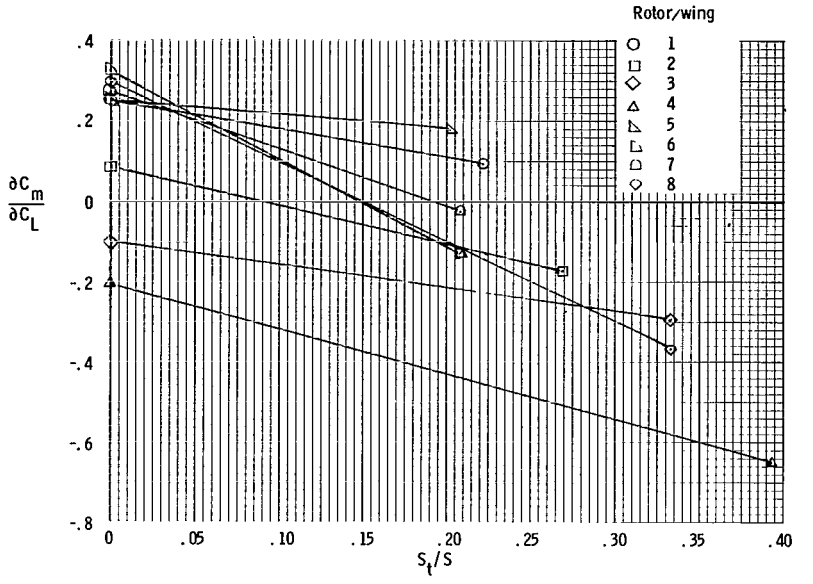

Figure 148.- Effect of tail size on longitudinal-stability characteristics. $\Theta = 0^{\circ}$.

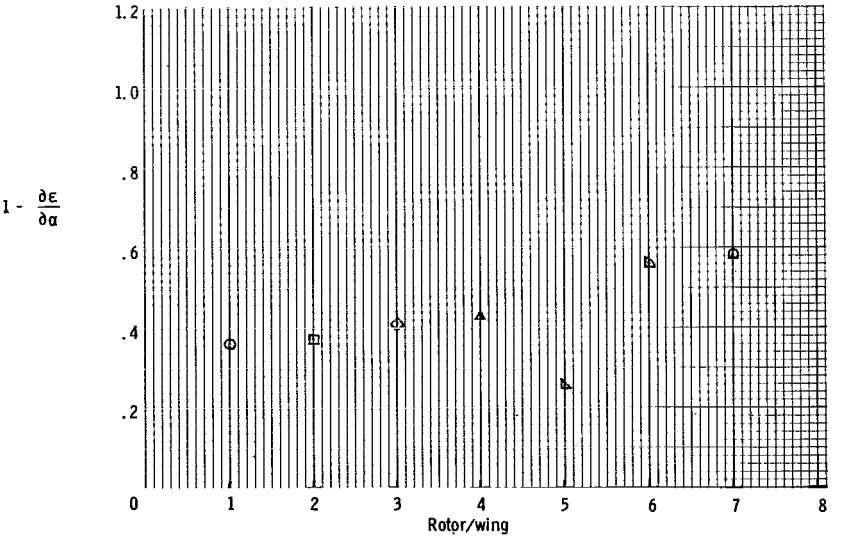

Figure 149.- Effect of rotor/wing planform on downwash characteristics. $\Theta = 0^{\circ}$.

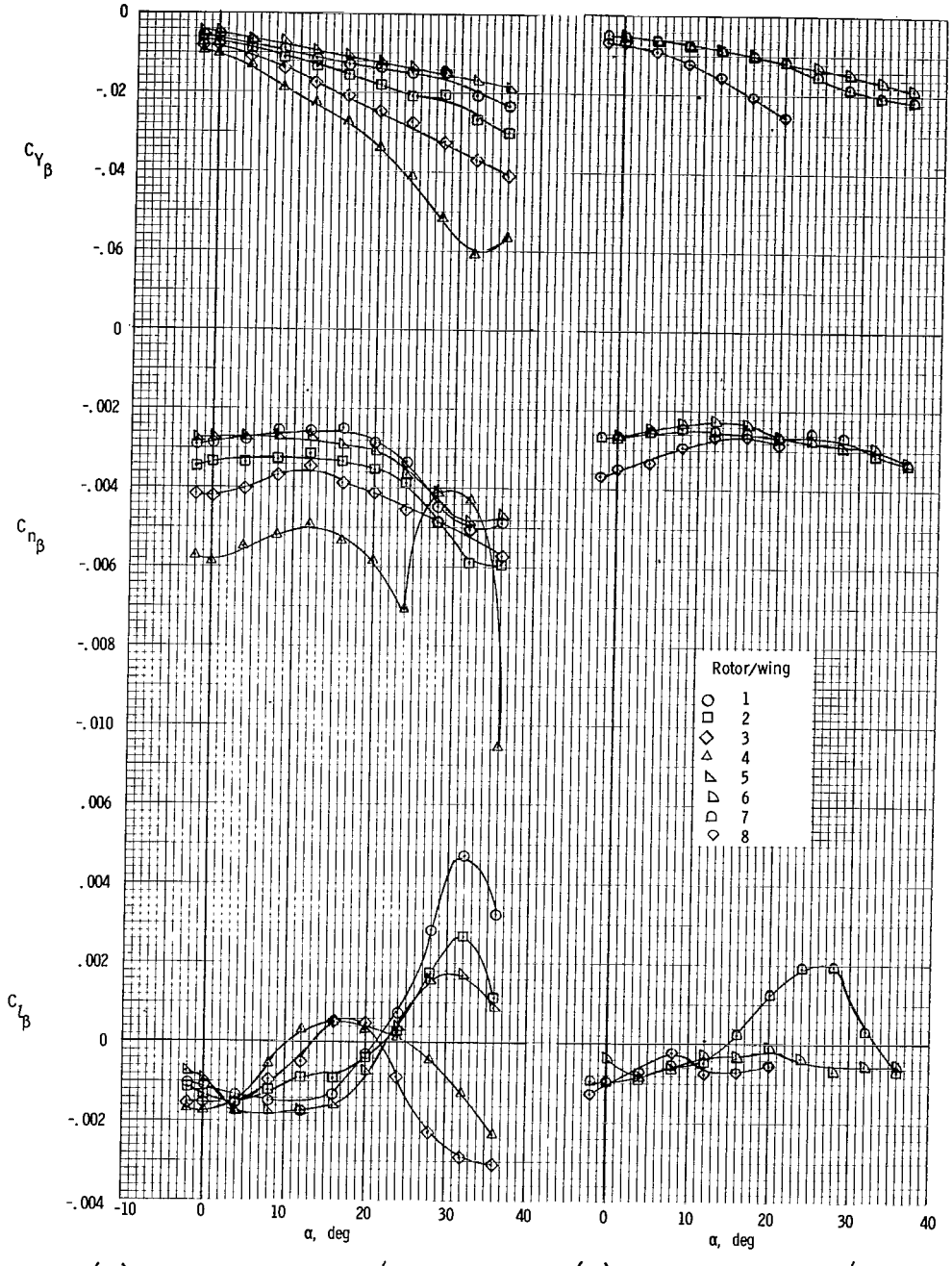

(a) Three-blade rotor/wing. (b) Four-blade rotor/wing.

Figure 150.- Effect of planform on static lateral-stability derivatives. Vertical tail off; $\Theta = 0^\circ$.

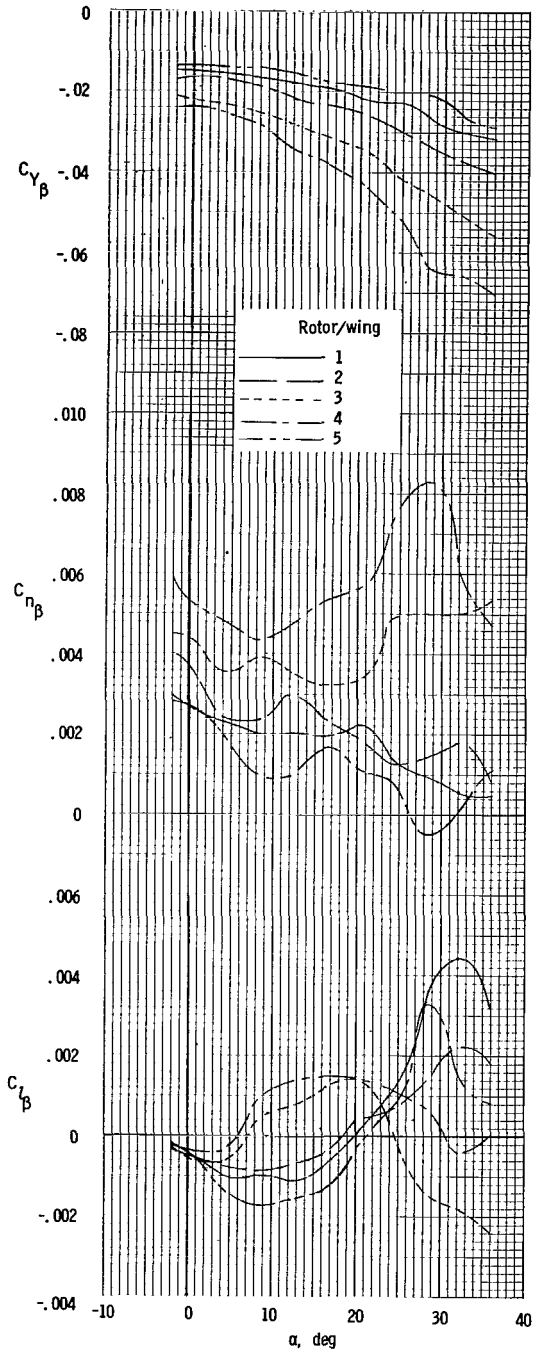

(a) Three-blade rotor/wing.

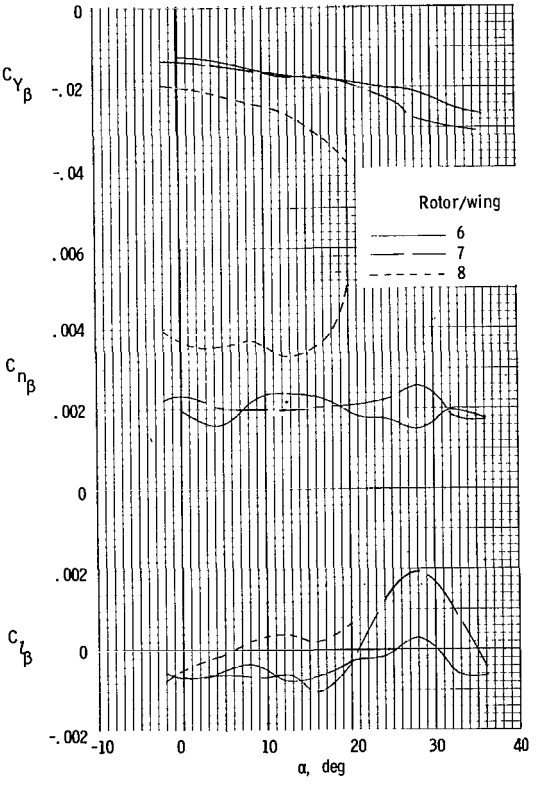

(b) Four-blade rotor/wing.

Figure 151.- Effect of planform on static lateral-stability derivatives. Horizontal tail at center fuselage; vertical tails at tip of horizontal tails; $\Theta = 0^{\circ}$.

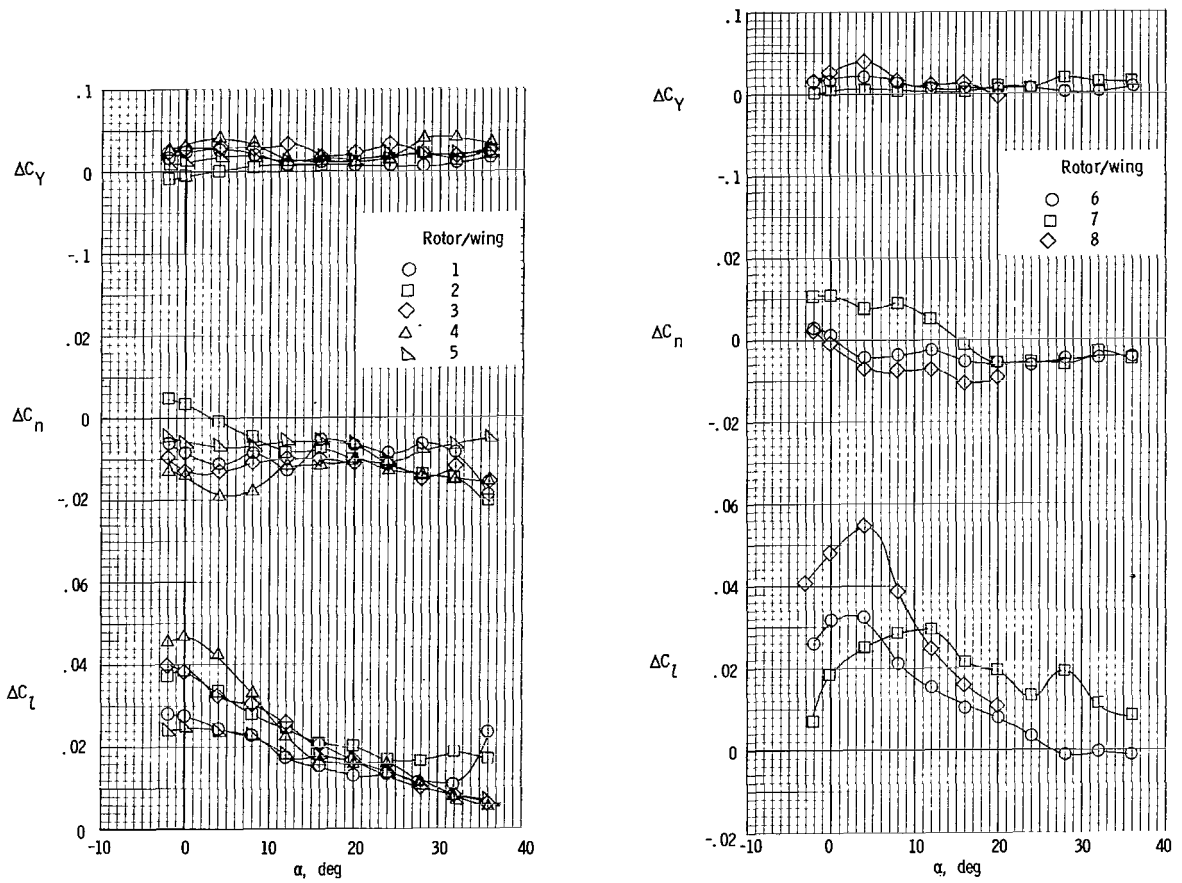

(a) Three-blade rotor/wing.

(b) Four-blade rotor/wing.

Figure 152.- Lateral-control characteristics with rotor blades differentially deflected ±10°.

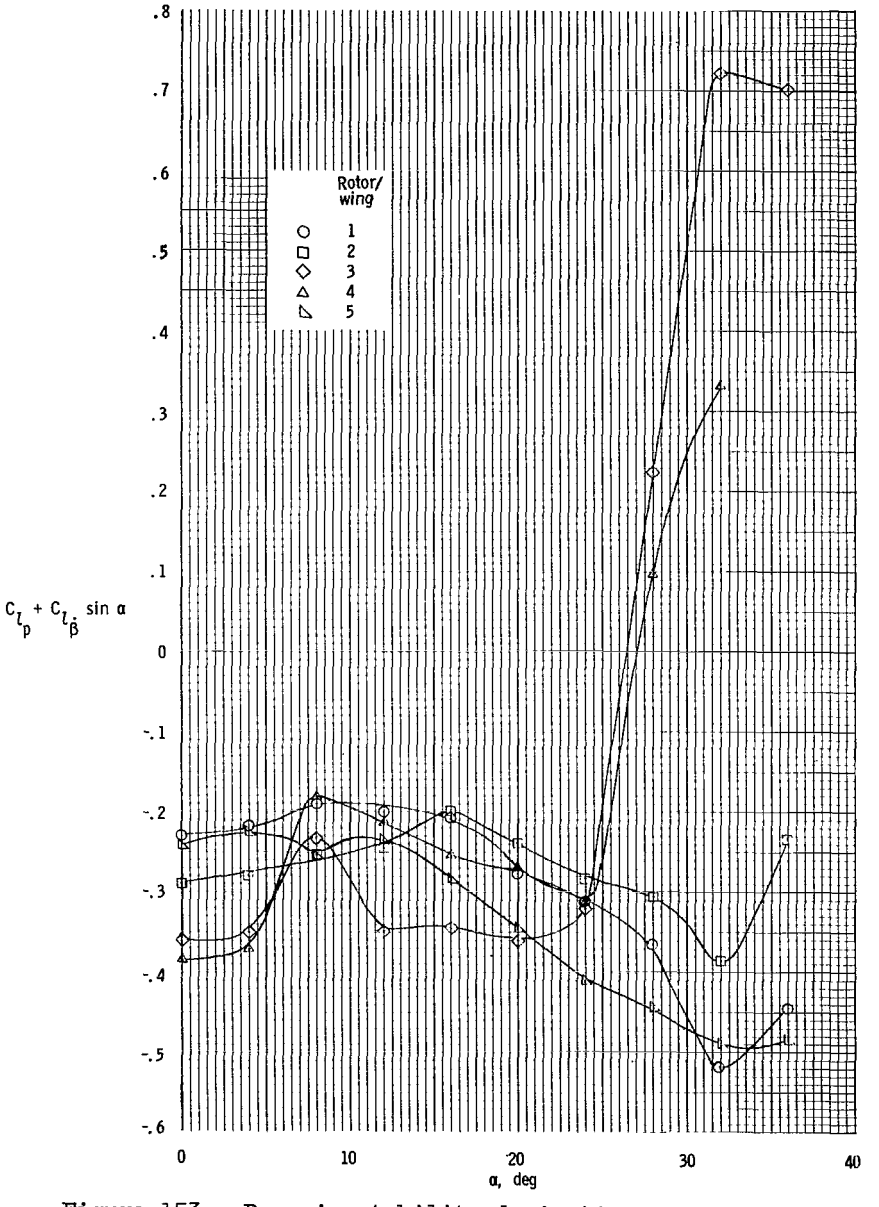

Figure 153.- Dynamic-stability derivatives measured in rolling-oscillation tests. Center vertical tail; mid-horizontal tail; $\Theta = 0^{\circ}$; $i_t = -10^{\circ}$.

"The aeronautical and space activities of the United States shall be conducted so as to contribute . . . to the expansion of human knowledge of phenomena in the atmosphere and space. The Administration shall provide for the widest practicable and appropriate dissemination of information concerning its activities and the results thereof."

— NATIONAL AERONAUTICS AND SPACE ACT OF 1958

NASA SCIENTIFIC AND TECHNICAL PUBLICATIONS

TECHNICAL REPORTS: Scientific and technical information considered important, complete, and a lasting contribution to existing knowledge.

TECHNICAL NOTES: Information less broad in scope but nevertheless of importance as a contribution to existing knowledge.

TECHNICAL MEMORANDUMS: Information receiving limited distribution because of preliminary data, security classification, or other reasons.

CONTRACTOR REPORTS: Scientific and technical information generated under a NASA contract or grant and considered an important contribution to existing knowledge.

TECHNICAL TRANSLATIONS: Information published in a foreign language considered to merit NASA distribution in English.

SPECIAL PUBLICATIONS: Information derived from or of value to NASA activities. Publications include conference proceedings, monographs, data compilations, handbooks, sourcebooks, and special bibliographies.

TECHNOLOGY UTILIZATION PUBLICATIONS: Information on technology used by NASA that may be of particular interest in commercial and other non-aerospace applications. Publications include Tech Briefs, Technology Utilization Reports and Technology Surveys.

Details on the availability of these publications may be obtained from:

SCIENTIFIC AND TECHNICAL INFORMATION DIVISION

NATIONAL AERONAUTICS AND SPACE ADMINISTRATION

Washington, D.C. 20546